Fibroblast subsets dictate the stromal set-point in the synovium to influence the outcome of joint inflammation.

by

Lucy-Jayne Marsh

A thesis submitted to the University of Birmingham for the degree of

DOCTOR OF PHILOSOPHY

Institute of Inflammation and Ageing

College of Medical and Dental Sciences

University of Birmingham

October 2024

Abstract

Fibroblast subsets cause inflammation and damage. While their diversity and pathogenicity in arthritis are understood, little is known about how this fibroblast landscape is remodelled during the course of arthritis. This thesis explored the role of fibroblast population in joint inflammation.

I performed a temporal analysis of fibroblasts at the single cell resolution in spontaneously resolving models of inflammatory arthritis. During inflammatory phases, I identified an enrichment in Wnt signalling in synovial fibroblasts. In particular, WNT5A was associated with disease chronicity. Local administration of rWnt5a protein in mice undergoing inflammatory arthritis, lead to worsened disease severity through recruitment of pro-inflammatory macrophages and dendritic cells. In contrast, inhibition of Wnt signalling in mice with inflammation arthritis lead to reduced joint swelling and leukocyte infiltration.

I also analysed fibroblasts during the resolving phase of arthritis, and identified a distinct subset of fibroblasts that exhibit a myofibroblast-like phenotype with a gene expression program linked to tissue repair. These fibroblasts express DKK3 (a member of the Dickkopf WNT Signalling Pathway Inhibitors with indeterminate biological function) and LRRC15 (a collagen binding protein), and show cross-talk with regulatory macrophages mediated by the TGF-β signalling pathway. In mice we observed that only these specific regulatory fibroblasts enhanced chromatin accessibility, gene expression, and protein expression of DKK3 during resolution. Direct administration of rDKK3 reduced joint swelling and inflammation in mice, potentially by mediating polarisation of regulatory T Cells.

Together, the findings implicate Wnt signalling as a major driver of fibroblast-mediated inflammation and suggest that targeting the Wnt pathway could be a therapeutically relevant approach to rheumatoid arthritis, particularly in patients who do not respond to conventional treatments. We discovered regulatory fibroblasts that suppress inflammation and promote tissue repair by activating DKK3 signalling. These fibroblasts are activated during the resolution phase of inflammatory arthritis through cross-talk with MerTK+ macrophages. DKK3 secretion by these fibroblasts transforms the stromal landscape towards pro-repair phenotypes that control inflammation.

Dedications

To Dad

Simon Andrew Jones

17th June 1971 – 2nd July 2021

At least you won't have to pretend you've read this

&

Snips

April 2021 – September 2024

I miss you, my little loaf

Acknowledgments

When I began this PhD journey in 2020, I had no idea what the next four years would hold. These years have brought some of the most challenging yet rewarding experiences of my life, and this thesis would not exist without the incredible support of those around me.

First, I would like to extend my deepest thanks to Prof. Crofty. You have been unwavering in your support of my work, and your encouragement during times when I lost faith in myself has been invaluable. You continually push us to be the best researchers we can be, while never compromising on compassion or integrity. Your support and understanding after the loss of my dad meant more than words can express, and it laid the foundation for a great working relationship. I look forward to seeing where the Croft Group goes in the future!

To the members of the Croft Group: I genuinely love being part of our team. We truly embody the "work hard, play hard" philosophy, and the mutual support we offer one another is something I will carry with me throughout my career. Special thanks to Annie Hackland for tolerating my quirks, never judging my meltdowns, and being my favourite Scorpio. I love you more than you love halloumi. To Dr. Sam Kemble, who has been there from day one—thank you for always having my back. And to Dr. Chris Mahony, whose patience knows no bounds, I am so grateful for your presence in my life. Charlotte Smith, our Research Technician Queen—I couldn't have made it through the past four years without you. Holly Adams, the RRG would fall apart without your hard work, and my life would be infinitely duller without your friendship. To the countless RRG members who have supported me along the way—thank you so much, even if I can't list you all by name here.

I also want to thank the original Lab 4 crew: Johnny, Julia, Laurence, KP, Mel, and Georgiana. I miss our days in the lab together, and I'm so grateful for the memories we created.

To my family: Though you may not fully understand what I do, your unwavering belief in me has been a constant source of strength.

A special shoutout to my second-favourite Scorpio, Jack—this thesis might never have been written without your monitor. I owe you some fried chicken!

To my wonderful friends, Emma and Will: I've never laughed as hard as I do when I'm with you. Thank you for your constant love and laughter.

To Yas: I probably need another thesis just to thank you properly. Even though I'm married, I believe you're my true soulmate. Being your friend for the past 13 years (?!) has meant the world to me. We've grown so much together, and I'm incredibly proud of who we've become. Thank you for everything—I love you.

And lastly, my deepest thanks go to my amazing husband, Aaron. We've been through so much together, but you've always been there with a calm and steady presence, supporting me and everyone around you. You are the best person I know, and I love you more than words can say.

Table of Contents

List of figures

List of tables

Contributions

Many generous colleagues contributed to this thesis's findings. Professor Adam Croft generated samples for the single-cell RNA sequencing atlas of inflammatory arthritis discussed in Chapter 3. Dr. Sam Kemble assisted in generating samples for single-cell multiome sequencing and participated in dissections, animal experiments, and library prep for scRNA-seq. Charlotte Smith also supported animal experiments, dissections, and library prep. Dr. Christopher Mahony analysed sequencing data from the single-cell ATAC-seq dataset and provided analyses of publicly available. Holly Adams sectioned tissue samples and assisted with H&E staining, along with Emily Powell. Annie Hackland and the Birmingham Tissue Analytics team collaborated on generating the RNA scope data. Professor Andrew Filer collected human synovial tissue which was used to generate immunofluorescence images kindly provided by Patricia Nisa and Dr. Christine Bolton. Dr. Ian Beh assisted with qPCR data generation and analysis, while Dr. Paulynn Chin helped with the overexpression of Dkk3. Chapter 4's work was produced through a collaboration with the Brenner Group at Brigham and Women’s Hospital and Harvard Medical School, with permission for its use. Special thanks to Professor Michael Brenner, Dr. Alisa Mueller, and Angela Zou for this successful collaboration.

1 INTRODUCTION & LITERATURE REVIEW

Declarations

Parts of this introduction have previously been published in a review paper, of which I am the primary author. [1]

1.1 Rheumatoid arthritis

RA is a prototypic immune-mediated inflammatory disease characterised by persistent synovial joint inflammation that, if untreated, leads to progressive joint damage.[2–4] While the introduction of biological disease-modifying anti-rheumatic drugs (bDMARDs) targeting either leukocytes or their derived products has led to a step change in the management of RA, 30%- 40% of patients do not respond to such therapies, regardless of the mechanism of action of the drug used.[5] These observations suggest the existence of additional pathways of disease persistence that remain to be identified and therapeutically targeted.[6] While autoimmunity and systemic immune dysregulation are fundamental underlying disease processes in RA, the primary site of pathology during the effector phase of the disease occurs in the lining of synovial joints (called the synovial membrane).[4] As a result, the pathogenic role of cells resident in synovial tissue, most notably fibroblasts and macrophages, has gained considerable attention as potential therapeutic targets in inflammatory joint disease.[7–10]

Synovial tissue architecture

The synovium is a thin mesenchymal tissue that encapsulates the joint cavity and provides a barrier and lubricates the joint during locomotion.[11,12] The membrane

comprises a complex cellular eco-system of tissue-resident macrophages, fibroblasts, nerves, and endothelial cells organised into a distinct microanatomy. The synovium is compartmentalised into histologically distinct zones: the lining layer and sub-lining layer with each compartment serving as a specialised tissue niche, adapted to perform specific tissue functions and unique roles in tissue homeostasis.[13]

In a healthy joint, the lining of the synovium is only 1-3 cell layers thick and is composed of tissue-resident macrophages and fibroblasts.[14] This zone of the synovium controls cellular and molecular trafficking between the synovial membrane and the joint cavity, maintaining the integrity of the joint and regulating the composition of the synovial fluid, which ensures sufficient lubrication for joint locomotion and exchange of nutrients between the synovial tissue and the synovial fluid. In contrast, the sub-lining is comprised of fibroblasts and tissue-resident macrophages distributed throughout a loose connective tissue that contains blood and lymphatic vessels to ensure effective transport of nutrients and cells to and from the systemic circulation to the joint.

The synovial membrane undergoes extensive remodelling in response to inflammation and can expand to as much as 10-20 cell layers thick.[15,16] Infiltrating immune cells and proliferation of fibroblasts result in synovial hyperplasia, characterised by a heterogeneous population of fibroblasts and macrophages that promote tissue inflammation and damage.[16,17] The formation of pannus tissue, a well-described architectural feature of the chronically inflamed joint,[18] is comprised of

hypertrophic synovium, composed of macrophages and fibroblasts that produce destructive enzymes that degrade articular cartilage and bone.[19] The cellular components and mechanisms underlying the disease-specific remodelling of the synovium have yet to be fully elucidated.[20]

1.2 Definitions of tissue fibroblasts in health and disease

Fibroblasts are ubiquitous mesenchymal cells that make up the stromal compartment of organ tissues.[21,22] Historically identified by their morphology, ability to adhere to plastic and absence of epithelial, vascular, and leukocyte lineage markers, their study has been compounded by a lack of fibroblast-specific cell markers.[23,24] Under steady-state conditions, fibroblasts are more generally defined by their expression of collagen 1-alpha (COL1A1), platelet-derived growth factor receptor-alpha (PDGFRα), and THY1 (CD90),[25–27] although these markers are not fibroblast- specific and expression does not reflect the underlying heterogeneity of this cellular population. Current evidence indicates that fibroblast populations consist of diverse cellular subsets based on their developmental origin,[28,29] anatomical location,[30,31] and tissue function.[32] Emerging single-cell profiling data of the transcriptional landscape of fibroblasts across different tissues are providing a framework for a consensus definition of fibroblast phenotypes and description of their heterogeneity. [21,33,34] This is the first crucial step in developing a universal definition of fibroblast phenotypes, but must now be extended to incorporate definitions based on cellular function that associate with the expression of specific gene programs.

Fibroblasts in synovial joints

Synovial fibroblasts are tissue-resident cells only found in the synovium of diarthrodial joints.[35] Specifically adapted to this microenvironment, these cells have an essential function in maintaining joint homeostasis and have key effector roles in inflammatory

joint disease. Their true phenotypic and functional heterogeneity has only recently been fully appreciated. The molecular mechanisms leading to the functional specialisation of synovial fibroblasts are an area of intense research and are leading to potentially new therapeutic avenues, including selectively targeting pathogenic subsets of fibroblasts in inflammatory joint disease.[19] It is hoped that targeting these cells directly in the joint microenvironment could break the therapeutic ceiling in RA and re-establish joint homeostasis.

Synovial fibroblasts in the healthy joint

Under resting conditions, the synovial microanatomy is characterised by a well-defined thin synovial lining layer containing a high density of fibroblasts and tissue-resident macrophages.[36,37] The sub-lining layer by contrast is less well defined, comprising a loose connective tissue, sparsely populated by fibroblasts within a collagenous extracellular matrix, interspersed with adipose cells and blood vessels. The healthy joint cavity is a fluid-containing sterile space that functions to lubricate the joint cavity and lacks immune cell trafficking.[12] Lining layer fibroblasts directly contribute to the composition of the synovial fluid by producing lubricin (proteoglycan 4, PRG4) and hyaluronic acid that lubricate the joint during locomotion.[12] These cells also regulate ion transport and deposit extracellular matrix made up of type III, IV, V, and VI collagen and laminin allowing nutrient exchange between the synovial fluid and the synovial membrane.[20]

The lining layer fibroblasts have traditionally been thought of as a loose association of cells that lack tight junctions but are supported by a porous basement-like

membrane.[36] A recent study in mice and humans has challenged our understanding of the cellular architecture of the synovium, demonstrating the presence of tissue-resident macrophages directly adjacent to the lining layer fibroblasts, on the outmost layer the synovial membrane[37] (**Error! Reference source not found.**). These macrophages express the protein CX_3CR1 and form an immunological barrier between the joint cavity and the synovial membrane that maintains immune privilege in the joint. This barrier is maintained by tight junctions forming a pseudo-epithelial structure that surrounds the joint. These macrophages may be similar to yolk sac–derived tissue-resident macrophages found in large cavities such as the peritoneum.[38] In the postnatal joint, these barrier macrophages are maintained through a pool of locally proliferating CX_3CR1^- $MHCII^+$ mononuclear cells that are embedded in the sub-lining tissue. An overview of synovial structure can be found in **Error! Reference source not found.**. The function of this anatomical localisation of barrier macrophages with lining layer fibroblasts has yet to be explored, but fibroblasts in this context may play a supportive role, helping to sustain an effective macrophage barrier. This reciprocal relationship is observed in large cavities, where fibroblasts act to prevent cavity lining macrophages from entering the tissue.[38] The potential for reciprocal fibroblast-macrophage relationship under steady-state and pathological conditions in the synovium requires further study.

The function of fibroblasts located in sub-lining tissue under resting conditions has yet to be fully defined; however, studies of global populations of fibroblasts isolated from the healthy joint display an immunosuppressive function similar to that observed in mesenchymal stem cells.[39,40] While significant progress has been made in

understanding fibroblast heterogeneity under pathological conditions,[34,41,42] little is known about the true heterogeneity of synovial fibroblasts under healthy conditions. In particular, it is not known whether the subsets of fibroblasts identified in the disease context also exist under resting healthy conditions or are simply a function of disease-driven differentiation or changes in cell activation state. The study of the resting joint has been compounded by a lack of access to healthy synovium, although this is being addressed through large cell atlas consortia studies, such as the human cell atlas.[43,44]

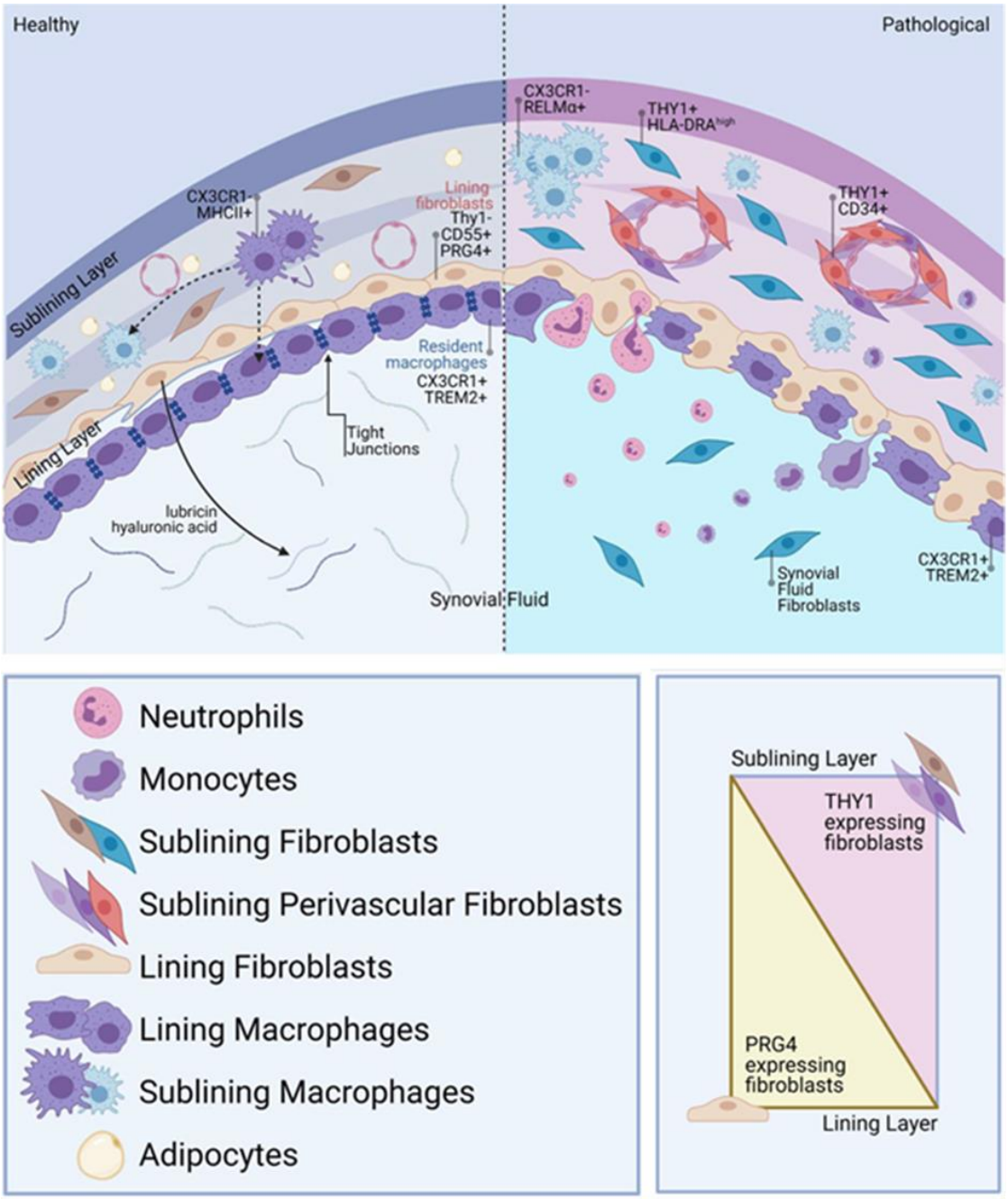

Figure 1.1 Schematic diagram of the synovium. The healthy synovium consists of a lining layer containing lubricin and hyaluronic acid secreting fibroblasts (THY1- CD55+ PRG4+) adjacent to an outer lining of tissue-resident barrier macrophages (CX3CR1+ TREM2+) that maintain immune privilege in the joint. This macrophage population is replenished from CX3CR1- MHCII+ macrophages embedded within the sub-lining layer. Under resting conditions, the sub-lining layer and the synovial membrane are not well defined. During chronic joint inflammation, the macrophage barrier is lost and there is pathological expansion and remodelling of the synovial sub-lining layer leading to extensive fibroblast heterogeneity. Some fibroblasts are detached from the synovium and found free-floating in the synovial fluid.

1.3 Fibroblasts in inflammatory joint pathology

It is now well established that synovial fibroblasts are key effectors in joint inflammation and damage.[45] They have diverse functions that impact on many disease pathways and as a result are an attractive therapeutic target.[8] However, they remain difficult to study in human disease largely due to a lack of specific cell surface markers which would allow for their identification from other cell types. The application of single-cell profiling technologies such as single-cell RNA sequencing and high dimensional imaging studies has revealed the true cellular diversity of synovial fibroblasts and defined their tissue-specific niches in the joint.[32,41,46,47] While progress has been made recently in our understanding of the phenotypic diversity of these cells, linking this phenotypic heterogeneity to cellular function and ultimately role in disease pathology is an essential part of future research.

Inflammatory remodelling of the synovium

During a chronic inflammatory insult, the synovial microenvironment is remodeled with the expansion and formation of a pathological, highly organised sub-lining tissue with diverse cellularity, including a significant expansion of tissue-resident synovial fibroblasts and the formation of an invasive hyperplastic pannus tissue. The synovial membrane expands to 10-20 cell layers thick, with remodeling involving selective expansion of distinct cellular populations both immune and non-immune and organisation of these cells into specialised compartments within the synovial tissue[47]. These changes in the synovial microenvironment also lead to changes in the phenotype of both tissue-resident synovial cells and infiltrating inflammatory

cells. These individual features of synovial remodeling all involve synovial fibroblasts which have a critical role in mediating inflammatory joint pathology, as emphasised by early studies of cadherin 11 (CDH11), an adhesion protein expressed by synovial fibroblasts during inflammation.[48] CDH11 determines adhesion between fibroblasts and is critical for the formation of synovial tissue hyperplasia, also increases fibroblast migration and invasion, and synergises in the activation of fibroblasts to produce matrix metalloproteinases (MMPs), cytokines, and chemokines.[36,49–51] The genetic deletion of *Cdh11* in mice results in the impaired formation of a hyperplastic synovium leading to attenuation of synovial inflammation in mice.[36] These studies emphasise the critical role of the synovial remodeling in driving inflammatory joint pathology and its importance as a potential site for modulating the disease process.

Cellular expansion

The mechanism of pathological cellular expansion in the synovium is multifactorial, including (a) active proliferation in response to growth factors and cytokines produced by immune cells[52]; (b) a low rate of apoptosis due to increased pro-survival factors and resistance to stress induced apoptosis (compared to other cell types); and (c) an increased accumulation of senescent cells.[53–55] The differential effects of these processes on different subsets of synovial fibroblasts and how this contributes to quantitative changes of different populations of fibroblasts during pathology are yet to be elucidated. In addition, the contribution of migrating cell populations from other tissue sources is still under active debate.

Cellular organisation

The synovial microanatomy also undergoes an organisational response to inflammation, resulting in well-defined synovial tissue niches that compartmentalise pathogenic synovial cells. Lining and sub-lining cell zones are present, but joint inflammation is associated with the loss of the CX_3CR1-expressing barrier macrophages[37] and the development of a more defined sub-lining tissue characterised by replacement of adipose tissue with dense cellular infiltrates of inflammatory cells and expansion of tissue-resident macrophages and fibroblasts.[56] Fibroblasts define this sub-lining cellular landscape, providing an address code to localise immune cells in this tissue compartment by contributing to chemokine gradients.[57] The positional identity of fibroblasts in the synovial tissue is mediated by microenvironmental instructive signals that polarise fibroblast phenotype, depending on tissue location, by regulating the expression of specific gene expression programs.[58] Using single-cell RNA sequencing followed by trajectory analysis and spatial localisation of fibroblast subsets within human RA synovial tissue, it has been shown that human synovial fibroblasts exhibit positional identity along a spatial axis that extends from the perivascular space in the sub-lining tissue to the synovial lining layer. This is mediated by endothelium-derived NOTCH3 signaling, which is a key positional determinant of perivascular fibroblast identity.[58] Other positional cues and polarising signals that facilitate fibroblast specialisation and positional identify have yet to be defined, but these could represent potentially important therapeutic avenues. In summary, the synovial architecture also has an organisational response to inflammation coordinated by synovial fibroblasts whose phenotype defines compartmentalised cellular niches within the synovial tissue that contain pathogenic

cells.[20]

Tissue pathotypes

Synovial histopathology in RA is heterogeneous and has been defined as pauci-immune (scant infiltration of immune cells and prevalence of tissue resident fibroblasts, diffuse-myeloid (predominant macrophages within the sublining tissue and lacking B/plasma cell aggregates) and lympho-myeloid (characterised by well-organised B or plasma cell aggregates and rich in macrophages).[59,60] Synovial tissue transcriptomic profiles from untreated RA patients suggest that synovial tissue pathotype signatures are associated with specific disease trajectories, treatment response, and disease outcomes.[61,62] Patients with a fibroid (pauci-immune) pathotype have an enriched fibroblast gene signature and tend to have the poorest response to treatment.[63] These findings support a role for fibroblasts as effector cells in treatment-refractory disease pathways. Understanding how fibroblast phenotype and heterogeneity contribute to treatment response will therefore be vital in our understanding of how and when to target fibroblasts in RA.

Pannus tissue represents another distinct cellular niche in the synovium, and pannus-resident fibroblasts may represent a distinct population of fibroblasts with specialised functions.[20] Galectin 3, a secreted β-galactosidase-binding protein, is present almost exclusively in the pannus of the inflamed RA synovium.[64,65] Its expression is upregulated at sites of cartilage invasion after the attachment of synovial fibroblasts to cartilage oligomeric matrix protein.[66] Galectin 3 is then able to directly activate pannus-resident fibroblasts, stimulating the secretion of pro-inflammatory cytokines,

chemokines, and MMP3, leading to the recruitment of inflammatory cells to the pathogenic tissue site.[67] At the pannus-cartilage interface, fibroblast-mediated production of MMPs, such as MMP1, MMP3, and MMP13, damages the collagen-rich structures of cartilage and enables fibroblasts to invade.[68,69]

Cellular phenotypes

The proliferative and organisational response to inflammation, observed at the tissue level in the synovium, is also associated with changes in cellular phenotypes leading to a diverse repertoire of tissue-resident cells.[70] There is also a global shift toward pro-inflammatory cell states with active suppression of pro-resolving cell states, resulting in a diverse cellular ecosystem that supports tissue inflammation and inhibits resolution.[15,16,71] Synovial fibroblasts can acquire a destructive phenotype, forming part of the invasive pannus tissue and along with macrophages, and release tissue destructive enzymes responsible for degradation of cartilage and bone. RA synovial fibroblasts attach to and invade cartilage directly, an effect that is independent of an intact adaptive immune system [68,72] The pannus microenvironment becomes hypoxic, and fibroblasts within this tissue niche upregulate tissue-degrading enzymes and apoptosis-inhibiting factors.[73–77] These destructive fibroblasts have been found to have an epigenetically imprinted phenotype that is maintained even when these cells are removed from the joint and cultured for prolonged periods of time, before being re-introduced into the cartilage implant.[68,78,79] This re-programming of fibroblast phenotype might explain why joint destruction and damage in RA do not always directly correlate with the severity of inflammation.

In summary, joint inflammation is associated with significant remodeling of the

synovial microenvironment observed at a spatiotemporal and phenotypic cellular level. These processes direct site-specific aspects of pathology and may underlie the clinical heterogeneity of RA. Synovial fibroblasts are critical cells in this process and orchestrate the synovial microanatomy into distinct anatomical compartments and drive the spatial organisation of synovial cells to develop functional cellular networks. As detailed cellular atlases emerge of the developing, healthy, and inflamed joints, we will gain further critical insights into the cellular ecosystem of the joint and its role in disease.

1.4 Synovial fibroblast phenotypic and functional diversity

Tissue fibroblasts have been considered functionally homogeneous cells, involved mainly in extracellular matrix production. However, it is now widely accepted that these cells perform a number of specialised functions.[80,81] In the joint, the lining and sub-lining of the synovial membrane are anatomically separated and contain morphologically distinct populations of fibroblasts.[49,82] Numerous human studies have demonstrated potential heterogeneity in the expression of cell surface marker proteins,[46] proteoglycans,[83] and various chemokines[32] between different compartments of the synovial membrane, consistent with the existence of different synovial fibroblasts within each of these tissue compartments. Early studies also implied a stratification of function between the lining and sub-lining layer fibroblasts, with a more pro-inflammatory function attributed to the sub-lining layer fibroblasts.[46,84] For example, a single-cell RNA-sequencing (scRNA-seq), analysis of the human RA synovial tissue initially identified two main fibroblast phenotypes: a $CD55^+$ population in the lining and a $THY1^+$ population in the sub-lining.[84] The $CD55^+$ fibroblasts were enriched for *HAS1* (encoding a hyaluronan synthase), and the $THY1^+$ fibroblasts were enriched for genes related to MMP expression and organisation of the extracellular matrix. The phenotypic diversity of synovial fibroblasts has, however, only recently been addressed comprehensively using single-cell profiling technologies from enzymatically digested synovial tissue in mice and humans.[32,58] These studies have clearly defined transcriptomically distinct populations of fibroblasts under inflammatory conditions. Initially, Mizoguchi *et al*[32] explored this diversity of human RA synovial fibroblasts by using flow cytometry to sort purify putative fibroblast subsets based on the expression of stromal markers

PDPN, CDH11, CD34, and THY1. These proteins were chosen as they were expressed at low levels under resting conditions and significantly upregulated during joint inflammation.[36,51,85–89] Following analysis by microarray and low-input, bulk-cell RNA sequencing followed by principal component analysis, three putative synovial fibroblast subsets were identified with unique transcriptomic profiles: *PDPN*$^{+}$ *CD34*$^{-}$ *THY1*$^{-}$ lining fibroblasts, *PDPN*$^{+}$ *CD34*$^{+}$ *THY1*$^{+}$ sub-lining fibroblasts, and *PDPN*$^{+}$ *CD34*$^{-}$ *THY1*$^{+}$ sub-lining fibroblasts.[32] Of these, the *THY1*$^{+}$ fibroblast subsets were expanded in the inflamed synovium in RA and correlated with the severity of joint inflammation. In contrast, in the synovia of patients with osteoarthritis (OA), a) non-inflammatory joint disease, the PDPN^{+} CD34^{-} THY1^{-} fibroblasts were expanded. Although these populations differed in their location within the joint, almost all subsets were positive for protein CDH11, which was previously shown to be associated with pathological behavior of fibroblasts in vitro and in experimental arthritis mouse models.[36]

The observation that sub-lining fibroblasts are expanded in inflamed synovia in RA has been confirmed in several studies including Zhang et al[41] The authors used mass cytometry and unbiased single-cell RNA-sequence clustering to identify four synovial fibroblast populations with distinct transcriptomic profiles in a collaborative study, as part of the Accelerating Medicines Partnership- Rheumatoid Arthritis/Systemic Lupus Erythematosus (AMP RA/SLE) Consortium. These subsets included a CD34^{+-}, THY1^{+-}, and HLA-DRA^{high}-expressing subset, found in both the sub-lining layer and a PRG4^{+} (gene encoding lubricin) lining layer population of fibroblasts. THY1^{+} HLA-DRA^{high} sub-lining fibroblasts were >15-fold expanded in RA synovium and are considered pro-inflammatory, expressing high amounts of IL-6,

CXCL12, and CCL2. In addition to the above, Zhang et al[41] identified a novel sub-lining fibroblast subset with high expression of DKK3 encoding Dickkopf[41], a protein upregulated in OA that prevents cartilage degradation in vitro.[90] DKK3 overexpression in fibroblasts suppresses cell proliferation and promotes apoptosis via TGFβ1/SMAD signaling[91] as well as impairing angiogenesis and inhibiting tumor growth through induction of endoplasmic reticulum stress.[92] Interestingly, Zhang et al[41] demonstrated that DKK3^{+} sub-lining fibroblasts also expressed high levels of OPG, CADM1, and MFAP2 which are involved in bone formation,[93] enhanced intestinal barrier function,[94] and elastic fiber structural formation.[95] Thus, DKK3^{+} fibroblasts may play a role in immuno-regulation and/ or restoring joint homeostasis. Finally, Zhang et al[41] demonstrated lining layer subsets consisting of (species-specific) CD55^{+} CD34^{-} THY1^{-} fibroblasts and express high levels of genes MMP1, MMP3, PRG4, HAS1, and CD55.[32,41,42,58] See Table 1.1 for a summary of fibroblast subsets, along with evidence of the proposed function.

Our work has defined the synovial fibroblast heterogeneity in both human and mouse arthritis.[42] We found that stromal markers were highly expressed in the inflamed synovia (tissue biopsy studies) in those patients who developed RA, compared to those in which joint inflammation resolved.[81] Of these markers, high expression levels of fibroblast activation protein-α (FAPα), a cell membrane di-peptidyl dipeptidase expressed by synovial fibroblasts,[96] were the strongest predictor of chronic joint inflammation.[81] This led us to develop the hypothesis that FAPα may be a biomarker of a pathogenic subset of synovial fibroblasts. Deletion of FAPα^{+} cells attenuated joint inflammation and bone erosion in serum transfer-induced arthritis in mice, suggesting that FAPα-expressing fibroblasts play an important

pathological role in arthritis. Flow cytometry confirmed FAPα^{+} fibroblasts were split into two discrete subsets: THY1^{+-} and THY1^{-} FAPα^{+} expressing cells. Bulk population RNA- seq of sorted purified populations confirmed that Fapα^{+} Thy1^{-} cells displayed a transcriptional signature of lining fibroblasts, whereas Fapα^{+} Thy1^{+} cells expressed a sub-lining phenotype. The most significant differences in transcriptional profiles were observed between the lining and sub-lining fibroblast populations, suggesting that anatomical location in the tissue was a major determinant of phenotype and gene expression programs.

Using single-cell transcriptomics of enzymatically digested mouse synovia, we confirmed the presence of several transcriptionally distinct populations of fibroblasts with one Thy1^{-} lining layer population (also expressing Cd55, Prg4, and Clic5) and three Thy1^{+} sub-lining layer subsets. A cross-comparison between human and mouse single-cell datasets revealed two Thy1^{+} subsets that are shared between human and mouse, including a CD34^{+} C3^{+} (this subset is localised within the perivascular zone around blood vessels and involved in immuno-inflammatory processes and stromal memory) and a COL8A1^{+}, COL1A1^{+} MDK^{+} (relating to bone, cartilage, and ECM remodeling). In addition, a single lining layer fibroblast phenotype was identified by a cassette of gene expression markers CLIC5^{+}, TSPAN15^{+}, and PRG4^{+}. Re-analysis of the Zhang et al[41], human synovial tissue dataset revealed FAPα expression within the pathogenic subset of fibroblasts (THY1^{+}HLA-DR^{high}) identified in this dataset and predominately within the sub-lining cell fibroblast populations.[42]

The transcriptional gene expression programs that define these fibroblast subsets correlate with different effector cell functions. As mentioned above, Zhang et al showed in human synovial tissue that THY1+ HLA-DR^{high} fibroblasts express the highest level of IL-6, CXCL12, CCL2, and interferon-stimulated genes, suggesting a pro-inflammatory phenotype.[41] In mouse studies, the Fapα^{+} Thy1^{+} subset is located in the sub-lining and has an immune effector profile characterised by high expression of a number of cytokines and chemokines, including IL-6, IL-33, and IL-34.[42] The Fapα^{+} Thy1^{-} subset is located in the lining and has a damage effector profile that includes high expression of inducers of osteoclast activity (CCL9 and TNFS11) and MMPs involved in cartilage degradation (MMP3, MMP9, and MMP13), indicating that the cells mediate bone and cartilage damage.[42] Consistent with these findings, subsets of synovial sub-lining fibroblasts have been found to have a secretory profile consistent with an inflammatory state in both mouse and human fibroblasts, secreting chemokines and cytokines (e.g., IL-6, CXCL12, and CCL2) in response to TNFα stimulation in vitro, that have the potential to modulate the inflammatory response in the joint.[32] The proportion of CD34^{-}THY1^{+} cells in the joint correlated positively with the proportion of leukocytes and the extent of synovitis in the human RA synovium.[32] In contrast, lining fibroblasts are the pre-dominant source of MMP1 and MMP3 and are able to stimulate osteoclastogenesis through the production of RANKL, and these findings are consistent with the lining fibroblasts having a destructive phenotype with the ability to invade and degrade articular cartilage and bone in mice.[42] We have previously shown that PDPN^{+} human synovial fibroblasts attached to, invaded, and degraded articular cartilage following implantation to immunodeficient mice.[46]

The definitive evidence that these transcriptionally distinct populations of fibroblasts have non-overlapping effector cell functions came from our adoptive transfer studies of selected fibroblasts in vivo using mouse models of arthritis.[42] We were able to demonstrate that the intra-articular injection of murine FAPα^{+} THY1^{+} immune effector sub-lining fibroblast subsets into the inflamed mouse synovium exacerbated joint inflammation, whereas the injection of FAPα^{+} THY1^{-} subsets did not affect the severity of inflammation but resulted in more joint damage. These data collectively demonstrate that the immune effector functions of synovial fibroblasts are conferred by sub-lining subsets, whereas damage is mediated predominately by the lining layer fibroblasts. The co-independence of these two cell populations remains uncertain as lining fibroblasts only had a destructive phenotype when stimulated ex vivo with pro-inflammatory cytokines, perhaps suggesting that damage also requires an intact pathological sub-lining layer in vivo. We further demonstrated an expansion of immune effector fibroblasts expressing FAPα and THY1 in the synovial tissue of individuals with RA, compared to patients with OA, consistent with previous studies demonstrating an expansion of sub-lining fibroblast subsets in RA.[32] The differential expansion of these two fibroblast populations in the synovium could explain the inflammatory pathotype of RA, in contrast to a more destructive pathotype observed in OA.

The molecular mechanism driving the expansion of sub-lining layer fibroblasts in RA has recently been elucidated. Wei et al[58] recognised that expansive fibroblast populations in the sub-lining were located around the endothelium in the perivascular

space, suggesting that vascular endothelial–derived signals could be important in modulating fibroblast phenotype. The investigators determined that the pathogenic sub-lining fibroblast phenotype and the expansion of this population are driven by endothelial-derived NOTCH3 signaling. The critical role of NOTCH3 signaling in arthritis was confirmed by the genetic deletion of the Notch3 gene and antibody blockade of NOTCH3 signaling during experimental arthritis in mice, with both approaches leading to attenuated synovial inflammation and damage. These studies demonstrate that the inhibition of NOTCH3 – mediated induction of pathogenic fibroblast differentiation could be an effective therapeutic approach in RA.

It is interesting that targeting a sub-lining layer fibroblast is also effective at inhibiting joint damage, given the observation that immune regulatory and joint destructive functions may be carried on two different effector fibroblast subsets. These findings suggest that an intact pathogenic synovial sub-lining may be required to mediate the destructive abilities of lining fibroblasts or that redundancy in function exists between fibroblast subsets in the synovium. Indeed, we only observed a destructive phenotype in lining layer fibroblasts in vitro following stimulation with TNFα.[32] The genetic deletion of Cdh11 gene which encodes the CDH11 protein that mediates cell-to-cell contact between synovial fibroblasts in mice disrupts the synovial membrane architecture, inhibiting synovial hyperplasia, and protects the joint against both damage and inflammation.[36] Collectively, these data suggest that the architectural re-organisation or function of cells in this compartment in response to inflammation can be protective.

In conclusion, recent studies have described a diverse repertoire of fibroblast

phenotypes with effector functions mapped to individual subsets. However, several challenges and uncertainties remain. Firstly, a detailed functional analysis of individual fibroblast subsets is still needed. Secondly, to understand the contribution of fibroblast heterogeneity to inflammatory joint pathology, it is important to understand the spatiotemporal changes of these fibroblast populations as disease progresses and in response to treatment. Thirdly, it is vital that we understand how changes in fibroblast phenotype and differentiation are regulated and whether pathogenic fibroblast subsets defined by single-cell analysis represent reversible changes in cell status. Collectively, this knowledge will allow us to determine the role of synovial fibroblasts in driving specific disease pathologies and determine how and when to utilise anti-fibroblast therapy in the future.

Table 1.1 Fibroblast subsets in Rheumatoid Arthritis

Subsets	Tissue location	Proposed function	Mouse homologous Subset	Disease pathology	Common markers
DKK3+	Sub-lining layer	Express genes related to the extracellular matrix. Bone formation, cell junction formation, and elastic fibre structural integrity.	Not yet defined	Not yet defined—may have a role in tissue remodelling.	DKK3, CADM1, Mfap2, OPG, Col8a2,
Thy1+ HLA-DRhi	Sub-lining layer (perivascular and interstitial)	Immunoregulatory, pro-inflammatory effect, NOTCH3-mediated differentiation.	Yes	Expanded by >15-fold in RA in synovial tissue containing high levels of leukocyte infiltration compared with synovial tissue in OA. IL-6 expression. Express genes related to MHC class II presentation and the IFNγ-mediated signalling pathway.	Col11a1, Mdk, Col8a1, Postn, MMP13, Col1a1,
CD55+ PRG4+	Lining layer	Lining layer function under resting conditions—secretes lubricin and hyaluronic acid.	Yes	Increased osteoclast activity and structural joint damage. Less abundant in RA in synovial tissue containing high levels of leukocyte infiltration than in synovial tissue in OA.	CLIC5, Tspan15, PRG4, Hbegf, Htra1, Sema3a
Thy1+ CD34+	Sub-lining layer (perivascular)	Immunoregulatory, tissue priming via C3 activation, pro-inflammatory effect, perivascular location, NOTCH3-mediated differentiation.	Yes	Expression of genes involved in complement activation, responsible for tissue priming response that underlies progression of arthritis. Express genes related to the extracellular matrix. Increased invasive and migratory properties in vitro. Increased ability to recruit peripheral blood monocytes in vitro.	Apod, C3, CD34, Mfap5, Clip, CXCL14

1.5 Synovial fibroblasts as immune effector cells

Two important functional changes occur during the progression of RA. Firstly, synovial fibroblasts lose their immunosuppressive capability and secondly become actively immune-stimulatory.[39,40,81,97] The persistent pathological phenotype of fibroblasts in established RA demonstrates that synovial fibroblasts are not merely "passive responders" to the inflammatory milieu, but can independently influence the inflammatory status of the joint.[47]

Fibroblast/endothelial cross talk determines immuno-phenotype

The interaction between leukocytes and synovial fibroblasts during an acute inflammatory response ultimately leads to resolution of the inflammatory focus. However, such interactions at sites of chronic inflammation lead to sustained leukocyte survival and retention within the joint, leading to the persistence of the inflammatory lesion.[7,98–100] For example, upon co-culture with endothelial cells (EC), fibroblasts isolated from patients with resolving synovitis and non-inflamed joints suppressed lymphocyte adhesion in response to TNFα stimulation.[39] This immune-protective effect was lost in fibroblasts isolated from patients with very early RA (≤3 months since disease onset), allowing increased lymphocyte recruitment. This stimulatory phenotype was characterised by high levels of IL-6 and TGF-β1 production. Hence, fibroblasts cultured from the synovial tissues of patients with divergent disease outcomes (resolving vs persistence) are also functionally distinct. Moreover, fibroblast – EC interactions evolve with RA progression. In contrast, fibroblasts from early RA have not yet acquired the ability to autonomously activate EC without exogenous cytokines.

IL-6 and TGF-β1 are each able to induce divergent pro-inflammatory or anti-inflammatory effects depending on the inflammatory context or cell type.[101] Emerging evidence reveals complex cross talk between IL-6 and TGF-β1 signaling pathways, in which each cytokine can positively or negatively regulate the expression or activity of the other depending on the inflammatory context.[102,103] IL-6 and TGF-β1 were identified as the bioactive agents required for the inhibitory effects on recruitment of cocultured resolving fibroblasts.[39] Furthermore, neutralisation of IL-6 and TGF-β1 inhibited the recruitment effect of cocultured very early RA fibroblasts. This suggests that in very early RA, IL-6 and TGF-β1 have not simply lost efficacy, but trigger stimulatory rather than inhibitory downstream events.

Synovial fibroblasts are a major source of IL-6 in RA.[104] Recent evidence suggests synovial fibroblasts isolated from patients with RA sustain IL-6 production (as well as heightened production of other chemotactic mediators such as IL-8) by creating a positive feedback loop involving autocrine LIF, LIF receptor, and STAT4 signaling.[104] IL-6 released during co-culture with EC signals through CD126 expressed by EC, but not fibroblasts.[39] Given that fibroblasts cannot respond to IL-6 generated during co-culture, distinct fibroblast-EC interactions must regulate EC responses to IL-6 and produce the discrete patterns of lymphocyte recruitment. High SOCS3 expression (i.e., negative regulation of *STAT* activation), as seen in the EC from co-cultures with fibroblasts isolated from patients with resolving synovitis, triggers an immuno-protective IL-6 response. Conversely, failure to induce SOCS3 was associated with loss of immunosuppressive responses in the EC from cocultures very early RA disease fibroblasts. In murine adjuvant-induced arthritis,

low endothelial SOCS3 levels, with negative regulation of IL-6 signaling, have been linked with more severe arthritis.[105] In summary, there are two distinct IL-6 signaling pathways in ECs, which are induced in a disease outcome-specific manner and elicit different functional consequences in EC.

Fibroblasts as innate immune cells

In addition to loss of immune-protective function, synovial fibroblasts also play an important role in RA pathology through cross talk with other cell types. Historical evidence has shown synovial fibroblasts can act as innate immune cells through the expression of pattern recognition receptors (PRRs) such as TLR2, TLR3, TLR4, TLR7, and TLR9. TLR4 recognises anti-citrullinated protein antibodies (ACPAs) and has been demonstrated to play an important role in RA pathology. [106,107] Recently, it has been shown that soluble CD14 can also induce the expression of inflammatory cytokines such as IL-6, TNFα, IL-8, adhesion molecules, MMPs, and RANKL through TLR4.[108] TNFα has been shown to activate TLR3 and induce the pro- duction of pro-inflammatory mediators through NFκB signaling.[109] Silencing of regulator of G-protein signaling (RGS1) inactivates TLR3 on synovial fibroblasts and suppresses inflammation and angiogenesis in collagen-induced arthritis in mice.[110] In addition, when cocultured with T cells, synovial fibroblast TLRs induce cell-cell contact and cytokine-mediated TH1 and TH17 expansion resulting in IFNγ and IL-17 production.[111] Thus, like innate cells, synovial fibroblasts are capable of recognising pathogen-associated molecular patterns and endogenous ligands which contribute to the pathogenesis of RA.

Fibroblast subsets promote T cell recruitment

It is well documented that synovial fibroblasts can present antigens to $CD4^+$ T cells during RA via MHCII.[112,113] In addition, the production of chemokines such as CXCL10 and CXCL19 by RA synovial fibroblasts is key promoters of lymphocyte recruitment.[114] A recent cross-disease analysis which included human fibroblasts isolated from the RA synovium has demonstrated *SPARC*$^+$ *COL3A1*$^+$ synovial fibroblasts interact with blood vessels via NOTCH signaling to alter the EC compartment, priming it to promote cellular infiltration which is further supported through the differentiation of $CXCL10^+$ $CXCLl9^+$ synovial fibroblasts.[34] $CXCL10^+$ $CXCL19^+$ fibroblasts interact directly with T cells and are likely analogous to Zhang et al [41] defined HLA-DRA^{high} pathogenic subset that displays a strong response to IFNγ (a pro-inflammatory molecule abundantly secreted by $CD8^+$ T cells). The expression of RA synovial fibroblast CX_3CL1 and CX_3CR1 by $CD8^+$ and $CD4^+$ T cells has also been shown to positively correlate with RA pathology. In support of this, treatment targeting CX_3CL1 production has shown efficacy in early phase clinical trials in RA.[115]

While the global effect of depleting sub-lining layer synovial fibroblast subsets has been determined to have an anti-inflammatory effect in mice,[42] the individual contribution of distinct sub-lining fibroblast subsets in regulating differential aspects of inflammation has yet to be determined. In RA, $THY1^+$ HLA-DRA^{high} fibroblasts express an interferon-stimulated phenotype suggesting that $IFN\gamma^-$ producing lymphocytes that infiltrate the tissue may stimulate an interferon-activated gene signature in this fibroblast population and drive their differentiation into a pro-

inflammatory phenotype.[41] It is likely that other critical interactions between synovial fibroblasts and other infiltrating inflammatory cells result in the modulation of the tissue fibroblast phenotype. It will be vital to define the effect of these cellular interactions on the regulation of individual fibroblast subset phenotypes in the future, since these interactions are likely to evolve as disease progresses, and in response to treatment with specific immunomodulatory therapies.

Fibroblast-macrophage coupling serves as an immune regulatory checkpoint in the synovium

Under steady-state conditions, the other major cellular component of the synovial membrane is macrophages. Macrophages derive from two main cellular lineages: bone-marrow-derived monocytes and monocyte-independent macrophages derived from cells that disperse into the tissues during embryonic development. The tissue-resident macrophages from the latter lineage have distinctive gene expression profiles that depend on the particular tissue in which they reside.[116] Under resting conditions in mice, 40% of synovial tissue macrophages are CX_3CR1^+ macrophages that constitute a barrier layer adjacent to lining layer fibroblasts.[37] These macrophages have an immunoregulatory phenotype expressing *Trem2* and genes encoding TAM receptors such as *Axl* and *Mfge8* that mediate the clearance of apoptotic cells. These barrier CX_3CR1^+ macrophages are derived from CX_3CR1^- $MHCII^+$ cells situated deep within the sub-lining layer. These $MHCII^+$ synovial macrophages also give rise to CX^3CR1^- $RELM\alpha^+$ sub-lining macrophages which are found to be expanded during experimental arthritis in mice and in synovial tissue in RA. Depletion of CX_3CR1^+ macrophages during experimental arthritis in mice leads

to synovial barrier breakdown and cellular infiltration of neutrophils and monocyte-derived cells into the synovium. Although CX_3CR1^+ lining macrophages do not expand during inflammation, they do, however, maintain an immunoregulatory phenotype and actively clear apoptotic cells.

These data suggest that CX_3CR1+ macrophages are the first immune-regulatory checkpoint that attempts to suppress or limit synovial inflammation and the failure of this checkpoint leads to established joint inflammation. The functional purpose of the anatomical coupling of lining macrophages with lining layer fibroblasts (which are functionally, spatially and anatomically distinct from sub-lining fibroblasts) is currently unknown. The loss of this spatial coupling during inflammation may lead to the emergence of a pathogenic lining layer fibroblast phenotype or a compensatory repair like phenotype.

In the sub-lining tissue, $MHCII^+$ interstitial macrophages replenish the end-stage CX_3CR1^+ macrophages, although the exact role of end-stage interstitial macrophages is currently unclear. However, as $MHCII^+$ macrophages also give rise to pro-inflammatory sub-lining RELMα-expressing macrophages, it is important to understand the mechanism in which CX_3CR1^+ and $RELM\alpha^+$ macrophage differentiation is determined. As lining and sub-lining macrophages are long-lived, it is also possible there is a pool of $MHCII^+$ macrophages which is rapidly depleted in response to an inflammatory stimulus. Further studies are required to explore the interactions between lining layer macrophages and fibroblasts and the molecular mechanisms that lead to disruption of the synovial macrophage barrier and

expansion of the invasive fibroblast population seen in RA. The second fibroblast-macrophage regulatory checkpoint is observed between fibroblasts and sub-lining macrophages. Sub-lining macrophages comprise heterogeneous populations of monocyte-derived and tissue-resident macrophages. A recent comprehensive analysis of their heterogeneity has releveled the transcriptional and functional diversity of synovial tissue macrophages.[70] The investigators isolated macrophages from patients with early/active RA, treatment-refractory/active RA, and RA in sustained clinical remission. The analysis revealed four distinct subsets that comprised nine discrete phenotypic states. Two of these subpopulations ($MERTK^+$ $TREM2^{high}$ macrophages and $MERTK^+$ $LYVE1^+$ macrophages) were enriched in the healthy synovium and in patients with RA whose disease was in remission compared with those with active disease. A reduction in these cellular subsets in the tissue was associated with an increased risk of future disease flare. In vitro evidence showed $MERTK^+$ macrophages produced high amounts of pro-resolving lipids and when cocultured with synovial fibroblasts induced a repair response in fibroblasts. In contrast MERTK macrophages are expanded during active disease compared to remission. This population comprises subsets of macrophages expressing alarmins ($CD48^+$ $S100A12^+$), bone remodeling molecules ($CD48^+$ $SPP1^+$), an interferon signature (HLA^+ $ISG15^+$ cluster), and an antigen-presenting cell signature (HLA^+ $CLEC10A^+$). $MERTK^-$ macrophages produce TNFα and IL-6 and induce pathological activation of fibroblasts.

As a result, $MERTK^+$ macrophages may act as an off switch by negatively regulating pro-inflammatory fibroblast phenotypes. We hypothesise the failure of this

checkpoint could lead to the emergence of persistently activated, pathogenic fibroblast subsets. In addition, another study has revealed the existence of macrophages in the RA synovium that are positive for the growth factor HBEGF.[117] These macrophages promoted fibroblast invasiveness in an epidermal growth factor receptor–dependent manner. Thus, indicating that intercellular networks between these pathogenic populations of synovial tissue cells can contribute to inflammatory joint pathology.

In summary, these studies demonstrate that fibroblast phenotypes can be regulated by synovial tissue macrophages. The coupling of these tissue-resident cell types appears to be critical in determining if joint inflammation either persists or resolves. If these checkpoints fail to limit or restrict inflammation, then disease persists. Certain macrophage subsets may therefore act as critical “off” switches, resulting in the suppression of pro-inflammatory fibro- blast phenotypes. It is not yet known, however, how inflammation-induced epigenetic changes and metabolic re-programming of fibroblasts observed in chronic disease might impact on their ability to respond to these regulatory changes in their phenotype induced by macrophages. In addition, quantitative changes in these two cell populations may underpin disease progression and treatment response. Understanding the nature of the functional networks established by these tissue-resident synovial cells at various stages of disease and in response to treatment will be critical in developing novel therapeutic approaches that aim to restore joint homeostasis.

1.6 Synovial fibroblasts – passive responders or transformed aggressors

Current evidence suggests that the phenotype (based on positional identity) of synovial fibroblasts is acquired from microenvironmental instructive signals from within the synovial tissue, rather than a pre-determined phenotype. One instructive signal of fibroblast phenotype and positional identity in the tissue has been identified as endothelial-derived NOTCH3 signaling which drives a sub-lining pathogenic fibroblast phenotype, responsible for driving arthritis pathology in the joint.[58] The removal of these fibroblasts from the joint resulted in the rapid loss of their tissue phenotype and the acquisition of a transitional fibroblast phenotype. These findings are consistent with observations that culture of synovial fibroblasts can lead to alterations in their phenotype over time.[118,119] These observations suggest a high degree of cellular plasticity in fibroblast phenotype that is dependent on external signals that regulate specific programs of gene expression within these tissue-resident cells. However, a large body of evidence supports the concept that disease-associated fibroblast phenotypes evolve with the chronicity of disease, resulting in a stably activated and aggressive phenotype in established disease.[47] The strongest evidence that an autonomous destructive fibroblast phenotype is established in chronic disease is the finding that invasive behavior is retained by human RA synovial fibroblasts in ex vivo invasion assays and in human RA fibroblast-cartilage co-implantation assays in mice.[19,47,120] Thus, the invasive phenotype of fibroblasts in RA is dependent on both autonomous and local microenvironmental signals and is highly likely to be epigenetically imprinted in chronic disease.[19,47] Epigenetic mechanisms can induce stable changes in gene expression without altering the genome, and have been extensively reviewed elsewhere.[121–123] These mechanisms

are essential during embryonic development and define tissue- and cell-specific gene expression.[124] In postnatal tissues, these mechanisms operate to allow cells to adopt to microenvironmental changes.[124]

However, changes in the epigenome can lead to stably, imprinted, and pathologically driven changes in gene expression.[122] These pathogenic programs of gene expression could lead to the emergence of disease-associated effector cell phenotypes that ultimately fail to respond to negative regulation by immunosuppressive signals, resulting in the persistence of joint inflammation.[47]

1.7 Concluding remarks

Synovial fibroblasts are specially adapted for their role in joint homeostasis, and this functional specialisation is retained within distinct anatomical compartments of the synovial membrane. These specialised synovial tissue niches undergo cellular remodeling in response to inflammation and contain specific subsets of fibroblasts.[20] The spatial and temporal heterogeneity of synovial fibroblasts underpins their pathogenic role in inflammatory joint disease.[42] Fibroblast heterogeneity is driven by anatomical location in the tissue,[46] microenvironmental instructive signals,[58] and interaction with tissue-resident leukocytes.[70] These regulatory signals and cellular interactions result in both subset differentiation and changes in cell activation status. This phenotypic heterogeneity gives rise to functional cellular diversity reflected in the existence of synovial fibroblast subsets with different effector cell functions.[32] The link between phenotypic heterogeneity and cellular function needs to be further explored to provide a clear link between transcriptional diversity and functional role in health and disease. Comprehensive analysis of synovial fibroblast subsets at distinct stages of disease in response to therapeutic intervention will be vital in exploring the role of specific fibroblast subsets in determining the response to treatment and disease progression and in dictating the most effective timing for the use of fibroblast targeted therapies. Yet the impact of chronic disease on fibroblast heterogeneity is unknown. The identification of key positional cues within the synovial tissue that regulate fibroblast identity/phenotype suggests a large degree of residual plasticity in phenotype. However, this plasticity may be modulated in chronic disease, as suggested by numerous previous studies that demonstrate the development of an epigenetically imprinted fibroblast phenotypes with chronicity of

joint inflammation.[47] This raises the possibility that the success of fibroblast targeted therapies is dependent on the stage of disease. For example, early changes in fibroblast phenotype may underpin a treatment-refractory disease trajectory and therefore targeting these cells in early disease may be more effective at altering the course of arthritis. Future research strategies should focus on linking single-cell transcriptomic analysis of cellular heterogeneity obtained from different pathogenic tissues to fibroblast function and build a consensus on the definition of fibroblast identity and heterogeneity, based on function rather than gene expression profiles. As we now define the cellular landscape of the joint, at various stages of disease and in different sub-groups of patients, it is vital to link these findings to function and this requires comprehensive in vitro and in vivo functional studies linked to the cell atlas of the tissue.

Furthermore, the exploration of shared and distinct fibroblast phenotypes across different tissues and inflammatory diseases will be vital for developing cross-indication therapeutic targeting of specific pathogenic fibroblasts in the future, perhaps as an adjuvant to existing biologic therapies such as anti-TNFα treatment, an approach that will hopefully break the ceiling of therapeutic response in RA.

1.8 Thesis aims and objectives

In this thesis, I have tested the hypothesis that firstly, synovial tissue fibroblasts exist as phenotypically and functionally distinct subsets that map to specific stages of joint inflammation. Secondly, that stage specific fibroblast phenotypes impact on the outcome of joint inflammation and thirdly, that fibroblast phenotypes are regulated by tissue, immune and stromal cell cues.

To test this hypothesis, I addressed the following aims:

1. Define the fibroblast subsets present in the synovium throughout the course of inflammatory arthritis from initiation to resolution of joint inflammation.
2. Determine the mechanisms underpinning the specialisation of fibroblasts during specific stages of inflammatory arthritis.
3. Investigate the specific role of synovial fibroblasts in the resolution of joint inflammation.

2 MATERIALS & METHODS

2.1 Materials

Table 2.1 Induction of inflammatory arthritis

Reagent	Supplier	Catalogue #
Dulbecco′s Phosphate Buffered Saline	Sigma Aldrich	D8537
Freund′s Adjuvant, Incomplete	Sigma Aldrich	F5506
Mycobacterium tuberculosis	ThermoFisher	10218823
Albumin methylated from bovine serum (mBSA)	Sigma Aldrich	A1009
Collagen II	Obtained from Richard Williams, Kennedy Centre, Oxford, UK	-
K/BxN Serum	Gifted by Harris Pearlman	-

Table 2.2 Experimental agents administered during inflammatory arthritis

Reagent	Supplier	Catalogue #
Recombinant Human/Mouse Wnt-5a Protein	Bio-Techne	645-WN-010
Recombinant Mouse DKK-3 Protein	SinoBiological	50247-M08H
LGK974	Cambridge Biosciences	L2540
Corn oil	Sigma Aldrich	C8267
Dimethyl sulfoxide (DMSO)	Sigma Aldrich	D4540

Table 2.3 Isolation of synovial joint cells (Collagenase D/Dispase method)

Reagent	Supplier	Cat #
RPMI-1640 Medium With sodium bicarbonate, without L-glutamine, liquid, sterile-filtered, suitable for cell culture	Sigma Aldrich	R0883
Foetal bovine serum (FBS)	Biosera	FB-1001
Collagenase D	Roche	11088866001
Collagenase Dispase	Roche	11097113001
Deoxyribonuclease I	Sigma Aldrich	DN25-10MG

Table 2.4 Isolation of synovial joint cells (Collagenase P method)

Reagent	Supplier	Cat #
RPMI-1640 Medium With sodium bicarbonate, without L-glutamine, liquid, sterile-filtered, suitable for cell culture	Sigma Aldrich	R0883
Foetal bovine serum (FBS)	Biosera	FB-1001
Collagenase P	Roche	11213857001
Collagenase Dispase	Roche	11097113001
Deoxyribonuclease I	Sigma Aldrich	DN25-10MG

Table 2.5 Isolation of bone marrow derived macrophages

Reagent	Supplier	Catalogue #
RPMI-1640 Medium With L-glutamine and sodium bicarbonate, liquid, sterile-filtered, suitable for cell culture	Sigma Aldrich	R8758
Foetal bovine serum (FBS)	Biosera	FB-1001

Table 2.6 Isolation of splenocytes and purification of T Cells

Reagent	Supplier	Catalogue #
RPMI-1640 Medium With L-glutamine and sodium bicarbonate, liquid, sterile-filtered, suitable for cell culture	Sigma Aldrich	R8758
Dynabeads Mouse T-Activator CD3/CD28	Gibco	11453D
Round-Bottom Polystyrene Test Tubes (14mL)	Falcon	352051
EasySep Mouse T Cell Isolation Kit	Stem Cell Technologies	19851
EasySep Magnet	Stem Cell Technologies	18001

Table 2.7 Mouse Fibroblast culture media

Reagent	Supplier	Catalogue #	Final Concentration
RPMI-1640 Medium With sodium bicarbonate, without L-glutamine, liquid, sterile-filtered, suitable for cell culture	Sigma Aldrich	R0883	-
Penicillin-Streptomycin (10,000 U/mL)	Gibco	15140122	1%
Foetal bovine serum (FBS) Heat inactivated	Biosera	FB-1001	10%
L-Glutamine (200 mM)	Gibco	25030081	1%

Table 2.8 Mouse BMDM culture media

Reagent	Supplier	Catalogue #	Final Concentration
RPMI-1640 Medium With L-glutamine and sodium bicarbonate, liquid, sterile-filtered, suitable for cell culture	Sigma Aldrich	R8758	-
Penicillin-Streptomycin (10,000 U/mL)	Gibco	15140122	1%
Foetal bovine serum (FBS) Heat inactivated	Biosera	FB-1001	10%
Recombinant human M-CSF	Peprotech	300-25	50ng/mL

Table 2.9 Mouse T Cell culture media

Reagent	Supplier	Catalogue #	Final Concentration
RPMI-1640 Medium With L-glutamine and sodium bicarbonate, liquid, sterile-filtered, suitable for cell culture	Sigma Aldrich	R8758	-
Penicillin-Streptomycin (10,000 U/mL)	Gibco	15140122	1%
Foetal bovine serum (FBS) Heat inactivated	Biosera	FB-1001	10%
L-Glutamine (200 mM)	Gibco	25030081	4mM
Sodium Pyruvate (100 mM)	Gibco	11360070	1mM
2-Mercaptoethanol (50 mM)	Gibco	31350010	50µM

Table 2.10 General cell culture

Reagent	Supplier	Catalogue #
Trypsin-EDTA solution (10x)	Sigma Aldrich	T4174
Phosphate buffered saline (PBS) tablets	Gibco	18912014
Ethylenediaminetetraacetic acid disodium salt solution (0.5M)	Sigma Aldrich	E7889
Cell culture flasks (T25, T75, T175)	Corning	CLS430372, CLS430641, CLS431079
Costar TC-Treated Multiple Well Plates (6-well, 12-well)	Corning	CLS3516, CLS3512
100 mm Culture Dish	Corning	CLS430591
Cell Strainer	Corning	CLS431751

Table 2.11 Cytokines, stimulants, inhibitors & recombinant proteins

Reagent	Supplier	Catalogue #
LPS	Enzo Life Sciences	ALX-581-010-L002
Dexamethasone	Sigma Aldrich	D8893-1MG
Recombinant Mouse TGF-beta 1	R&D Systems	7666-MB-005/CF
TGF beta-1,2,3 Monoclonal Antibody	Invitrogen	MA5-23795
Recombinant Mouse DLL4	BioLegend	776702
DAPT	Sigma Aldrich	D5942
Recombinant Mouse DKK-3 Protein	SinoBiological	50247-M08H
Recombinant Murine IL-1β	Peprotech	211-11B
Recombinant mouse Interferon alpha 1 protein	Abcam	ab259386
Recombinant Murine IFN-γ	Peprotech	315-05
Recombinant Murine TNF-α	Peprotech	315-01A

Table 2.12 Antibodies for flow cytometry

Target	*Fluorochrome*	*Clone*	*Supplier*	*Cat #*
APOE	AF700	WUE-4	Novus Bio	NB110-60531AF700
B220	FITC	RA3-6B2	Biolegend	103206
Biotinylated α-rabbit	-	Polyclonal	Invitrogen	A16122
Biotinylated α-sheep	-	GT-34	Sigma Aldrich	B3148
CCL2	FITC	2H5	Invitrogen	11-7096-81
CD11b	FITC	M1/70	Biolegend	101206
CD11c	BV650	N418	BioLegend	117339
CD201	APC-eFluor660	1560	eBioscience	47-2012-82
CD25	BV650	PC61	BioLegend	102037
CD31	SuperBright-645	390	eBioscience	64-0311-82
CD34	BV421	MEC14.7	BioLegend	119321
CD3e	APC-e780	145-2C11	Biolegend	100329
CD4	BV421	RM4-5	Biolegend	100543
CD44	PERCP-CY5.5	IM7	Biolegend	103031
CD45	PE-CY7	30-F11	Biolegend	103113
CD45	APC-CY7	30-F11	Biolegend	103116

CD62L	PE-CY5	MEL-14	Biolegend	104410
CD55	APC	RIKO-3	Biolegend	131811
CD64	PE-CY7	X54-5/7.1	Biolegend	139314
CD8a	PE/Dazzle 594	53-6.7	Biolegend	100761
CD90.2	APC-CY7	30-H12	Biolegend	105327
CX_3CR1	PerCP-Cy5.5	SA011F11	Biolegend	149010
DKK3	-	Polyclonal	Proteintech	10365-1-AP
F4/80	BV421	BM8	Biolegend	123131
FAPα	-	Polyclonal	BioTechne	AF3715
Fixable Viability	BV510	-	Biolegend	423101
FOXP3	PE	FJK-16s	Invitrogen	12-5773-82
LY6C	PE-CY7	HK1.4	BioLegend	128017
LY6G	AF700	1A8	BioLegend	127622
LYVE1	PE	ALY7	Invitrogen	12-0443-82
MerTK	APC	2B10C42	BioLegend	151508
MHC II	BV650	M5/114.15.2	BioLegend	107641
PDPN	PE	8.1.1	Biolegend	127407
SIGLEC-F	PE-e610	1RNM44N	Invitrogen	46-1702-2
SPP1	PE	Polyclonal	R&D Systems	IC808P

Streptavidin	APC	-	Biolegend	405207
TOP2A	APC	1361	Novus Bio	NBP2-54546APC
TruStain FcX (anti-mouse CD16/32)	-	S17011E	Biolegend	156603

Table 2.13 Preparation of samples for single-cell RNA sequencing

Reagent	Supplier	Cat #
Chromium Single Cell 3' Library Kit v2	10X Genomics	120234
Chromium Single Cell 3' Gel Bead Kit v2	10X Genomics	120235
Dynabeads™ MyOne™ SILANE	10X Genomics	2000048

Table 2.14 R packages used for bioinformatics analysis

Package name	Developer page	Version
Seurat	https://github.com/satijalab/seurat	5.1.0
Harmony	https://github.com/immunogenomics/harmony	1.2.0
Clustree	https://github.com/lazappi/clustree	0.5.1
Nebulosa	https://github.com/powellgenomicslab/Nebulosa	1.13.0
Monocle	https://github.com/cole-trapnell-lab/monocle3	2.30.0
CellChat	https://github.com/sqjin/CellChat	1.6.1
Ggplot2	https://github.com/tidyverse/ggplot2	3.5.0
Cowplot	https://github.com/wilkelab/cowplot	1.1.3
Gsfisher	https://github.com/sansomlab/gsfisher	0.2
EnhancedVolcano	https://github.com/kevinblighe/EnhancedVolcano	1.20.0
RColorBrewer	https://github.com/cran/RColorBrewer	1.1.3
Liana	https://github.com/saezlab/liana	0.1.12
SCpubr	https://github.com/enblacar/SCpubr	3.0
DoubletFinder	https://github.com/chris-mcginnis-ucsf/DoubletFinder	2.0

Table 2.15 RNA isolation, cDNA conversion & RT PCR reagents

Item	Supplier	Cat #
RNeasy Mini Kit	Qiagen	74104
iScript cDNA Synthesis Kit	BioRad	1708891
TaqMan™ Universal Master Mix II, with UNG	ThermoFisher	4440038

Table 2.16 TaqMan Gene Expression Assays

Gene	Assasy ID	Supplier
Cthrc1	Mm01163611_m1	ThermoFisher
Postn	Mm01284919_m1	
Col1a1	Mm00801666_g1	
Mmp14	Mm00485054_m1	
Lrrc15	Mm01169717_m1	
Dkk3	Mm00443800_m1	
Pi16	Mm00470084_m1	
Thy1	Mm00493681_m1	
Hprt	Mm00446968_m1	

Table 2.17 H&E of FFPE tissue

Item	*Supplier*	*Cat #*
Haematoxylin (Harris) (Mercury Free) (Acidified)	Pioneer Research Chemicals	PRC/R/51
Eosin (1% Aqueous)	Pioneer Research Chemicals	PRC/66/1
1% Acid Alcohol	Pioneer Research Chemicals	PRC/R/75
Ammonium hydroxide solution	Sigma-Aldrich/Merck	09859-250ML
DPX	Sigma-Aldrich/Merck	06522-500ML
Leica Slides X-tra Adhesive	Leica	3800200AE

2.2 Methods

2.2.1 Animal Experiments

All animal experiments were approved by the UK Home Office and conducted in accordance with the UK's Animals (Scientific Procedures) Act 1986 and the UK Home Office Code of Practice. The project and experimental protocols were approved by the University of Birmingham Animal Ethics Review Committee who provided ethical oversight of the study. C57BL/6 mice were purchased from Charles River. All mice were housed at a barrier and specific pathogen-free facility at the Biomedical Services Unit, University of Birmingham. All mice used in experimental studies were aged 6-10 weeks and unless otherwise stated, male.

DKK3-/- mice

Embryos from DKK3$^{-/-}$ C57BL/6 mice were obtained from Professor Christof Niehrs and re-derived at the Biomedical Services Unit. Following genotyping breeding colonies were established. Pups were genotyped at ~2 weeks old and homozygous mice were used for subsequent experiments at 6-10 weeks old.

K/BxN serum transfer induced arthritis

K/BxN Serum Transfer Induced Arthritis (STIA) was induced by intravenous injection of 100µl of serum from KRN mice (K/BxN). Inflammation of ankle and wrist joints was assessed daily, by measuring thickness, using callipers. Persistent inflammatory arthritis was induced by 100 µl intravenous injection of serum at day 0, then 50µl of the same serum once a week.

Collagen induced arthritis

Male DBA/1 mice were immunised with 100 µg of rat CII emulsified 1:1 in Freund's incomplete adjuvant (IFA) containing Mycobacterium tuberculosis H37Ra (Difco; 3.33 mg/ml). Mice were boosted 3 weeks later with 100 µg CII in IFA.

Antigen induced arthritis

Antigen Induced Mono-Arthritis (AIA) was initiated by injection of CFA (as above) containing 1mg/mL methylated-bovine serum albumin (m-BSA), subcutaneously into either side of the base of the tail (50µL per injection site). 14-21 days following subcutaneous injections (Day 0), 100µg m-BSA (in PBS) is injected locally into the knee joint via intra-articular (IA) injection, to induce inflammation.

Injection of recombinant DKK3 protein

6-8-week-old C57BL/6 mice were induced with AIA as previously described. 48 hours following induction of inflammation, the knee was injected (IA) with 10µL recombinant DKK3 protein, or a PBS control. Severity of arthritis was determined by measurement of the knee joint, and a global arthritis score.

Injection of recombinant Wnt5a in murine inflammatory arthritis

6-8-week-old C57BL/6 mice were induced with AIA as previously described. 48- and 96-hours following induction of inflammation, the knee was injected (IA) with 10µL recombinant Wnt5a protein, or a PBS control. Severity of arthritis was determined by measurement of the knee joint, and a global arthritis score.

Injection of LKG974 in murine inflammatory arthritis

6-8-week-old C57BL/6 mice were induced with AIA as previously described. LGK974 or a control substance (corn oil + 10% DMSO) was administered via intraperitoneal

injection daily for 7 days. Severity of arthritis was determined by measurement of the knee joint, and a global arthritis score.

2.2.2 Isolation of primary cells from mouse tissue

Collagenase D/Dispase method

Bones with intact joints were dissected and transferred into RPMI-1640 (+2% FCS) containing 0.1 g/mL collagenase D (Roche), 0.01 g/mL of DNase I (Sigma-Aldrich). Samples were incubated at 37 °C for 45 min, followed by incubation with medium containing 0.1 g/mL collagenase dispase (Roche) and 0.01 g/mL DNase I at 37 °C for 30 min. The cell suspension was filtered through 50µm cell strainer, and red blood cell lysis was performed. The resulting cells were pelleted by centrifugation at 400g for 5 minutes.

Collagenase P method

Bones with intact joints were dissected and transferred into RPMI-1640 (+2% FCS) containing 0.8 g/mL collagenase Dispase, 0.2 mg/mL collagenase P and 0.1 mg/mL of DNase I. Samples were incubated at 37 °C for 30 minutes, followed a second incubation with fresh digest medium for 20 minutes. The cell suspension was filtered through 50µm cell strainer, and red blood cell lysis was performed. The resulting cells were pelleted by centrifugation at 400g for 5 minutes.

Isolation of fibroblasts

Synovial stromal cells were extracted using the Collagenase D/Dispase method as described above. Pelleted cells from a single joint were resuspended in 12mL fibroblast media (Table 2.7) and transferred to a T75 flask (37°C, 5% CO2). 1/3 of the culture media was replaced after 48 hours, then weekly. Cells were passaged using

trypsin (2X) at 70-80% confluency. Contaminating cells are removed with each passage and the resulting culture is >99% fibroblasts following P3. Fibroblasts were used between passages 3-7.

Isolation of bone marrow derived macrophages

Mouse bone marrow-derived macrophages (BMDMs) were isolated from hind legs of C57BL/6 wild type mice. Bones were cleaned of muscle tissue, cut at both ends and centrifuged (4000rpm, 3min) inside a pierced eppendorf within a second tube. Bone marrow from each mouse was resuspended in 50ml macrophage medium (Table 2.8) with 50ng/ml M-CSF and seeded into five 10cm dishes. On day 5, old media was exchanged for fresh media. Macrophages were harvested at day 7 by washing with PBS, then incubating with cell dissociation buffer (5mM EDTA in PBS) for 15 minutes at 37°C. Lifted with a cell lifter, pelleted, counted and seeded for experiments in media not containing M-CSF. Isolated macrophages were not passaged or cultured for extended time periods.

Isolation of splenocytes and purification of T Cells

Mouse splenocytes were isolated by mashing the spleen through a 70µM cell strainer and washing with RPMI, then pelleted at 250g for 5 minutes at 4°C. T Cells were isolated using the EasySep mouse T Cell isolation kit, according to supplier instructions. T cells were resuspended at 2x106 cells per well in a 12 well plate in T Cell media (RPMI 1640, 10% FBS, 1% P/S, 4mM L-Glutamine, 1mM pyruvate, 50µM BME) containing CD3/CD28 mouse activator DynaBeads (4x106) and recombinant mouse IL-2 (100U/mL). 0.5mL T Cell media (Table 2.9) containing 100U/mL IL-2 was added to each well 24 hours following isolation. Purified T Cells were collected 48 hours following isolation by de-beading the cell suspension, according to supplier

instructions. T Cells were cultured in T Cell media containing 100U/mL IL-2 for further experiments, but not passaged or cultured for extended time periods.

Primary cells were seeded at the appropriate density (Table 2.18) and allowed to rest for 24 hours prior to stimulation. Treatments were added as detailed in table 2.11. and used alongside suitable vehicle controls. For BMDMs, stimulation medium did not include M-CSF. Following treatment, cells were harvested for analysis via flow cytometry or RT-PCR.

Table 2.18 Seeding of primary mouse cells

Cell Type	*Seeding Density*	*Culture plate*
Fibroblasts	$0.25x10^6$ cells/well	6 well
BMDMs	$1x10^6$ cells/well	6 well
T Cells	$2x10^6$ cells/well	12 well

2.2.3 Fibroblast/Macrophage co-culture assays

0.5×10^6 fibroblasts and 0.5×10^6 macrophages per well were seeded onto 6 well plates in fibroblast culture medium. Cells were allowed to rest for 24 hours prior if any experimental treatments were added. Co-cultures were incubated for 24-48 hours. Cells were collected using cell dissociation buffer as previously described and analysed with flow cytometry.

2.2.4 Single Cell RNA Sequencing

Preparation of samples

Isolated synovial cells were stained at 4°C and dead cells excluded using 7-Aminoactinomycin D (7-AAD) staining (Invitrogen). Antibodies used were anti-CD45 (30-F11). Cell sorting was performed immediately after staining using a MoFlo Astrios EQ machine (Beckman Coulter). Cells were captured with the 10X Genomics Chromium system, and sequencing libraries were generated using the 10X Genomics Single Cell 3′ Solution (version 2) kit then sequenced with Illumina sequencing (HiSeq 4000, read 2 sequenced to 75 bp). Alignment, quantitation and aggregation of sample count matrices was performed using the 10X Genomics Cell Ranger pipeline (v.2.1.0) and mouse reference sequences (v.2.1.0). Downstream analysis was performed using the Seurat R package (v.4.1.1).

Quality Control and Filtering

Doublets were removed from each sample using DoubletFinder. To ensure high-quality data, quality control (QC) metrics were applied to each sample. Specifically, I assessed the percentage of mitochondrial features and the total UMI counts and number of features for each sample individually to establish QC metrics that were applied to exclude low quality cells. Per-cell counts were normalised and scaled.

Sample integration using Seurat integration and/or the ‘Harmony package’ was optimised for each dataset. Downstream spatial mapping and clustering analysis was generated from the integrated data slot, whilst any RNA expression analysis was taken from the RNA metadata. PCA, UMAP and tSNE projections were generated, and cells were clustered using the Louvain algorithm. Table 2.14. provides packages used for data analysis.

Data availability

Raw counts for the human fibroblast atlas were kindly sent from Prof. Korsunsky and are publicly available at: https://sandbox.zenodo.org/record/772596#.YGsi6BRKg-Q. Processed scRNAseq data from Alivernini et al., 2024[70] were kindly provided by Prof. Kurowska Stolarska and are publicly available at: E-MTAB-8322, E-MTAB-8873 and EMTAB-8316. ScRNA-seq data from Zhang et al., 2019[41] was obtained from Immport (SDY998).

Code availability

All code used for analysis of scRNA-seq datasets can be found at: https://github.com/LMarshx/Thesis_Script.

2.2.5 Single Cell ATAC sequencing

Preparation of samples

Synovial cells were isolated stained, and sorted as previously described. Live CD45-CD31- cells were sorted and kept at 4 °C. Nuclei isolation was optimised to determine the optimal incubation period in cell dissociation buffer (**Error! Reference source not found.**). Nuclei were isolated from cells according to 10X Genomics standard operating procedure and resuspended in 1X nuclei buffer. Samples were

then passed onto The University of Birmingham Genomics Department who performed library preparation and sequencing.

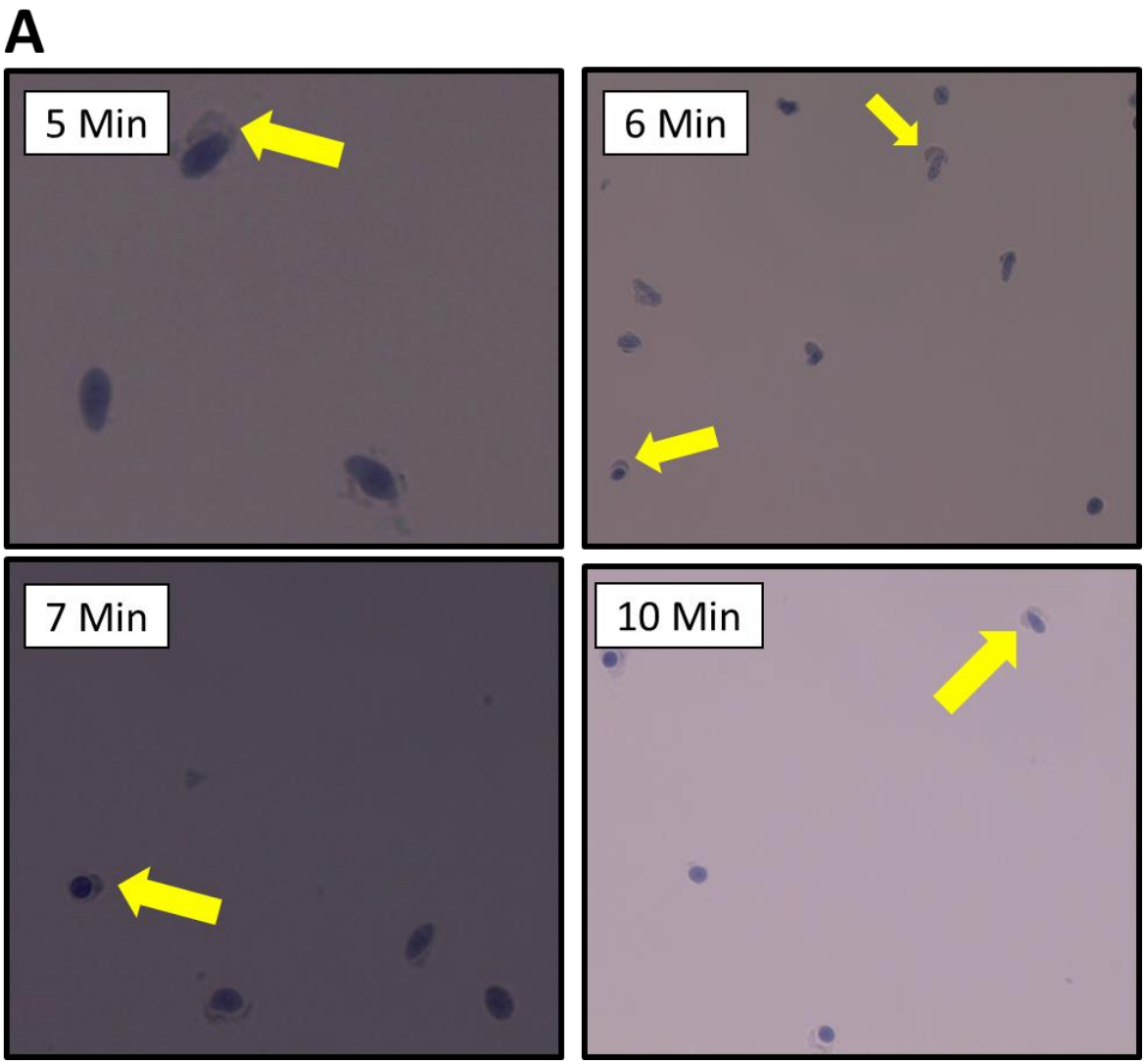

Figure 2.1 Optimisation of nuclei isolation of mouse synovial fibroblasts. Following isolation of cells, nuclei were isolated according to supplier instructions. The length of time in nuclei isolation buffer was optimised to remove the cytoplasm without inducing damage to the nucleus. Nuclei were imaged with trypan blue staining (A). Yellow arrows indicate regions where cytoplasm is still intact.

2.2.6 Flow Cytometry

General Staining Procedure

Cells were harvested using the appropriate digest protocol, as described above, and pelleted (400g, 5 minutes, 4°C). All staining was conducted in the dark, on ice, unless stated otherwise. Once staining was completed, the volume of each sample was measured before addition of counting beads. Samples were run on a BD LSRFortessa X-20 and analysed using FlowJo v10.

Procedure for staining cell surface markers

Cells were washed twice with PBS before incubating with fixable viability dye (20 minutes). Antibody cocktails were prepared using FACS buffer (PBS + 0.1% BSA). Cells were washed twice with FACS buffer and stained with antibody mix (30 minutes). Cells were washed twice with FACS buffer and prepared for running.

Procedure for staining intracellular markers

Following staining of cell surface markers, cells were fixed/permeabilised using BD cytofix/perm kit (20 minutes). Cells were washed twice with 1X BD cytofix/perm buffer, and incubated with the intracellular antibody cocktail (prepared with cytofix buffer, 30 minutes). Cells were washed twice with FACS buffer and prepared for running.

Procedure for staining nuclear markers

Following staining of cell surface markers, cells were fixed/permeabilised using Foxp3 / Transcription Factor Staining Buffer Set (20 minutes). Cells were washed twice with 1X permeabilisation buffer, and incubated with mouse FC block (15 minutes), then α-FOXP3 was added (30 minutes, prepared with permeabilisation

buffer, 30 minutes). Cells were washed twice with FACS buffer and prepared for running.

Fibroblast staining

Synovial cells were isolated using the Collagenase D/Dispase protocol. Novel markers of fibroblast subsets were identified from previous single cell RNA sequencing data[42]. They were then evaluated and optimised for use in flow cytometry and excluded where necessary (Supplementary Figure 1). Two final panels were developed for analysis of fibroblasts (Table 2.19, Table 2.20), gating strategies in Figure 2.2. For DKK3/FAPα staining amplification was required. Following staining of cell surface markers, cells were incubated with mouse FC block (15 minutes), then either α-DKK3 or α-FAPα (30 minutes). Cells were washed twice with FACS buffer. Cells were incubated with mouse FC block (15 minutes), then biotinylated anti-rabbit (30 minutes). Cells were washed twice then incubated with streptavidin APC (30 minutes), then washed twice and prepared for running.

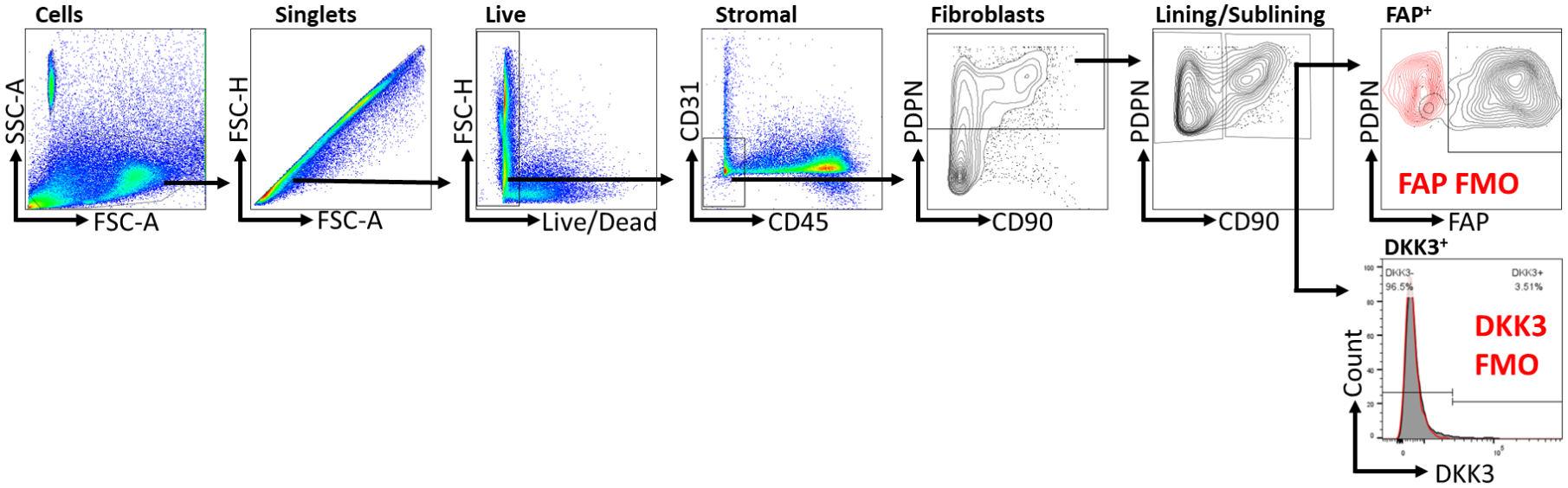

Figure 2.2 Gating strategy for staining murine synovial fibroblasts.

Table 2.19 Staining for DKK3+ Fibroblasts

Target	*Fluorochrome*	*Clone*	*Dilution*
CD45	PE-CY7	30-F11	1/500
CD31	SuperBright-645	390	1/500
PDPN	PE	8.1.1	1/150
CD90.2	APC-CY7	30-H12	1/100
DKK3	-	Polyclonal	1/50
Biotinylated α-rabbit	-	Polyclonal	1/1000
Streptavidin	APC	-	1/400
TruStain FcX (anti-mouse CD16/32)	-	-	1/100
Fixable Viability	BV510	-	1/500

Table 2.20 Staining for FAP+ Fibroblasts

Target	*Fluorochrome*	*Clone*	*Dilution*
CD45	PE-CY7	30-F11	1/500
CD31	SuperBright-645	390	1/500
PDPN	PE	8.1.1	1/150
CD90.2	APC-CY7	30-H12	1/100
FAPα	-	Polyclonal	1/50
Biotinylated α-sheep	-	Polyclonal	1/1000
Streptavidin	APC	-	1/400
TruStain FcX (anti-mouse CD16/32)	-	-	1/100
Fixable Viability	BV510	-	1/500

Macrophage staining

Synovial cells were isolated using the Collagenase D/Dispase protocol. Novel markers of macrophage subsets were identified from literature review. They were then evaluated and optimised for use in flow cytometry and excluded where necessary. RELMα was cleaved by the enzymatic digest process, thus excluded from the panel (Supplementary Figure 2). A final panel was developed for analysis of macrophages (Table 2.21), gating strategy shown in .

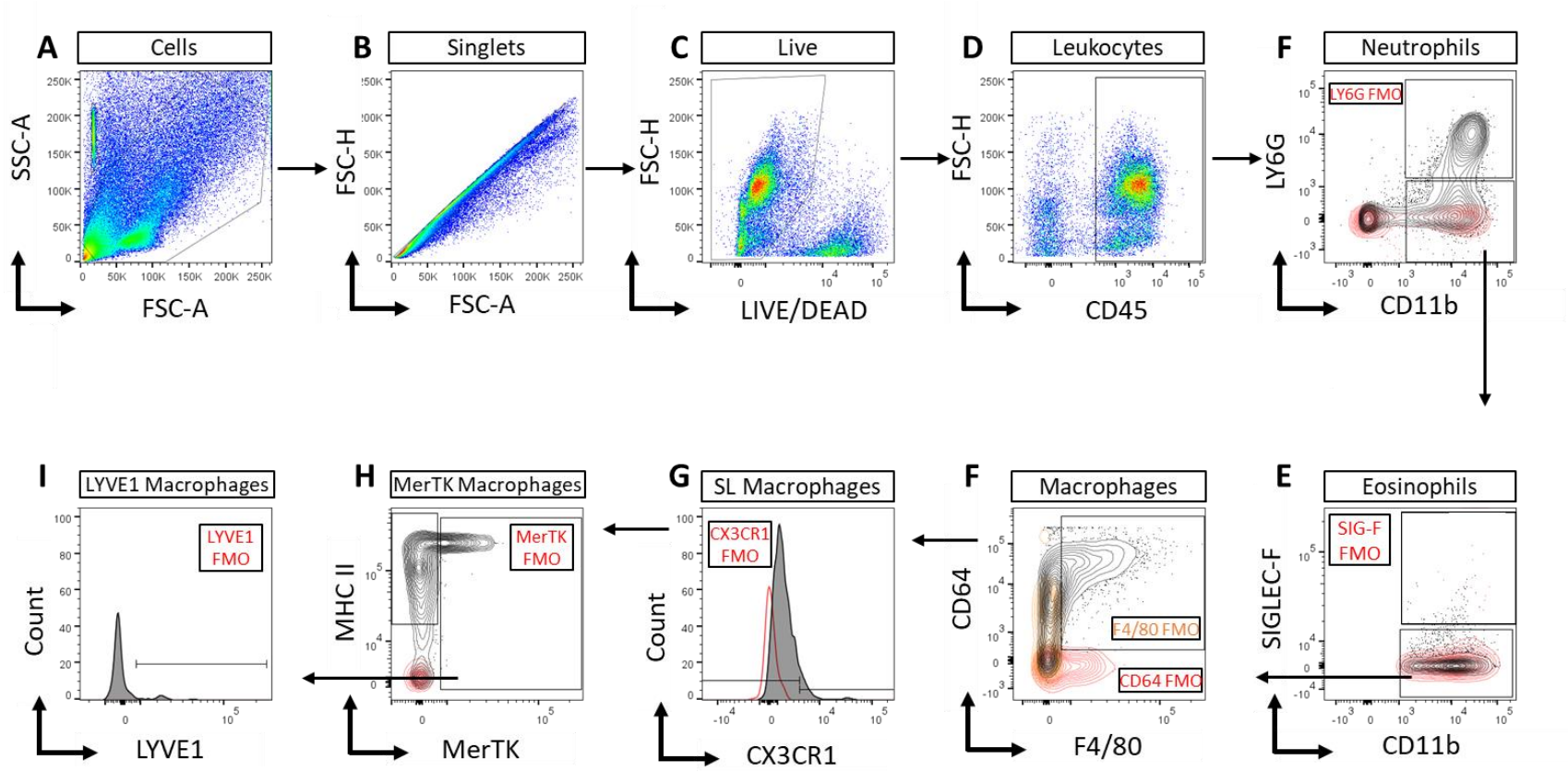

Figure 2.3 Optimisation of mouse macrophages markers. Mouse synovial macrophages were isolated and stained as indicated. Gating strategy used to quantify macrophage populations.

Table 2.21 Staining for synovial macrophage subsets

Target	*Fluorochrome*	*Clone*	*Dilution*
CD45	APC-CY7	30-F11	1/500
CD11b	FITC	M1/70	1/100
LY6G	AF700	1A8	1/100
SIGLEC-F	PE-e610	1RNM44N	1/200
CD64	PE-CY7	X54-5/7.1	1/100
F4/80	BV421	BM8	1/100
CX_3CR1	PerCP-Cy5.5	SA011F11	1/100
MHC II	BV650	M5/114.15.2	1/200
LYVE1	PE	ALY7	1/100
MerTK	APC	2B10C42	1/100
Fixable Viability	BV510	-	1/500

Myeloid staining

Synovial cells were isolated using the Collagenase D/Dispase protocol. Markers of myeloid populations were obtained from literature review and a final panel was developed for analysis of myeloid cells (Table 2.22).Gating strategy shown in Figure 2.4.

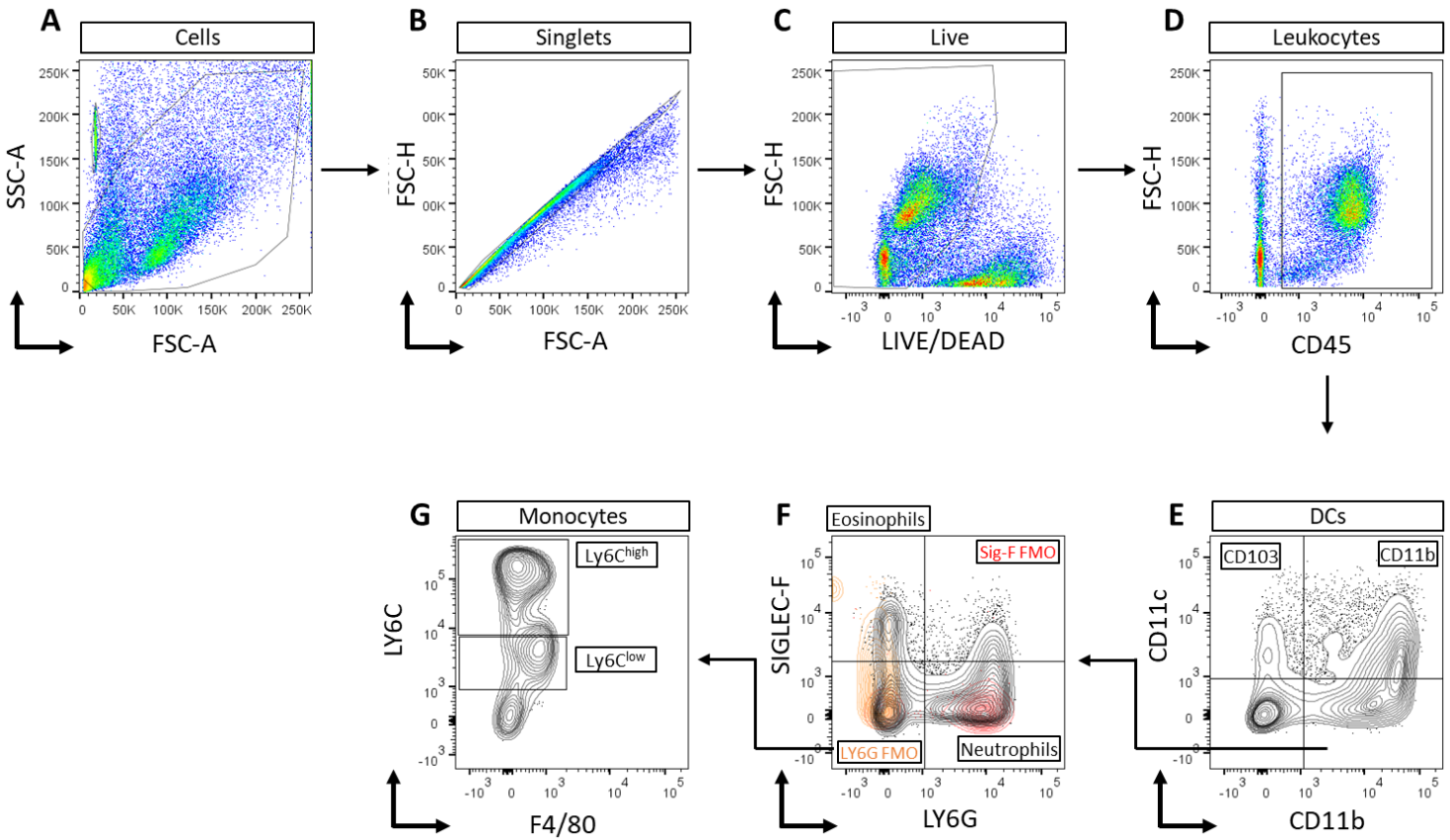

Figure 2.4 Myeloid flow cytometry gating strategy. Optimisation of mouse myeloid markers. Mouse synovial cells were isolated and stained as indicated. Gating strategy shown used to quantify myeloid populations.

Table 2.22 Staining for myeloid populations

Target	*Fluorochrome*	*Clone*	*Dilution*
CD45	APC-CY7	30-F11	1/500
CD11b	FITC	M1/70	1/100
CD11c	BV650	N418	1/100
SIGLEC-F	PE-e610	1RNM44N	1/200
LY6G	AF700	1A8	1/100
LY6C	PE-CY7	HK1.4	1/200
F4/80	BV421	BM8	1/100
Fixable Viability	BV510	-	1/500

Lymphoid staining

Synovial cells were isolated using the Collagenase P protocol, following the discovery that some T Cell markers were cleaved during the Collagenase D/Dispase digest (not show, previous work). Markers of lymphoid populations were obtained from literature review and a final panel was developed for analysis of lymphoid cells (Table 2.23). Gating strategy in Figure 2.5

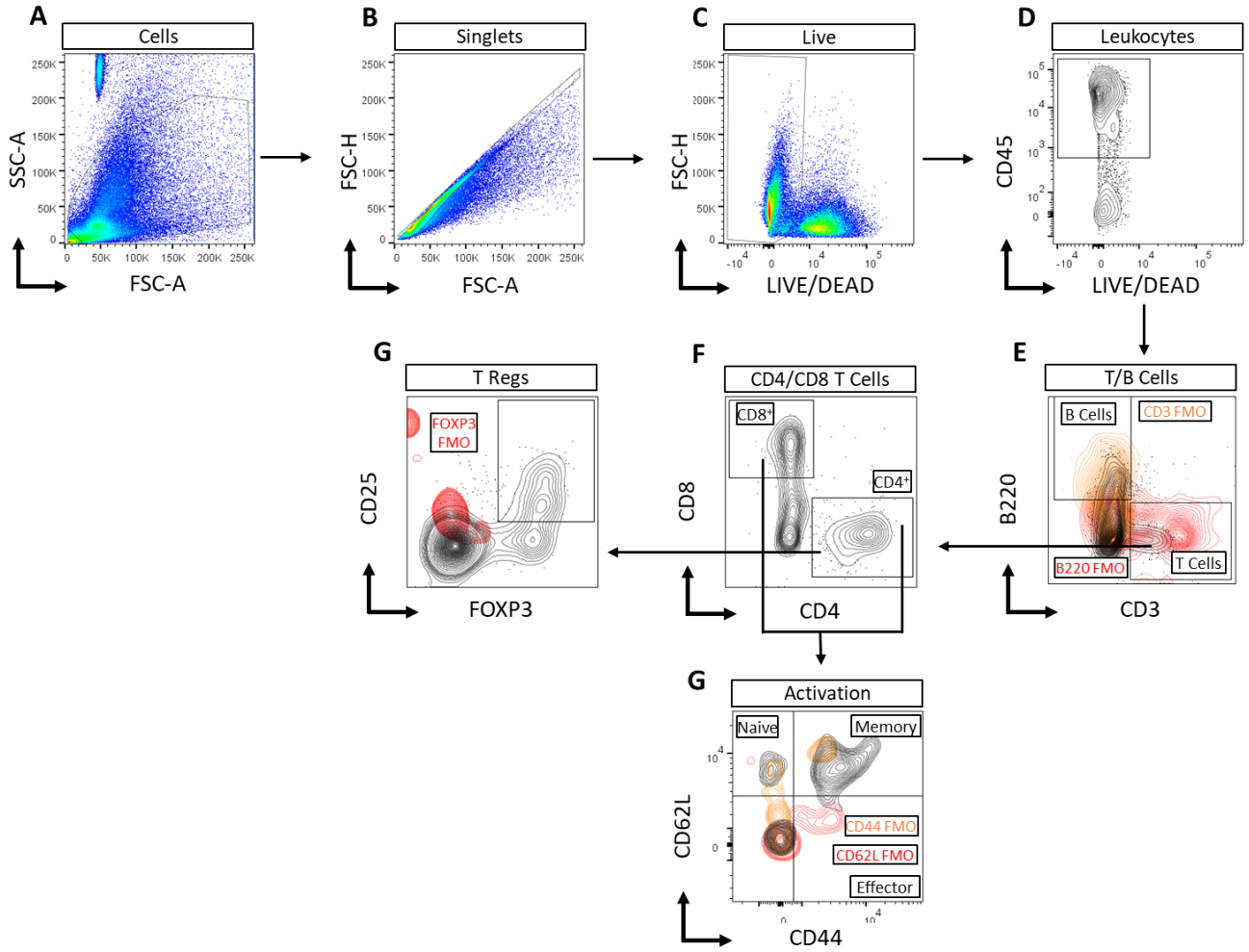

Figure 2.5 Lymphoid flow cytometry gating strategy. Optimisation of mouse myeloid markers. Mouse synovial cells were isolated and stained as indicated. Gating strategy shown used to quantify lymphoid populations.

Table 2.23 Staining for lymphoid populations

Target	*Fluorochrome*	*Clone*	*Dilution*
CD45	PE-CY7	30-F11	1/300
CD8a	PE-Texas Red	53-6.7	1/100
CD3e	APC-e780	145-2C11	1/80
B220	FITC	RA3-6B2	1/100
CD4	BV421	RM4-5	1/80
CD44	PERCP-CY5.5	IM7	1/100
CD25	BV650	PC61	1/80
CD62L	PE-CY5	MEL-14	1/100
FOXP3	PE	FJK-16s	1/50

2.2.7 RT Q-PCR

RNA was isolated from single-cell suspensions using the RNeasy Micro Kit according to the manufacturer's instructions, including the DNase digestion step to remove any contaminating DNA. cDNA synthesis was performed on all samples (500 ng of RNA was transcribed) using iScript cDNA synthesis kit (Bio-Rad) on a Techne 312 thermal cycler PCR machine. Reverse transcription with quantitative PCR (RT−qPCR) was performed using Taqman assays (Table 2.16) and Taqman universal Mastermix on a real-time PCR detection system (CFX96 Touch Real-Time PCR Detection System). Relative fold gene expression was normalised to Hprt and calculated with the $2^{-\Delta\Delta Ct}$ method. Assistance with RT PCR was kindly provided from Dr Ian Beh.

2.2.8 Histology

Preparation and processing of tissue

Tissue was fixed for 24 hours in 10% formalin, then decalcified in EDTA (10% w/v, pH7.4). Tissue was processed and embedded in formalin (Table 2.24). 4µM sections were cut and incubated at 56°C overnight, then stored at 4°C.

Table 2.24 Paraffin embedding of mouse legs

Reagent	Concentration	Time
Ethanol	70%	1h
Ethanol	95%	1h
Ethanol	95%	1h
Ethanol	100%	1h
Ethanol	100%	1h
Ethanol	100%	Overnight
Xylene	-	1h
Xylene	-	1h
Paraffin (60°)	-	Change every 15 minutes for 4 hours
Embed in paraffin and leave to set at RT		

H&E

Sections were stained with H&E following the procedure in Table 2.25. Imaged with the AxioScan Slide Scanner, and analysed using ZenBlue v. A scoring system to assess the level of synovitis was adapted from published works[125] (Table 2.25).

Table 2.25 H&E Scoring of murine synovitis

Score	**Synovial hyperplasia**	**Synovial cellularity**	**Synovial Inflammation**
0	Lining layer 1 cell thick	Normal	None
1	Lining layer 2-3 cells thick	Slightly increased	Occasional scattered inflammatory cells
2	Lining layer 4-5 cells thick	Moderately increased with few multinucleated cells	Focal areas of dense infiltrate, few aggregates
3	Lining layer 6+ cells thick	Greatly increased, pannus that extends over cartilage surface	Widespread dense infiltrate, follicle formation and numerous aggregates

Table 2.26 H&E staining of FFPE tissue

Reagent	Concentration	Time
Xylene	-	5 minutes
Xylene	-	5 minutes
Xylene	-	10 minutes
Ethanol	100%	2 minutes
Ethanol	90%	2 minutes
Ethanol	80%	2 minutes
Ethanol	70%	2 minutes
Ethanol	50%	2 minutes
dH_20	-	2 Minutes
dH_20	-	2 Minutes
dH_20	-	2 Minutes
Harris haematoxylin	-	8 minutes
Running tap water	-	5 minutes
Acid alcohol	1%	30 seconds
Running tap water	-	1 minute
Ammonia water	0.1%	1 minute
Running tap water	-	5 minutes
Ethanol	95%	10 dips
Eosin	-	5 minutes
Ethanol	95%	2 minutes
Ethanol	100%	5 minutes
Ethanol	100%	5 minutes
Xylene	-	5 minutes
Xylene	-	5 minutes
Mount with DPX		

2.2.9 Statistical Analysis

Statistical analyses were carried out using GraphPad Prism v6 and R Studio (v4.4.1).

Statistical tests and corrections utilised are indicated in figure legends. * $p<0.05$; ** $p<0.01$; *** $p<0.001$; **** $p<0.0001$.

3 CELLULAR ATLAS OF MURINE INFLAMMATORY ARTHRITIS

3.1 Introduction

Inflammatory arthritis encompasses a range of autoimmune conditions characterised by joint inflammation and tissue damage, with rheumatoid arthritis (RA) being one of the most prevalent and debilitating forms[15,16]. Despite extensive research, the complex interplay of cellular and molecular mechanisms driving the onset and progression of RA remains incompletely understood. Recent advancements in single-cell RNA sequencing (scRNA-seq) have provided unprecedented resolution in dissecting the heterogeneity of cellular populations and their dynamic responses during disease progression[126,127]. This chapter leverages scRNA-seq technology to construct a comprehensive cellular atlas of inflammatory arthritis in mouse models, capturing the temporal evolution of cellular landscapes across various stages of disease.

To achieve this, we utilised three well-established mouse models of inflammatory arthritis, each representing distinct aspects of the disease: Collagen-Induced Arthritis (CIA), Antigen-Induced Arthritis (AIA), and Serum Transfer-Induced Arthritis (K/BxN). These models were examined at critical timepoints to capture the resting, peak, resolving, resolved, and persistent phases of arthritis. Specifically, the CIA model was analysed at the resting and peak stages; the AIA model at resting, peak, resolving, and resolved stages; and the K/BxN model at resting, peak, resolving, resolved, and persistent stages **Error! Reference source not found.**.

Single-cell RNA sequencing

One of the major advantages of scRNA-seq is its ability to capture the dynamic changes in cellular composition and gene expression over time. In the context of inflammatory arthritis, this means we can monitor how different cell types emerge, expand, or diminish across various stages of disease. This temporal resolution is critical for understanding the progression from initial inflammation to chronic disease, and potentially to resolution or persistence of inflammation. By applying scRNA-seq to our mouse models of arthritis at multiple timepoints, we can create a detailed cellular atlas that maps these changes comprehensively.

Murine models of arthritis

To study the complex pathogenesis of RA and develop potential therapeutic interventions, researchers employ various mouse models of inflammatory arthritis. These models mimic key aspects of human RA, providing insights into disease mechanisms and progression. This chapter focuses on three widely used mouse models: Collagen-Induced Arthritis (CIA), Antigen-Induced Arthritis (AIA), and Serum Transfer-Induced Arthritis (K/BxN). Each model captures distinct features of RA and contributes uniquely to our understanding of the disease (Table 3.1).

Collagen-Induced Arthritis (CIA)

CIA is one of the most extensively used models for studying RA. This model is typically induced in genetically susceptible mouse strains, by immunising them with type II collagen (CII) emulsified in an adjuvant, usually complete Freund's adjuvant (CFA)[128–132]. The immune system mounts a response against the collagen, leading to inflammation and joint destruction[129,133,134]. Immunisation with CII leads to the activation of T and B cells, which recognise and respond to collagen epitopes[135,136].

The production of anti-collagen antibodies forms immune complexes that deposit in the joints[136–139]. These immune complexes activate the complement system, driving inflammation and recruitment of immune cells[139–141]. Pro-inflammatory cytokines such as TNF-α, IL-1β, and IL-6 play a pivotal role in sustaining the inflammatory response and causing tissue damage[142–147]. CIA closely mimics several aspects of human RA, including synovial hyperplasia, pannus formation, and joint erosion.[45,79,148–156]

Antigen-Induced Arthritis (AIA)

AIA involves the injection of an antigen, such as methylated bovine serum albumin (mBSA), directly into the joint of a previously immunised mouse[157–159]. Direct injection of the antigen into the joint induces a localised inflammatory response. The model involves both innate and adaptive immune responses, with significant roles for T cells, macrophages, and neutrophils[157,160–162]. Key cytokines such as IL-1, TNF-α, and IL-17 are involved in mediating joint inflammation and damage[163–167].

Serum Transfer-Induced Arthritis (STIA)

STIA is induced by transferring serum from K/BxN mice, which spontaneously develop arthritis due to a transgenic T cell receptor recognising a self-antigen, to recipient mice[168]. The serum contains autoantibodies that cause arthritis in the recipients[168]. The transfer of serum containing autoantibodies against glucose-6-phosphate isomerase (GPI) leads to immune complex formation and deposition in the joints[169]. Activation of the complement system and engagement of Fc receptors on immune cells drive inflammation and tissue destruction[170]. Neutrophils and macrophages are key effectors in this model, mediating joint inflammation and

damage through the release of reactive oxygen species and proteolytic enzymes[171,172].

Conclusion

Each of these mouse models of inflammatory arthritis offers unique insights into several aspects of RA pathogenesis. By leveraging these models, we can dissect the cellular and molecular mechanisms driving RA, identify potential therapeutic targets, and evaluate new treatments. The combination of these models in this chapter enables a comprehensive exploration of the temporal dynamics and heterogeneity of inflammatory arthritis, providing a robust foundation for advancing RA research.

3.2 Chapter aims

The main objectives of this chapter are:

1. To construct a comprehensive cellular atlas of synovial tissues from the AIA, CIA, and STIA mouse models using scRNA-seq.
2. To compare the cellular and molecular changes across different mouse models and at various stages of disease progression.
3. To identify key cell types, pathways, and gene expression patterns that are associated with disease onset and progression, with the goal of elucidating potential therapeutic targets for inflammatory arthritis.
4. To integrate these findings to identify key cellular and molecular targets in the treatment of RA.

Table 3.1 Murine models of inflammatory arthritis

Model	Main Cell Types Involved	Mechanisms	Pathways Involved	Pros	Cons
KBxN Serum Transfer-Induced Arthritis (STIA)	• Neutrophils • Macrophages • Synovial fibroblasts • Mast cells	• Passive transfer of arthritogenic serum containing autoantibodies • Immune complex deposition in the joints • Activation of innate immune cells	• Fcγ receptor signalling • Complement activation • TNF, IL-1, IL-6 pathways	• Rapid, reproducible arthritis • Does not require T-cell involvement • Useful for studying effector phase of inflammation	• Lacks adaptive immune component (T/B cells) • Non-specific nature of serum limits antigen-specific insights
Collagen-Induced Arthritis (CIA)	• T cells (Th1, Th17) • B cells • Dendritic cells • Synovial fibroblasts	• Autoimmune response to type II collagen • Production of collagen-specific autoantibodies • Synovial inflammation and cartilage destruction	• Th1/Th17 pathways • IL-17, IL-1, TNF-α, IL-6 • MMPs	• The most widely used RA model • Involves both innate and adaptive immunity • Human relevance (collagen involvement)	• Time-consuming to induce (weeks) • Strain-dependent variability
mBSA Antigen-Induced Arthritis (AIA)	• CD4+ T cells (Th1, Th17) • Macrophages • Synovial fibroblasts • Neutrophils	• Injection of mBSA antigen in the joint or subcutaneously • Local antigen-specific immune response • Chronic inflammation in joint	• NF-κB, IL-1, TNF-α, and IL-6 pathways • Involvement of MMPs and cytokines like IL-17	• Simple and reproducible • Localised inflammation useful for joint-specific studies • Useful for testing therapies targeting joint-specific inflammation	• Not systemic, limited to one joint • Not spontaneous or progressive • Artificial model due to reliance on a foreign antigen

3.3 Building a single cell atlas of murine inflammatory arthritis

Introduction to the Dataset

We generated a comprehensive cellular atlas of inflammatory arthritis using scRNA-seq across three mouse models: AIA, CIA, and STIA To capture the dynamic changes in cellular composition and gene expression profiles over the course of diseases progression, samples were collected at various timepoints throughout the course of disease (**Error! Reference source not found.**). Specifically, we harvested synovial tissue samples from the joints of mice at early, intermediate, and late stages of disease in each model, resulting in a robust dataset that spans the entire disease course.

Our primary objective was to analyse this dataset to construct a detailed cellular atlas and to investigate how cellular populations and gene expression profiles change across different models and timepoints. By integrating and comparing these data, we aim to uncover key cellular and molecular mechanisms underlying the initiation and progression of inflammatory arthritis, which could inform the development of targeted therapies.

Data Integration and Quality Control

Following sample preparation and sequencing, low quality cells were excluding by assessing metrics shown in Figure 3.2**Error! Reference source not found.**. Then the dataset was integrated to remove any batch effects Figure 3.3.

Once QC and integration are complete, cell types can be identified, rendering the dataset ready for exploration and analysis.

Cellular Atlas

Following QC filtering and integration, the atlas was clustered using Seurat, and cell types were identified by comparing top Differentially Expressed Genes (DEGs) with common cell markers. Contaminating cells, such as Myoblasts (Tnnt1, Myod1), Erythrocytes (Hba-a1, Hba-a2), Cycling Cells (Cdk1, Cenpa), and Skeletal Muscle (Actn3, Aldoa) were removed. Major cell types identified in the atlas are shown in Figure 3.4A, i), defined by common markers Figure 3.4 A, ii). Where feasible I further clustered cell types into sub-populations Figure 3.4B), defined by either common markers reported in literature or top DEGs if the sub-population is novel Figure 3.5.

Fibroblasts were identified as Pdgfra+ Pdpn+ Figure 3.4A, ii), and were further subdivided into five subpopulations Figure 3.5A). Lining versus Sub-Lining (SL) populations were distinguished via Thy1 expression (Figure 8.3). The lining subpopulation was identified through expression of established lining markers Prg4 and Tspan15[12,139,150,155,173,174]. All other subpopulations were Thy1+ and defined by top DEGs, Cd34+ Apod+, Cd34+ Pi16+, Cthrc1+ Postn+, and Cxcl9+ Cxcl10+. Although fibroblast subsets are not currently well established, clusters defined in this data set closely resembled other, more recent scRNAseq studies of murine fibroblasts, so I was confident in the clustering and annotation[32,41,42,58,175].

Dendritic Cells (DCs) were identified as Itgax+ (CD11c) H2-Ab1+ (MHC-II) (Figure 3.4**Error! Reference source not found.**A, ii), and were further subdivided into three subpopulations (Figure 3.5**Error! Reference source not found.**B). These subpopulations are defined by gene expression and can also be identified in current literature: CD11b+ DCs, CD11b- CD103- DCs, and Plasmacytoid DCs (pDCs).

Macrophages were first divided into tissue resident or tissue infiltrating by evaluating expression of Adgre1, Cx3cr1, Mertk, Ly6c and Ccr2. Despite claims in published works that resident macrophages should be F4/80high Cx3cr1+ Mertk+ Ly6c- Ccr2-, and infiltrating macrophages should be F4/80low Cx3cr1- Mertk- Ly6c+ Ccr2+, the reality was much more complex. Many of these markers are generic for macrophages/monocytes and can be differentially regulated under inflammatory conditions. This context was considered when defining clusters (Figure 8.4).

Tissue-Resident Macrophages (referred to as Macrophages) were ultimately identified as Mertk+ Adgre1+ (F4/80) Cd68+ (Figure 3.4A, ii), and were further subdivided into six subpopulations (Figure 3.5**Error! Reference source not found.**C). These subpopulations are defined by top DEGs, Spp1+, S100a9+ S100a8+, Cx3cr1+ Vsig4+ Mertkhi, Retnla+ (Relma) Lyve1+, Aqp1+ Lyve1+ Mertkhi, and MHC-IIhi. Again, characterisation of tissue resident synovial macrophages in murine tissues is sparse. The most comprehensive data comes from Culemann et al[37]. Despite some crossover with clusters described in Culemann et al, not all macrophage subsets described could be identified in our dataset. This could be due to inadequate exclusion of monocytes before sequencing in the Culemann methodology.

Monocytes were identified as Ly6chi Itgam+ (CD11b) Cd14+ (**Error! Reference source not found.**A, ii), and were further subdivided into two subpopulations defined by current literature (D): Classical Monocytes (C-Monocytes) and Non-Classical Monocytes (NC-Monocytes).

B Cells were identified as Cd79a+ Cd19+ (Figure 3.4A, ii), and were further subdivided into three subpopulations (**Error! Reference source not found.**E) defined by current literature: Memory B Cells (Bmem), Early Activated B Cells (EA B), and Mature Activated B Cells (MA B).

T Cells were identified as Cd3e+ Cd3d+ (Figure 3.4A, ii), and were further subdivided into three subpopulations defined by current literature (**Error! Reference source not found.**F): CD4+ T Cells, CD8+ T Cells, and T Regulatory Cells (Treg).

Innate Lymphoid Cells (ILCs) (Rora+ Tox+), Natural Killer (NK) Cells (Ncr1+ Klrb1c+), Mast Cells (Fcer1a+ Mcpt4+), Pericytes (Des+ Acta2+), Osteoblasts (Bglap+ Alpl+), Chondrocytes (Cilp+ Chad+), and Vascular Endothelial Cells (Emcn+ Cdh5+) were not clustered into further subpopulations either due to low cell numbers or lack of biological relevance and understanding to reliably sub-cluster these cell types(Figure 3.4A, ii).

All identified cell types were represented within each arthritis model (Figure 3.6

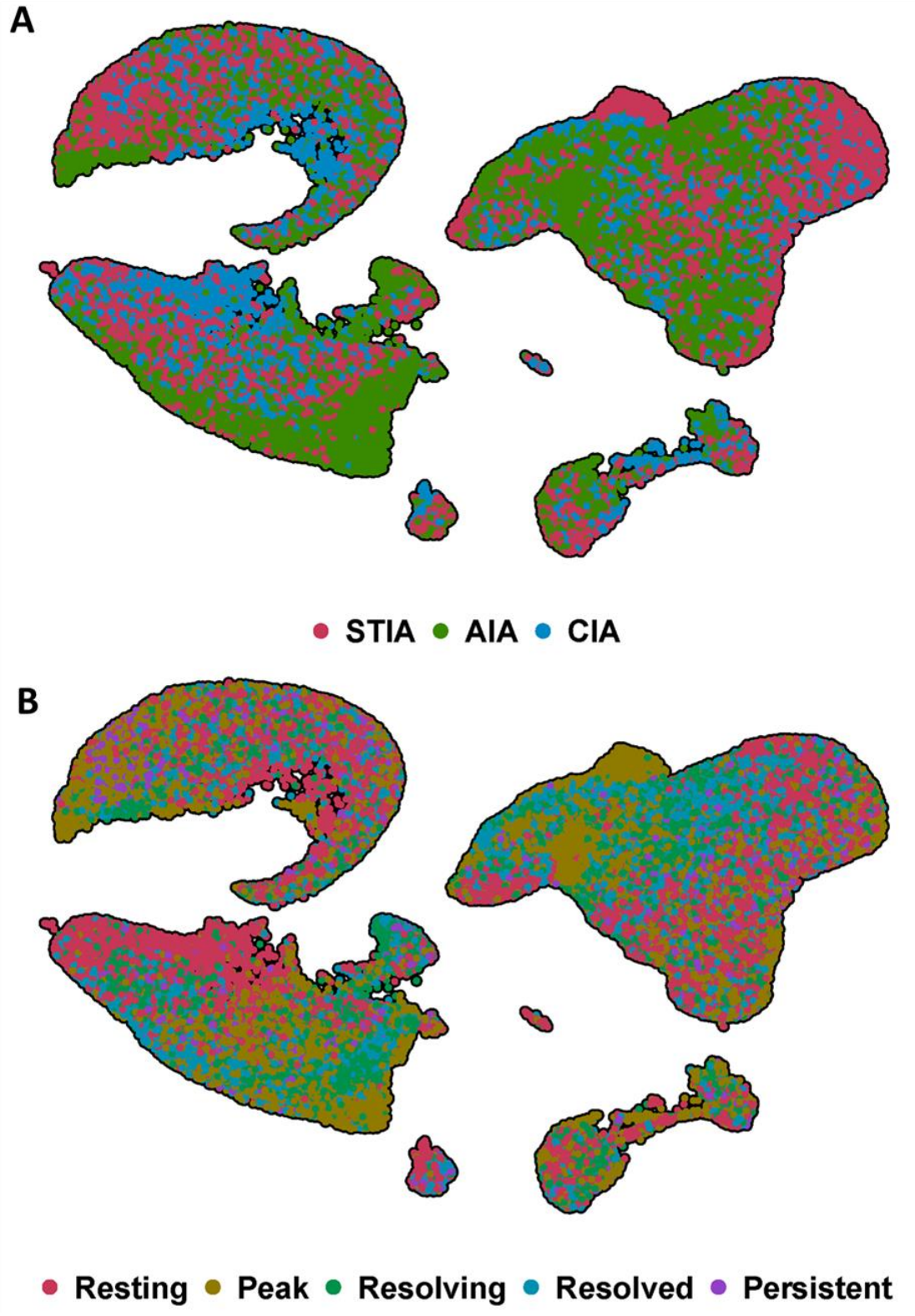

A)

and across each timepoint (Figure 3.6

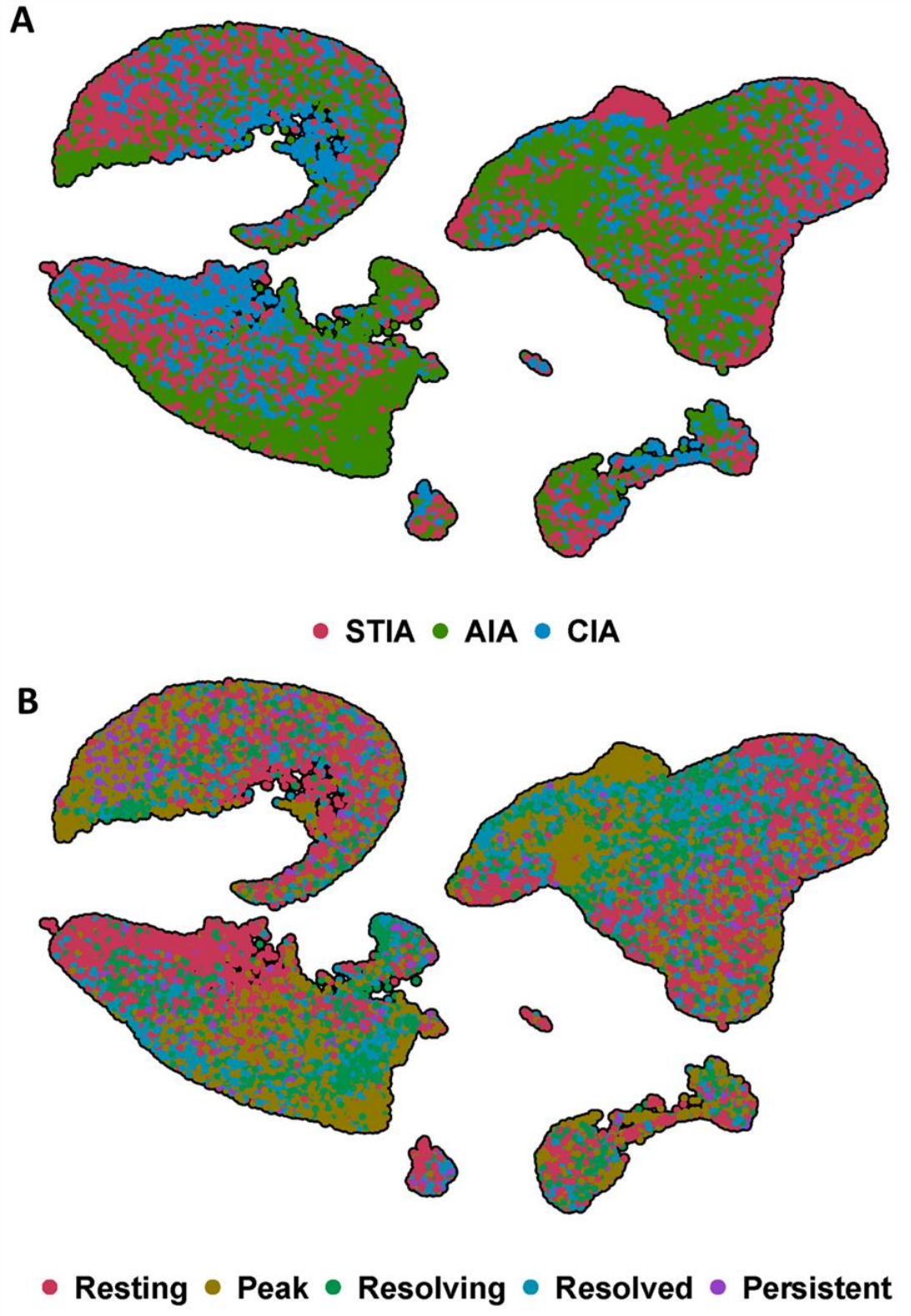

B)

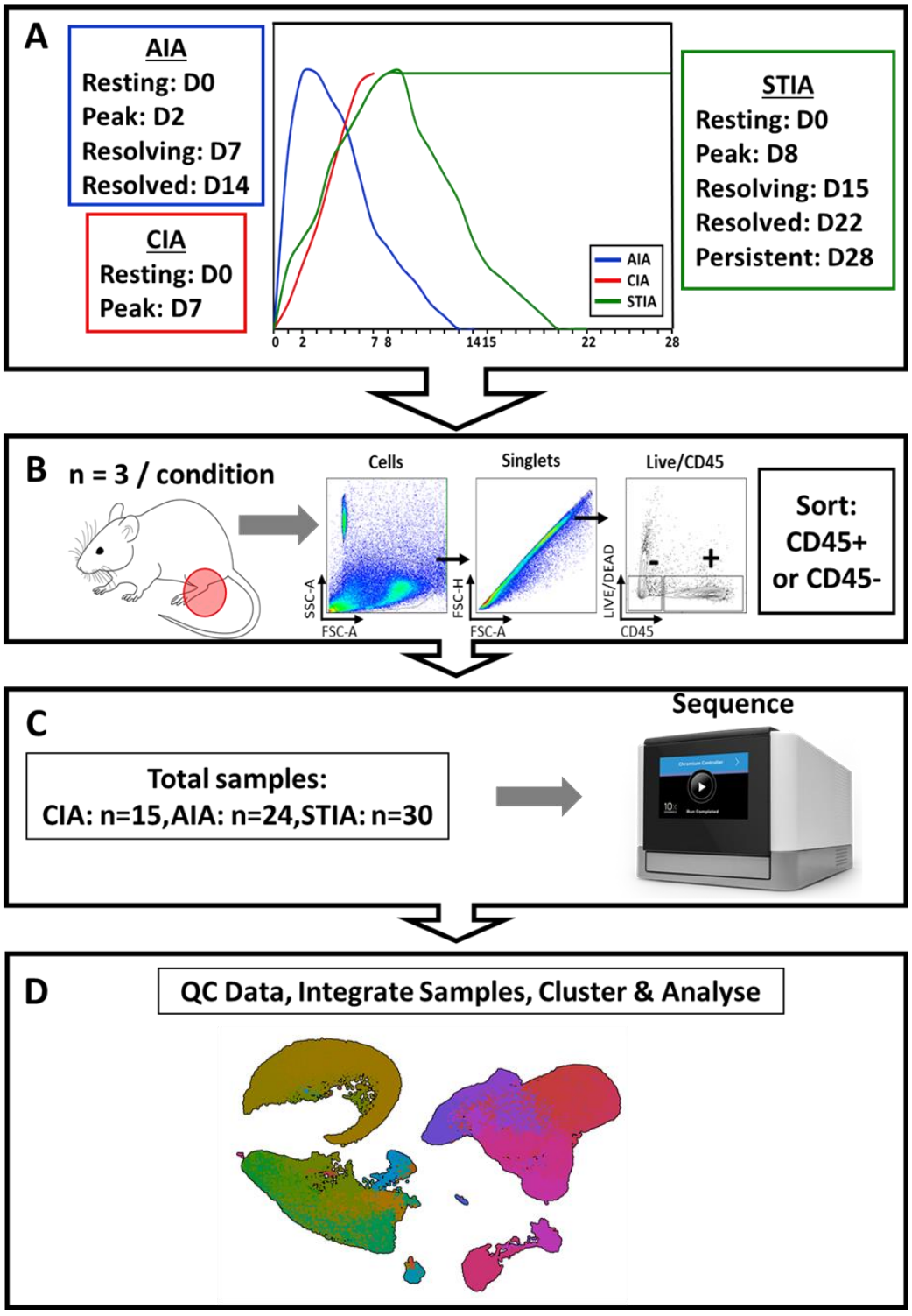

Figure 3.1 Generation of a cellular atlas of murine models of inflammatory arthritis. A) Mice were induced with either AIA, CIA or STIA; and key timepoints throughout the course of their disease were identified. B) Tissue was extracted from mice at each timepoint, synovial cells were isolated, stained and collected into either CD45+ or CD45- fractions. C) Each sample was prepared and sequenced using the 10X platform. D) Sequencing data underwent processing and integration to generate the final atlas containing all models and timepoints.

Table 3.2 Samples sequenced for the murine single cell atlas.

Model	Timepoint	Sort Condition	Replicate	# Cells Post-QC	orig.ident
CIA	Resting (Day 0)	CD45+	1	1927	Con1_CD45pos
			2	1958	Con3_CD45pos
			3	2907	CIA_Control_pos_CR5
			4	2640	Con2_CD45pos
		CD45-	1	422	Con1_CD45neg
			2	1095	Con2_CD45neg
			3	2910	Con3_CD45neg
			4	2928	Con4_CD45neg
	Peak (Day 7)	CD45+	1	1464	Infla1_CD45pos
			2	2883	Infla2_CD45pos
			3	2730	Infla3_CD45pos
			4	2940	Infla4_CD45pos
		CD45-	1	2168	Infla1_CD45neg
			2	2140	Infla2_CD45neg
			3	2904	Infla3_CD45neg
	Total samples:				15
AIA	Resting (Day 0)	CD45+	1	2826	AIA_rest1_cd45pos
			2	770	rest_pos_renamed
			3	2907	Day0pos_cr_V5
		CD45-	1	2772	AIA_rest1_cd45neg
			2	2745	rest_neg_renamed
			3	2826	Day0neg_cr_V5
	Peak (Day 2)	CD45+	1	2760	AIA_infla1_cd45pos
			2	2760	AIA_infla2_cd45pos
			3	466	Day2_pos3
		CD45-	1	2793	AIA_infla1_cd45neg
			2	2772	AIA_infla2_cd45neg
			3	634	Day2_neg3
		CD45+	1	2640	Day7pos1

	Resolving (Day 7)		2	2670	Day7pos2
			3	2520	Day7pos3
		CD45-	1	2397	Day7_neg1
			2	2850	Day7_neg2
			3	2817	Day7_neg3
	Resolved (Day 14)	CD45+	1	2781	D14_1_pos_renamed
			2	2850	D14_2_pos_renamed
			3	2769	D14_3_pos_renamed
		CD45-	1	2793	D14_1_neg_renamed
			2	2880	D14_2_neg_renamed
			3	2793	D14_3_neg_renamed
	Total samples:				24
STIA	Resting (Day 0)	CD45+	1	1127	S7_CONTROLposB_r
			2	2883	S7_ControlposC
			3	1127	CD45P
		CD45-	1	1219	S8_CONTROLnegB_r
			2	2838	S8_ControlnegC
			3	1428	CD45N
	Peak (Day 8)	CD45+	1	2817	S1_DAY8posA
			2	2856	S3_DAY8posB
			3	2895	S5_DAY8posC
		CD45-	1	1711	S4_Day8negB
			2	2700	S2_DAY8negA
			3	2883	S6_DAY8negC
	Resolving (Day 15)	CD45+	1	1487	S1_Day15posB
			2	1502	S3_Day15posC
			3	2883	S7_DAY15posA
		CD45-	1	898	S2_Day15negB
			2	2196	S4_Day15negC
			3	2862	S8_DAY15negA
	Resolved (Day 22)	CD45+	1	898	S1_Day22posA
			2	778	S3_Day22posB
			3	813	S5_Day22posC

		CD45-	1	719	S2_Day22negA
			2	2660	S4_Day22negB
			3	1778	S6_Day22negC
	Persistent (Day 28)	CD45+	1	1761	S5_Day28posA
			2	2352	S7_Day28posB
			3	900	S1_Day28posC
		CD45-	1	973	S6_Day28negA
			2	1667	S8_Day28negB
			3	720	S2_Day28negC
	Total samples:				30

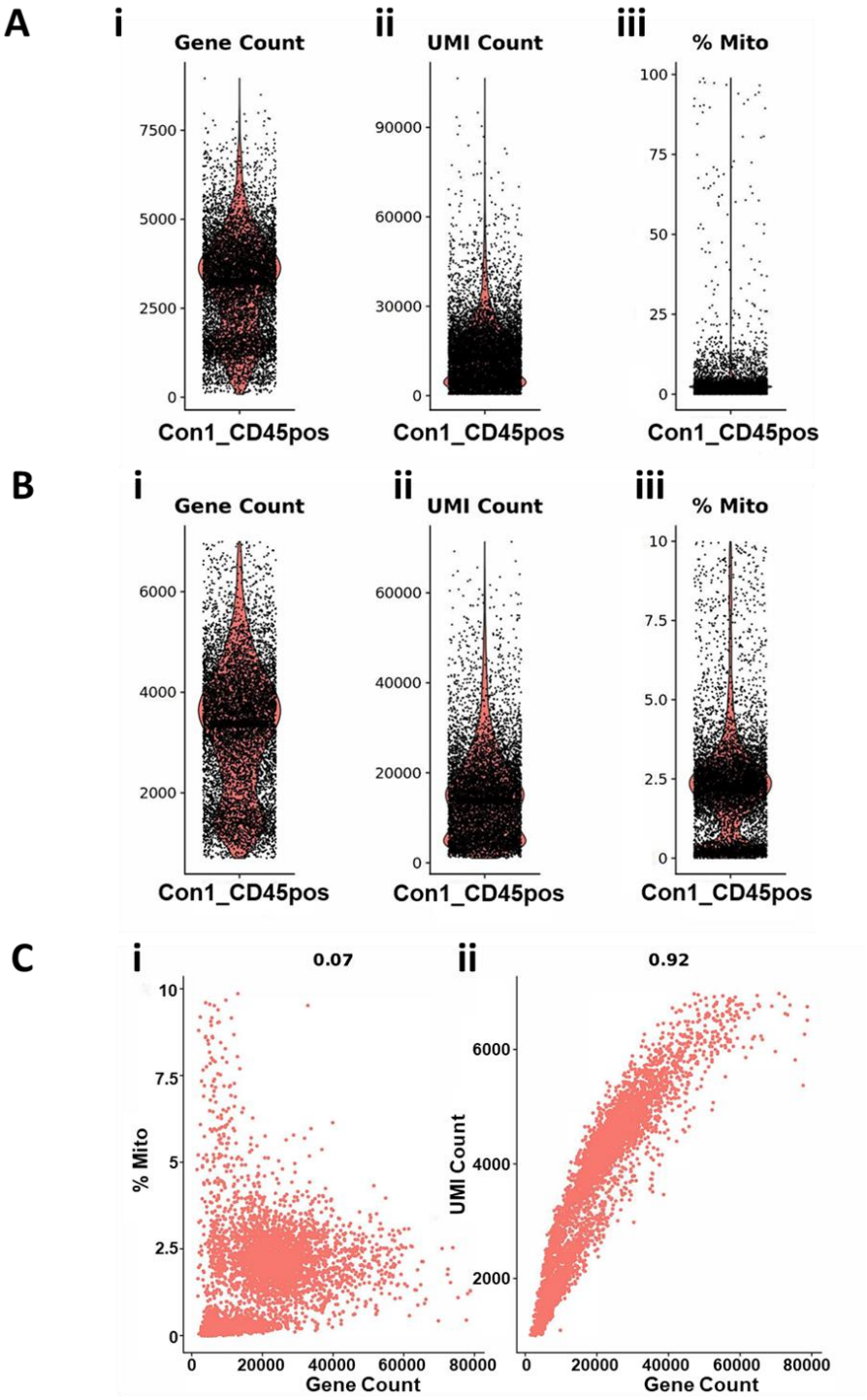

Figure 3.2 Quality control checks of single cell RNA sequencing samples. A) A representative sample before any quality control measures have been applied. Parameters shown are i) Gene Count before QC, ii) UMI Count before QC, iii) % Mito before QC. B) The same sample following QC filtering. i) Gene Count filter: > 500, < 7000, ii) UMI Count filter: < 7000, iii) % Mito filter: < 10. C) Scatter plots of parameters after QC filtering on the same sample. i) % Mito vs Gene Count, ii) UMI Count vs Gene Count. Correlation values are displayed at the top of each plot.

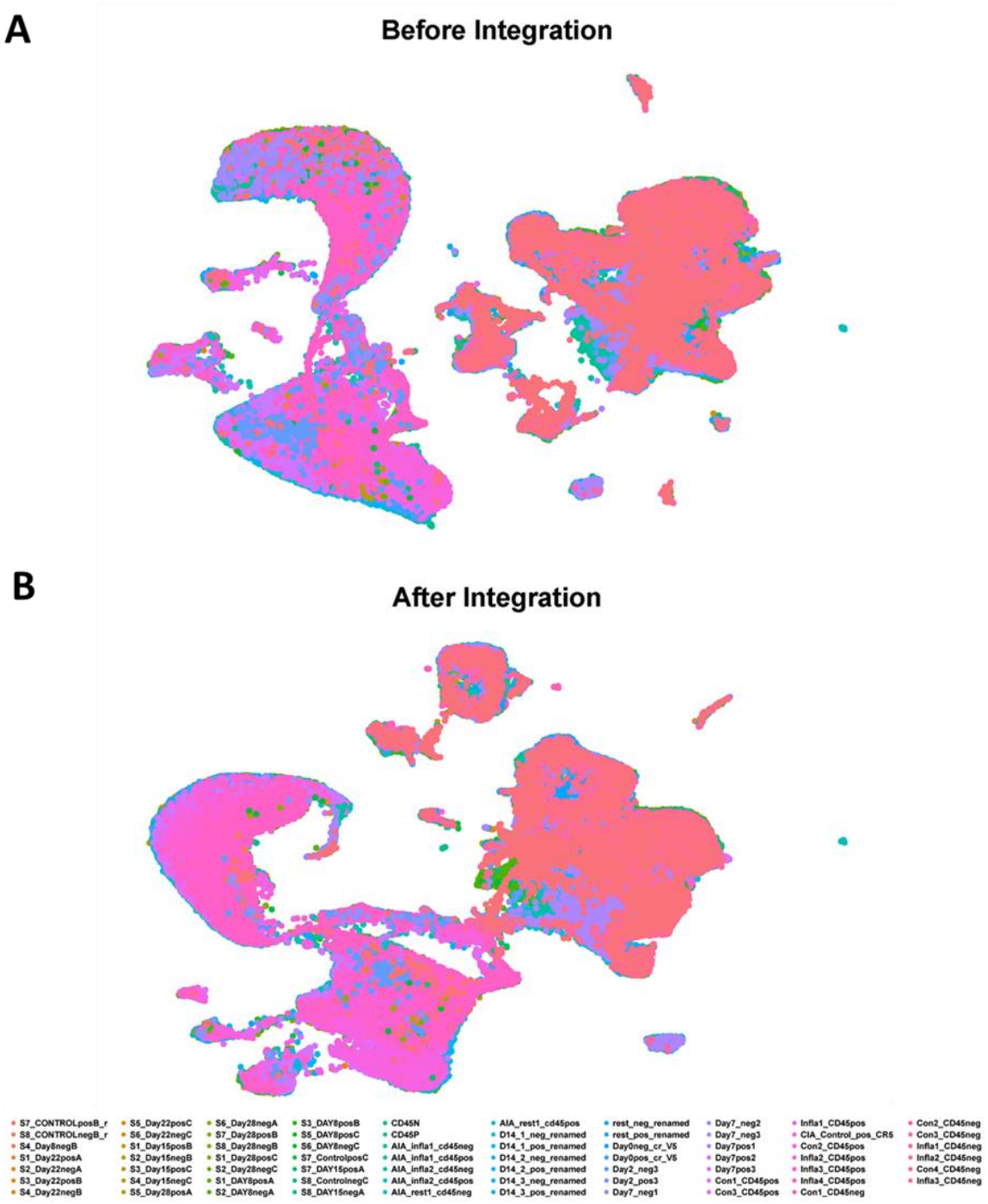

Figure 3.3 Integration of samples. A) UMAP of all samples before any integration. B) UMAP of all samples following integration.

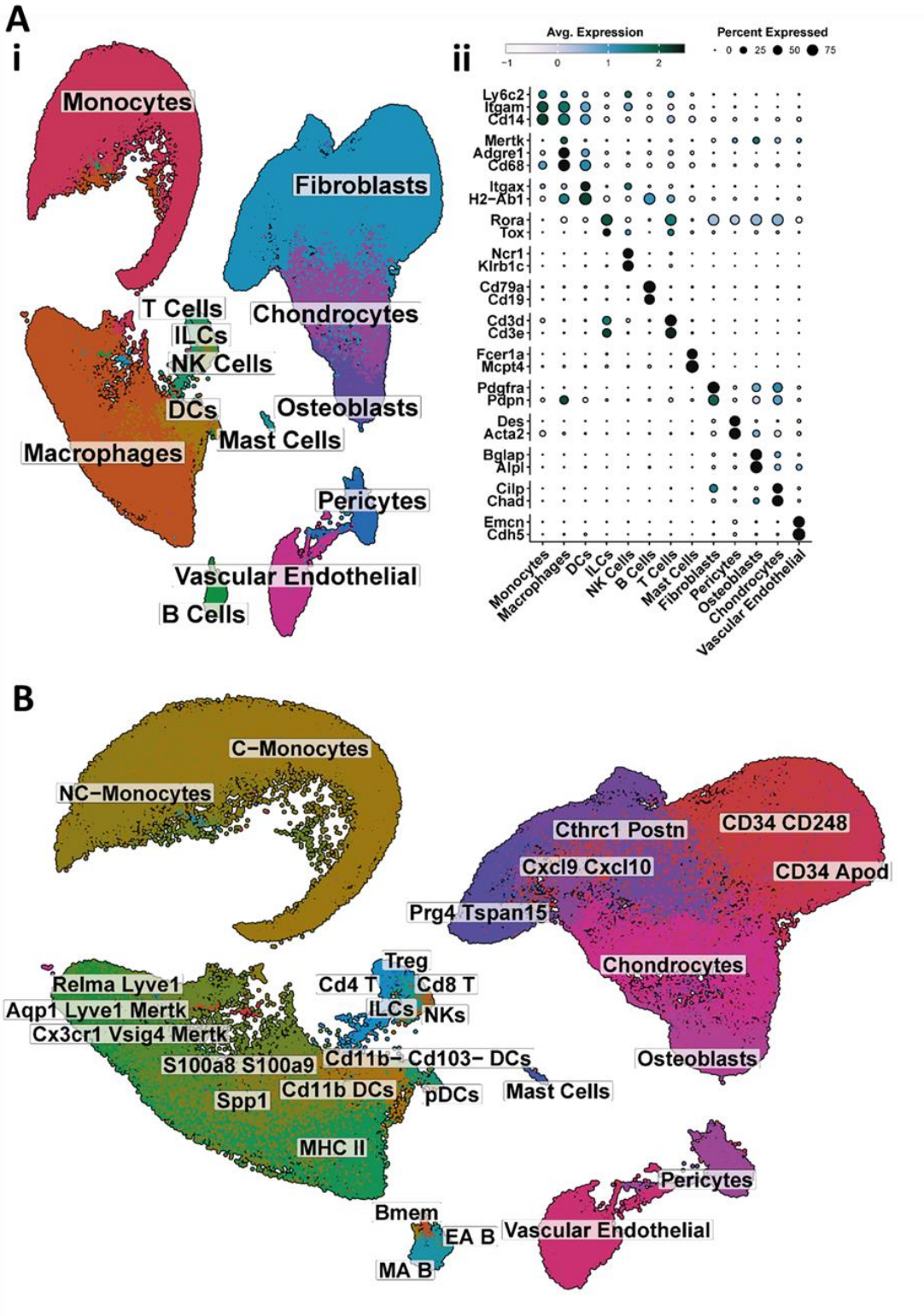

Figure 3.4 Identification of cell types in the atlas. A) Clustering of global cell types across the atlas. i) UMAP of global cell populations identified following clustering. ii) Dot plot showing scaled RNA expression of marker genes for each cell type. B) UMAP showing all identified cell types following further clustering.

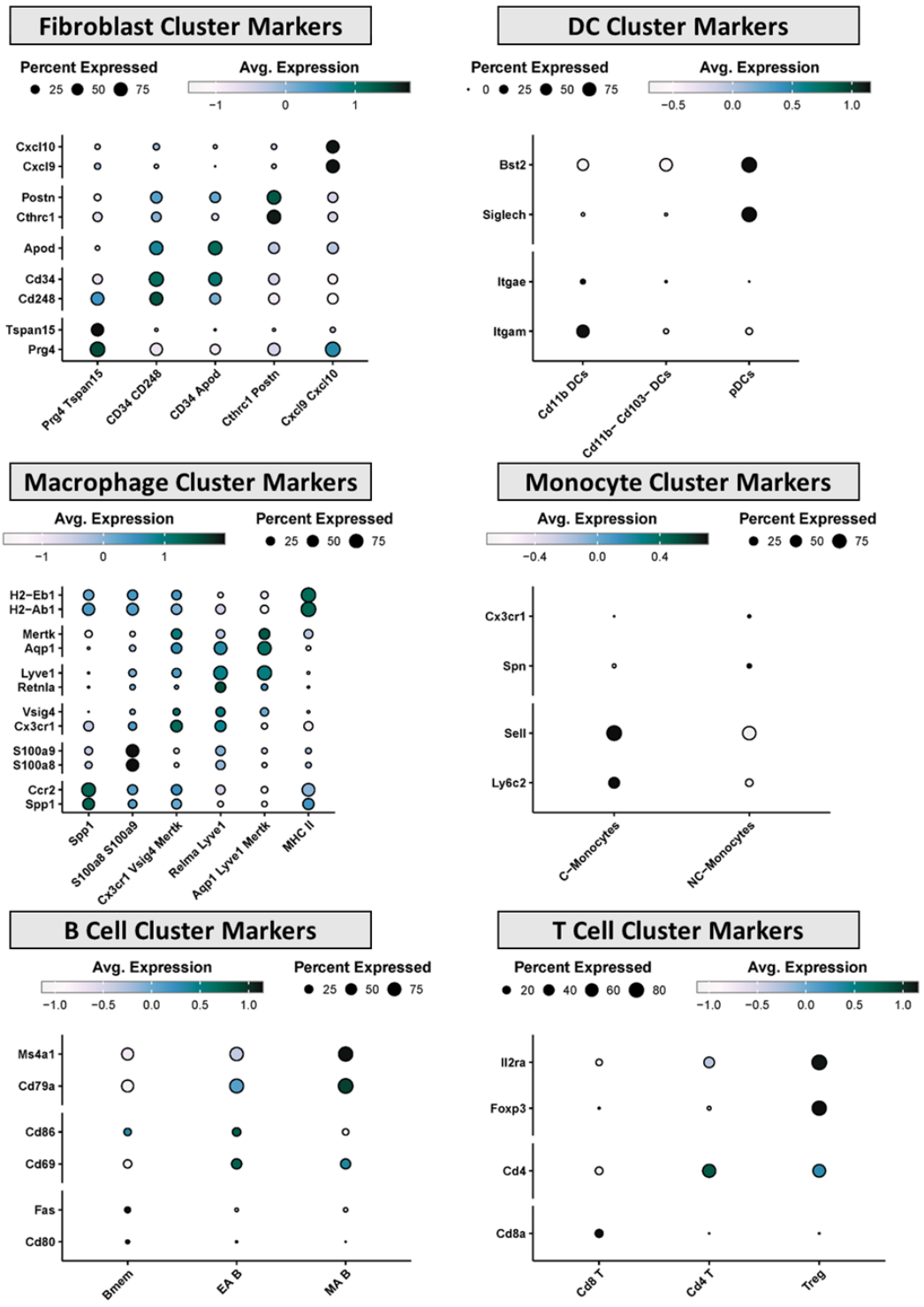

Figure 3.5 Markers of subpopulations. Dot plots showing scaled expression of marker genes for A) fibroblast subpopulations. B) dendritic cell subpopulations. C) macrophage subpopulations. D) monocyte subpopulations. E) B Cell subpopulations. F) T Cell subpopulations.

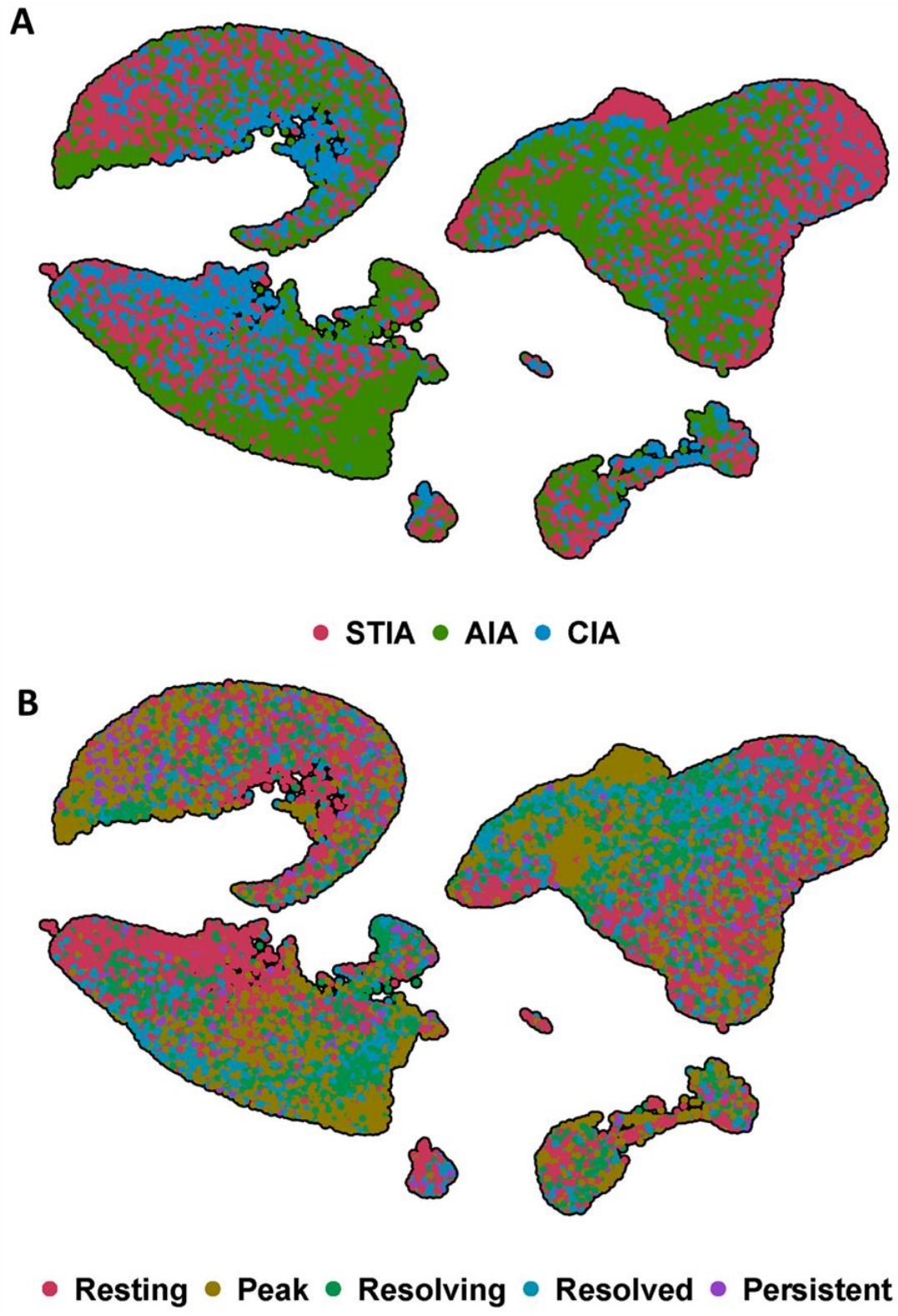

Figure 3.6 Representation of models and timepoints within the cell atlas. A) UMAP showing the distribution of cells from each model of arthritis. B) UMAP showing the distribution of cells from each timepoint

3.4 Comparison Across Mouse Models

Generating a single-cell atlas that encompasses several models of inflammatory arthritis offers numerous benefits for understanding the disease. While sc-RNAseq is often employed with these models to investigate specific hypotheses, to our knowledge, an in-depth cellular atlas elucidating the general mechanisms of these models has not previously been created.

Spatial Mapping

Spatial representation of the data, such as UMAP plots, displays how cells cluster based on their transcriptomic profiles. While useful for initial cell type identification, these plots also help evaluate condition-specific changes linked to cell states or functions.

In order to observe how fibroblast sub-populations change between models, I examined UMAP plots of fibroblasts in each model (Figure 3.7). Model-specific changes in the spatial distribution of fibroblasts can clearly be observed. Notably, subpopulations display distinct spatial distributions across conditions. For example, the Cthrc1 Postn cluster's right portion is prominent in STIA (Figure 3.7A), the centre in AIA (Figure 3.7,**Error! Reference source not found.**B), and the top portion in CIA (Figure 3.7**Error! Reference source not found.**C).

Similar spatial distributions are observed in other subpopulations. Macrophage subpopulations show similar variability (Figure 3.8). This in the Spp1 cluster, where the centre population is dominant in STIA (A), top portion in AIA (Figure 3.8**Error! Reference source not found.**B), and a population at the right of the cluster is observed in CIA (**Error! Reference source not found.**C).

Proportional Changes

Whilst spatial distribution of clusters can infer model-specific changes at the gene level, quantifying proportional changes across conditions can elucidate the functions of cell types within specific models by assessing their relative abundance.

The proportion of total fibroblasts across models is consistent: STIA (33%), AIA (31%), and CIA (28%) (Figure 3.9), indeed confirming that they play a key role in all models. However, the abundance of fibroblast subpopulations is model-specific (Figure 3.10A).

Some fibroblast populations appear to be key populations, abundant in all models. Such as CD34 CD248 fibroblasts, which are present at 41%, 31% and 24% in AIA, STIA and CIA, respectively; Cthrc1 Postn fibroblasts which make up 39% of the population in CIA, 29% in AIA and 19% in STIA; and Lining fibroblasts (Prg4 Tspan15) at 8% in STIA, 8% in CIA, and 14% in AIA. Other populations are more model-specific, for instance, in STIA, 41% of fibroblasts are CD34 Apod+, compared to 29% in CIA and just 4% in AIA, suggesting their role is redundant in the mechanisms of AIA. The Cxcl9 Cxcl10 population is specific to AIA (13%) and represents less than 1% in STIA and CIA.

Similarly, macrophages are present in each model, 17% in STIA, 23% in AIA, and 24% in CIA (Figure 3.9). With model-specific changes in proportions of subpopulations (Figure 3.10**Error! Reference source not found.**B).

Cx3cr1 Vsig4 Mertk macrophages are mostly specific to STIA (40%), representing only 7% and 1% in AIA and CIA, respectively. MHC II macrophages dominate in AIA

(60%), making up just 2% in STIA and 0.6% in CIA. Relma Lyve1 macrophages comprise 33% of macrophages in CIA and less than 1% in STIA and AIA. Interestingly, CIA lacks a dominant macrophage population, with Relma Lyve1, S100a9 S100a8, and Spp1 macrophages each representing approximately 30%.

Other notable changes include the presence of T Cells, mainly in AIA (3%) but not in STIA or CIA (<1%); Mast Cells, which primarily appear in CIA; and Monocytes, which are less prevalent in AIA (20%) than in STIA (28%) and CIA (29%).

Pathway Enrichment Analysis

The differences in spatial distribution and relative abundance across models suggest that some cell types are more dominant in specific contexts, and that some populations may transitional over the course of inflammation. To investigate this further, pathway enrichment analysis was conducted to identify the functional roles of tissue-resident subpopulations.

Regardless of their abundance, some populations are consistently involved in similar pathways in all models. Such as Prg4 Tspan15 lining fibroblasts, involved in aerobic respiration, vesicle formation, secretion, and cell-matrix adhesion (Figure 3.11**Error! Reference source not found.**). Surprisingly, despite the model-specific changes observed in spatial distribution, Cthrc1 Postn fibroblasts are consistently involved in bone and tissue remodelling and leukocyte apoptosis regulation across models (Figure 3.11).

Likewise, Spp1 macrophages primarily facilitate T Cell migration and activation in all models (Figure 3.12**Error! Reference source not found.**). Aqp1 Lyve1 Mertk macrophages and MHC II macrophages also display similar functions across models.

Other populations show model-specific enrichment patterns, suggesting they may be genetically altered depending on the model deployed. For example, CD34 CD248 fibroblasts are enriched for mitochondrial respiration in STIA (Figure 3.11**Error! Reference source not found.**A), mechanical roles in vasculogenesis and tissue migration in AIA (Figure 3.11B), and involvement in B Cell-mediated immunity and complement activation in CIA (Figure 3.11C). Cx3cr1 Vsig4 Mertk macrophages regulate leukocyte migration, cell-cell junction organisation, and tissue remodelling in STIA and AIA (Figure 3.12A and B), but take on an inflammatory role in CIA, involving both T and B Cell pathways (C).

Additionally, whilst the specific mechanisms involved appear altered, some populations display a similar overall function throughout each model. S100a8 S100a9 macrophages are always implicated in regulation of the adaptive immune response, but though B Cell activation and leukocyte proliferation in STIA (Figure 3.12**Error! Reference source not found.**A), mast cell activation in AIA (Figure 3.12**Error! Reference source not found.**B), and T Cell and MHC-II receptor complex formation and endocytosis-related pathways in CIA (Figure 3.12**Error! Reference source not found.**C).

Relma Lyve1 macrophages, were only detectable in sufficient numbers to perform pathway analysis in CIA, where they engage in pro-inflammatory pathways like TNF response and IL-1 production (Figure 3.12**Error! Reference source not found.**C).

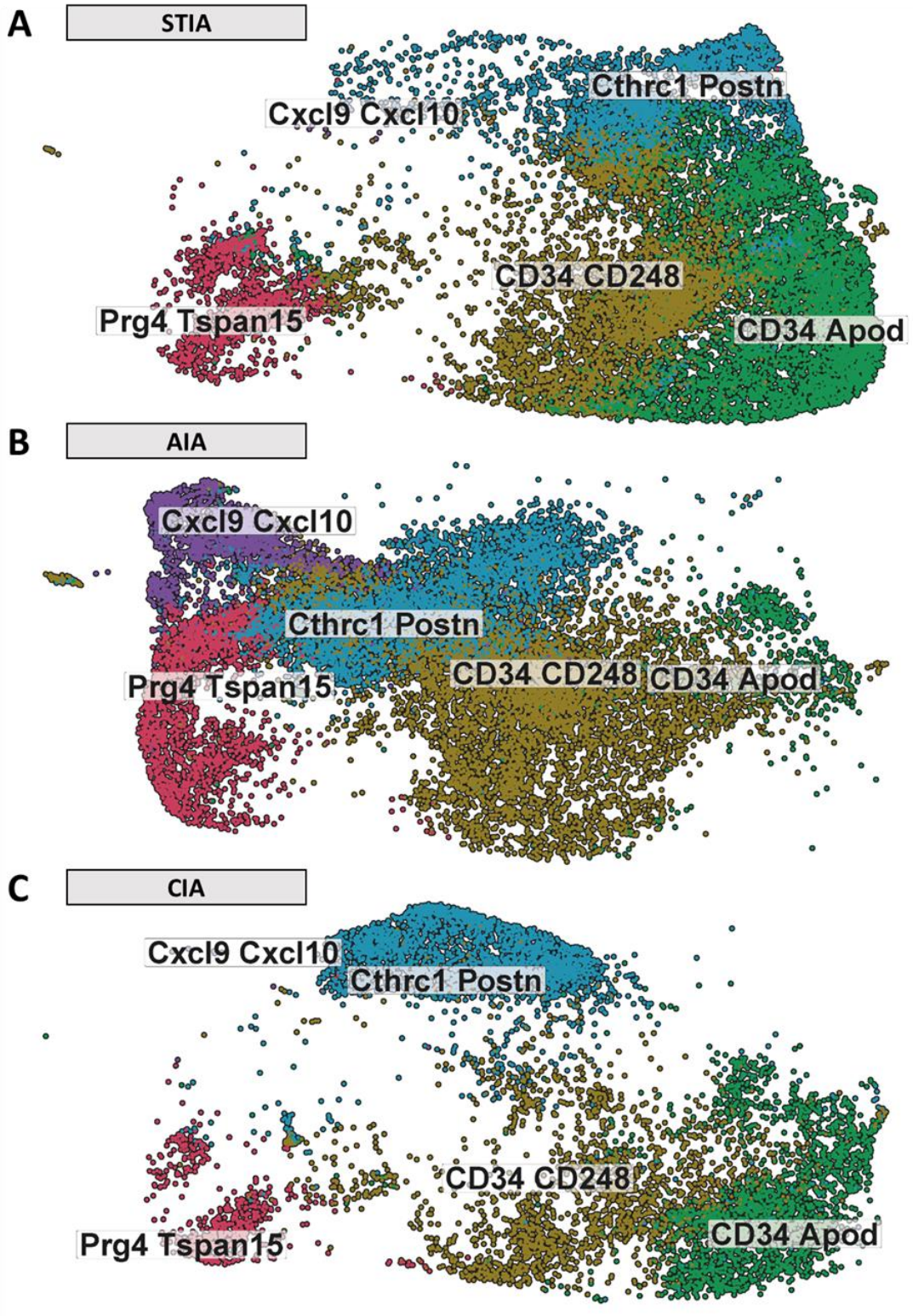

Figure 3.7 Spatial distribution of fibroblast subpopulations across models of inflammatory arthritis. A) UMAP of fibroblast subpopulation within the STIA model. B) UMAP of fibroblast subpopulation within the AIA model. C) UMAP of fibroblast subpopulation within the CIA model.

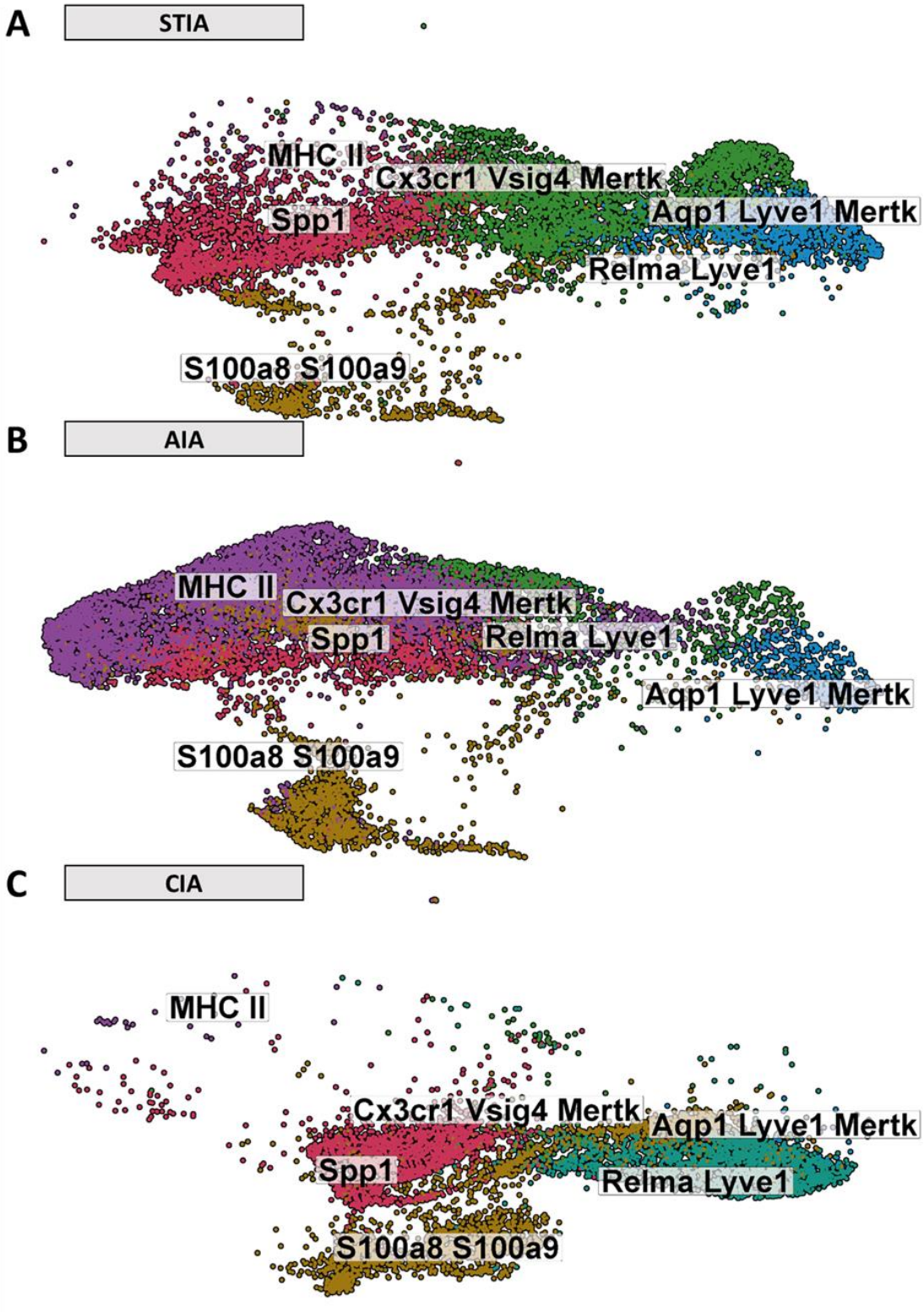

Figure 3.8 Spatial distribution of macrophage subpopulations across models of inflammatory arthritis. A) UMAP of macrophage subpopulation within the STIA model. B) UMAP of macrophage subpopulation within the AIA model. C) UMAP of macrophage subpopulation within the CIA model.

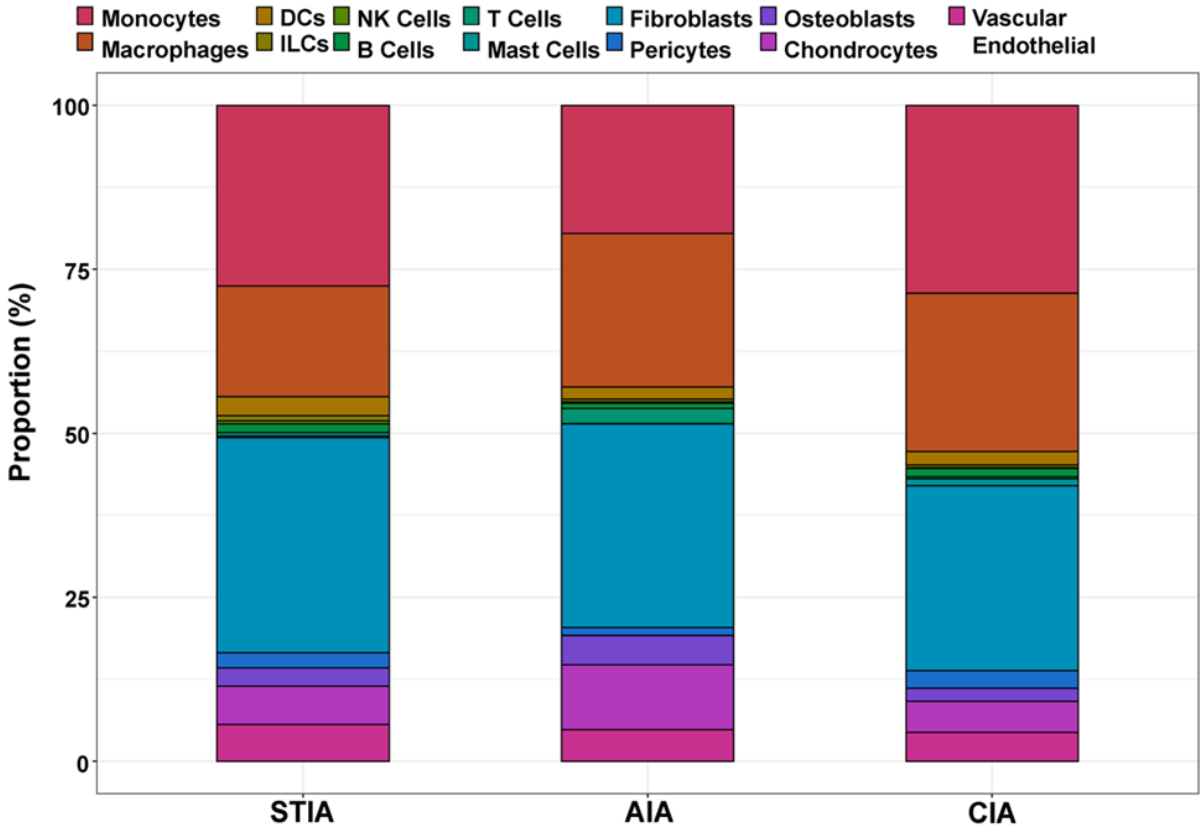

Figure 3.9 Proportions of general cell populations in each model of arthritis. Stacked bar plot showing the relative proportion of each cell type of the whole cell population in each model of arthritis.

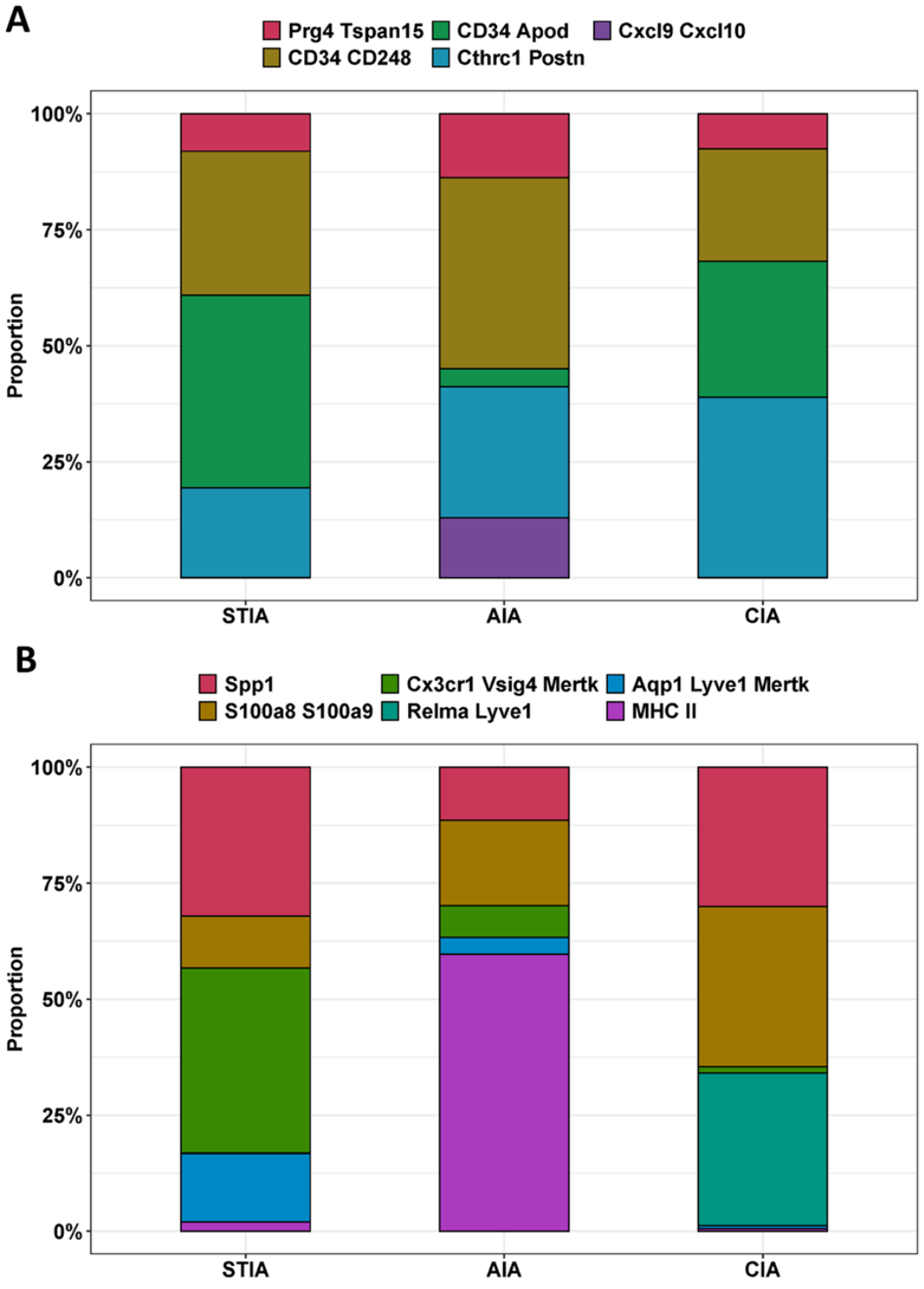

Figure 3.10 Proportions of fibroblast and macrophage populations in each model of arthritis. A) Stacked bar plot showing the relative proportion of each fibroblast subpopulation, of all fibroblasts, in each model of arthritis. B) Stacked bar plot showing the relative proportion of each macrophage subpopulation, of all macrophages, in each model of arthritis.

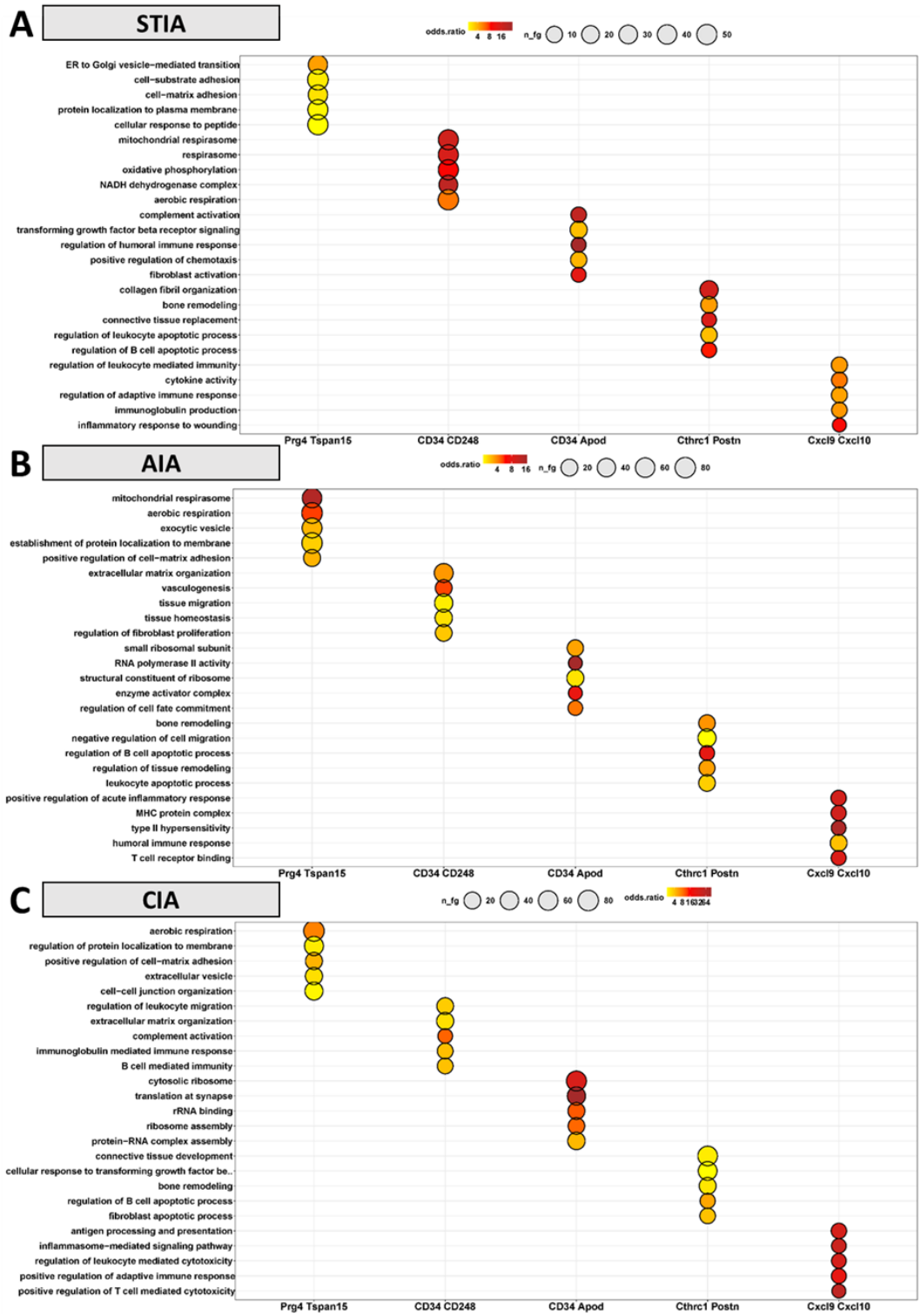

Figure 3.11 Pathway enrichment analysis of fibroblast populations across arthritis models. A) Dot plot showing enrichment of 5 significant Gene Ontology (GO) pathways in each fibroblast population during STIA. B) Dot plot showing enrichment of 5 significant Gene Ontology (GO) pathways in each fibroblast population during AIA.C) Dot plot showing enrichment of 5 significant Gene Ontology (GO) pathways in each fibroblast population during CIA.

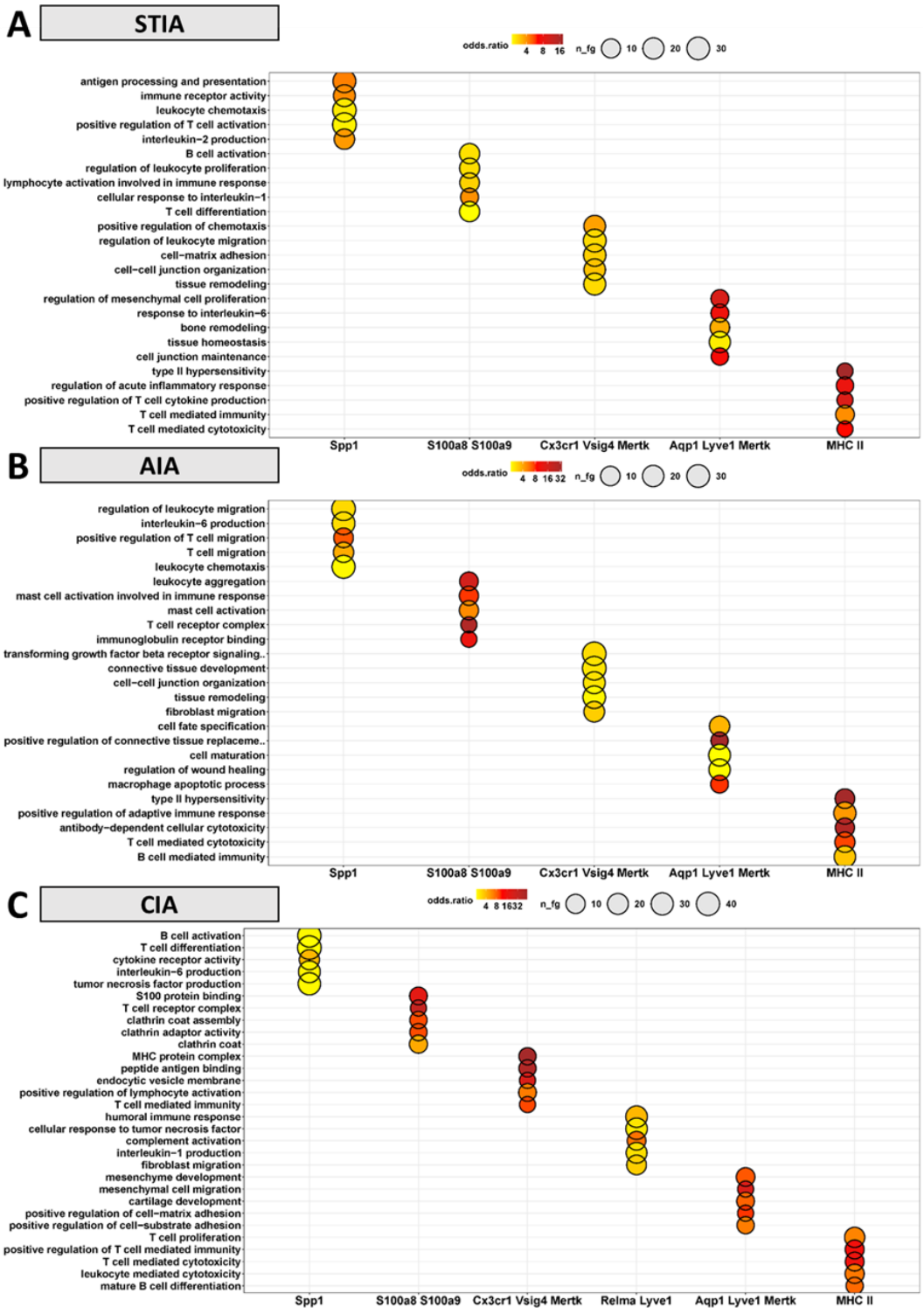

Figure 3.12 Pathway enrichment analysis of macrophage populations across arthritis models. A) Dot plot showing enrichment of 5 significant Gene Ontology (GO) pathways in each macrophage population during STIA. B) Dot plot showing enrichment of 5 significant Gene Ontology (GO) pathways in each macrophage population during AIA.C) Dot plot showing enrichment of 5 significant Gene Ontology (GO) pathways in each macrophage population during CIA.

3.5 Temporal Dynamics

As well as characterising model-specific changes, understanding the dynamic cellular and molecular changes that occur in arthritis is crucial for developing effective treatments and interventions. By analysing time-course data from different mouse models of arthritis, we can identify key transitional states and pivotal time points critical for disease progression or resolution.

Spatial Mapping

This time, spatial distribution plots were employed to display transitional cell-state changes across the time course. The spatial representation of Prg4 Tspan15 fibroblasts changes significantly over the disease course, suggesting they undergo changes in gene expression.

At resting, these cells are mainly in the lower portion of the cluster (Figure 3.13**Error! Reference source not found.**A). Then, at the peak of inflammation there is a shift to the centre of the cluster (Figure 3.13**Error! Reference source not found.**B). During resolution, the central zone of cells is lost, and the lower portion re-emerges along with a group of cells in the upper left-hand side of the cluster (Figure 3.13C), which shift to densely populate the upper left of the plot at the resolved timepoint (D). Similar to the peak of inflammation, during persistent inflammation Prg4 Tspan15 cells are localised in the central zone of the cluster (Figure 3.13**Error! Reference source not found.**E). In contrast, the Cthrc1 Postn cluster remains consistent over time, however, a unique group of cells appears in the upper right part of the plot at the peak of inflammation, not present at other time points (Figure 3.13**Error! Reference source not found.**B). This same group of cells is also seen in persistent inflammation (Figure 3.13**Error! Reference source not found.**E).

Spatial distribution plots also highlight potential changes within macrophage populations across the time course. Cx3cr1 Vsig4 Mertk macrophages are tightly localised to the upper right side of the plot in resting conditions (Figure 3.14A), however, when it re-emerges at the resolving timepoint and in the resolved point it shifts to the left (Figure 3.14**Error! Reference source not found.** C-D), indicating a potential state change or transition following inflammation.

Similarly, MHC II macrophages emerge with a compact cluster on the left of the plot at the peak of inflammation (Figure 3.14**Error! Reference source not found.** B), but as resolution progresses the cluster expands and shifts to the right (Figure 3.14**Error! Reference source not found.** C); the initial cluster is lost all together as the resolved time point (Figure 3.14**Error! Reference source not found.** D). Due to lower cell numbers, the macrophage populations are more difficult to interpret at the persistent timepoint and there don't appear to be any positional shifts that could indicate a state change (Figure 3.14**Error! Reference source not found.** E).

Proportional Changes

Proportional changes across the disease course are observed in both general cell types and sub-populations, and can infer the involvement of a particular cell during that phase of disease.

Some cell types are diminished by the onset of inflammation, such as chondrocytes which are reduced by more than 50% from the resting to peak and persistent time points; however, are recovered once inflammation resolves (Figure 3.15). Vascular

Endothelial cells follow a similar trend, but are not recovered at the resolved timepoint (Figure 3.15**Error! Reference source not found.**).

Other populations increase following the onset of inflammation. Monocytes dominate the initial stages of inflammation, increasing from 24% to 30% from resting to peak, then reducing to 19% and 17% at the resolving and resolved time points, respectively (Figure 3.15**Error! Reference source not found.**). Interestingly, T Cells and DCs increase in proportion during resolution rather than at the peak of inflammation (Figure 3.15).

Fibroblasts are involved in each stage of inflammation, expanding throughout the time course from 26% in the resting joint to 30% at peak then 33% at the resolving time point; they continue to make up a larger proportion (39%) of the resolved joint. They also increase to 29% of the total population in persistent inflammation (Figure 3.15). Similarly, tissue resident macrophages increase with inflammation, but return to their original 20% with resolution (Figure 3.15). Interestingly, macrophages are less prominent in persistent inflammation, making up on 10% of cells (Figure 3.15**Error! Reference source not found.**).

Similar changes in fibroblast and macrophage subpopulations throughout the time course can be observed (Figure 3.16), and may illustrate their importance throughout the course of disease.

Prg4 Tspan15 lining fibroblasts are diminished during inflammation, and even further in persistent inflammation, but do recover upon resolution (Figure 3.16A). Similar dynamics are observed in the Cx3cr1 Vsig4 Mertk lining macrophage population, however in contrast this population expands in persistent inflammation (Figure 3.16B). In the resting joint, most fibroblasts are CD34 C248+ (50%) (Figure 3.16**Error! Reference source not found.**A), and Relma Lyve1 (30%) S100a8 S100a9 (32%) make up most of the macrophage population (B). The synovial environment changes at the peak of inflammation where Cthrc1 Postn (40%), Cxcl9 Cxcl10 (20%) and Cd34 Apod (20%) fibroblasts, and Spp1 macrophages (50%) expanding Figure 3.16A,B). Interestingly, Cxcl9 Cxcl10 fibroblasts and Spp1 macrophages are highly specific to the peak of inflammation, diminished to <1% and 4% of their respective populations at the resolving timepoint (Figure 3.16**Error! Reference source not found.**A,B). They are replaced by a re-expansion of the CD34 CD248 fibroblast population, and emergence of Aqp1 Lyve1 Mertk and MHC II macrophages (Figure 3.16**Error! Reference source not found.**A,B). In the resolved joint, both populations appear to be permanently altered from the resting joint with Cthrc1 Postn fibroblasts, and MHC II macrophages retaining large proportions of the population (Figure 3.16A,B). Interestingly Cxcl9 Cxcl10 fibroblasts, which expand during the peak of inflammation are not present in persistent inflammation, but Spp1 macrophages are dominant in both types on inflammation (Figure 3.16**Error! Reference source not found.**A,B).

These findings highlight the dynamic nature of cellular and molecular changes in arthritis, underscoring the importance of temporal analysis in understanding disease progression and identifying potential therapeutic targets.

Pathway Enrichment Analysis

Under resting conditions, Prg4 Tspan 15 fibroblasts are involved in pathways involved in exocytosis and plasma membrane organisation (Figure 3.17A). During the peak of inflammation, pathways shift focusing on regulation of cell junctions and monocyte activation (Figure 3.17B). During the resolving and resolved phases, Prg4 Tspan15 cells become enriched for pathways associated with respiration and the Golgi membrane (Figure 3.17**Error! Reference source not found.**C,D). In addition, lining fibroblasts at the resolving timepoint become associated with antigen presenting pathways (Figure 3.17C). There is a prominent shift towards cell and tissue migration during persistent inflammation, as well as enrichment in the hyaluronan catabolic process (Figure 3.17,E).

Cd34 Cd248 fibroblasts are associated with regulation of regulation of the development of vasculature and connective tissue at the resting timepoint (Figure 3.17**Error! Reference source not found.**A), and become increasingly enriched for inflammatory pathways and mitochondrially active during the peak of inflammation (Figure 3.17B). They remain associated with pathways involved in cellular stress during the resolving phase (C). Interestingly, following resolution CD34 CD248 fibroblasts become enriched for new pathways involving leukocyte differentiation and

fibroblast proliferation (Figure 3.17**Error! Reference source not found.**D). They appear to be highly active during persistent inflammation, enriched for pathways associated with cytokine production and binding, but also cell stress (**Error! Reference source not found.**E).

CD34 Apod fibroblasts are associated with regulatory pathways at the resting timepoint (Figure 3.17A), however become enriched for osteoclast associated pathways during the peak of inflammation (B). Again, they show signs of cellular stress during the resolving phase, as well as fibroblast proliferation and activation (Figure 3.17C). At the resolved phase, they are still displaying signs of cell stress. They also exhibit enrichment in pathways involved in chromatin regulation (**Error! Reference source not found.**D). During persistent inflammation CD34 Apod fibroblasts are highly enriched for pro-inflammatory pathways, mainly associated with B Cells and the humoral immune response (**Error! Reference source not found.**E).

Cthrc1 Postn fibroblasts as consistently enriched in pathways associated with tissue remodelling, homeostasis and transforming growth factor beta (TGFβ) signalling (**Error! Reference source not found.**A-E). Interestingly, during the peak, resolving and resolved phases of inflammation, these fibroblasts become more associated with apoptosis of leukocytes (**Error! Reference source not found.**B-D). At the resolved timepoint, they are enriched for pathways involved in tolerance induction and negative regulation of inflammation (Figure 3.17D).

Cxcl9 Cxcl10 fibroblasts are consistently associated with pro-inflammatory pathways throughout the time course (Figure 3.17A-E). During peak, resolving and resolved timepoints they are enriched for T Cell associated pathways, CD8 T Cell mediated cytotoxicity (Figure 17B-D). During persistent inflammation, these fibroblasts are more enriched for pathways involved in cytokine and chemokine activity (Figure 3.17E).

Together, these data display the dynamic changes in fibroblast function and state throughout arthritis progression, highlighting key biological processes at various stages of the disease.

Pathway analysis could only be completed for the resting, peak, resolving and resolved timepoints; due to insufficient macrophage numbers at the persistent timepoint.

The Spp1 macrophage population is consistently involved in immune response, antigen processing and T cell activity across all timepoints (Figure 3.17A-D).

Under resting conditions, the S100a8 S100a9 population is involved in pathways related to cell adhesion and granulocyte macrophage colony stimulating factor production (Figure 3.18**Error! Reference source not found.**A). At the peak of inflammation, this population becomes enriched for pathways involved in leukocyte chemotaxis and migration (Figure 3.18**Error! Reference source not found.**B). They switch to B and T Cell related pathways at the resolving timepoint (C), and show

signs of cell stress and chromatin regulation at the resolved timepoint (Figure 3.18**Error! Reference source not found.**D).

Cx3cr1 Vsig4 Mertk lining macrophages switch from a regulatory barrier associated role at resting conditions (Figure 3.18**Error! Reference source not found.**A), to pro-inflammatory pathways at the peak of inflammation (Figure 3.18B). Interestingly, during the resolving and resolved timepoints they become enriched for pathways associated with tissue remodelling, homeostasis and TGFβ signalling (Figure 3.18C-D).

Relma Lyve1 macrophages display enrichment for B Cell associated signalling pathways both at the resting and peak timepoints (Figure 3.18A-B). Pathway analysis could not be performed on this population at the resolving and resolved timepoints due to insufficient cell numbers.

Aqp1 Lyve1 Mertk macrophages display a potential regulatory role, enriched for tissue remodelling and TGFβ signalling during resting conditions (Figure 3.18**Error! Reference source not found.**A). At the peak of inflammation pathways involved in vasculature regulation are enhanced (B). Interestingly, during resolution, another switch is observed to pathways involving mesenchymal regulation and development (Figure 3.18C). At the resolved timepoint, Aqp1 Lyve1 Mertk macrophages are shown to be enriched for pathways involved in responding to inflammation and damage (Figure 3.18D).

MHC II macrophages are consistently enriched in MHC class II protein complex and antigen presentation processes throughout the time course (Figure 3.18A-D), although they do show signs of cell stress at the resolved timepoint (Figure 3.18D).

Overall, when observing the genetic pathways enriched in tissue resident fibroblast and macrophage populations, the intensity and variety of enriched processes change significantly at peak inflammation, with a broader range of immune and inflammatory responses observed. During resolution and resolved phases, there's a shift towards antigen processing, tolerance induction, and tissue remodelling, indicating a transition from active inflammation to immune regulation and tissue repair. Persistent inflammation involves separate and unique inflammatory pathways to the spontaneously resolving course of inflammation.

Pseudotime Trajectory analysis

Pseudotime trajectory analysis was performed on the fibroblast and macrophage subpopulations, as these are novel and less understood. Viewing the trajectory over each point in the time course can help to identify the progression of each subpopulation and transitional states during disease.

At the resting timepoint, fibroblasts are primarily concentrated at the beginning of the pseudotime trajectory, indicating a resting or initial state (Figure 3.19**Error! Reference source not found.**A). Prg4 Tspan 15 fibroblasts form a distinct and separate cluster (Figure 3.19Ai) and are the starting point of the trajectory (Figure 3.19A,ii). All other form two distinct clusters, one for the CD34 Apod population, and

the other for all other cells (Figure 3.19Ai). Both clusters fall at the latest pseudotime timepoint, potentially indicating two separate developmental routes (**Error! Reference source not found.**Aii).

At the peak of inflammation fibroblasts span a wider range of pseudotime, showing progression from an early to a later state. The clusters start to spread out more, indicating diversification in cell states (Figure 3.19B). There's a more distinct progression in pseudotime, with cells spanning from early to later pseudotime states. The Prg4 Tspan15 and CD34 Apod clusters are more dispersed compared to the resting state. CD34 CD248 and Cthrc1 Postn fibroblast clusters are more spread out than previously, indicating diversification or state changes (Figure 3.19Bi). Additionally, Cxcl9 Cxcl10 and Cthrc1 Postn clusters form two distinct branches, which can indicate a response state. Both are at the end point in pseudotime, thus could indicate a responsive state change (**Error! Reference source not found.**Bii).

At the resolving state, more complex branching is evident, indicating a greater diversity of cell states (Figure 3.19C). The pseudotime trajectory shows a wider distribution of cells across the timeline, with clear paths branching out, suggesting differentiation and resolution of cell states.

Prg4 Tspan15 cluster shows further branching and remains spread out (Figure 3.19Ci), and forms a mixed cluster at the end of the pseudotime trajectory (Cii). CD34 Apod cells are still spread out with some branching, but begin to resemble more

distinct clusters again (Figure 3.19Ci). They appear at the start to mid-phase of pseudotime, but are not present at the end of the trajectory (Figure 3.19Cii). CD34 CD248 and Cthrc1 Postn clusters exhibit complex branching patterns, suggesting various resolving states (Figure 3.19Ci). Both cell types are present throughout the pseudotime trajectory, however Cthrc1 Postn fibroblasts form a large cluster as the end stage (Figure 3.19Cii).

At the resolved timepoint the cell states show a more defined structure, but display distinct paths compared to earlier timepoints (Figure 3.19Di). Fibroblasts are distributed across a broader range of pseudotime, indicating that the resolution phase encompasses various cell states from early to late pseudotime (Figure 3.19Dii).

Prg4 Tspan15 fibroblast form a defined and separate cluster (Di), which is once again the starting point in pseudotime (**Error! Reference source not found.**Dii). CD34 Apod cells form a distinct path and cluster (**Error! Reference source not found.**Di), as a mid-stage in pseudotime (Figure 3.19Dii). CD34 CD248 and Cthrc1 Postn clusters are now more distinct and well-separated (**Error! Reference source not found.**Di). Cthrc1 Postn fibroblasts form a branched cluster at the end of the pseudotime, potentially indicating end stage state change or differentiation (**Error! Reference source not found.**Dii).

With persistent inflammation several distinct clusters and branches can be observed indicating distinct cell states (**Error! Reference source not found.**Ei). Fibroblasts appear to be spread out across the pseudotime trajectory, suggesting that persistent cell states have fully developed and maintained their positions (Figure 3.19Eii). Prg4 Tspan15 cluster remains distinct (Figure 3.19Ei), and the starting point of the pseudotime trajectory (Eii). CD34 Apod cells are evenly distributed across the trajectory plot, forming a final densely populated cluster (Figure 3.19Ei). This cluster is the end stage in pseudotime, potentially indicating a transition and state change to this cell type (Figure 3.19Eii). Cthrc1 Postn fibroblasts disperse into a distinct and branched cluster (Ei), that occurs at the mid-stage in pseudotime (Eii); indicating a transitional change that results in a developed and separate population. Looking at the pseudotime trajectory analysis, Prg4analysis, Prg4 Tspan15, Cthrc1 Postn, and CD34 Apod fibroblasts appear to be terminally differentiated cell states that emerge at different points along the time course. They also display evidence of diversity within the population over the time course. CD34 CD248 and Cxcl9 Cxcl10 fibroblast appear to be more responsive, transitional states than differentiated fibroblast subsets.

Key transitional states can also be identified in pseudotime trajectory analysis of macrophage populations. Under resting conditions, the clusters are distinct and compact and show a smooth trajectory (Figure 3.20A). S100a8 S100a9 macrophages forming a clear and distinct cluster, indicating a separate cell state (Figure 3.20Ai). Relma Lyve1 are the dominant cell type the beginning of the trajectory, with other macrophage populations emerging later (Figure 3.20Aii).

At the peak of inflammation more branching and dispersing of cells is observed (Figure 20 B). There is a transitional phase to Spp1 macrophages that occurs early in the trajectory, resulting in two distinct clusters of either Spp1 or S100a8 S100a9 macrophages) (Figure 3.20Bi,ii). MHC II macrophages form a more dispersed population (Figure 3.20i), that emerges at the end of the trajectory (Bii). During resolution, a smoother and less branched trajectory returns (C).

A transition is shown from MHC II macrophages, to either S100a8 S100a9 or Cx3cr1 Vsig4 Mertk and Aqp1 Lyve1 Mertk macrophages (Figure 3.20C I,ii). The trajectory at the resolved state is highly distinct from the resting state, suggesting cell state changes may have occurred (Figure 3.20 D). Aqp1 Lyve1 and Cx3cr1 Vsig4 Mertk macrophages form distinct clusters at the beginning of the trajectory (Figure 3.20**Error! Reference source not found.**D I,ii).

MHC II macrophages emerge later in the time course, interestingly forming 3 distinct clusters indicating potential transition into different terminally differentiated states (Figure 3.20D, I,ii). Macrophages are sparse in persistent inflammation but indicate a transition from Aqp1 Lyve1 Mertk and Cx3cr1 Vsig4 Mertk macrophages to either MHC II or S100a8 S100a9 macrophages as the pseudotime progresses (Figure 3.20E I,ii).

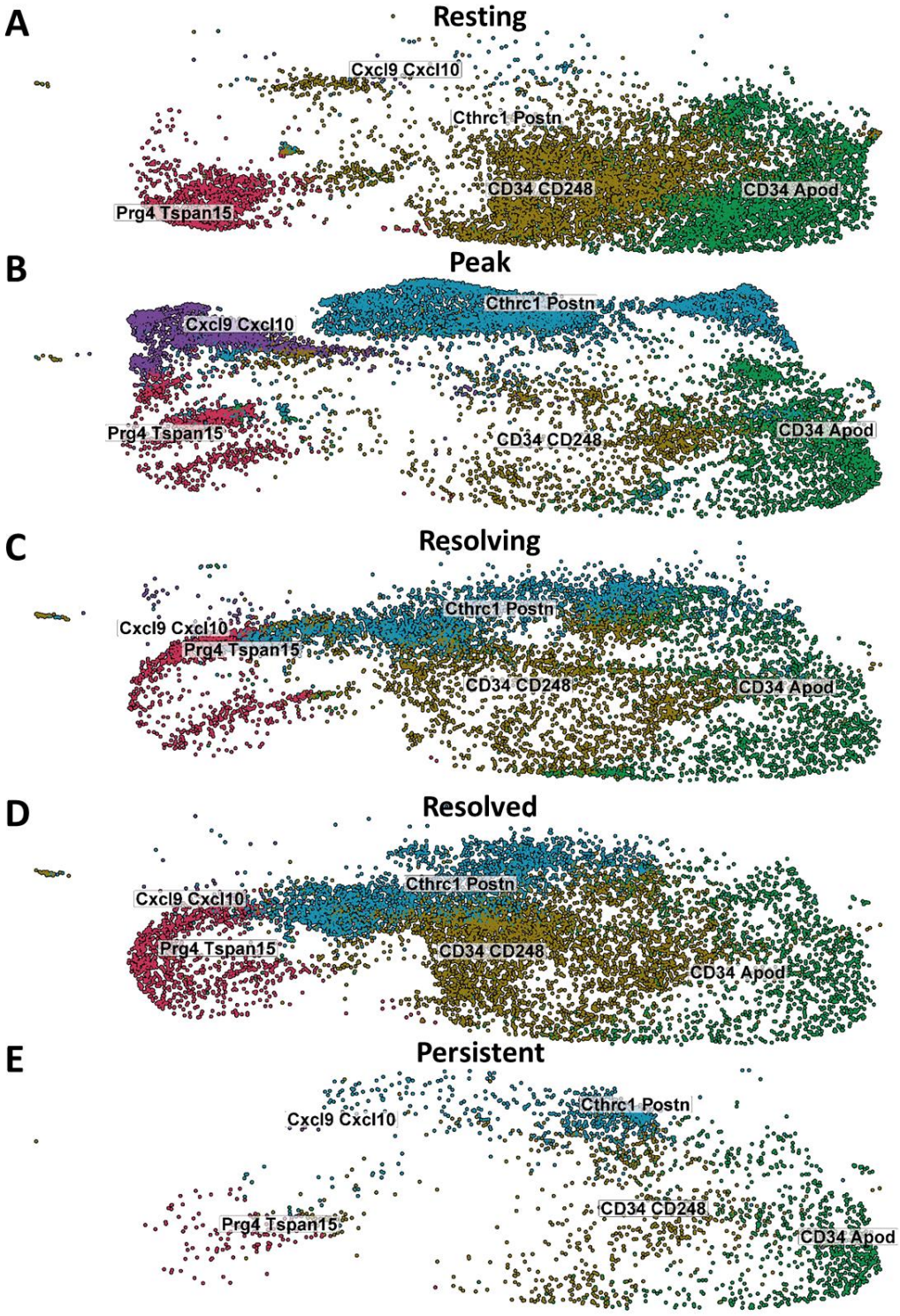

Figure 3.13 Temporal spatial distribution of fibroblast subpopulations. A) UMAP of fibroblast subpopulations at the resting timepoint. B) UMAP of fibroblast subpopulations at the peak timepoint. C) UMAP of fibroblast subpopulations at the resolving timepoint. D) UMAP of fibroblast subpopulations at the resolved timepoint. E) UMAP of fibroblast subpopulations at the persistent timepoint.

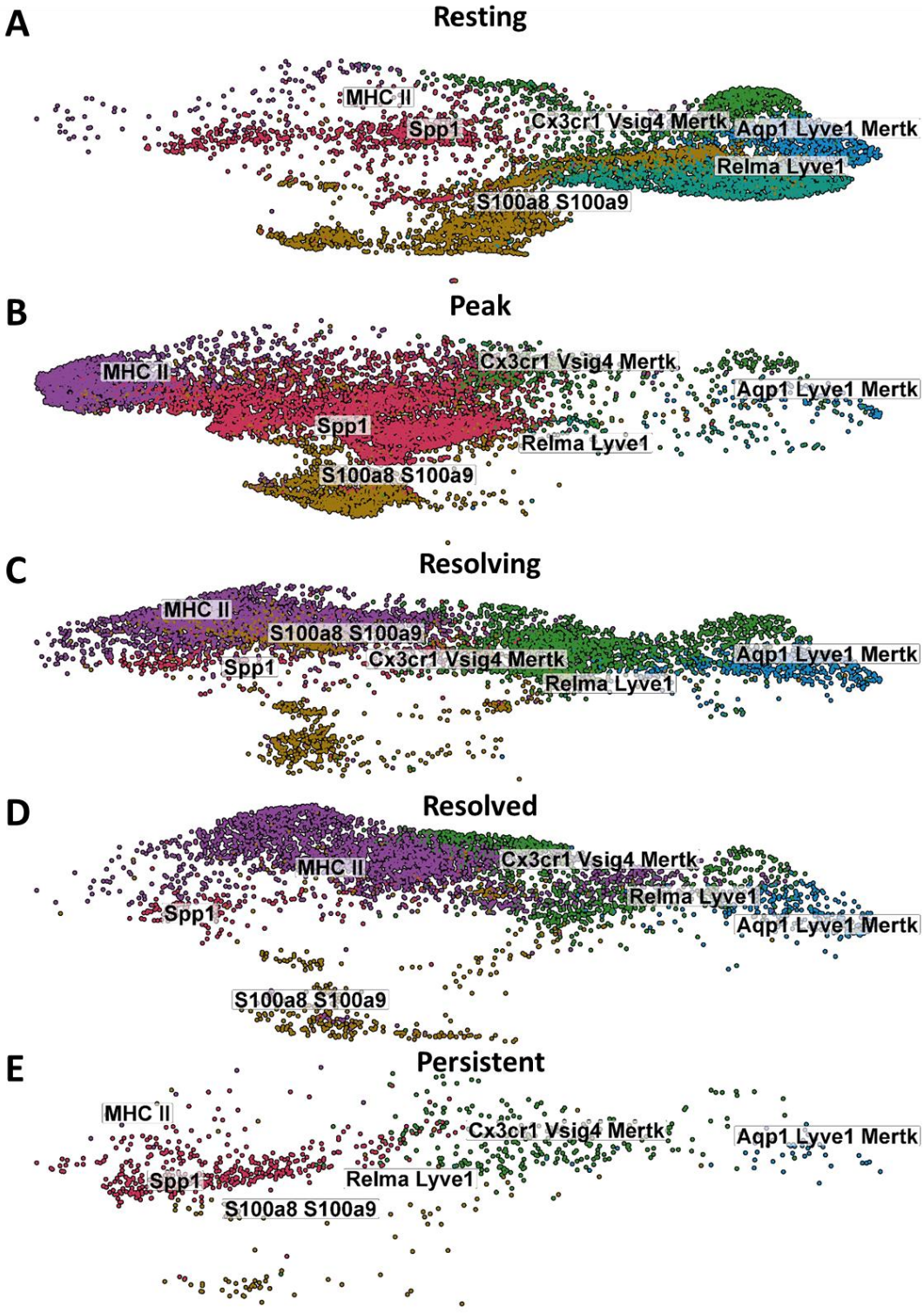

Figure 3.14 Temporal spatial distribution of macrophage subpopulations. A) UMAP of macrophage subpopulations at the resting timepoint. B) UMAP of macrophage subpopulations at the peak timepoint. C) UMAP of macrophage subpopulations at the resolving timepoint. D) UMAP of macrophage subpopulations at the resolved timepoint. E) UMAP of macrophage subpopulations at the persistent timepoint.

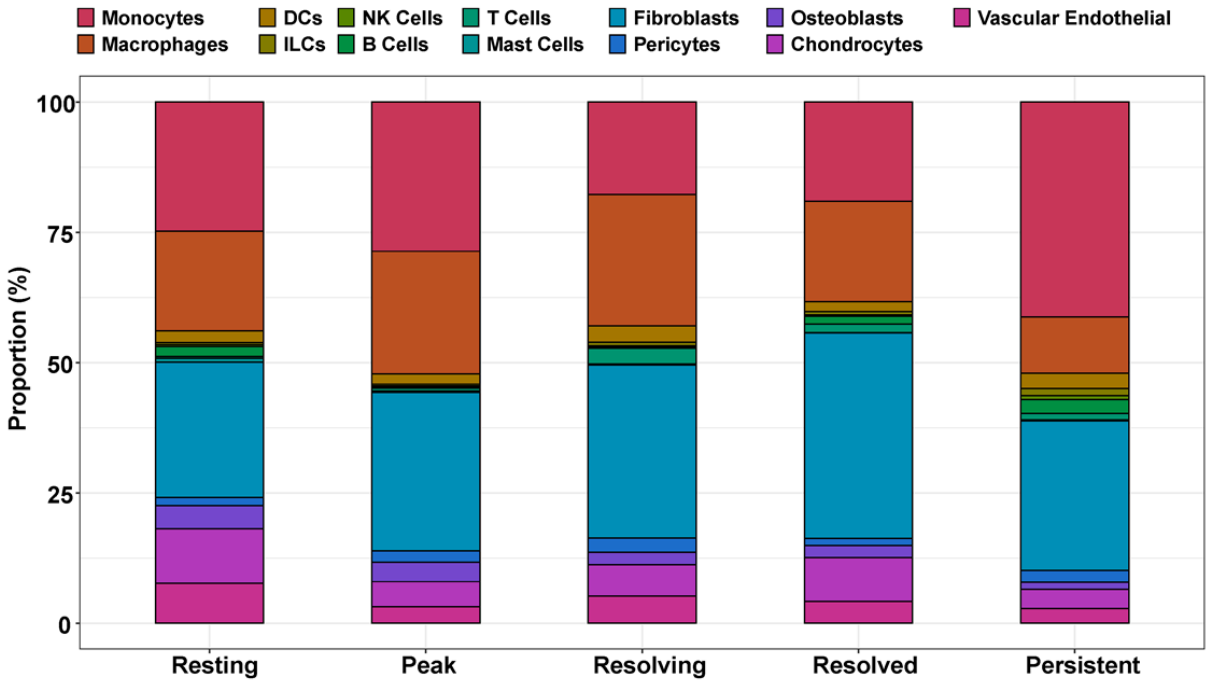

Figure 3.15 Proportions of general cell populations across the time course of inflammatory arthritis. Stacked bar plot showing the relative proportion of each cell type of the whole cell population at each disease state.

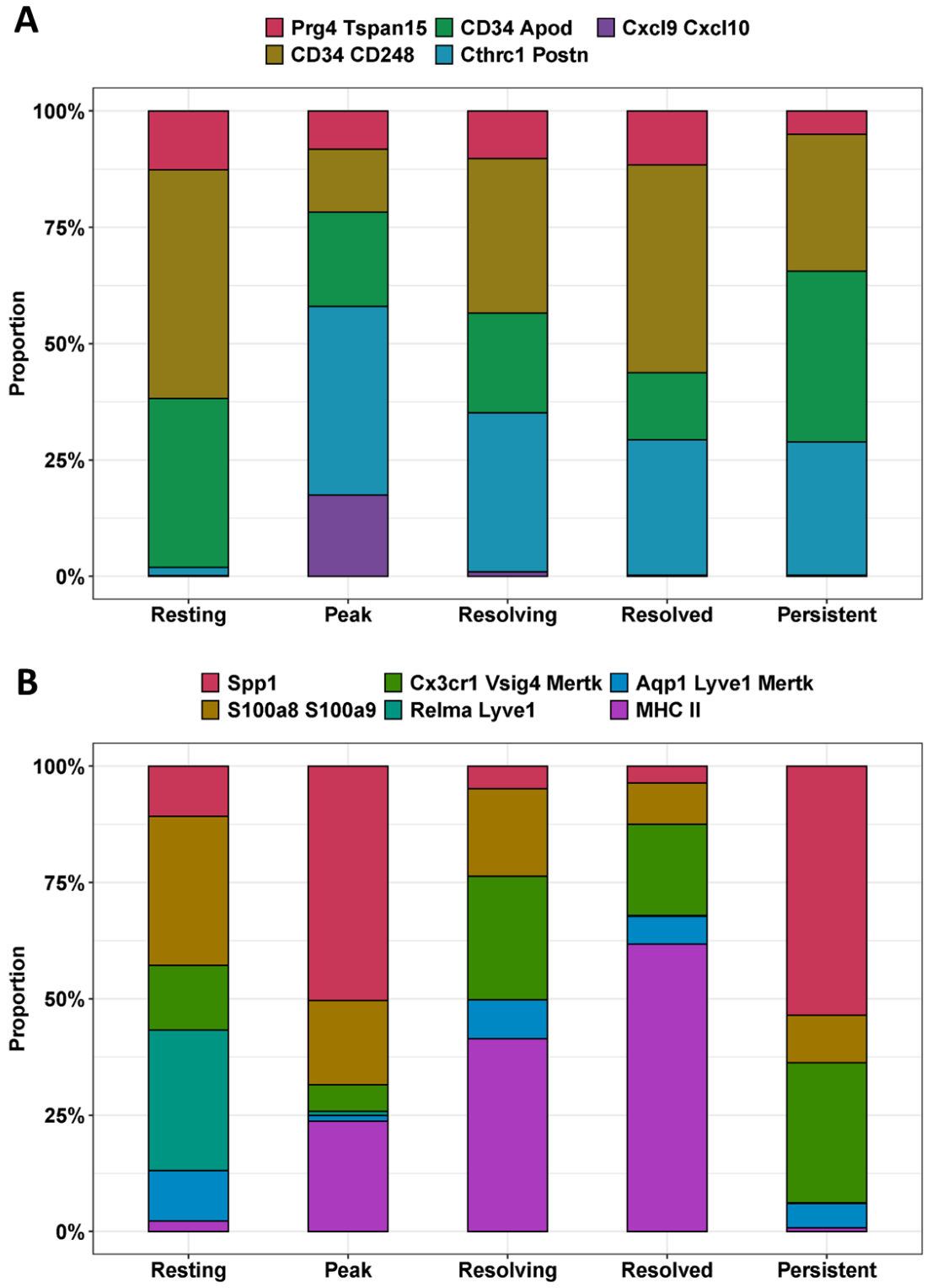

Figure 3.16 Proportions of fibroblast and macrophage populations across the time course of inflammatory arthritis. A) Stacked bar plot showing the relative proportion of each fibroblast subpopulation, of all fibroblasts, at each time point. B) Stacked bar plot showing the relative proportion of each macrophage subpopulation, of all macrophages, at each time point.

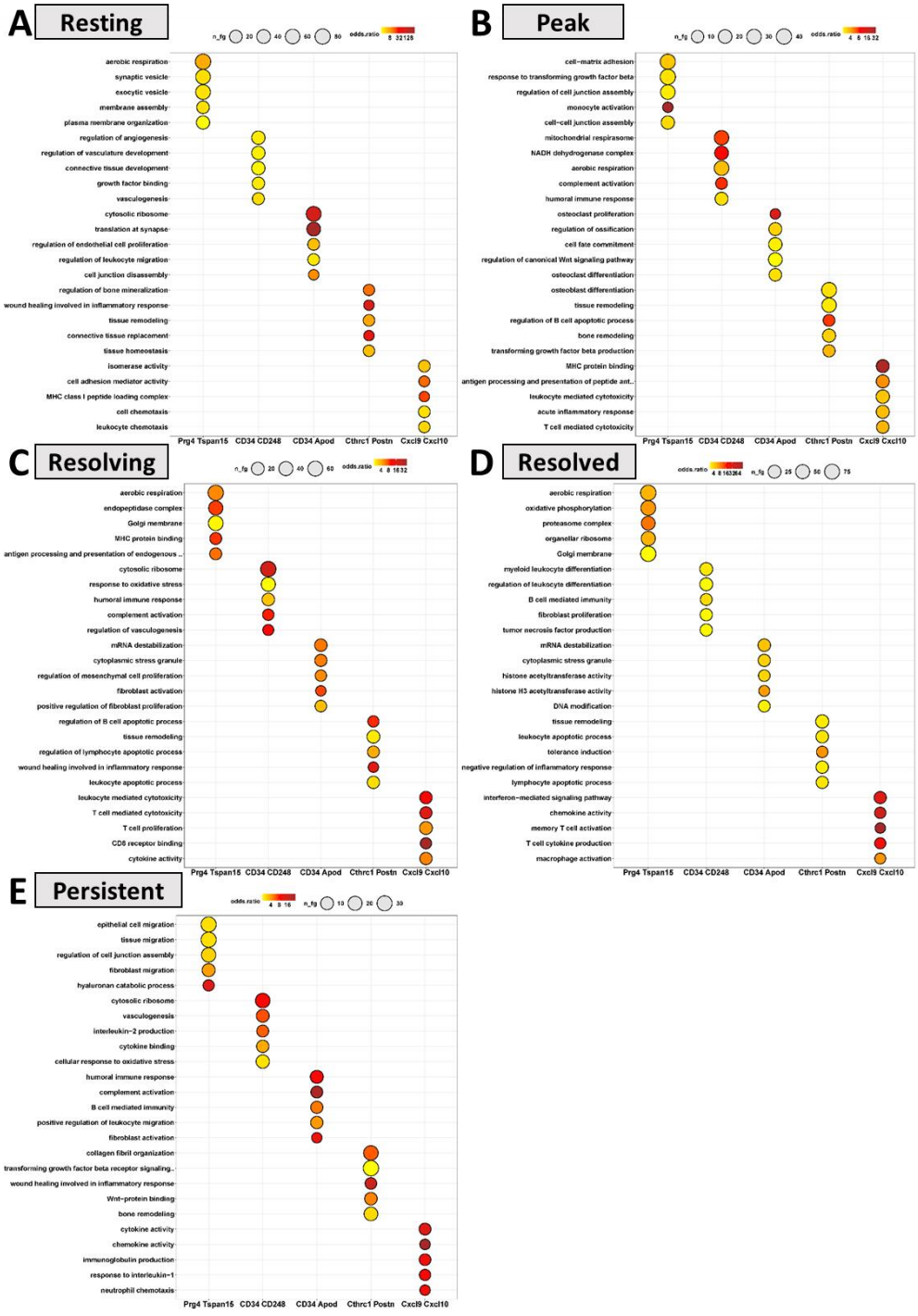

Figure 3.17 Pathway enrichment analysis of fibroblast populations at each time point. Gene Ontology (G) pathways enriched in each fibroblast population at A) the resting time point. B) the peak time point. C the resolving time point. D) the resolved time point. E) the persistent time point.

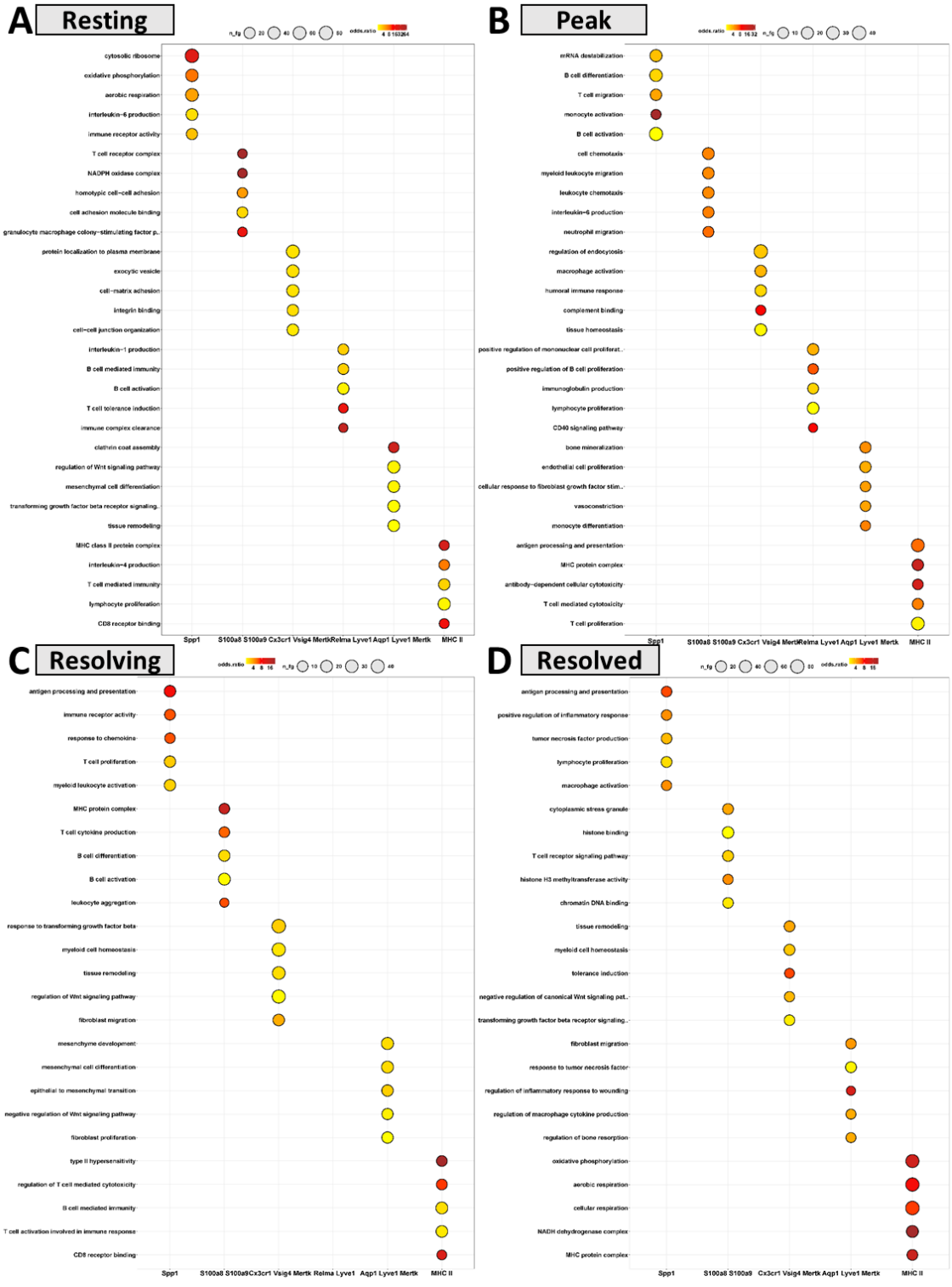

Figure 3.18 Pathway enrichment analysis of macrophage populations at each time point. GO pathways in each macrophage population at A) the resting time point. B) the peak time point. C) the resolving time point. D) the resolved time point.

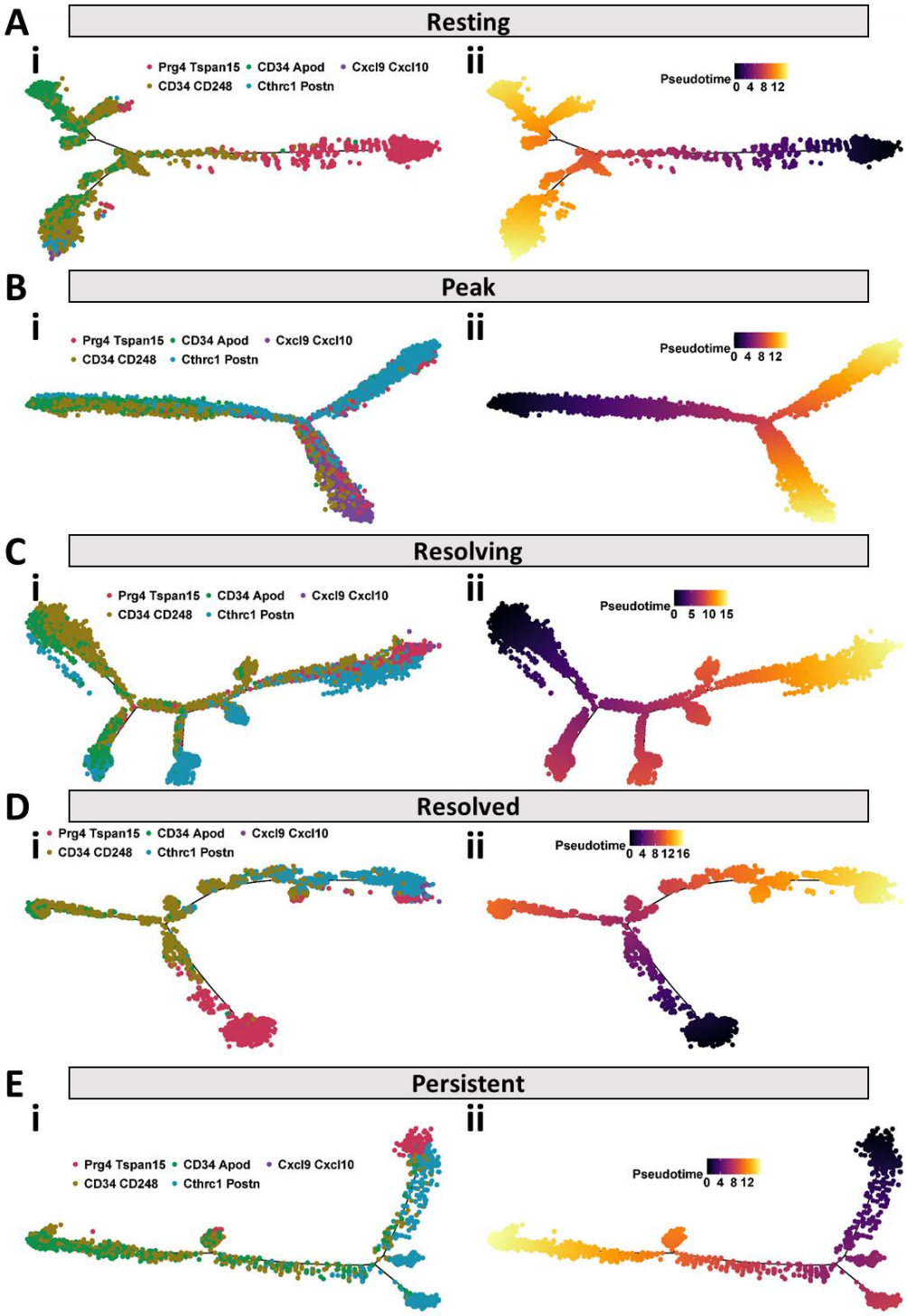

Figure 3.19 Pseudotime trajectory analysis of fibroblast populations at each time point. (A-E) Spatial projection plots representing cellular states at: Resting (A), Peak (B), Resolving (C), Resolved (D), and Persistent (E). (i) Each plot shows cells coloured by fibroblast population. (ii) Corresponding pseudotime trajectories for each stage, where cells are coloured based on their pseudotime values. The pseudotime scale ranges are shown in the legend next to each plot, indicating progression through the biological process.

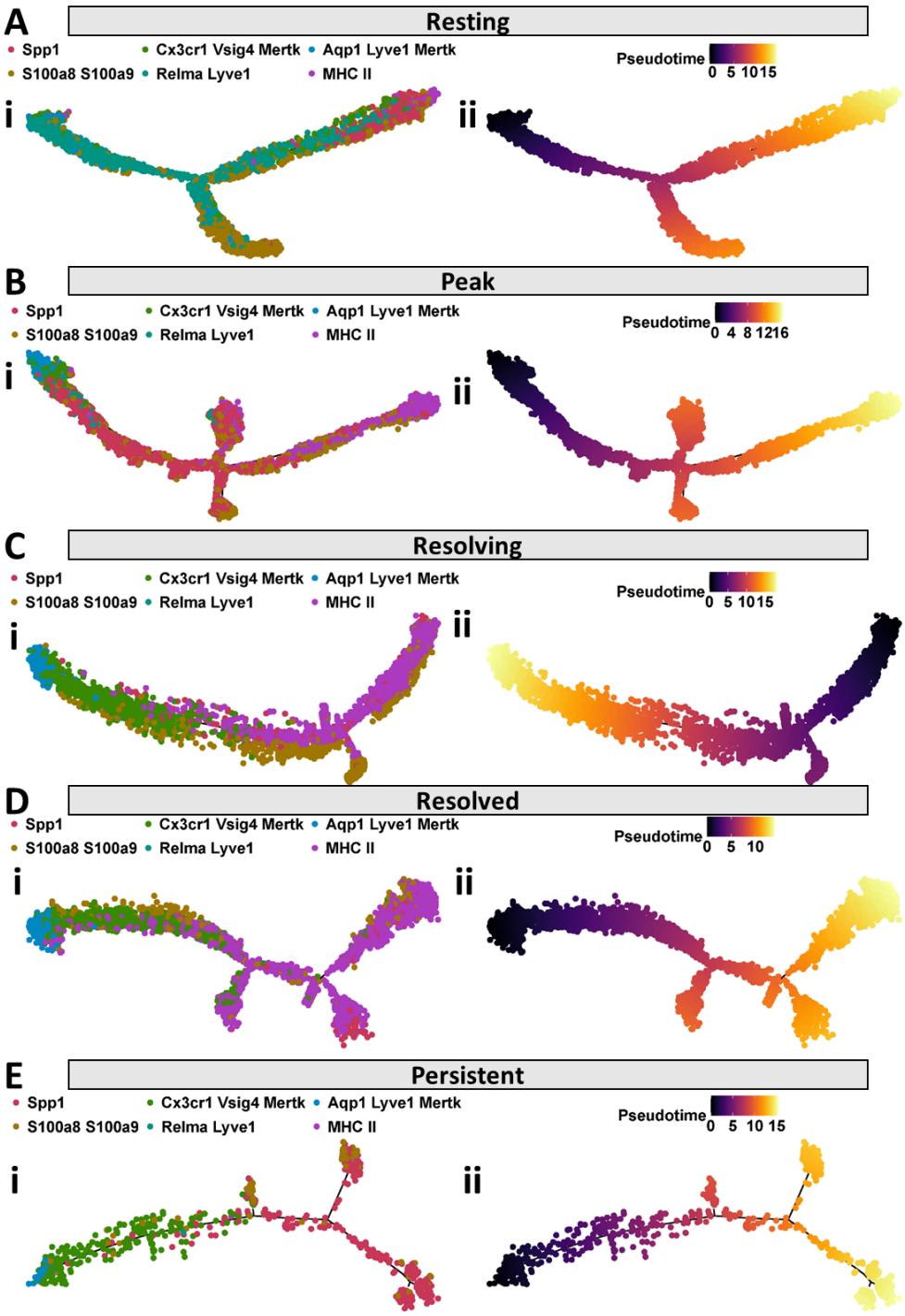

Figure 3.20 Pseudotime trajectory analysis of macrophage populations at each time point. (A-E) Spatial projection plots representing cellular states at: Resting (A), Peak (B), Resolving (C), Resolved (D), and Persistent (E). (i) Each plot shows cells coloured by macrophage population. (ii) Corresponding pseudotime trajectories for each stage, where cells are coloured based on their pseudotime values. The pseudotime scale ranges are shown in the legend next to each plot, indicating progression through the biological process.

3.6 Chapter discussion

3.6.1 Meeting the aims

I have successfully met the aims of this chapter, by defining the tissue resident fibroblast and macrophages subpopulations within the mouse synovium within an atlas of murine inflammatory arthritis. I have outlined the key populations present in each model and their predicted roles (Table 3.3) as well as the temporal dynamics of inflammatory arthritis Table 3.4 & Table 3.5. The mechanisms driving the transition between disease states in human and mouse inflammatory arthritis are poorly understood. I have used this atlas to identify key targets and mechanisms for disease pathology and resolution.

3.6.2 Overall findings

Although a comprehensive overview of fibroblast and macrophage populations within the mouse synovium has not yet been conducted, the subpopulations identified within this atlas align with recent publications.

Prg4+ Tspan15+ fibroblasts are well established as lining layer fibroblasts in the synovium. They play a critical role in lubricating joints and maintaining cartilage health during homeostasis, but have been shown to promote bone erosion in murine inflammatory arthritis[42].

Cd34+ fibroblasts have previously been characterised as vascular associated cells involved in tissue regulation and homeostasis[32,42,58]. CD34+ CD248+ fibroblasts were recently described in myocardial fibrosis, and associated with vascular regulation[176]. CD34+ Apod+ fibroblasts are thought to be involved in pro-inflammatory pathways and NOTCH3-mediated differentiation[32,42,58]. More recently, they have been

described as a universal fibroblast population, and suggested as potential progenitors to myofibroblast populations[177] .

Fibroblasts expressing elevated levels of Cxcl9 and Cxcl10 have been described in various cancer settings, and are associated with pro-inflammatory responses particularly involving T Cells[177–179].

Cthrc1 Postn fibroblasts in this dataset closely resemble myofibroblasts, which have been associated with tissue repair, fibrosis and remodelling (reviewed in [180]). Recently, Dakin et al[181] described a population of DKK3+ myofibroblasts in adhesive capsulitis, commonly known as frozen shoulder, responsible for driving resolution of inflammation and tissue repair.

Identifying macrophage populations within this atlas was challenging due to limited literature and conflicting results with published works. Markers to distinguish tissue resident from infiltrating macrophages in mouse synovium are poorly defined. While some studies consider F4/80 (Adgre1 in mice) a specific macrophage marker[182–184] it is increasingly viewed as outdated, with expression noted in various monocyte populations[185–191], and even myofibroblasts[192]. Some studies suggest F4/80 can distinguish tissue resident from infiltrating macrophages[193,194], but this remains contested [191].

Similarly, while MerTK is cited as a marker of tissue residency, evidence shows it is also expressed in various macrophages. CD64 (Fcgr1 in mice) has been proposed as a marker of tissue residency in murine macrophages, yet evidence is inconsistent[195,196]. Current scRNAseq studies examining macrophages in humans

and mice utilise varying identification strategies for tissue resident macrophages, often lacking specificity and allowing for contamination by infiltrating macrophages and monocytes. For example, Culemann et al. performed a comprehensive scRNAseq analysis of synovial macrophages, finding that those in the lining layer expressed high CX3CR1 levels and exhibited protective barrier functions. They identified four additional macrophage populations but did not exclude monocytes in their sorting strategy, potentially compromising downstream analysis[37]. This may account for discrepancies between the macrophage populations identified in this atlas, and other studies.

Defining monocytes and infiltrating macrophages proved challenging. High Ly6C and CCR2 expression mark both cell types present in the entire monocyte/macrophage population. I classified monocytes (Ly6chi Ccr2hi F480low Cd64low Mertklow), tissue infiltrating macrophages (Ly6chi Ccr2hi F480 moderate/high Cd64low MerTKmoderate/high), and tissue resident macrophages (Ly6Clow Ccr2low F480hi Cd64hi MerTKhi) using Ly6C, CCR2, F4/80, CD64, and MerTK (Supplementary figure 4). While these profiles align with recent literature, the cell types demonstrated gene expression like either monocytes or tissue resident macrophages, lacking clear distinction between tissue resident and infiltrating macrophages. Some monocyte populations, like Spp1 and S100a8 S100a9, resembled highly inflammatory tissue infiltrating populations, but their high F4/80, MerTK, and CD64 expression contradicted this.

Further insights into specific markers of macrophage tissue residency, particularly in the synovium, are necessary to confidently define these populations.

The assigned cell types align with recent standards, allowing me to proceed with the cellular atlas analysis. A key advantage of scRNAseq data is the potential for future re-analysis and re-clustering as new studies emerge and more definitive methods for defining synovial cell populations are developed.

Model-specific mechanisms

The mechanisms of each model in inflammatory arthritis featured in the atlas are well characterised. This atlas can confirm those findings and uncover potential novel mechanisms involving newly identified cell populations.

STIA involves a complex humoral immune response to immune complexes formed by autoantibodies in K/BxN serum, driven by Cd34+ Apod+ fibroblasts and Spp1+ and S100a8 S100a9 macrophages. Notably, Cd34+ Cd248+ fibroblasts uniquely upregulate genes related to mitochondrial respiration, likely due to increased oxidative stress from monocyte influx.

CIA is governed by an adaptive immune response led by T and B Cells. Our data indicate that Cd34+ Apod+ and Cd34 Cd248+ fibroblasts are crucial, with Cd34+ Cd248+ fibroblasts specifically involved in B Cell-mediated immunity and complement response. Unlike other models, Cx3cr1+ Vsig4+ Mertk+ macrophages become more pro-inflammatory in CIA. Notably, Spp1+ and S100a8 S100a9 macrophages shift roles compared to STIA; Spp1 macrophages now participate in B Cell response, while S100a8 S100a9 macrophages regulate T Cell responses and

antigen presentation. Relma Lyve1 macrophages also play a distinct pro-inflammatory role in CIA, where they are most abundant.

AIA features significant monocytic infiltration driven by T cell responses to joint antigens, influenced by Cxcl9 and Cxcl10 fibroblasts, along with MHC II and S100a8/S100a9 macrophages. Abundant CD34/CD248 fibroblasts are notably involved in vasculogenesis, potentially supporting the inflammatory response. The abundance of MHC II macrophages in the AIA model is also an interesting area to further explore. The large abundance of these cells in AIA compared to other models could be due to the direct administration of antigen to the joint in order to initiate joint inflammation. This could make AIA a key model for use in exploring the mechanisms of antigen presentation in RA.

Remarkably, Aqp1/Lyve1/Mertk macrophages are specific to STIA and AIA, where they contribute to wound healing and tissue repair. Similarly, Cthrc1/Postn fibroblasts, present in all three models, play roles in matrix remodelling and tissue homeostasis, suggesting their importance in inflammation resolution, as CIA lacks both populations and does not resolve spontaneously. Indeed, MerTK^{hi} macrophages are linked to remission and repair in rheumatoid arthritis[70].

A review analysing scRNAseq data from human and mouse macrophages reached somewhat conflicting conclusions [197]. It identified Aqp1 MHC II macrophages as a pro-inflammatory tissue-infiltrating phenotype, though these had been previously classified as two distinct tissue-resident macrophage populations[37]. The review

highlighted significant differences between human and mouse macrophage populations, indicating that caution is necessary when comparing them, and further research is needed to fully characterise these cells.

Temporal Mechanisms

The resting synovium mainly comprises Prg4 Tspan15 lining layer fibroblasts, CD34 CD248 and Cd34 Apod sublining fibroblasts, as well as Cx3cr1 Vsig4 Mertk lining layer macrophages and Aqp1 Lyve1 Mertk, Relma Lyve1, and Spp1 sublining macrophages. Excluding Spp1 macrophages, this aligns with our understanding of a healthy joint. Lining fibroblasts produce lubricin and hyaluronic acid, aiding joint movement, while lining macrophages create a barrier to maintain the synovial membrane's structure and integrity.

CD34+ fibroblasts are linked to tissue homeostasis and represent the resting fibroblast phenotype in the synovium. Recent fate mapping showed that MHC II macrophages repopulate Cx3cr1+ and Relma+ macrophages in the synovium[37]. Aqp1+ macrophages were noted in the same study, but their role remains unclear. The presence of Spp1 macrophages is concerning since they exhibit a pro-inflammatory phenotype and haven't been identified as a resident population.

Additionally, the abundant monocytes at rest are puzzling, as they are typically thought to infiltrate the joint only during inflammation. A recent study identified tissue resident monocytes[198], but I could not correlate the populations in that study with those in this atlas, making this an intriguing area for further research. Small populations of various leukocytes in the resting joint indicate that the prevailing view

of healthy synovium as comprising solely tissue-resident fibroblasts and macrophages may be incomplete.

At the peak of inflammation, previously unidentified tissue resident populations play distinct roles. Pro-inflammatory Cxcl9 and Cxcl10, along with anti-inflammatory and tissue remodelling Cthrc1 Postn, emerge alongside each other, highlighting their opposing functions. CD34+ Apod+ fibroblasts are implicated in osteoclast regulation and Wnt signalling. Additionally, the emergence of pro-inflammatory MHC II, Spp1, and S100a8 S100a9 macrophages indicates specific subsets driving inflammation in the synovium.

During resolution, the loss of Cxcl9 Cxcl10 fibroblasts is striking, and the mechanisms involved in clearing or re-programming these cells would be an interesting area to investigate. A return to the resting joint is observed, with the re-emergence of CD34 CD248 fibroblasts and Aqp1 Lyve1 Mertk macrophages. The maintained expansion of Cthrc1 Postn fibroblasts could suggest they play a role in driving and maintaining resolution, and at this time point they also become associated with apoptotic clearance of inflammatory infiltrate.

The resolved joint largely resembles the resting joint, but some populations, such as Cd34 Cd248 fibroblasts, exhibit changes due to inflammation, maintaining a proinflammatory phenotype. Cx3cr1 lining macrophages play a greater role in tissue remodelling and homeostasis, engaging in anti-inflammatory pathways like TGFβ signalling and negative Wnt signalling regulation, indicating they may be involved in repairing joint damage. Meanwhile, MHC II macrophages remain abundant at the

resolved timepoint but show signs of stress and exhaustion, likely working to replenish homeostatic macrophage populations. An exploration of a later timepoint would be valuable to determine whether this population decreases or persists. Cthrc1 postn fibroblasts and Aqp1 Lyve1 Mertk macrophages persist after joint inflammation resolves, contributing to tissue remodelling, immune tolerance, and wound healing. This supports the hypothesis that these populations play a crucial role in resolving joint inflammation.

The synovial environment in persistent inflammation distinctly differs from other stages, representing a separate model of inflammation rather than merely an additional time point in arthritis. The fibroblast population in persistently inflamed joints primarily consists of Cthrc1 Postn and Cd34 Apod fibroblasts, which have opposing functions. The absence of a Cxcl9 Cxcl10 proinflammatory fibroblast population is expected, as this appears to be specific to the AIA model. Spp1 macrophages dominate in persistent inflammation, yet there is no disruption of Cx3cr1 Vsig4 Mertk barrier macrophages, unlike in other models, suggesting this disruption is not critical for initiating synovial inflammation, which was previously thought to be the case. The presence of Cthrc1 Postn fibroblasts might indicate induction by inflammatory signals. Furthermore, the lack of Aqp1 Lyve1 Mertk macrophages and resolution of inflammation may signify a key relationship between these cell types in the resolution process.

3.6.3 Conclusion

In summary, whilst further functional work is required to validate the findings within this work, it highlights the dynamic changes that occur synovial fibroblast and macrophage populations over the course of inflammatory arthritis. It can be used to identify novel cellular and molecular targets, in particular for treatment resistant RA patients. Additionally, the insight into model-specific mechanisms can help to streamline the research process and select the best model for each research hypothesis.

Table 3.3 Fibroblast and macrophage subsets in a murine atlas of inflammatory arthritis

Cell Type	Subset	STIA	CIA	AIA
Fibroblasts	Prg4+ Tspan15+	Synovial lining cells, maintain cartilage health	Present, support lubrication	Present, support lubrication
	Cd34+ Apod+	Pro-inflammatory, involved in osteoclast regulation, Wnt signalling	Drive B cell immunity, complement response	Contribute to vasculogenesis and inflammation
	Cd34+ Cd248+	Upregulate mitochondrial respiration due to oxidative stress	Regulate B cell-mediated immunity, complement response	Support vasculogenesis and T cell response
	Cxcl9+ Cxcl10+	Not detected	Emergent in peak inflammation, support T cell responses	Highly pro-inflammatory, drive T cell responses
	Cthrc1+ Postn+	Tissue repair, matrix remodelling	Absent	Tissue repair, matrix remodelling
Macrophages	Spp1+	Drive inflammation, possibly tissue infiltrating	Shift to B cell response, regulate antigen presentation	Involved in regulating T cell response
	S100a8+ S100a9+	Inflammatory, may regulate monocyte recruitment	Regulate T cell response, antigen presentation	Regulate T cell response, antigen presentation
	Cx3cr1+ Vsig4+ Mertk+	Pro-inflammatory role	Shift toward pro-inflammatory function	Barrier function disrupted
	Relma+ Lyve1+	Tissue remodelling and repair	Pro-inflammatory	Contribute to tissue repair
	Aqp1+ Lyve1+ Mertk+	Wound healing, resolution of inflammation	Absent	Present, contribute to tissue repair
	MHC II+	Promote pro-inflammatory responses	Regulate T cell responses	Pro-inflammatory, drive T cell response

Table 3.4 Fibroblast subsets across the time course of murine inflammatory arthritis

Cell Type	Subset	Resting	Peak	Resolving	Resolved	Persistent
Fibroblasts	Prg4+ Tspan15+	Lubricate joints, maintain cartilage health	Present, maintain synovial lubrication	Present, still functioning to lubricate joints	Restored to normal function	Reduced, but may persist for lubrication
	Cd34+ Apod+	Homeostasis, resting fibroblast phenotype	Pro-inflammatory, osteoclast regulation, Wnt signalling	Start to revert to homeostasis, some remain pro-inflammatory	Restored to homeostatic fibroblast population	Promote chronic inflammation
	Cd34+ Cd248+	Homeostasis, resting fibroblast population	Pro-inflammatory, involved in immune regulation	Begin returning to homeostasis, contribute to tissue repair	Restored to homeostasis	Persist with pro-inflammatory phenotype
	Cxcl9+ Cxcl10+	Absent	Emerge as pro-inflammatory fibroblasts, drive T cell response	Begin clearing, involved in reducing T cell responses	Cleared during resolution	Absent
	Cthrc1+ Postn+	Absent/low	Involved in tissue remodelling and repair	Tissue remodelling, begin apoptosis clearance	Persist, involved in tissue homeostasis	Drive tissue remodelling and chronic inflammation

Table 3.5 Macrophage subsets across the time course of murine inflammatory arthritis

Cell Type	Subset	Resting	Peak	Resolving	Resolved	Persistent
Macrophages	Spp1+	Absent or very low levels	Pro-inflammatory, regulate immune cell infiltration	Begin decreasing, contribute to tissue repair	Return to homeostasis, involved in apoptotic cell clearance	Dominant pro-inflammatory macrophage population
	S100a8+ S100a9+	Absent or very low levels	Pro-inflammatory, involved in T cell regulation and antigen presentation	Start reducing, shift towards anti-inflammatory roles	Reduced to resting levels	Persist with pro-inflammatory functions
	Cx3cr1+ Vsig4+ Mertk+	Barrier function, maintain synovial structure	Barrier function disrupted	Restoring barrier function, tissue repair	Fully restored, maintain tissue homeostasis	Maintain barrier, involved in homeostasis
	Relma+ Lyve1+	Tissue homeostasis, regulate tissue integrity	Pro-inflammatory, involved in inflammation	Shift towards tissue repair and resolution	Persist, involved in tissue repair and homeostasis	Persist, involved in tissue repair and immune regulation
	Aqp1+ Lyve1+ Mertk+	Absent or unclear role	Contribute to tissue repair and wound healing	Active in tissue remodelling and inflammation resolution	Persist, support tissue repair and immune tolerance	Absent
	MHC II+	Absent or low levels	Pro-inflammatory, regulate immune responses	Show signs of exhaustion, involved in clearing apoptotic cells	Exhibit exhaustion, still working to replenish macrophage populations	Exhibit exhaustion, involved in tissue homeostasis

4 INVESTIGATING FIBROBLAST-MEDIATED MECHANISMS OF PERSISTENCE IN INFLAMMATORY ARTHRITIS

4.1 Introduction

As discussed in Chapter 1, synovial fibroblasts play a significant role in the pathogenesis of RA. These specialised mesenchymal cells not only perpetuate inflammation but also actively participate in the recruitment of immune cells into the joint, contributing to tissue destruction and disease progression [45]. Historically, treatment of RA has been highly focused on immune cells, however fibroblasts are now recognised as key players in both the initiation and persistence of chronic joint inflammation [46], and targeting them could be the key to breaching the therapeutic ceiling of intervention observed in RA.

It has been observed that patients who do not respond to conventional treatments often exhibit an enrichment of fibroblasts within their synovium, in contrast to treatment responders who tend to show increased leukocyte infiltration. Despite the critical role of fibroblasts in RA, the development of therapeutics targeting these cells remains a challenge [42], and no current therapies targeting fibroblasts are used in the treatment of RA.

Early studies into fibroblast heterogeneity identified several markers, such as Cadherin-11 [48], THY1, and fibroblast activation protein (FAP)[199] , which define inflammatory fibroblast subsets. However, it has become clear that even within these subsets, a more complex functional diversity exists. For example, while THY1+ FAP+ fibroblasts have been shown to drive inflammation [42], more recent work has revealed that certain THY1+ fibroblast subsets may also contribute to the resolution of

inflammation and tissue homeostasis [35]. This highlights the need for a deeper understanding of fibroblast biology to inform the development of more targeted and effective therapies for RA.

Wnt Signalling in RA

One promising area of research into synovial fibroblast biology is the role of Wnt signalling. The Wnt pathway, known for its role in tissue development and homeostasis, has also been implicated in pathological processes such as cancer and fibrosis [200]. In the context of RA, dysregulated Wnt signalling appears to contribute to the aberrant behaviour of synovial fibroblasts, driving both inflammation and tissue damage [201].

Wnt Signalling in Health and Disease

The Wnt signalling pathway is highly conserved and regulates a wide array of biological processes, including cell proliferation, migration, and differentiation [200]. The pathway can be divided into two main branches: canonical (β-catenin dependent) Figure 4.1 and non-canonical (β-catenin independent)Figure 4.2 [202]. While canonical Wnt signalling is more commonly associated with cell fate determination and tissue regeneration, non-canonical signalling, plays a critical role in regulating cellular motility, immune responses, and inflammation[203].

Wnt Signalling in Fibroblasts in RA

Recent studies have shown that Wnt signalling is active in RA, particularly within fibroblast populations [204]. Inflammatory stimuli within the synovium can induce the expression of Wnt ligands, which in turn amplify inflammatory responses [205]. Despite mounting evidence of the importance of Wnt signalling in pathogenic fibroblasts, the

exact mechanisms by which Wnt signalling regulates synovial fibroblast activity in RA are still under investigation.

WNT5A – A Key Driver of Fibroblast-Mediated Pathology in RA

WNT5A has emerged as a critical mediator of inflammation in RA synovial fibroblasts. WNT5A expression is significantly upregulated in synovial fibroblasts from RA patients[206], and studies in animal models have demonstrated that WNT5A knockout mice show reduced severity of inflammatory arthritis[125]. This suggests that WNT5A is not only involved in the initiation of inflammation but may also play a vital role in maintaining chronic inflammatory states.

WNT5A primarily signals through non-canonical pathways, which are known to drive pro-inflammatory responses[203] (Figure 4.3). Specifically, WNT5A has been shown to promote the production of key inflammatory cytokines such as TNF-α, IL-6, and IL-1β [205]. These cytokines are major drivers of joint inflammation and destruction in RA, suggesting that WNT5A may be a critical regulator of synovial inflammation. In addition, WNT5A enhances the migratory and invasive properties of fibroblasts, further contributing to joint damage[207,208]. Emerging evidence suggests that WNT5A could be a key target in the treatment of RA.

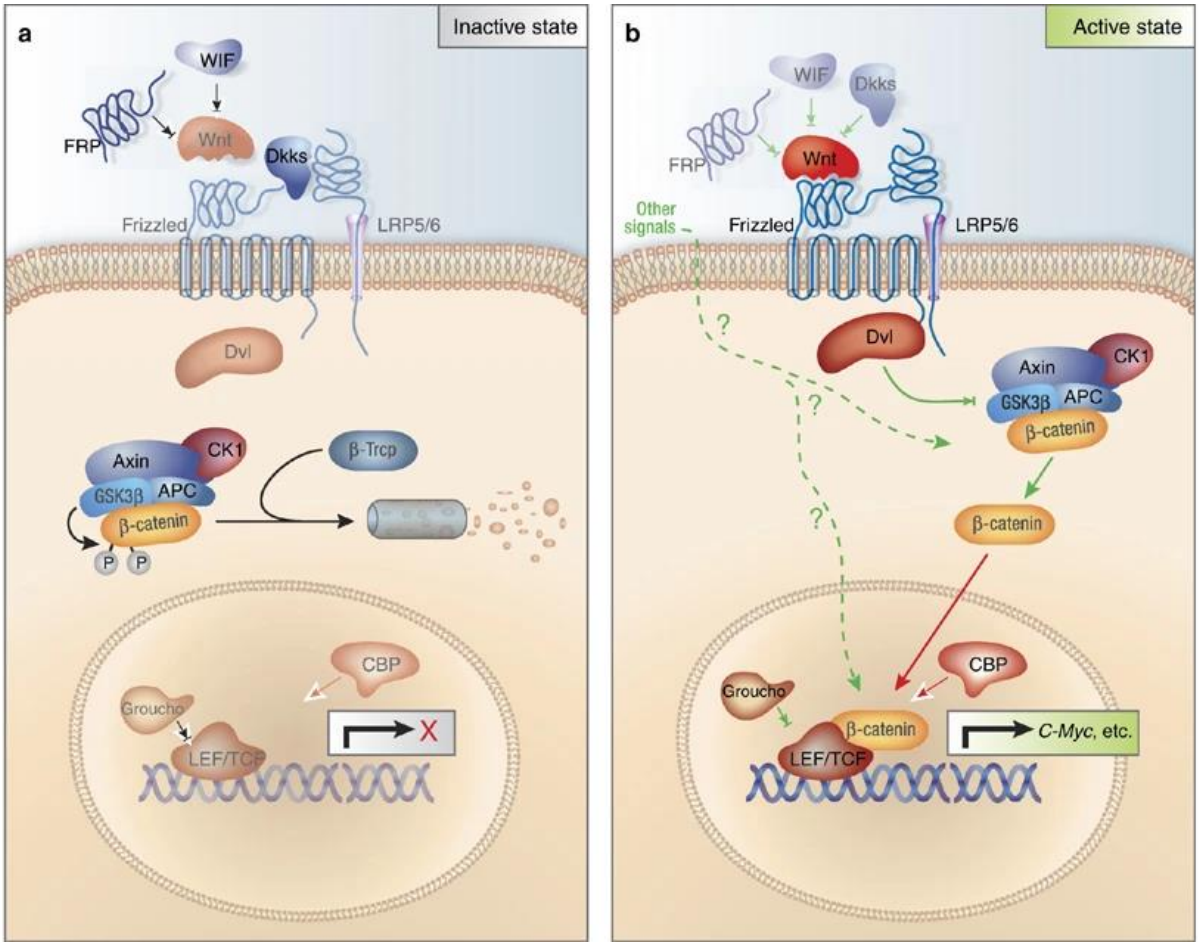

Figure 4.1 Schematic representation of the canonical Wnt/β-catenin signaling pathway taken from Jinyong Luo, Jin Chen et al[209]. (a) In the absence of Wnt signal, β-catenin is recruited into the APC/Axin/GSK3β complex, and phosphorylated by GSK3β at the N-terminal 'destruction box'. The phosphorylated β-catenin binds to β-Trcp of the proteosome machinery and is targeted for degradation. As the result, no free β-catenin enters nucleus to form transcriptional complex with LEF/Tcf and to regulate downstream gene expression. (b) Wnt binds to its Fz receptor and LRP5/6 co-receptor and activates Dvl, leading to the inhibition of APC/Axin/GSK3β-mediated β-catenin degradation. Stabilized β-catenin forms a transcriptional complex with LEF/Tcf and activates downstream targets such as c-Myc. Negative regulators, such as Dkks, WIF and FRPs, inhibit the interactions between Wnt ligands and their receptors. There is crosstalk between Wnts and other signaling pathways, such as growth factors that activate receptor tyrosine kinases.

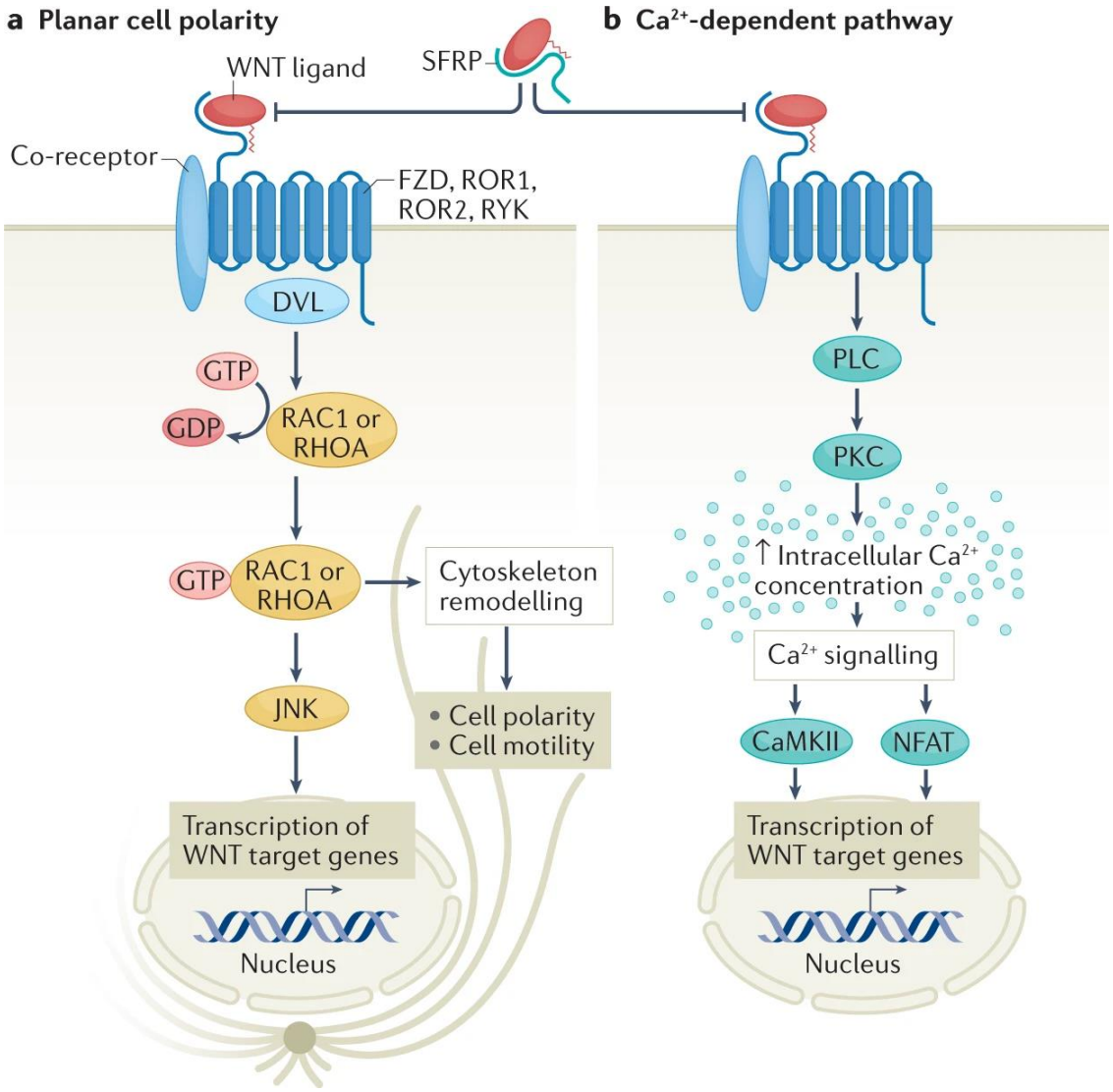

Figure 4.2 Non-canonical WNT signalling pathways involve the planar cell polarity pathway (part a) and the Ca2+-dependent pathway (part b). Taken from Akoumianakis et al. [209]Both pathways are initiated by binding of a WNT ligand to WNT receptors, such as Frizzled (FZD) receptors, the tyrosine-protein kinase transmembrane receptors ROR1 and ROR2, and tyrosine-protein kinase RYK, which belong to the family of G protein-coupled receptors (also known as seven-transmembrane receptors), with the potential contribution of various co-receptors. Binding of WNT ligands to secreted FZD-related proteins (SFRPs) blocks the WNT–receptor interaction. The downstream events involved in the planar cell polarity pathway are not well defined, but include Dishevelled (DVL) and lead to GTP-dependent activation of small GTPases, such as RAC1 and RHOA, which in turn activate JUN N-terminal kinase (JNK), and ultimately regulate cell polarity and motility and gene transcription. The Ca2+-dependent pathway involves activation of PLC and protein kinase C (PKC), which leads to increased intracellular Ca2+ concentration, triggering the activation of calcium/calmodulin-dependent protein kinase II (CaMKII) and the nuclear factor of activated T cells (NFAT) pathway, leading to transcriptional regulation.

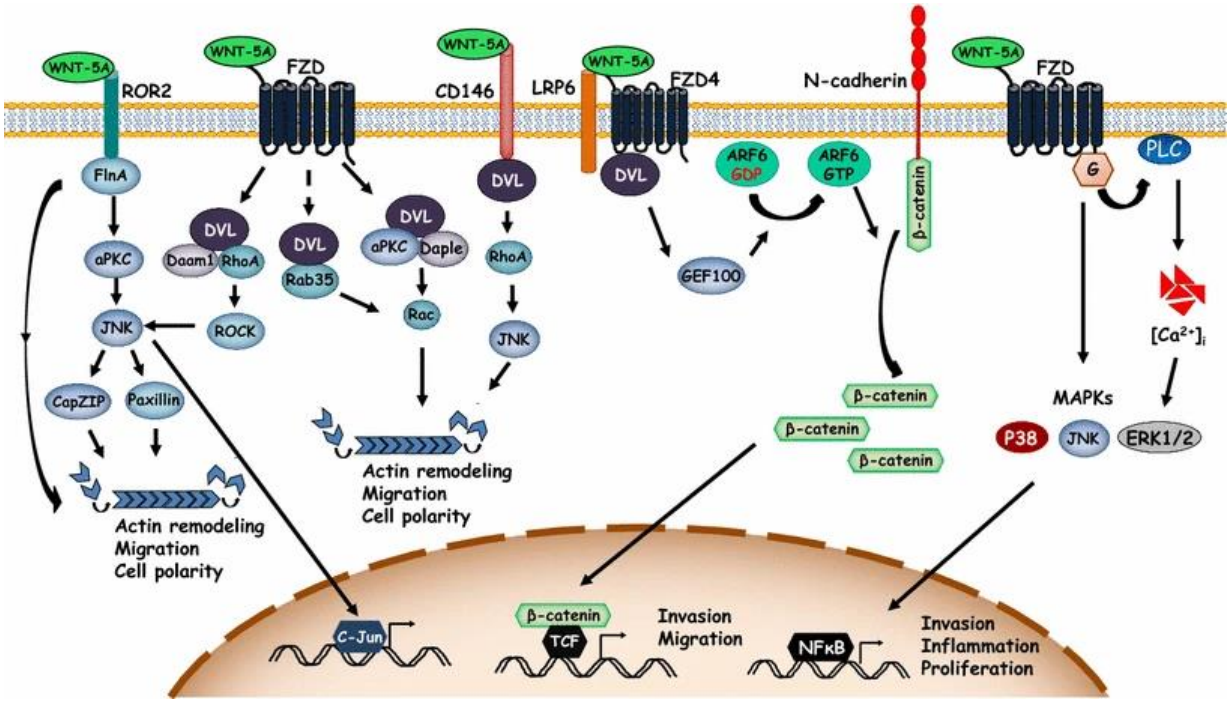

Figure 4.3 WNT-5A-activated signalling cascades in cell migration. Taken from Kumawat & Gosens [209]Diagrammatic representation of few key signalling cascades engaged by WNT-5A to regulate actin cytoskeletal remodelling and cell migration. ARF6 ADP-ribosylation factor 6, GEF100 ARF-guanine nucleotide exchange protein 100, FlnA filamin A, aPKC atypical protein kinase C, JNK c-Jun N-terminal protein kinase, CapZIP CapZ-interacting protein, DVL disheveled, Daam1 DVL-associated activator of morphogenesis 1, Daple DVL-associating protein with a high frequency of leucine residues, ROCK rho-associated kinase, LRP6 low-density lipoprotein receptor-related protein 6, G G proteins, [Ca 2+] i intracellular calcium release

4.2 Chapter Aims

The overall aims of this chapter are:

1. To investigate the role of WNT signalling in fibroblasts in inflammatory arthritis.
2. Assess the role of WNT5A in inflammatory arthritis and determine its effects on joint inflammations and immune cell recruitment.
3. To evaluate the therapeutic potential of WNT inhibition in inflammatory arthritis and identify key cellular and molecular targets.

Results

4.3 Wnt signalling is implicated in pathogenic synovial fibroblasts

I decided to use the cellular atlas developed in Chapter 3 to explore the potential of WNT5A as a key regulator of inflammation and pathology in RA synovial fibroblasts.

Increased enrichment of Wnt signalling was observed at both peak and persistent inflammation, in all synovial cells, but not in the resolving phases Figure 4.4. I generated gene modules associated with Wnt signalling, and calculated a module score of averaged expression of Wnt signalling pathways. I saw an enrichment of Wnt activation associated with fibroblasts Figure 4.5, A. I then assessed enrichment of the same modules in fibroblasts across the time course of inflammatory arthritisFigure 4.5. Wnt receptors, downstream target genes and genes associated with the Ca^{2+} pathway were enriched in fibroblasts at the peak timepoint, and even further enrichment of Wnt activation was observed in persistent inflammation; confirming that Wnt signalling is upregulated during inflammation.

Following recent identification of Wnt5a as a potential pathogenic marker in RA, I examined its expression within fibroblastsFigure 4.6, A and saw expression of Wnt5a across the total fibroblast population, excluding Cthrc1 Postn fibroblastsFigure 4.6. In contrast, fibroblasts expressed very low levels of Wnt5b.

Figure 4.4 Wnt signalling is associated with inflammation. Top GO enriched pathways in murine inflammatory arthritis for each timepoint.

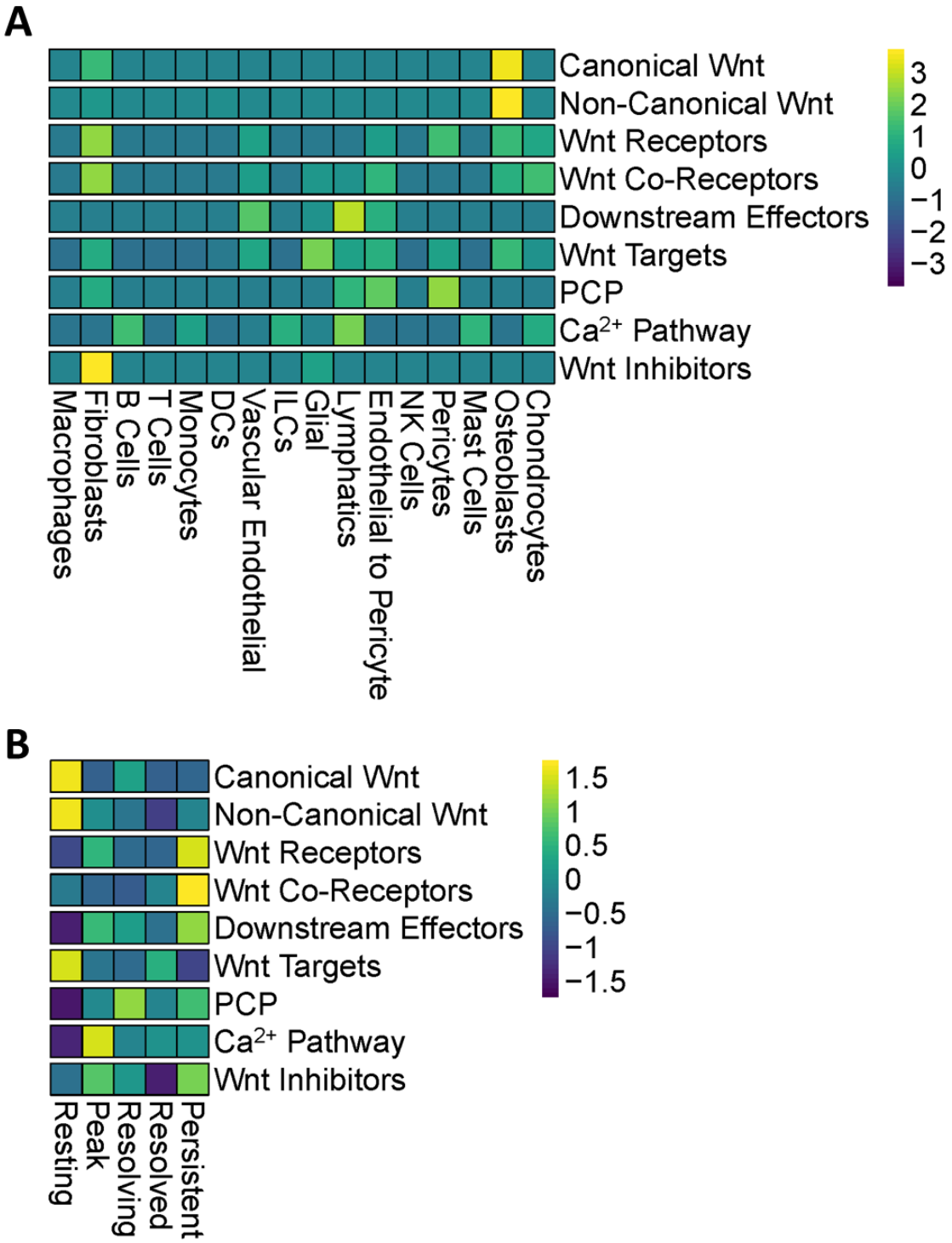

Figure 4.5 Wnt signalling is associated with fibroblasts in inflammation. Heatmaps showing expression of enrichment scores for wnt signalling pathways and related genes in A) All cell types in the cellular atlas of murine inflammatory arthritis. B) Fibroblasts across the timecourse of murine inflammatory arthritis.

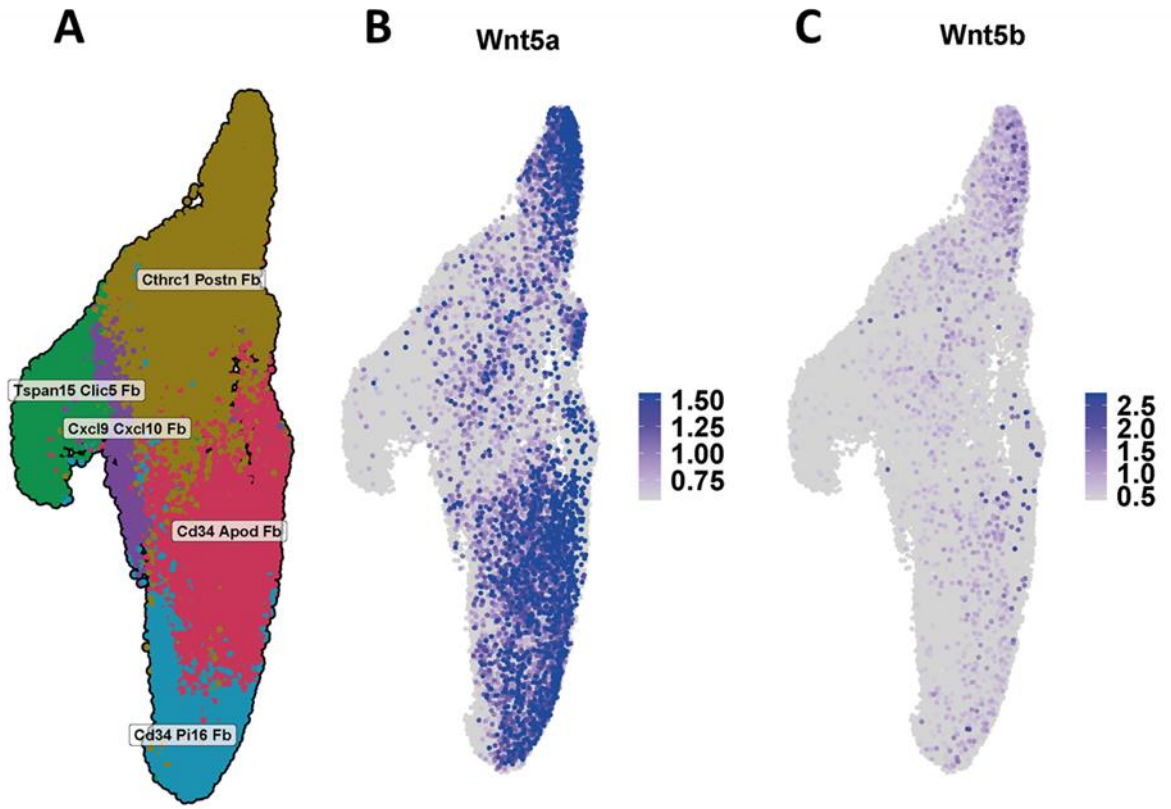

Figure 4.6 Wnt5a is enriched in fibroblasts in inflammatory arthritis. UMAP plots showing A) Fibroblast clusters in inflammatory arthritis. B) Wnt5a expression in fibroblasts. C) Wnt5b expression in fibroblasts.

4.4 WNT5A is upregulated during inflammation

Following confirmation that WNT5A is implicated in fibroblast-mediated inflammation in inflammatory arthritis, I decided to assess its direct impact on inflammatory mouse models. I injected recombinant Wnt5a protein into the knee joints of mice during AIA. I first determined the optimal dose and the impact of one or two doses of rWnt5a (Figure 8.5). For further experiments I determined that two doses or rWnt5a (1000 ng/µL per dose) into the knee joint at days 2 and 4 of AIA were sufficient to observe a change in AIA.

Mice injected with rWnt5a displayed significantly increased knee swelling at days 3,4,5,6 and 7 of AIA,Figure 4.7 A,i and an overall increase in knee swelling determined by calculated the area under the curve of knee swelling over timeFigure 4.7 Figure 4.7,A,ii. Additionally, mice are assessed for overall arthritis severity and a global arthritis score is calculated (Table 8.2). Mice injected with rWnt5a had significantly increased arthritis severity at days 3,4,5,6 and 7 of AIA, Figure 4.7B,i; and again an increased overall arthritis severity, Figure 4.7B,ii.

The effect of rWnt5a was most significant at days 5, 6 and 7, with no difference in the level of significance between the three timepoints. For this reason, I chose day 7 of AIA to conduct further experiments.

I isolated synovial cells from the knee joints of mice at day 7 of AIA injected with either rWnt5a or a PBS control, and assessed frequencies of cell populations using flow cytometry. Gating strategies can be found in Chapter 2. I saw that rWnt5a did

not appear to impact the total number of fibroblasts Figure 4.8,A, the number of lining vs sub-lining fibroblasts Figure 4.8,B,C, or the number of activated sub-lining fibroblasts Figure 4.8.

However, rWnt5a significantly increased the total number of Leukocytes Figure 4.9Figure 4.9, A, and macrophages Figure 4.9,D. With non-significant but increasing trends in the number of Neutrophils, Eosinophils, B Cells and T Cells Figure 4.9, B,C,E,F.

I also recorded increased numbers of both CD11b+ DCs Figure 4.10,A, CD103+ DCs Figure 4.10,B and Ly6Clow monocytes Figure 4.10,D; but not Ly6Chigh monocytes, although there was a trend towards an increase Figure 4.10,C.

I also wanted to assess the impact of rWnt5a on the macrophage populations previously discussed in chapters 1 and 3. I stained for Cx3cr1+/- , Cx3cr1- MHC II+ and Cx3cr1- Mertk+ Lyve1+ macrophages populations, I was unable to capture the other discussed populations with flow cytometry. Whilst I did not observe any significant differences in any of the macrophage populations Figure 4.11, there was an observable trend towards a decrease in Cx3cr1+ macrophages following injection with rWnt5a Figure 4.11,B.

Finally, I captured T Cell populations, due to their implications in both AIA and RA. Within the CD4+ T cell subset I captured naïve, memory, effector and regulatory cells; and within the CD8+ T Cell subset, naïve, memory and effector cells. Again, I did not see any significant differences in these populations Figure 4.12. However, trends towards an increase in CD4+ T cells Figure 4.12,A, and naïve CD8+ T cells Figure 4.12, G, and a decrease in Regulatory T Cells Figure 4.12, F are shown.

Whole knee joints from the same tissue were sectioned and stained for H&E. representative examples showing a resting joint Figure 4.13,A,i, PBS injected joint during AIA Figure 4.13,A,ii, and rWnt5a injected joint Figure 4.13,A,iii, are shown. In addition, I developed a scoring system for mouse tissue in AIA, discussed in chapter 2. I saw that rWnt5a increased synovial hyperplasia Figure 4.13, B,i, and synovial inflammation Figure 4.13 B,ii, but not synovial cellularity Figure 4.13, B,iii. Overall, more synovitis was observed in the joints of rWnt5a injected mice Figure 4.13, B,iv.

To further explore the impact of Wnt5a in AIA, I conducted scRNA-seq of isolated synovial cells from AIA mice at day 7, following injection with PBS or rWnt5a at days 2 and 4. Total cell populations identified can be seen in Figure 4.14,A. I also examined the frequency of cell populations within this data set but saw no significant difference in total fibroblasts Figure 4.14,B,i, resident macrophages Figure 4.14,B,ii, DCs Figure 4.14,B,iii or regulatory T Cells Figure 4.14,B,iv. Although there is a visual trend towards an increase in fibroblasts and resident macrophages.

I assessed GO pathways in the rWnt5a injected mice compared to the control condition, and saw significant enrichment of pro-inflammatory associated pathways in both the total cell population Figure 4.15,A, and fibroblast population Figure 4.15,B.

Several genes associated with inflammation and DC and macrophage recruitment were upregulated with rWnt5a, whilst genes associated with tissue remodelling and, interestingly lining fibroblasts, were downregulated Figure 4.16. When plotting sole expression of key genes associated with RA and inflammation, I observed significant

increases in expression in Csf1 Figure 4.17,A, Nfkb1 Figure 4.17,B, Ccl2 Figure 4.17,C and Il6 Figure 4.17,D.

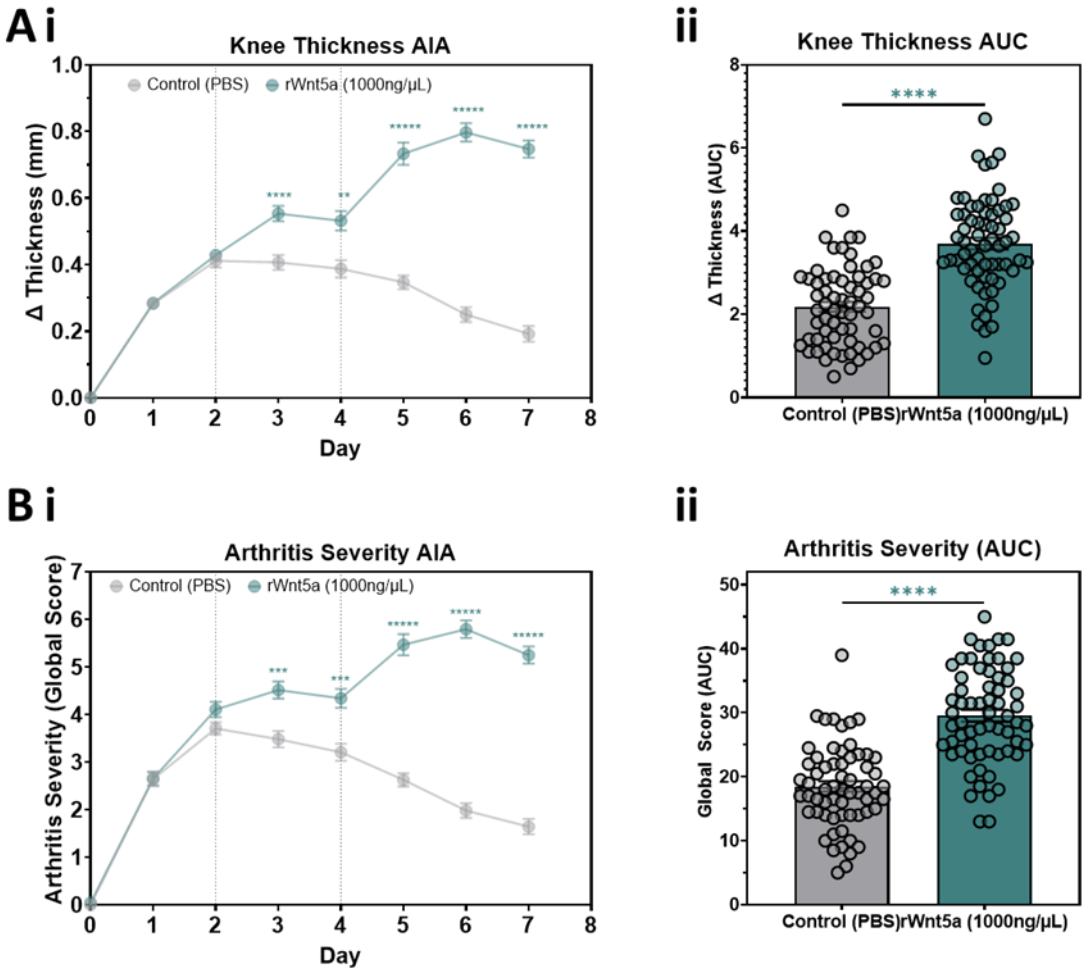

Figure 4.7 rWnt5a worsens AIA in mice. (A) Measurements of knee swelling in mice subjected to antigen-induced arthritis (AIA), injected on day 2 and 4 with either PBS control or murine rWnt5a protein. (i) Change in knee swelling over time. (ii) Change in knee swelling quantified by the area under the curve. (B) Arthritis severity assessed using a global arthritis score sheet: (i) over time and (ii) calculated area under the curve. Statistical analyses were performed using Two-Way ANOVA followed by Tukey's Post Hoc test and unpaired t-tests. * p<0.05; ** p<0.01; *** p<0.001; **** p<0.0001. Control n=67, rWnt5a n=69.

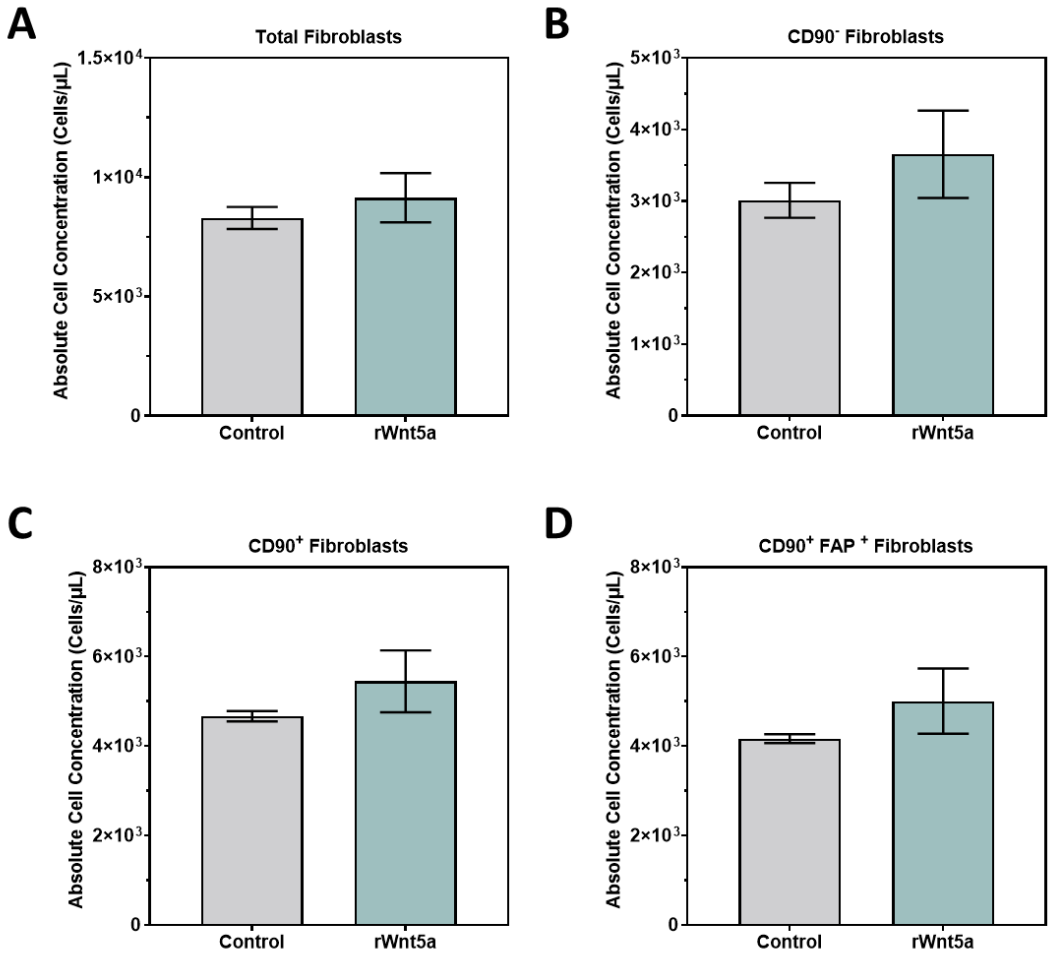

Figure 4.8 Fibroblast proportions are not impacted by rWnt5a. Bar plots showing the absolute concentrations of (A) Total fibroblasts, (B) Thy1- fibroblasts, (C) Thy1+ fibroblasts, and (D) Thy1+ FAP+ fibroblasts on day 7 of AIA, following injection of PBS or rWnt5a on day 2 and 4. n = 4 per condition. Statistical analyses were performed using unpaired t-tests. n = 4 per group.

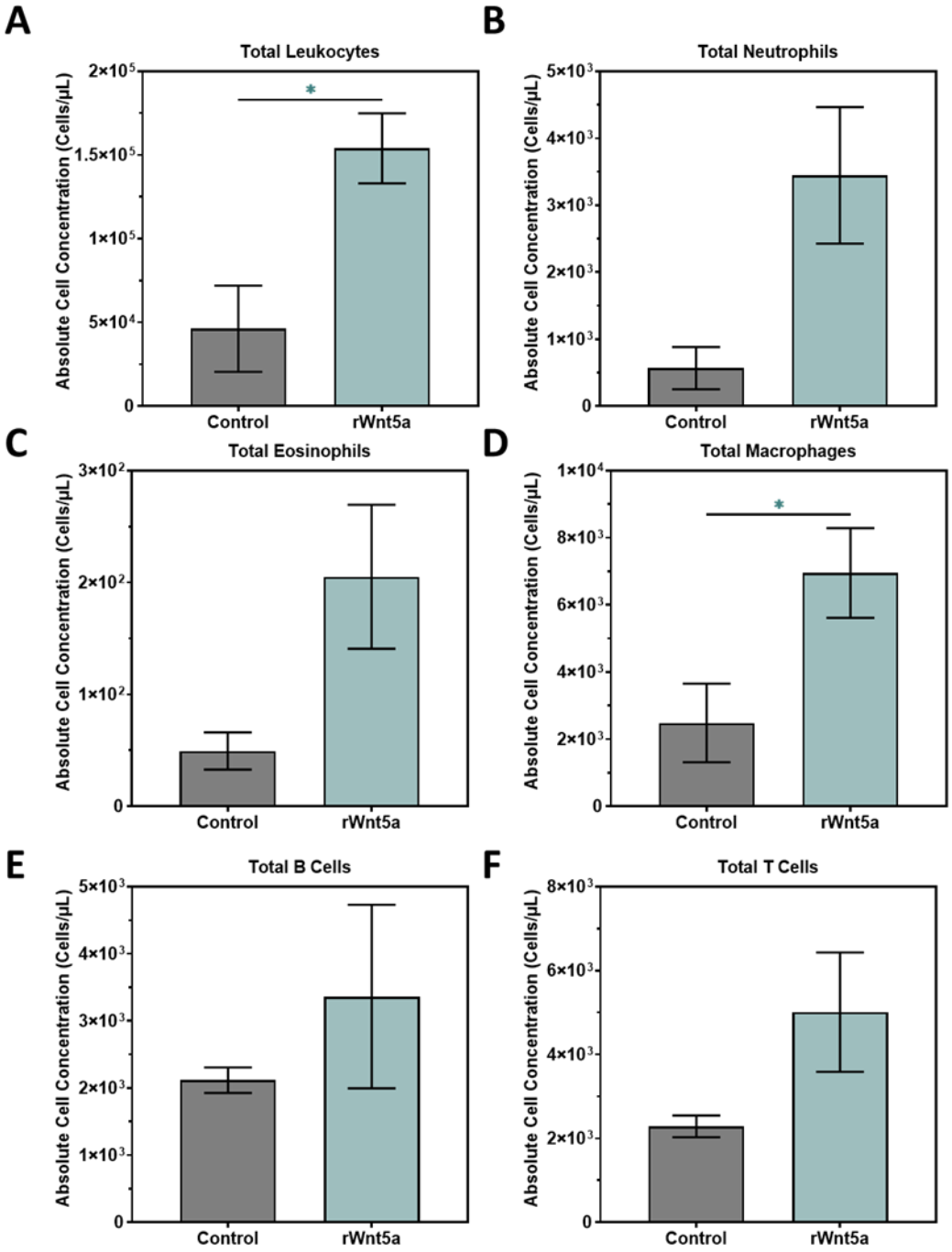

Figure 4.9 Leukocyte frequencies following rWnt5a in AIA. Bar plots showing the absolute concentrations of (A) Total Leukocytes, (B) Total Neutrophils, (C) Total Eosinophils, (D) Total Macrophages, E) Total B Cells and F) Total T Cells on day 7 of AIA, following injection of PBS or rWnt5a on day 2 and 4. n = 4 per condition. Statistical analyses were performed using unpaired t-tests. * $p<0.05$; ** $p<0.01$; *** $p<0.001$; **** $p<0.0001$. n = 4 per group.

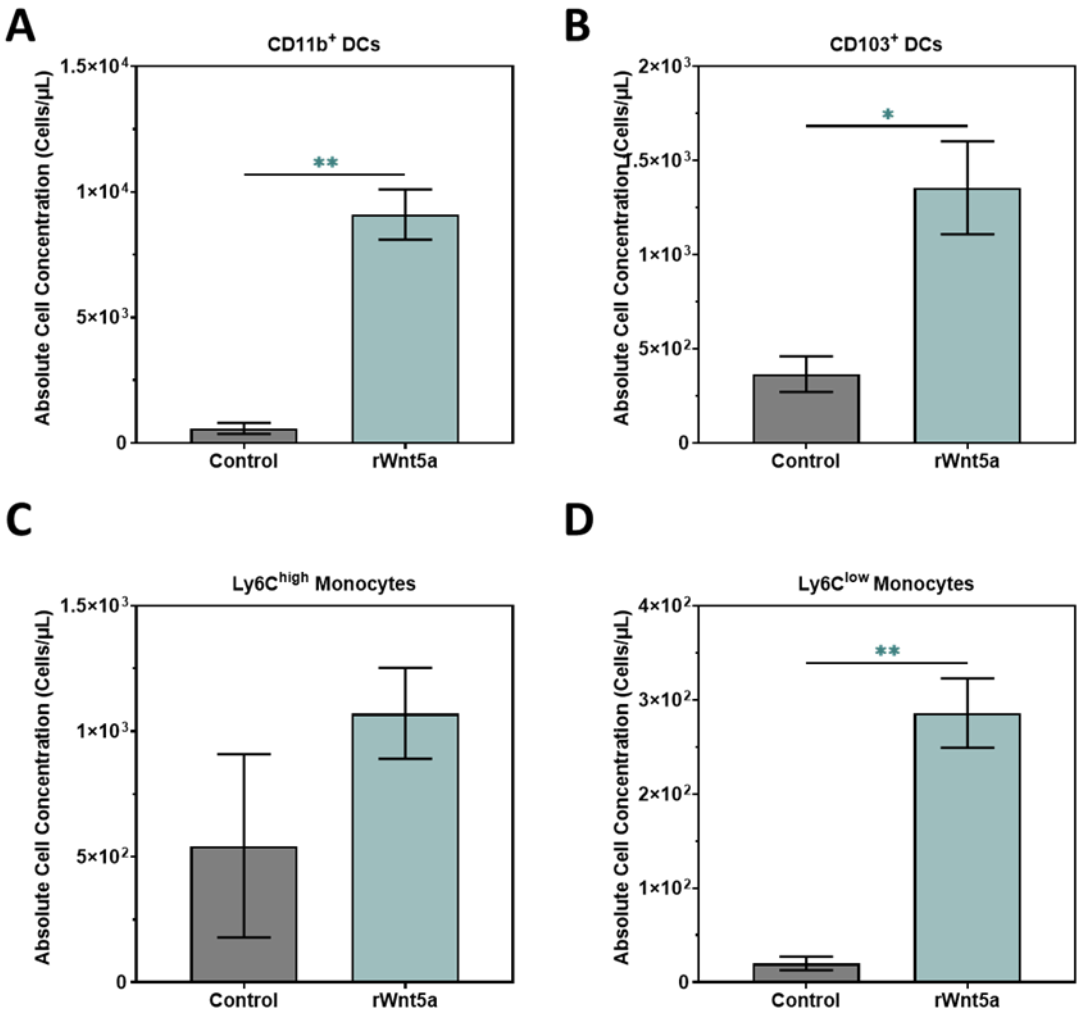

Figure 4.10 Myeloid frequencies following rWnt5a in AIA. Bar plots showing absolute concentrations of A) CD11b+ DCs, B) CD103+ DCs, C) Ly6Chigh monocytes and D) Ly6clow on day 7 of AIA following injection of PBS or rWnt5a on day 2 and 4. n = 4 per condition. Statistical analyses were performed using unpaired t-tests. * p<0.05; ** p<0.01; *** p<0.001; **** p<0.0001. n = 4 per group.

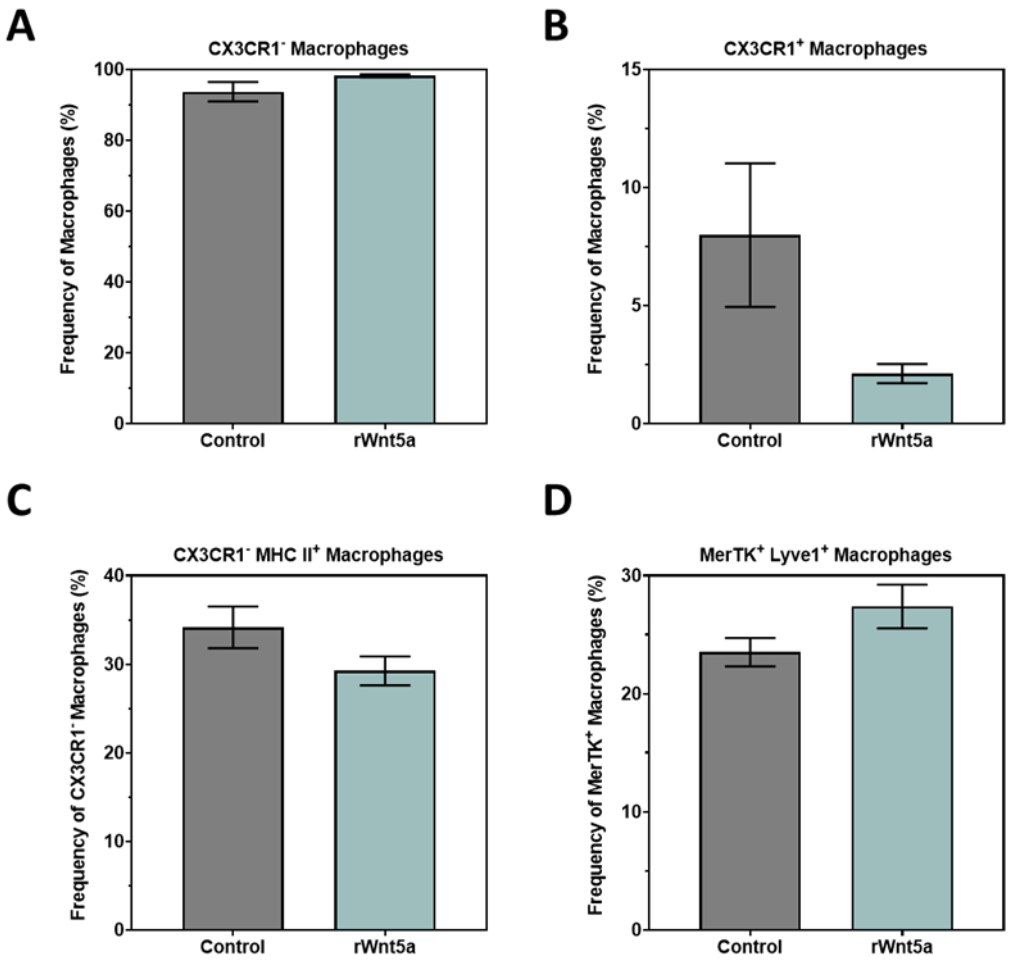

Figure 4.11 Macrophage frequencies following rWnt5a injection in AIA. Bar plots showing cell frequencies of A) Cx3cr1- macrophages, B) Cx3cr1+ macrophages, C) Cx3cr1+ MHC II+ macrophages and D) Mertk+ Lyve1+ macrophages on day 7 of AIA, following injection of PBS or rWnt5a on day 2 and 4. n = 4 per condition. Statistical analyses were performed using unpaired t-tests. n = 4 per group.

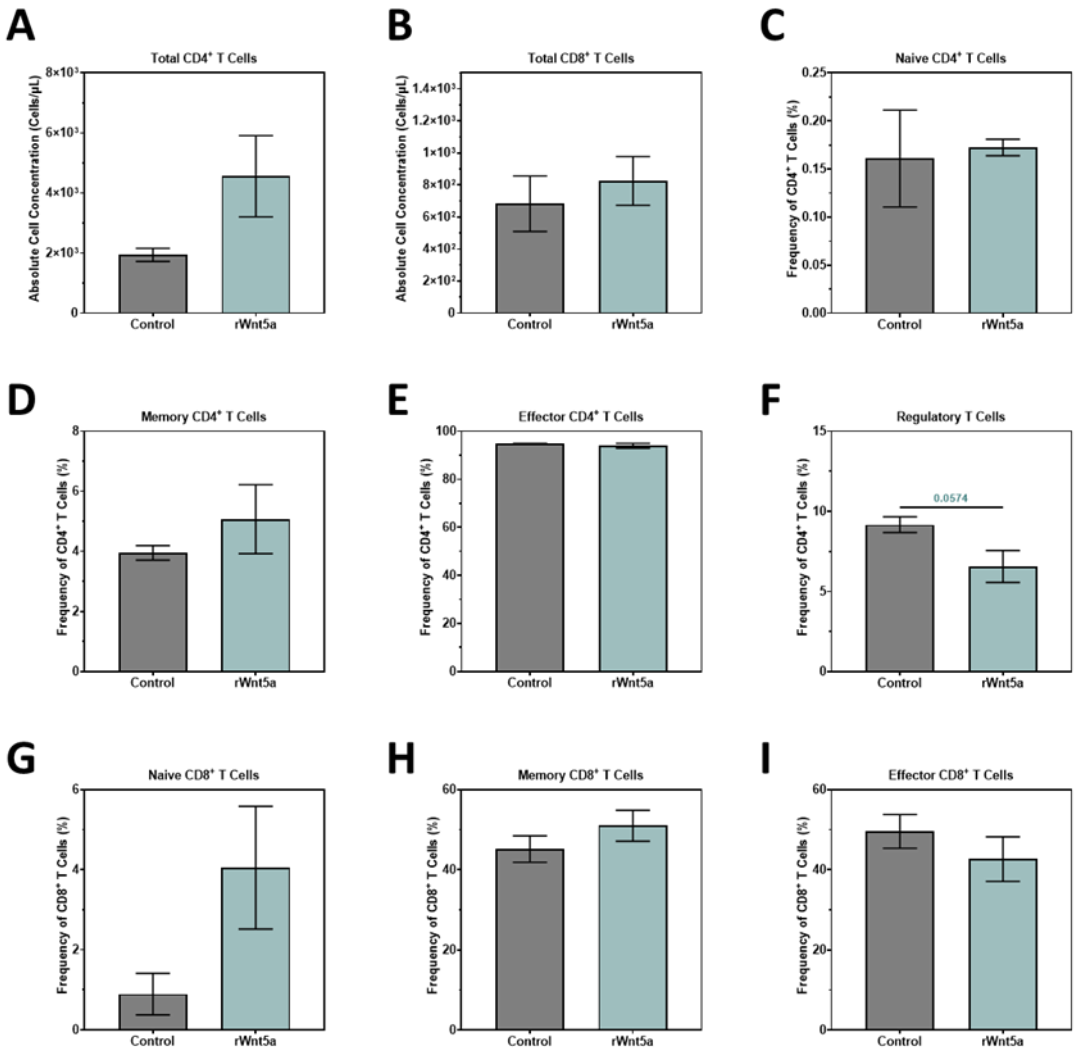

Figure 4.12 T Cell frequencies following rWnt5a injection in AIA. Bar plots showing absolute concentrations of A) CD4+ T Cells, B) CD8+ T Cells, and frequencies of C) Naïve CD4+ T Cells, D) Memory CD4+ T Cells, E) Effector CD4+ T Cells, F) Regulatory CD4+ T Cells, G) Naïve CD8+ T Cells, H) Memory CD8+ T Cells, I) Effector CD8+ T Cells on day 7 of AIA, following injection of PBS or rWnt5a on day 2 and 4. n = 4 per condition. Statistical analyses were performed using unpaired t-tests. * $p<0.05$; ** $p<0.01$; *** $p<0.001$; **** $p<0.0001$. n = 4 per group.

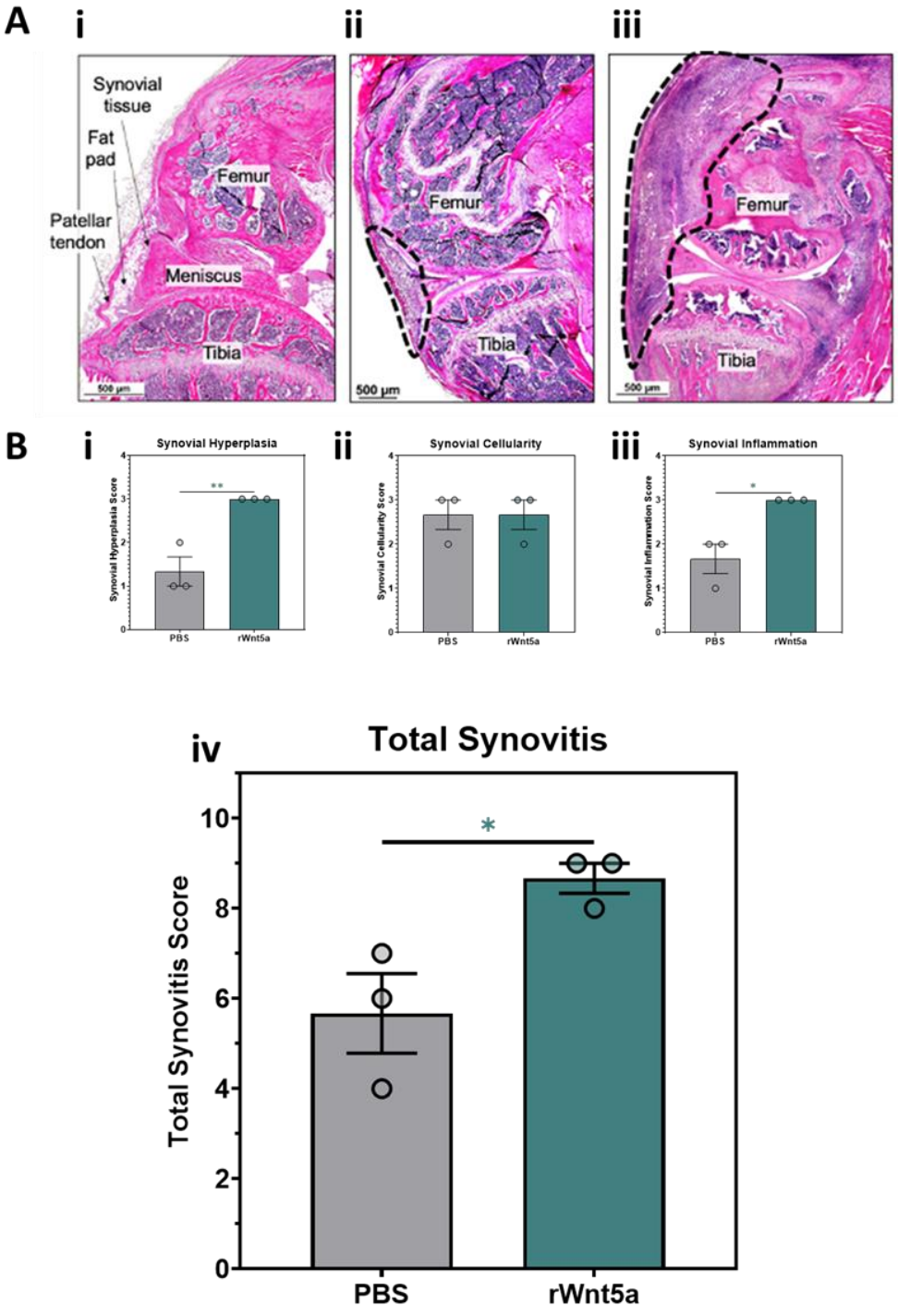

Figure 4.13 rWnt5a worsens synovitis in AIA. A) H&E-stained tissue sections of the mouse knee at i) Day 0 (No AIA), ii) Day 7 of AIA with PBS injections at days 2 and 4, iii) Day 7 of AIA with rWnt5a injections at days 2 and 4. Synovial tissue is highlighted within dotted lines. B) H&E sections were scored for arthritis severity, assessing (i) synovial hyperplasia, (ii) synovial cellularity, (iii) synovial inflammation, and (iv) a combined score for total synovitis. n = 3 per condition. Statistical analyses were performed using unpaired t-tests. * $p<0.05$; ** $p<0.01$; *** $p<0.001$; **** $p<0.0001$. n = 4 per group.

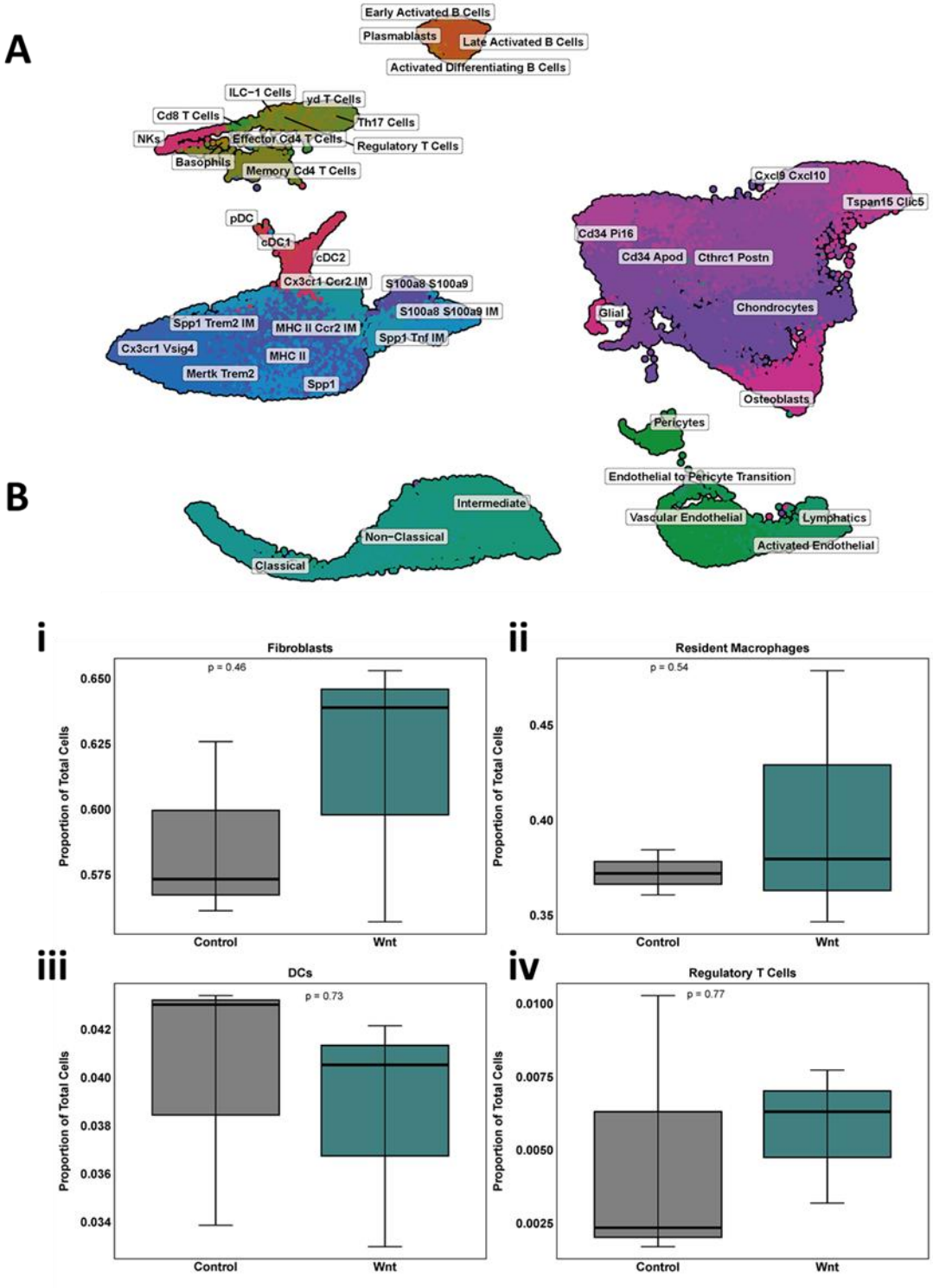

Figure 4.14 scRNA-sequencing of rWnt5a injected mice during AIA. A) UMAP plot of cell populations identified in a scRNA-seq dataset of isolated synovial cells at day 7 of AIA following injection at days 2 and 4 with either PBS (Control) or rWnt5a. B) Box plots of cell frequencies of i) Fibroblasts, ii) Resident macrophages, iii) Dendritic Cells and iv) Regulatory T Cells, shown as a proportion of the total cell population. n=3 per condition. Statistical analyses performed using unpaired t-tests.* p<0.05; ** p<0.01; *** p<0.001; **** p<0.0001.

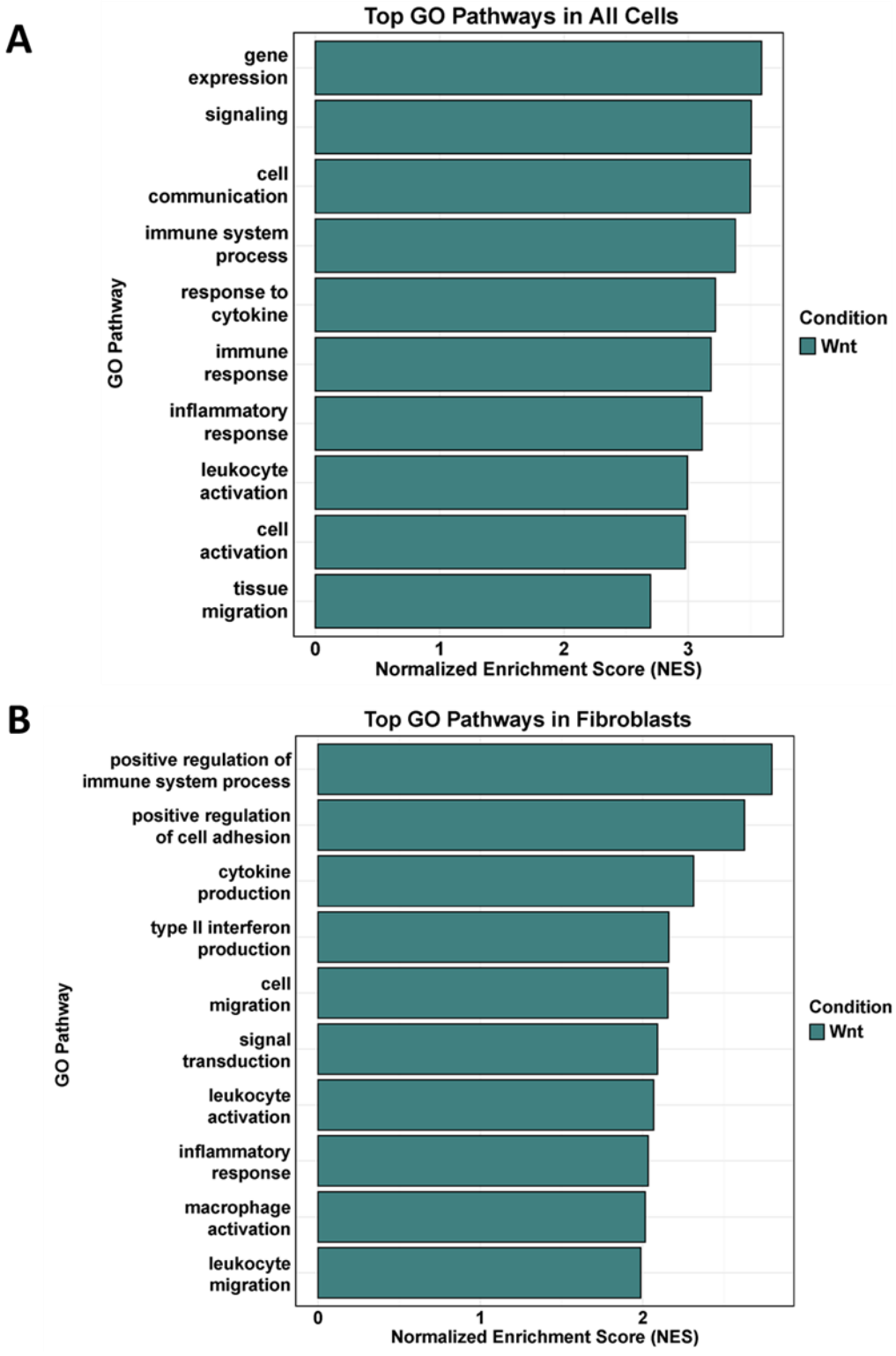

Figure 4.15 Wnt5a promotes inflammation in AIA. Bar plots of top significant GO pathways enriched following rWnt5a injection in A) All synovial cells and B) Fibroblasts.

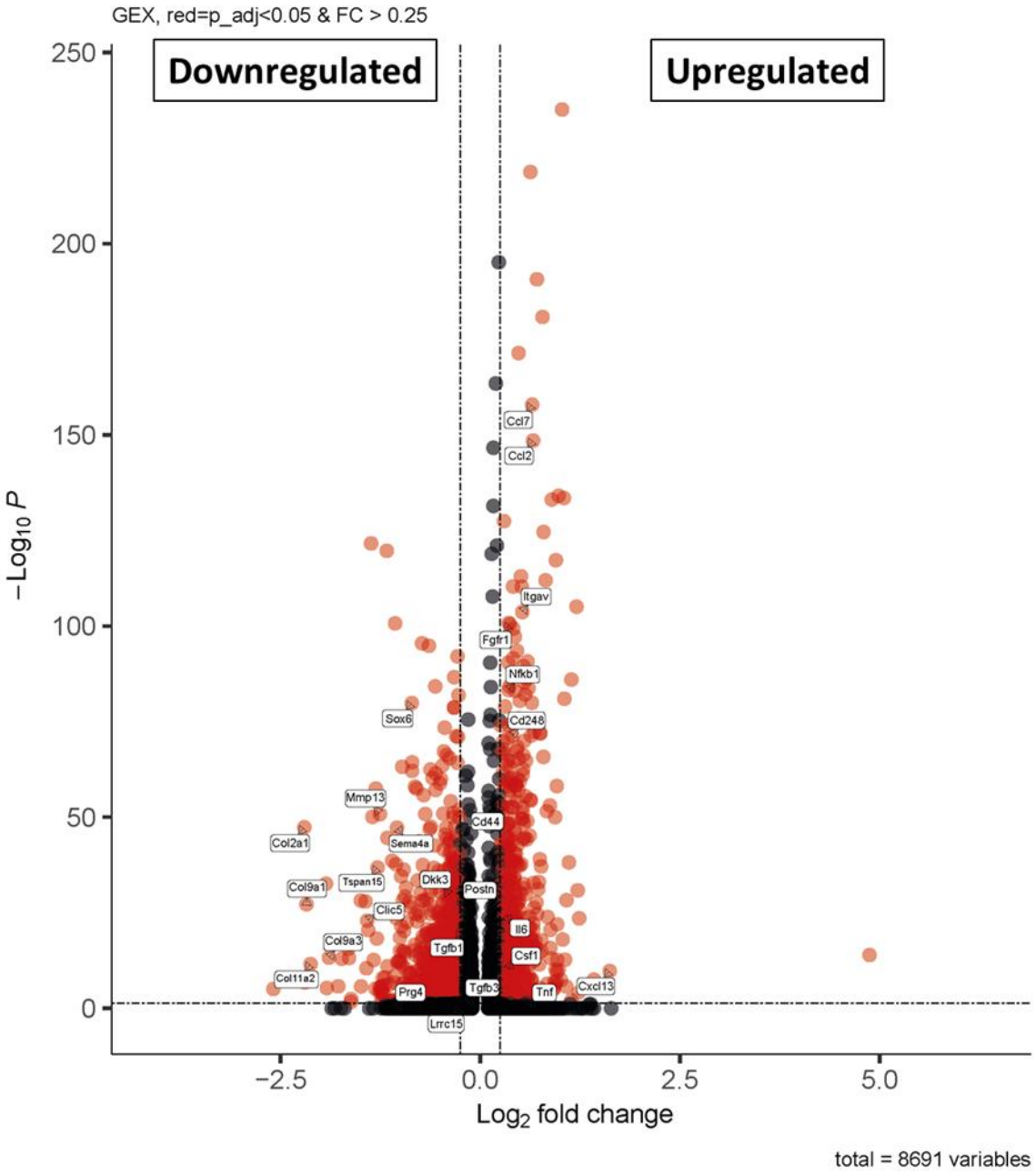

Figure 4.16 rWnt5a modifies gene expression in AIA. Enhanced volcano plot showing top upregulated and down regulated genes in AIA following injection with rWnt5a, compared to injection with PBS.

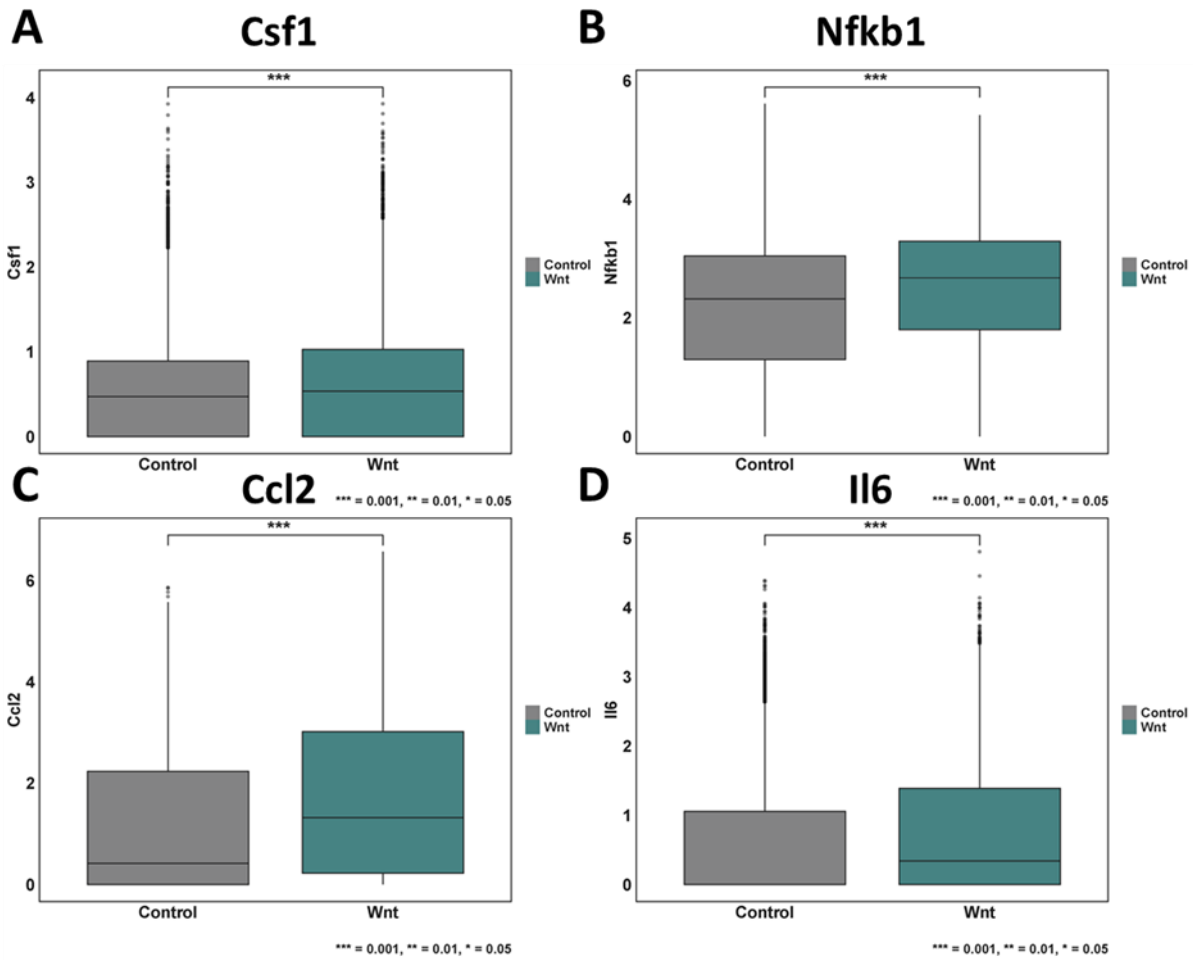

Figure 4.17 rWnt5a promotes expression of key pro-inflammatory genes. Box plots showing expression of A) Csf1, B) Nfkb1, C) Ccl2 and D) Il6 in PBS and rWnt5a injected mice. Statistical analyses performed using unpaired t-tests.* p<0.05; ** p<0.01; *** p<0.001; **** p<0.0001. n = 3 per condition.

4.5 Inhibition of WNT signalling can improve arthritis in mice

To further confirm the role of Wnt signalling in RA synovial fibroblasts, I administered Wnt inhibitor, LGK974, during AIA. LGK974 is a small molecule inhibitor that specifically targets the Wnt/β-catenin signalling pathway. LGK974 works by inhibiting Porcupine (PORCN), an enzyme essential for the post-translational modification (palmitoylation) of Wnt proteins, which in turn prevents the release of active Wnt ligands[210,211]. LGK974 has shown to be safe in animal models[210,212,213], and is even being assessed in a phase 1 study for the treatment of solid tumours[214]. Thus, LGK974 was deemed an ideal inhibitor to test, as it acts independently of the Wnt signalling pathway involved and directly on the Wnt ligands.

As use of this molecule is more widely reported in the literature, I first tested a dose of 3mg/kg of LGK974, injected intraperitoneally daily. No further dose optimisations were deemed necessary as we saw an effect with this dose, and the inhibitor was not well tolerated with mice showing signs of discomfort and weight loss.

Mice dosed with LGK974 displayed a significant reduction in knee swelling at days 3,4 and 5 of AIA, Figure 4.26,A,i, this time the overall knee swelling over time was not significant Figure 4.26,A,ii. Additionally, LGK974 treated mice displayed a decreased trend arthritis severity, but this was not significant at any of the timepoints Figure 4.26,B,i, or the overall arthritis severity, Figure 4.26B,ii.

The effect of LGK974 was most significant at day 4 of AIA, so I collected all further tissue samples at this timepoint

I isolated synovial cells from the knee joints of mice at day 4 of AIA injected with either LGK974 or a vehicle control (corn oil + 10% DMSO) and assessed frequencies of cell populations using flow cytometry. LGK974 did not appear to impact the total number of fibroblasts Figure 4.19,A, the number of lining vs sub-lining fibroblasts Figure 4.19,B,C, or the number of activated sub-lining fibroblasts Figure 4.19,D.

Additionally, LGK974 did not significantly influence any of the other cell populations captured (Figure 4.20, Figure 4.21, Figure 4.22, Figure 4.23), save for a significant increase in the frequency of Regulatory T Cells Figure 4.23,F.

As in the previous section, whole knee joints from the same tissue were sectioned and stained for H&E. Representative examples the control Figure 4.24,A,i, and LGK974Figure 4.24,A,ii, conditions are shown. When quantitively scored for synovitis, LGK974 significantly decreased synovial hyperplasia Figure 4.24, B,i, and synovial inflammation Figure 4.24Figure 4.13, B,iii, but not synovial cellularity Figure 4.24, B,ii. Overall, reduced synovitis was observed in the joints of LGK974 mice Figure 4.24, B,iv.

I conducted scRNA-seq of isolated synovial cells from AIA mice at day 4, following injection with Control orLGK974. Total cell populations identified can be seen in Figure 4.25,A. I also examined the frequency of cell populations within this data set but saw no significant difference in total fibroblasts Figure 4.25,B,i, resident macrophages Figure 4.25,B,ii, DCs Figure 4.25,B,iii or regulatory T Cells Figure 4.25,B,iv. Although there is a visual trend towards a decrease in all populations.

I assessed GO pathways in LGK974 treated mice compared to the control condition, and saw significant enrichment of anti-inflammatory associated pathways, as well as interferon-β signalling and apoptosis in both the total cell population Figure 4.26,A, and fibroblast population Figure 4.26,B.

I saw downregulation of genes associated with inflammation, and fibrosis in the LGK974 treated mice, and upregulation of anti-inflammatory genes as well as lining fibroblast markers Figure 4.27. A significant decrease in Csf1 Figure 4.28,A, and Nfkb1 Figure 4.28,B, is, is, is shown the in the LGK974 condition, however Ccl2 Figure 4.28,C, and Il6 Figure 4.28,C, were increased.

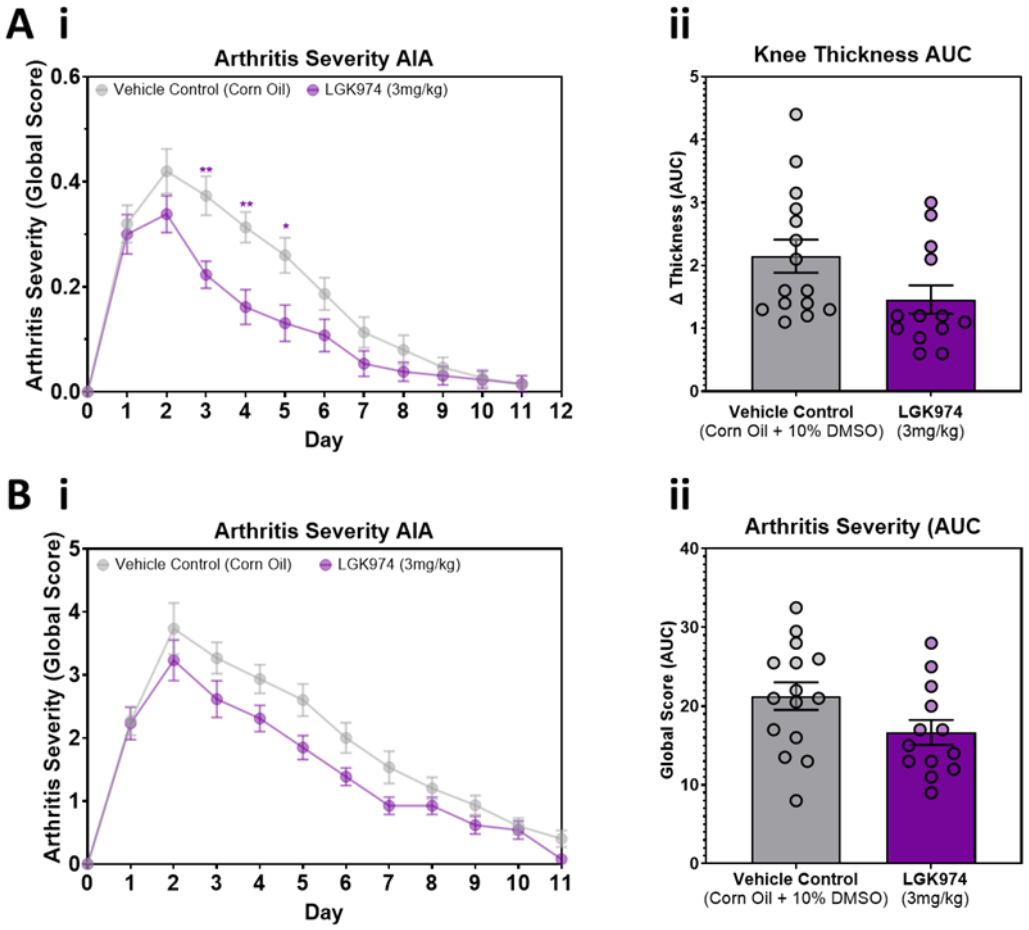

Figure 4.18 Inhibition of Wnt reduces AIA in mice. (A) Measurements of knee swelling in mice subjected to antigen-induced arthritis (AIA), injected daily for 7 days with either corn oil + 10% DMSO (Control) or LGK974. (i) Change in knee swelling over time. (ii) Change in knee swelling quantified by the area under the curve. (B) Arthritis severity assessed using a global arthritis score sheet: (i) over time and (ii) calculated area under the curve. Statistical analyses were performed using Two-Way ANOVA followed by Tukey's Post Hoc test and unpaired t-tests.* p<0.05; ** p<0.01; *** p<0.001; **** p<0.0001. Control n = 15, LGK974 n = 13.

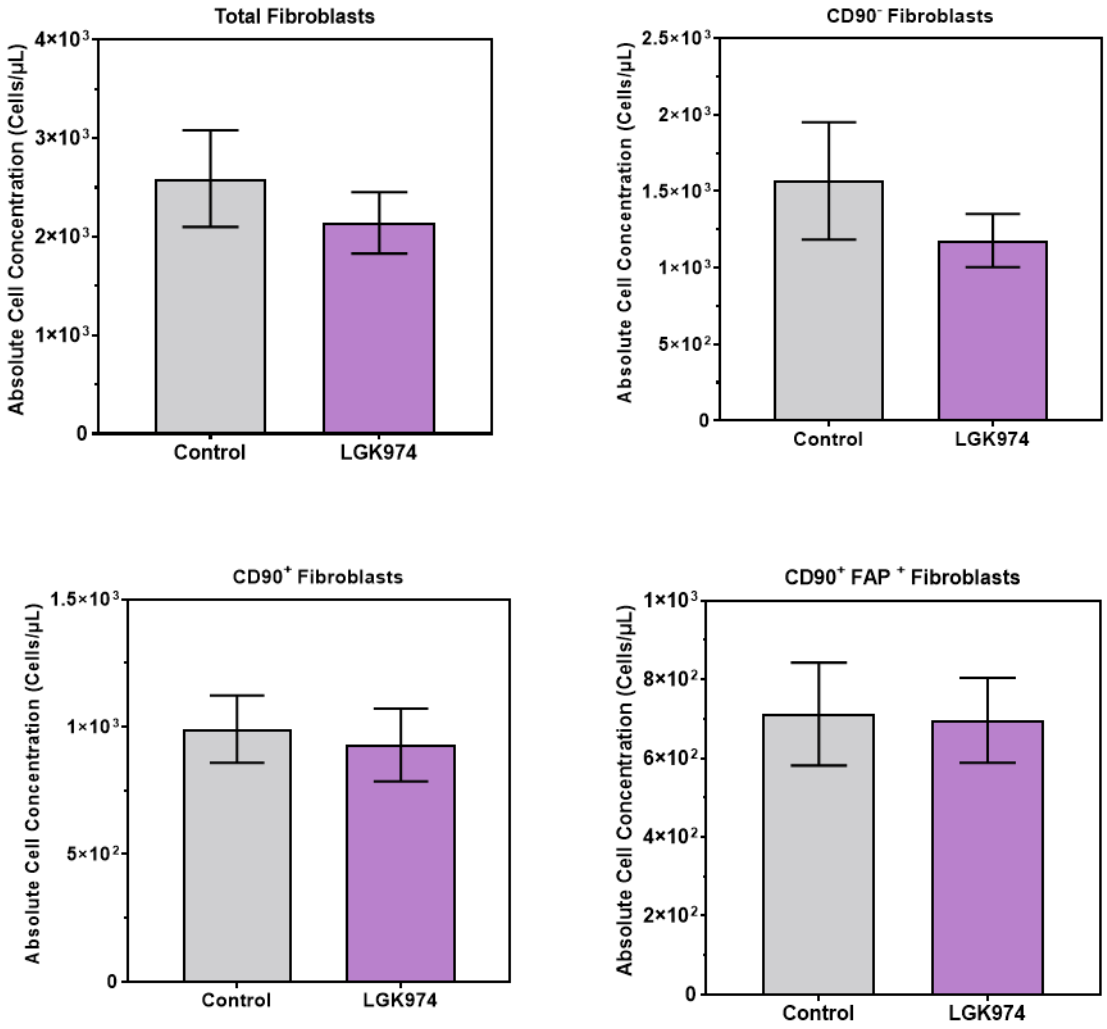

Figure 4.19 Fibroblast proportions are not affected by Wnt inhibition. Bar plots showing the absolute concentrations of (A) Total fibroblasts, (B) Thy1- fibroblasts, (C) Thy1+ fibroblasts, and (D) Thy1+ FAP+ fibroblasts on day 4 of AIA, following injection of corn oil + 10% DMSO (Control) or LGK974 daily. n = 4 per condition. Statistical analyses were performed using unpaired t-tests. * $p<0.05$; ** $p<0.01$; *** $p<0.001$; **** $p<0.0001$. n = 4 per group.

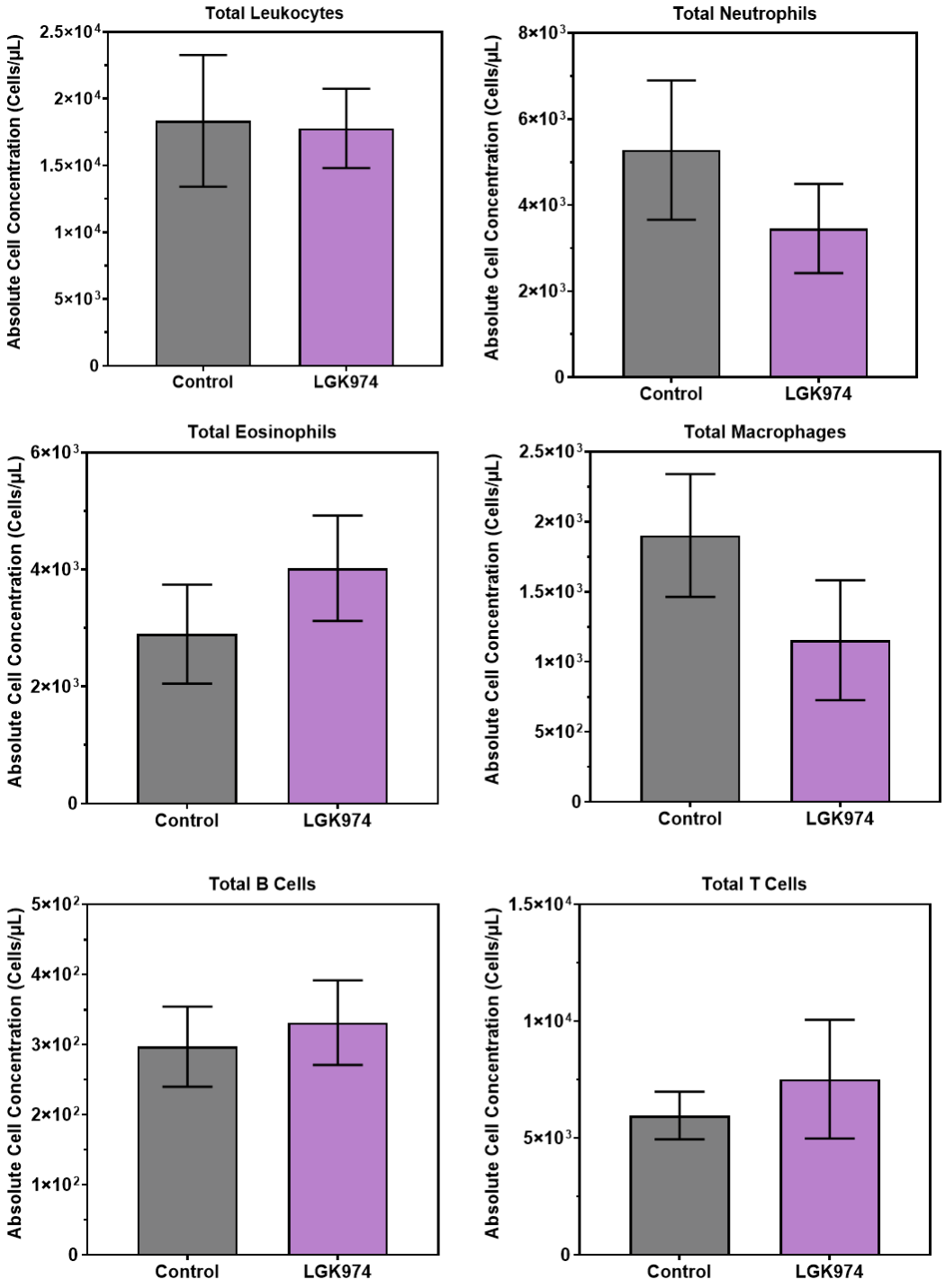

Figure 4.20 Leukocyte frequencies following Wnt inhibition in AIA. Bar plots showing the absolute concentrations of (A) Total Leukocytes, (B) Total Neutrophils, (C) Total Eosinophils, (D) Total Macrophages, E) Total B Cells and F) Total T Cells on day 4 of AIA, following injection of corn oil + 10% DMSO (Control) or LGK974 daily. n = 4 per condition. Statistical analyses were performed using unpaired t-tests. * $p<0.05$; ** $p<0.01$; *** $p<0.001$; **** $p<0.0001$. n = 4 per group.

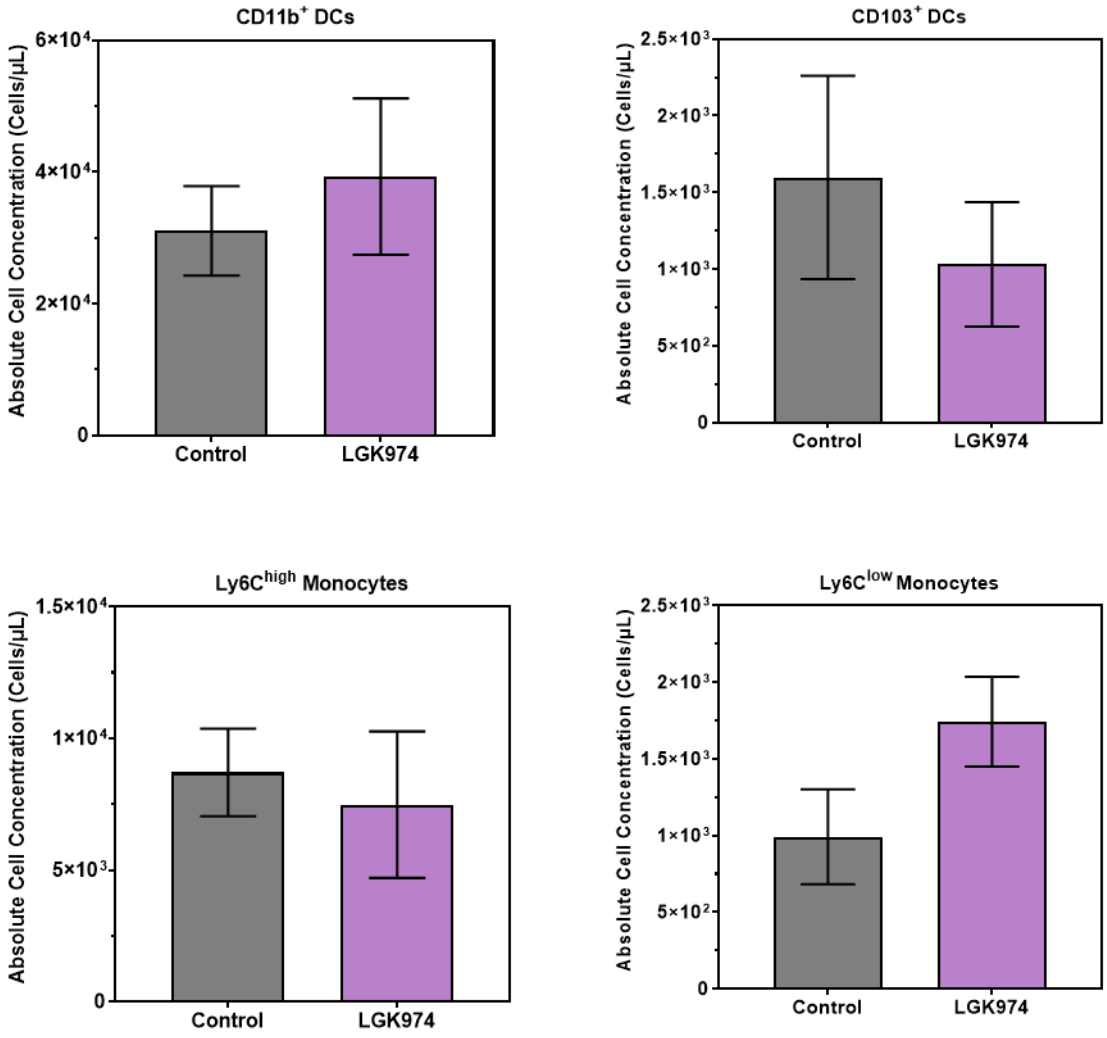

Figure 4.21 Myeloid frequencies following Wnt inhibition in AIA. Bar plots showing absolute concentrations of A) CD11b+ DCs, B) CD103+ DCs, C) Ly6Chigh monocytes and D) Ly6clow on day 4 of AIA, following injection of corn oil + 10% DMSO (Control) or LGK974 daily. n = 4 per condition. Statistical analyses were performed using unpaired t-tests.* $p<0.05$; ** $p<0.01$; *** $p<0.001$; **** $p<0.0001$. n = 4 per group.

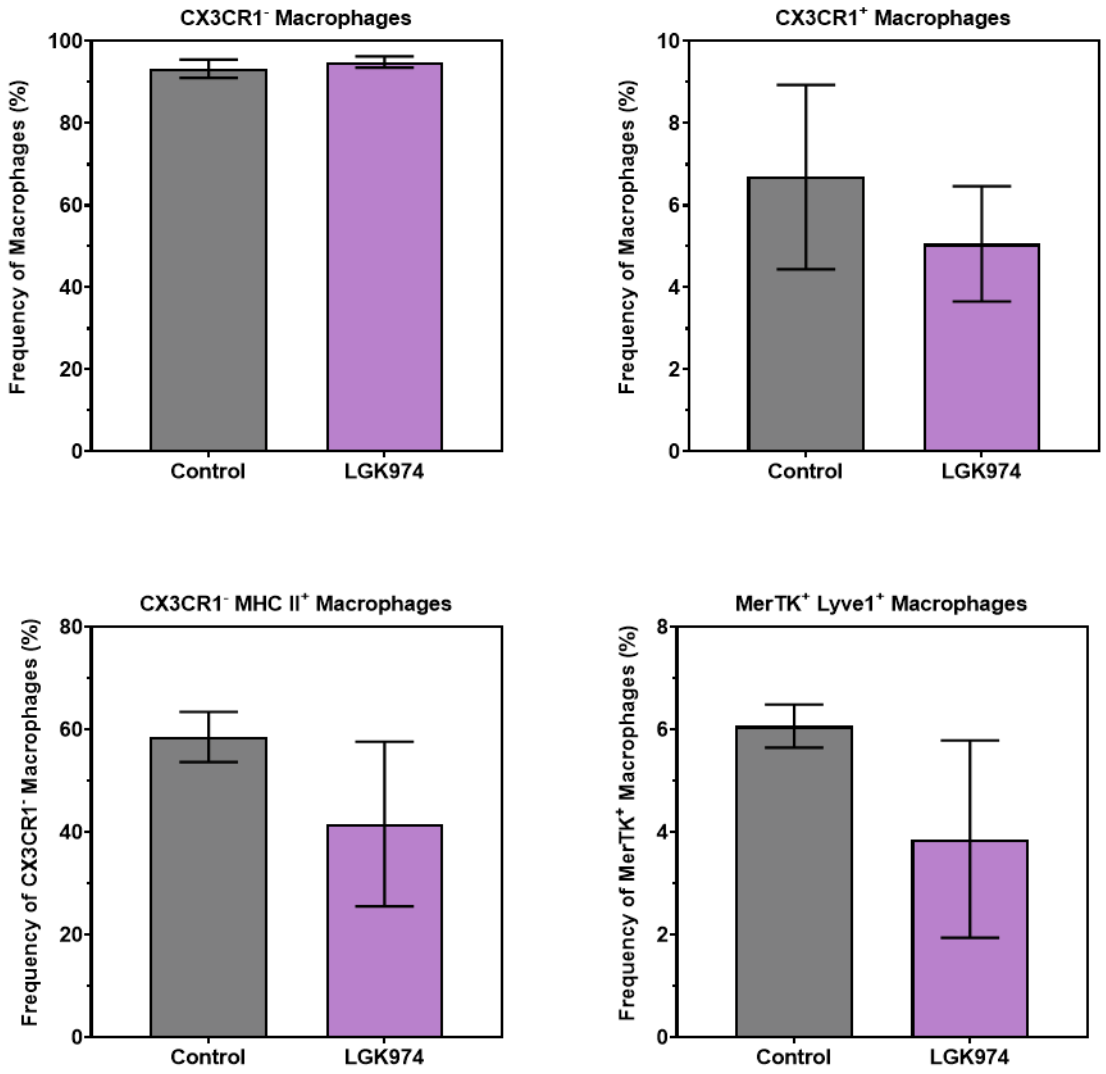

Figure 4.22 Macrophage frequencies following Wnt inhibition in AIA. Bar plots showing cell frequencies of A) Cx3cr1- macrophages, B) Cx3cr1+ macrophages, C) Cx3cr1+ MHC II+ macrophages and D) Mertk+ Lyve1+ macrophages on day 7 of AIA, following injection of PBS or rWnt5a on day 4 of AIA, following injection of corn oil + 10% DMSO (Control) or LGK974 daily. n = 4 per condition. Statistical analyses were performed using unpaired t-tests. * $p<0.05$; ** $p<0.01$; *** $p<0.001$; **** $p<0.0001$. n = 4 per group.

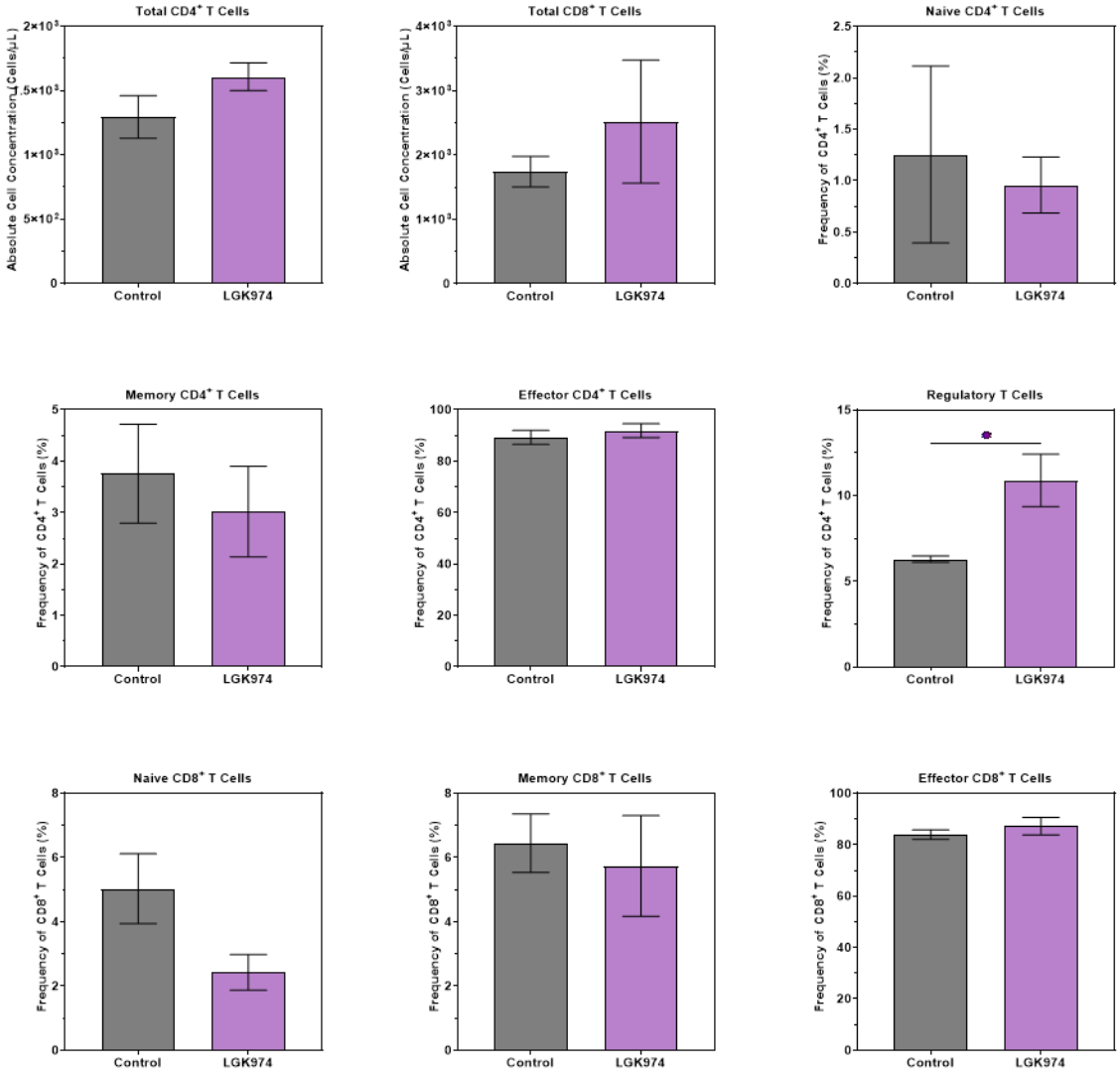

Figure 4.23 T Cell frequencies following Wnt inhibition in AIA. Bar plots showing absolute concentrations of A) CD4+ T Cells, B) CD8+ T Cells, and frequencies of C) Naïve CD4+ T Cells, D) Memory CD4+ T Cells, E) Effector CD4+ T Cells, F) Regulatory CD4+ T Cells, G) Naïve CD8+ T Cells, H) Memory CD8+ T Cells, I) Effector CD8+ T Cells on day 7 of AIA, following injection of PBS or rWnt5a on day 4 of AIA, following injection of corn oil + 10% DMSO (Control) or LGK974 daily. n = 4 per condition. Statistical analyses were performed using unpaired t-tests. * $p<0.05$; ** $p<0.01$; *** $p<0.001$; **** $p<0.0001$. n = 4 per group.

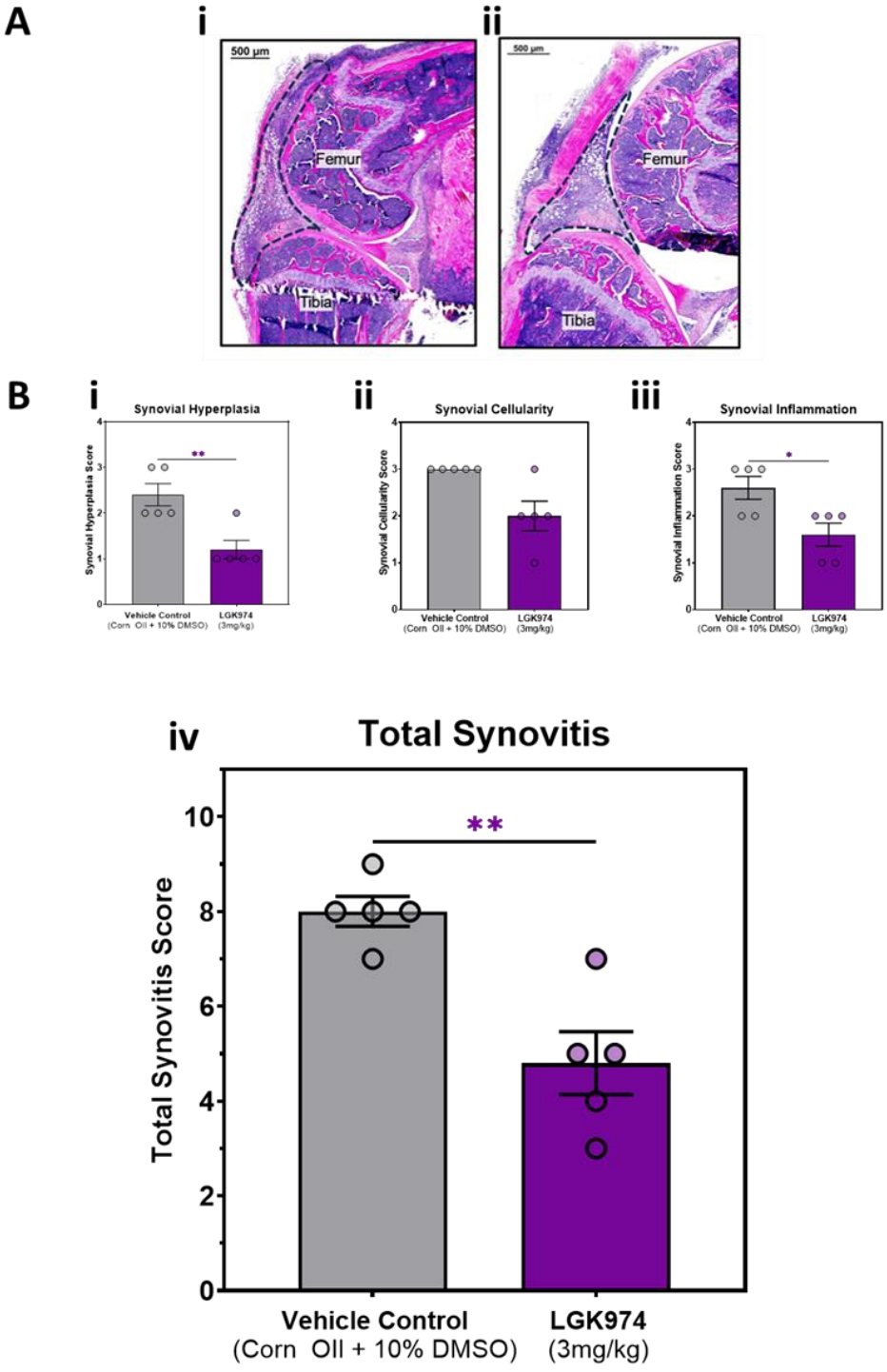

Figure 4.24 Wnt inhibition improves synovitis in AIA. A) H&E stained tissue sections of the mouse knee at i) Day 4 of AIA with daily injections of corn oil + 10& DMSO (Control) ii) Day 5 of AIA with daily injections of LGK974. Synovial tissue is highlighted within dotted lines. B) H&E sections were scored for arthritis severity, assessing (i) synovial hyperplasia, (ii) synovial cellularity, (iii) synovial inflammation, and (iv) a combined score for total synovitis. n = 5 per condition. Statistical analyses were performed using unpaired t-tests. * p<0.05; ** p<0.01; *** p<0.001; **** p<0.0001. n = 5 per group.

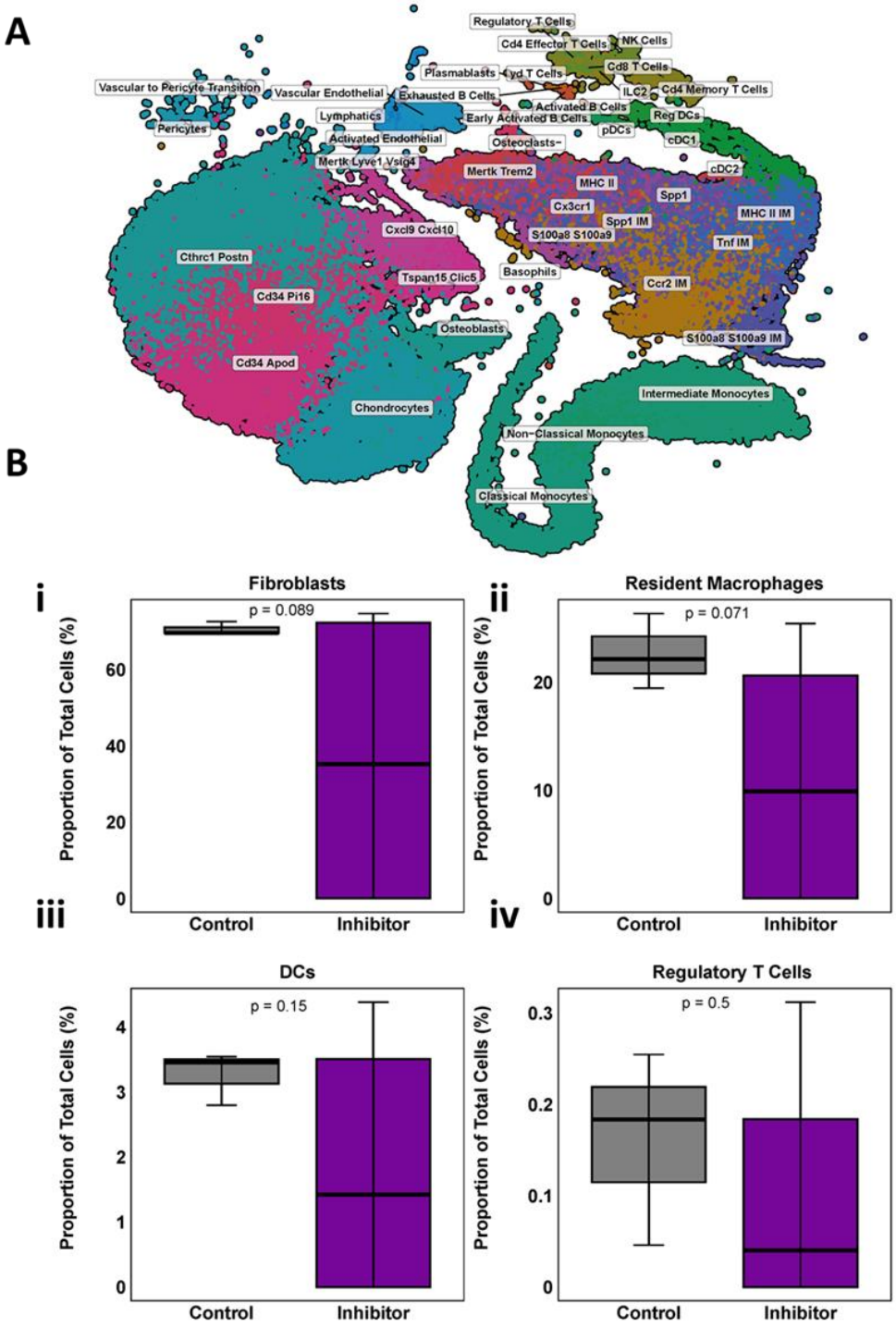

Figure 4.25 scRNA-sequencing of LGK974 injected mice during AIA. A) UMAP plot of cell populations identified in a scRNA-seq dataset of isolated synovial cells at day 4 of AIA following daily injections of corn oil + 10% DMSO (Control) or LGK974. B) Box plots of cell frequencies of i) Fibroblasts, ii) Resident macrophages, iii) Dendritic Cells and iv) Regulatory T Cells, shown as a proportion of the total cell population. n=3 per condition. Statistical analyses performed using unpaired t-tests. * p<0.05; ** p<0.01; *** p<0.001; **** p<0.0001.

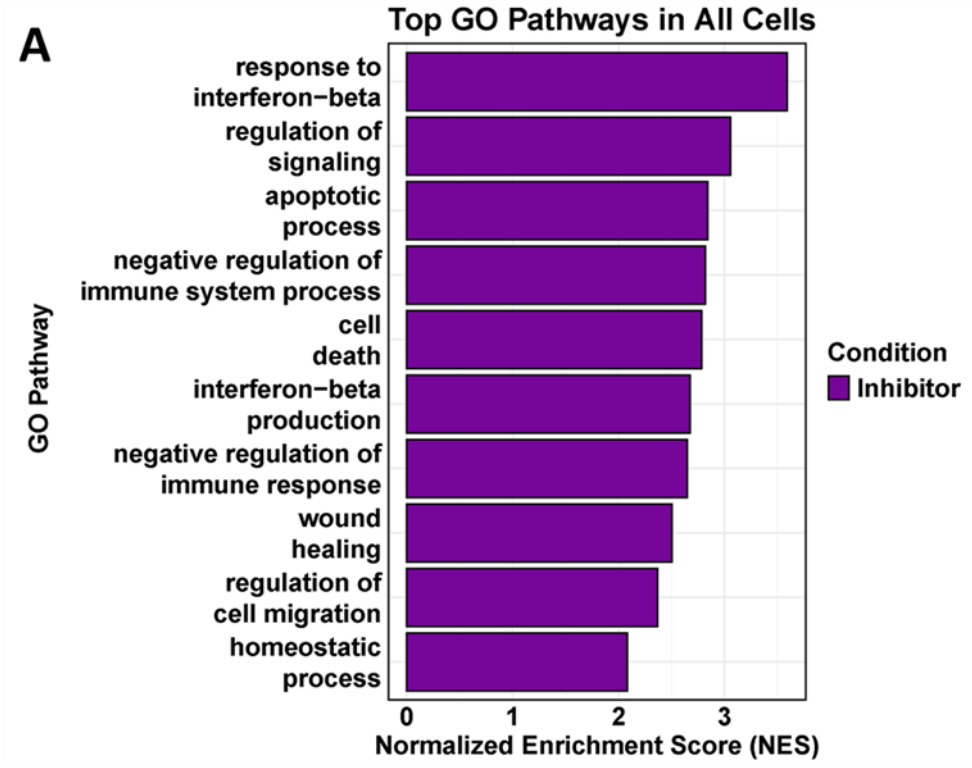

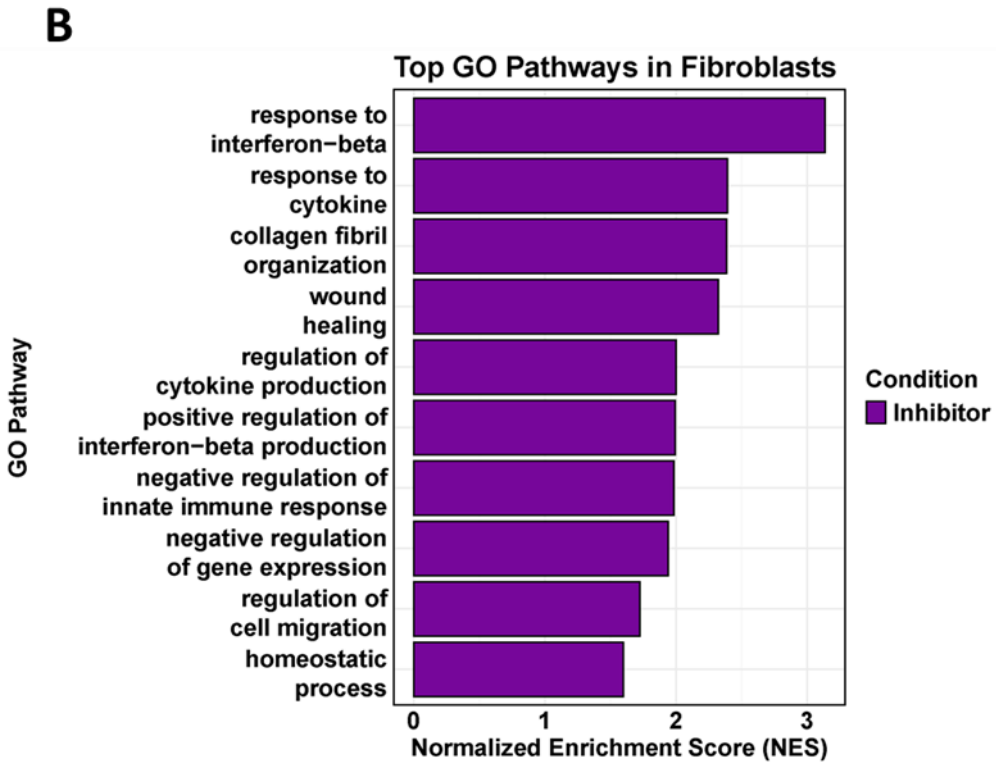

Figure 4.26 Wnt inhibition impedes inflammation in AIA. Bar plots of top significant GO pathways enriched following LGK974 treatment in A) All synovial cells and B) Fibroblasts.

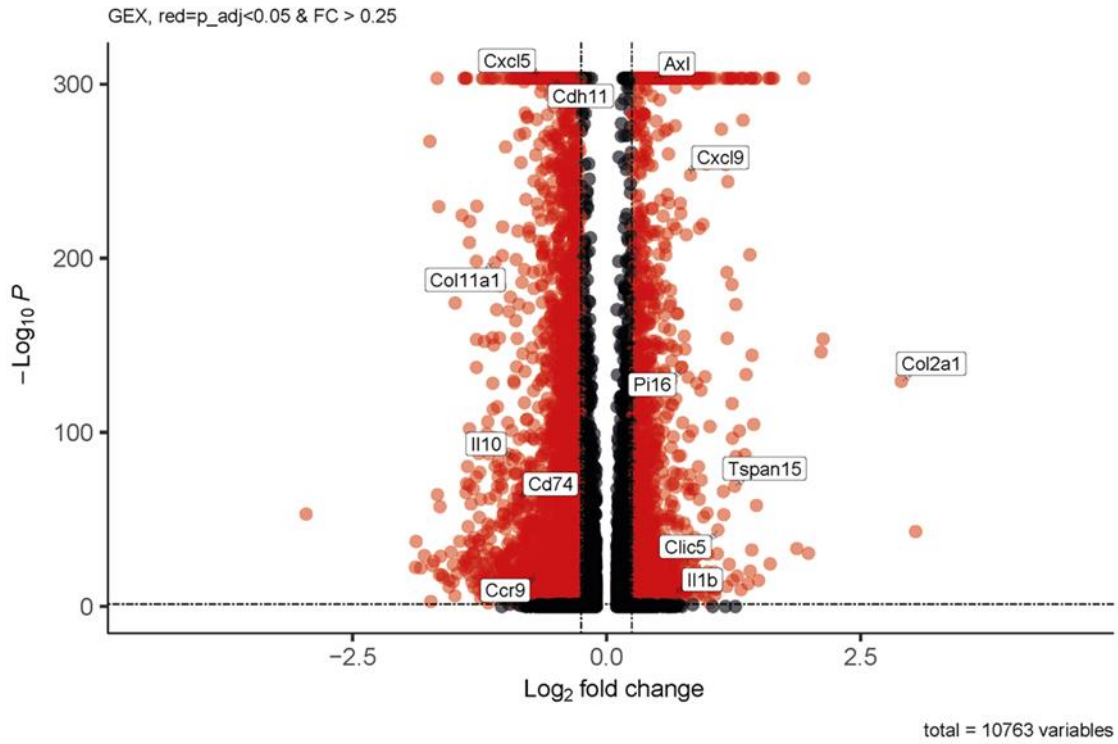

Figure 4.27 Wnt inhibition changes gene expression in AIA. Enhanced volcano plot showing top upregulated and down regulated genes in AIA following treatment with LGK974 compared to injection with control substance.

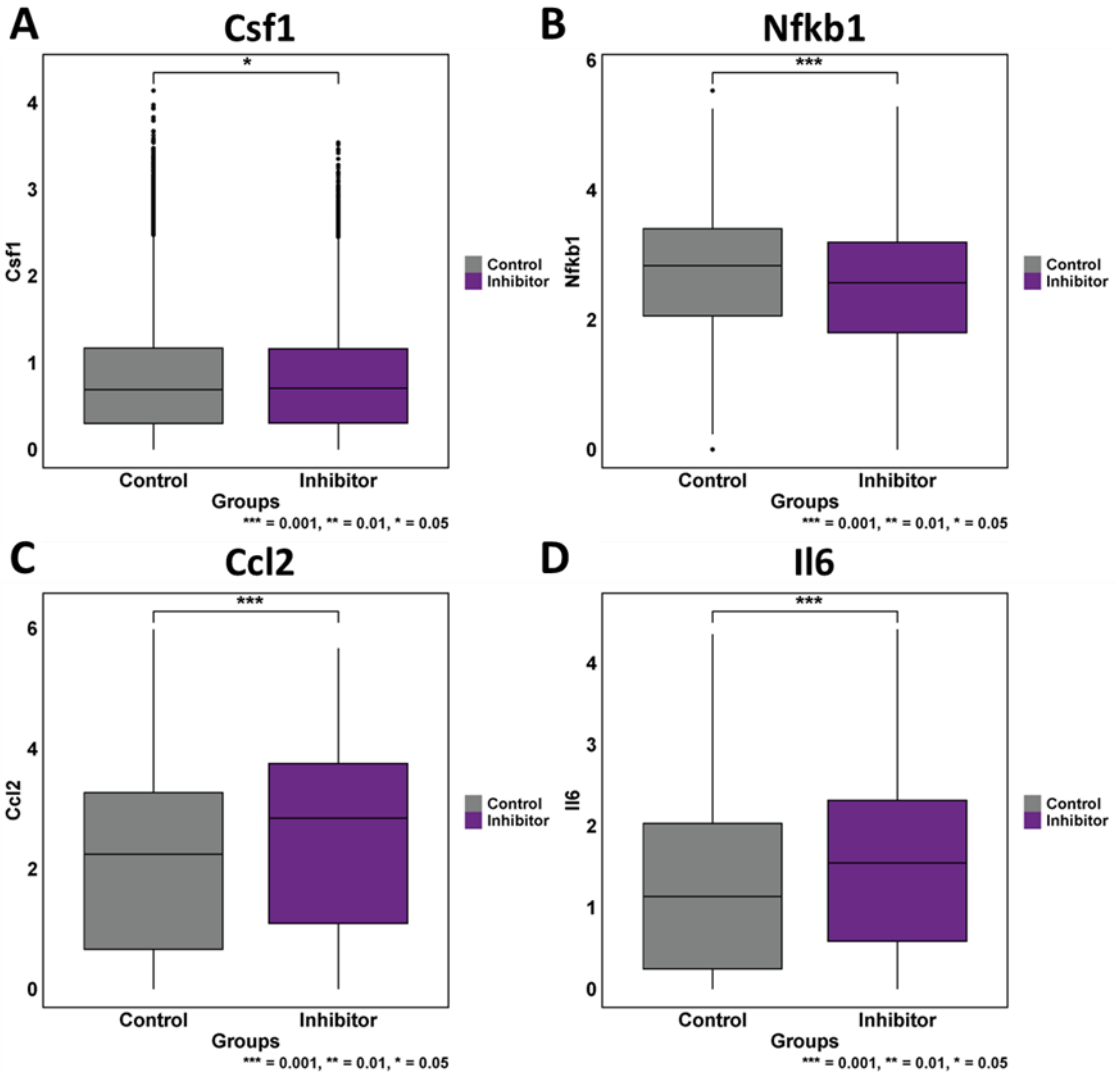

Figure 4.28 Wnt inhibition influences expression of key pro-inflammatory genes. Box plots showing expression of A) Csf1, B) Nfkb1, C) Ccl2 and D) Il6 in Control and LGK974 treated mice. Statistical analyses performed using unpaired t-tests. * p<0.05; ** p<0.01; *** p<0.001; **** p<0.0001. n = 3 per condition.

4.6 Chapter Discussion

4.6.1 Meeting the aims

I have used data generated by myself, and published literature to highlight a key role of WNT signalling in fibroblasts during inflammatory arthritis. Using a combination of single cell transcriptomics and in vivo experiments, I have demonstrated the role of WNT5A in inflammatory arthritis. Specifically identifying the impact of WNT5A on leukocyte recruitment, particularly macrophages and dendritic cells. I successfully showed that inhibition of WNT signalling can improve disease severity, with opposing effects to WNT5a, identifying a key target to disrupt chronic inflammation in the treatment of RA.

4.6.2 Overall findings

WNT5A Enrichment and Fibroblast Activation in RA

My research confirms that WNT signalling is enriched in fibroblasts during the peak and persistent phases of arthritis, aligning with published works where the role of WNT signalling is well established in inflammation[215–218], fibroblasts [219–222]and specifically RA[223–225,225–228].

More recently, WNT5A has emerged as a specific regulator of fibroblast mediated inflammation in RA. Patients with RA had elevated levels of WNT5A[206], in vitro stimulation of cells with WNT5A upregulated expression of several cytokines associated with the pathogenesis of RA[205], and WNT5A conditional knockout mice displayed improved arthritis severity[229]. I found that WNT5A is highly enriched in fibroblasts at peak and persistent phases of inflammatory arthritis. In particular, the

exclusion of WNT5A from Cthrc1+ Postn+ fibroblasts, which are thought to be involved in resolution, suggests that WNT5A's role is tied specifically to inflammatory fibroblast subpopulations.

The further enrichment of Wnt signalling in persistent inflammation would be an interesting area for further exploration. It has previously been shown that Wnt5a can induce a feedback loop within a tissue microenvironment, leading to sustained and chronic inflammation[223,224,230–232]. This could be one of the key mechanisms of chronic inflammation in RA and a key target for treatment.

Impact of Recombinant WNT5A on Synovial Inflammation

The in vivo experiments injecting recombinant WNT5A (rWNT5A) into murine knee joints confirmed that WNT5A is not merely a marker of inflammation, but actively drives synovial pathology. Mice injected with rWNT5A exhibited significantly greater knee swelling, arthritis severity, and synovial hyperplasia compared to controls. Flow cytometry and scRNA-seq analyses further revealed that rWNT5A increased the recruitment of leukocytes, macrophages, and dendritic cells into the synovium. These observations are supported by claims in the literature that Wnt5a is a crucial mediator of inflammatory cell recruitment[204,230,231]. Notably, the upregulation of Csf1 suggests recruitment of macrophages is key to the proinflammatory actions of Wnt5a, which has also been reported elsewhere[233–235].

Interestingly, I did not see significant changes in fibroblast numbers or activation markers, despite reports that Wnt5a induces fibroblast activation, proliferation and migration[207,208,220,228,231]. This could be a caveat of the experimental set up, locally

injecting Wnt5a into the joint, rather than inducing specific upregulation from fibroblasts, it could be that this is required to have an impact on the fibroblast population. The trends saw towards increased CD4+ T cells and decreased regulatory T cells also highlight WNT5A's role in modulating adaptive immunity, an area worth exploring in future studies, it has been previously shown that Wnt signalling negatively modulates regulatory T Cells[226].

Inhibition of WNT and Therapeutic Implications

Administration of the Wnt inhibitor LGK974 significantly reduced synovial inflammation, synovial hyperplasia, and the frequency of leukocytes, including regulatory T cells. Validating previous reports that inhibition of Wnt signalling can reduce the severity of inflammation and arthritis[224,227,236,237].

These findings are consistent with earlier studies that demonstrate the therapeutic potential of Wnt pathway inhibition in modulating fibroblast-driven inflammation. However, it is noteworthy that LGK974 did not significantly reduce arthritis severity across the whole-time course, suggesting that Wnt inhibition may be most effective during specific windows of disease progression.

The scRNA-seq data indicated significant downregulation of pro-inflammatory pathways. Although the upregulation of Il6 with LGK974 warrants further investigation. This could potentially be a caveat of the experimental design. The small molecule LGK974 was injected intraperitoneally in a solution of corn oil and DMSO, which was also used as the vehicle control. I observed that both conditions induced negative side effects on the mice, including weight loss and increased

observations of the mouse grimace scale. Conversely, I wonder if the daily IP injections of either solution induced a systemic inflammatory response.

The enriched involvement of interferon-β signalling, and expression of lining fibroblast markers further suggests that Wnt inhibition promotes a shift towards tissue homeostasis, and presents an interesting area to further investigate. Several studies have implicated a connection between IFN-β, Wnt signalling and dendritic cells[226,238–240], which further supports the findings of this chapter, and the impact of rWnt5a and LGK974 on DCs shown in the flow cytometry analysis.

4.6.3 Conclusion

In summary, Wnt signalling in pathogenic synovial fibroblasts proves to be a key target in RA. It could be a crucial mechanism of disease, particularly in treatment resistant patients with Pauci-immune tissue pathotypes. Wnt5a is produced by synovial fibroblasts and promotes leukocytes recruitment, specifically macrophages and DCS, and potentially induces a positive feedback loop leading to chronic and sustained inflammation of the joint. Inhibition of Wnt signalling may reverse these actions, and is presented as a potential therapeutic target in the treatment of RA.

5 INVESTIGATING FIBROBLAST-MEDIATED MECHANISMS OF RESOLUTION IN INFLAMMATORY ARTHRITIS

5.1 Introduction

Joint inflammation in inflammatory arthritides, such as RA, can resolve spontaneously, although this is uncommon or alternatively, following therapeutic intervention[241,242]. In addition, despite its chronicity RA also has a relapsing remitting course with episodes of joint inflammation that resolve[241–243]. Understanding the mechanisms underlying the resolution of joint inflammation and clinical remission in arthritis is crucial for advancing new treatment strategies. Currently, these mechanisms are poorly understood. It is still unclear why some patients experience spontaneous or drug-induced remission, while others do not and although it likely involves multiple disease associated factors, such as early, targeted and aggressive treatment. As previously discussed, the disease pathotype may also be a critical and less variable factor[61,62].

In my previous studies, I identified fibroblast and macrophage populations that were enriched during the resolution phase of inflammatory arthritis. The robust presence of these subsets in both the synovial tissue of mice and the joints of individuals with RA suggests a potential conserved mechanism of the resolution of joint inflammation, however the exact causal role of these fibroblast populations in arthritis are currently unknown.

Previous research indicates that the histological pathotype of the disease can predict responses to targeted therapies. For instance, individuals with a leukocyte-rich

pathotype tend to respond better, while those with a fibroblast-rich pathotype typically respond less favourably[61–63]. In cases of joint inflammation resolution, clearing inflammatory infiltrates from the synovium, repairing tissue damage, and restoring joint homeostasis are essential steps. For patients with the pauci-immune pathotype, restoring homeostasis among tissue-resident fibroblasts is critical, but no current therapies directly target fibroblasts.

Potential mechanisms underlying resolution may involve the development of immune tolerance to reduce autoimmune responses, the recruitment of Treg cells to support tolerance and prevent excessive inflammation, and the restoration of cytokine balance within the joint[244–247]. Notably, certain murine models of inflammatory arthritis, such as AIA and STIA, also exhibit spontaneous resolution without intervention. These models are valuable tools for unravelling the mechanisms driving resolution in inflammatory arthritis and for identifying new therapeutic targets.

Dkk3 (Dickkopf-related protein 3) is a member of the Dickkopf (Dkk) family of proteins, which are known for their roles in Wnt signalling[248]. However, Dkk3 behaves somewhat differently from other members of the Dkk family, which makes its role in Wnt signalling more complex and context dependent. While Dkk1, Dkk2, and Dkk4 primarily act as inhibitors of the canonical Wnt/β-catenin signalling pathway[248], Dkk3's function is less well defined, with reports suggesting both pro- and anti-Wnt activities depending on the biological context. For example, other DKK ligands block Wnt signalling by binding to Wnt co-receptors LRP-5/6[249,250], but DKK3 is not able to bind these receptors[250,251]. There are some examples of DKK3 reducing β-Catenin availability[251–254], but since it has not been shown to bind any of the known members of DKK-mediated Wnt inhibition signalling cascade, the mechanism by which this

occurs in unknown. In fact, little is known about the molecular mechanisms of DKK3 at all, and no receptors that bind DKK3 have currently been identified. Instead, it appears that DKK3 has biological action independent of Wnt inhibition. DKK3 has been implicated in a number of Wnt independent mechanisms. It has been implicated as a protective agent in osteoarthritis[255], and aid the differentiation of fibroblasts into endothelial cells[256]. DKK3 has been shown to play a key role in regulation of proliferation and apoptosis[257], as well as regulating T Cell tolerance and polarisation of regulatory T Cells[258].

5.2 Chapter aims:

The aims of this chapter are:

1. To explore the roles of fibroblast and macrophage populations in the resolution of inflammatory arthritis.
2. To evaluate the cellular and molecular mechanisms involved in promotion of resolution of inflammation in the joint.
3. To evaluate the role of DKK3 as a key marker of pro-resolving fibroblasts and assess its therapeutic potential in inflammatory arthritis.

5.3 Fibroblasts and Macrophages are implicated in the resolution of inflammatory arthritis

I previously identified subsets of fibroblasts (Cthrc1 Postn) and tissue-resident macrophages (MerTK Lyve1) that were proportionally expanded during the resolution phase of inflammatory arthritis and are associated with tissue repair and inflammation clearance. My objective was to examine the role of these cells in inflammatory arthritis. For these studies, I excluded the CIA model from our dataset as it does not exhibit spontaneous resolution, thus focusing specifically on mechanisms of resolution.

Analysis of STIA and AIA inflammatory arthritis models revealed that both fibroblast and macrophage subsets remain enriched during the resolution phase (Figure 5.1). Recent studies have identified similar populations, such as LRRC15+ myofibroblasts in frozen shoulder[181] and MerTK+ macrophages in RA[70], as key drivers of resolution and remission. Comparisons of gene expression profiles show these populations align with their mouse equivalents in our dataset (Figure 5.2).

I further investigated the gene signature of Cthrc1 Postn fibroblasts, finding its presence and that of the frozen shoulder signature across several human diseases/datasets (Figures 5.3 – 5.5). Key marker genes specific to each population were identified (Figure 5.6), and where possible, antibodies were used to validate these findings in murine synovium during STIA and AIA by flow cytometry of digested synovia at specific time points. Numbers of both cell types, in each arthritis model aligned with proportions from the atlas scRNA-seq dataset (Figures 5.7, 5.8).

Additionally, detected PDPN+ POSTN+ fibroblasts were detected in human synovial tissue, specifically in the perivascular region of the sublining tissue (Figure 5.9).

These findings confirmed the enrichment of specific fibroblast (Cthrc1 Postn) and macrophage (MerTK Lyve1) subsets during the resolution of inflammation, particularly in inflammatory arthritis.

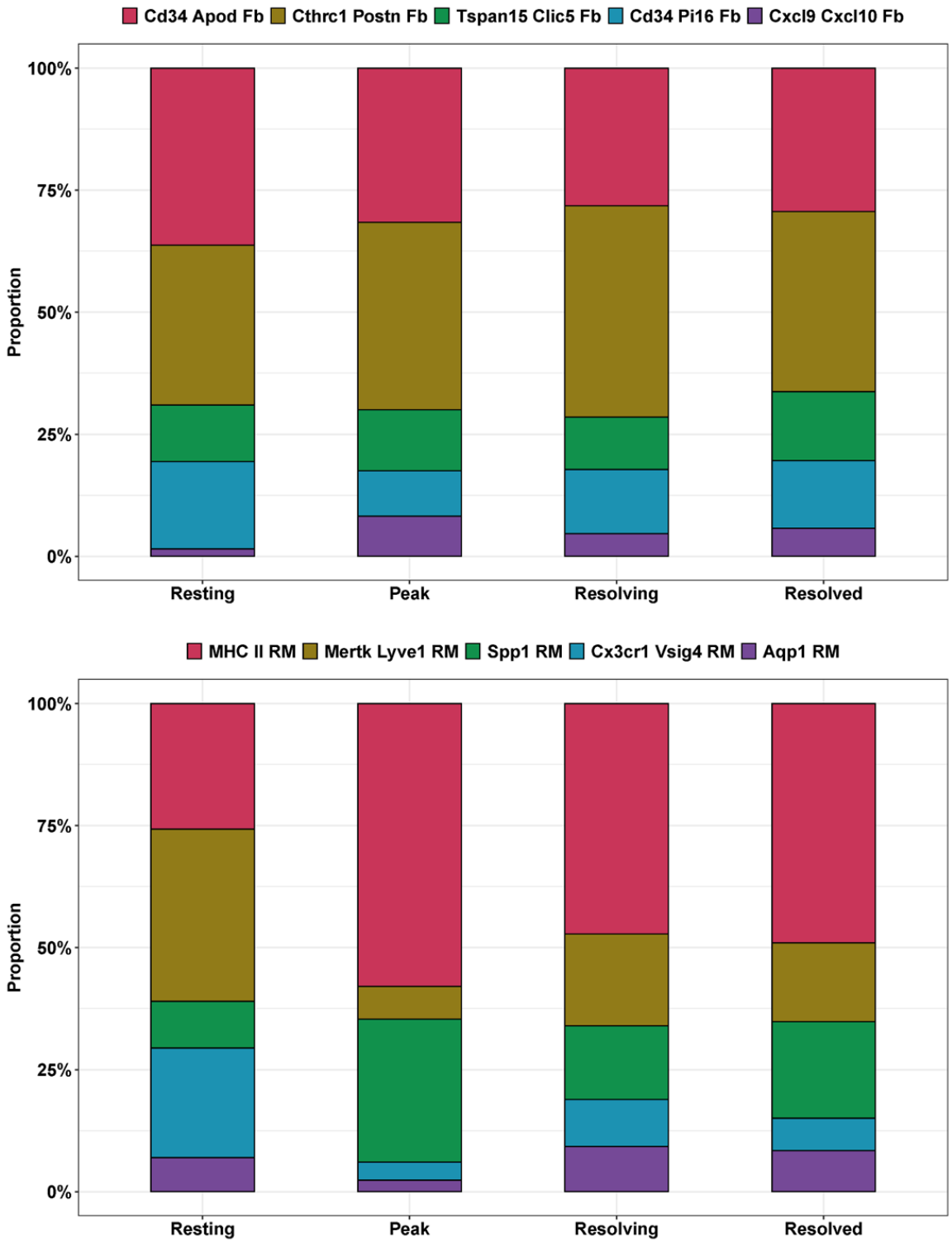

Figure 5.1 Proportional representation of fibroblast (Fb) and tissue-resident macrophage (RM) clusters over the course of inflammatory arthritis. (A) Relative proportions of fibroblast clusters at five distinct stages of arthritis: Resting, Peak, Resolving, Resolved, and Persistent. (B) Proportions of five tissue-resident macrophage clusters at the same time points in both models.

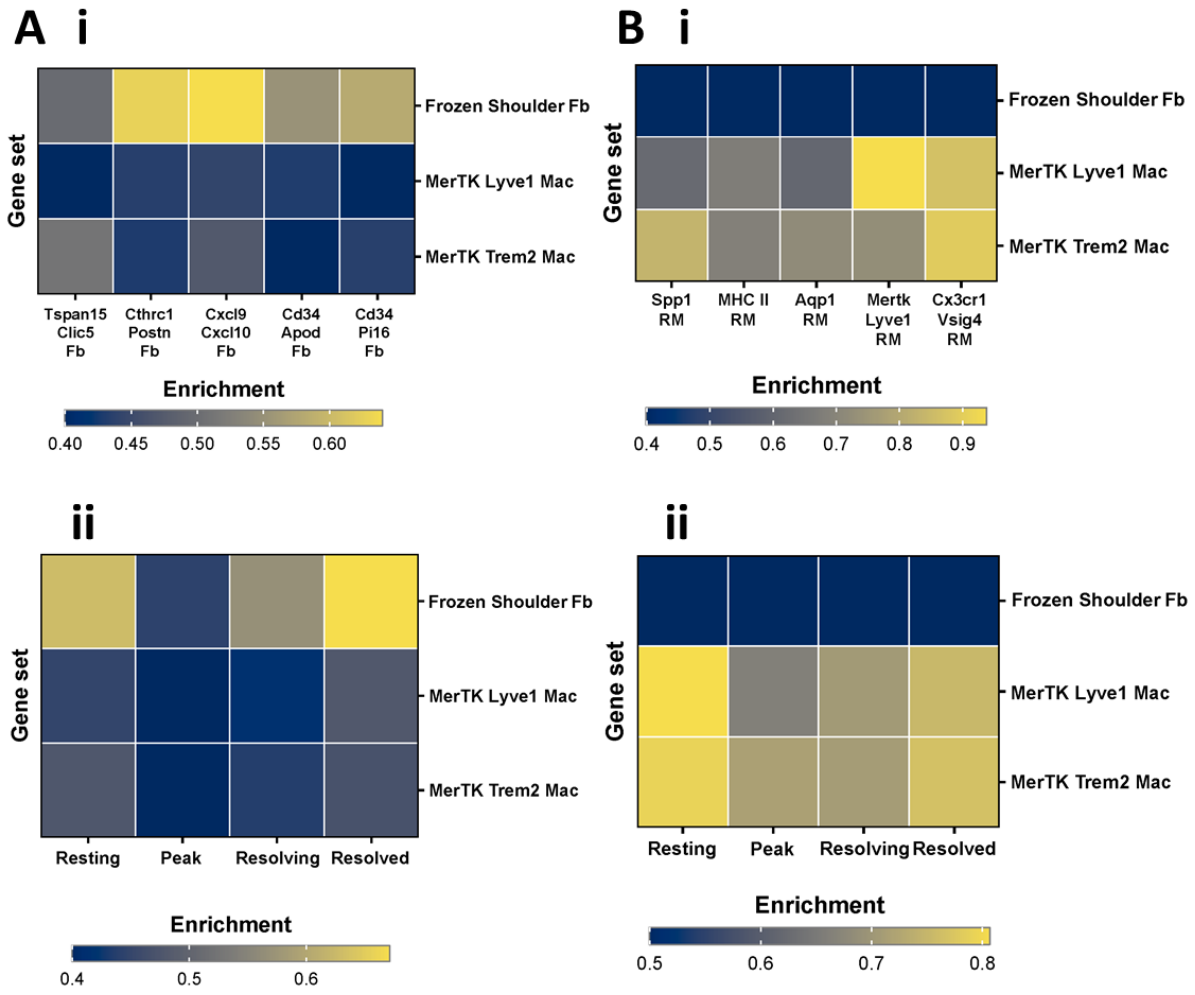

Figure 5.2 Mapping of fibroblast and macrophage gene signatures from external studies onto arthritis clusters. (A) Heatmap showing the expression of gene modules in fibroblasts derived from the frozen shoulder fibroblast subsets identified by the Dakin Lab, and MerTK+ macrophage subsets identified by Alvernini et al., per fibroblast cluster (i) and timepoint (ii). (B) Enrichment of the same modules in resident macrophages per macrophage cluster (i) and timepoint (ii). Module scores were calculated for each gene set, and averaged across cells at each timepoint, then expressed as scaled enrichment.

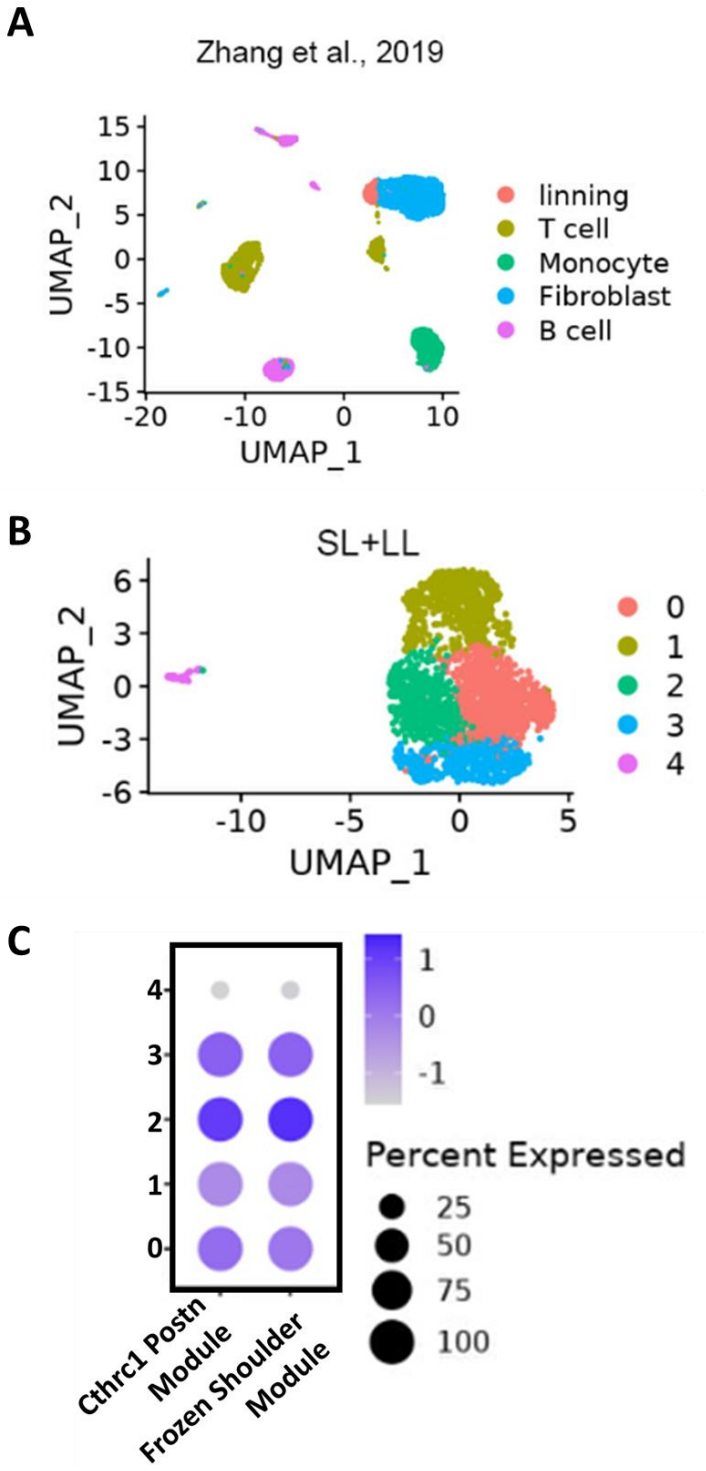

Figure 5.3 Mapping of Cthrc1 Postn and Frozen Shoulder gene modules onto a publicly available scRNA-seq dataset from Zhang et al. (2019). A) UMAP plot showing the clustering of cells from the publicly available dataset by Zhang et al. (2019). (B) UMAP plot showing only fibroblasts from the same dataset, resulting in 5 fibroblast clusters (0-4). (C) Dot plot representing the expression of the Cthrc1 Postn module and the Frozen Shoulder module per fibroblast clusters identified in the Zhang et al. dataset.

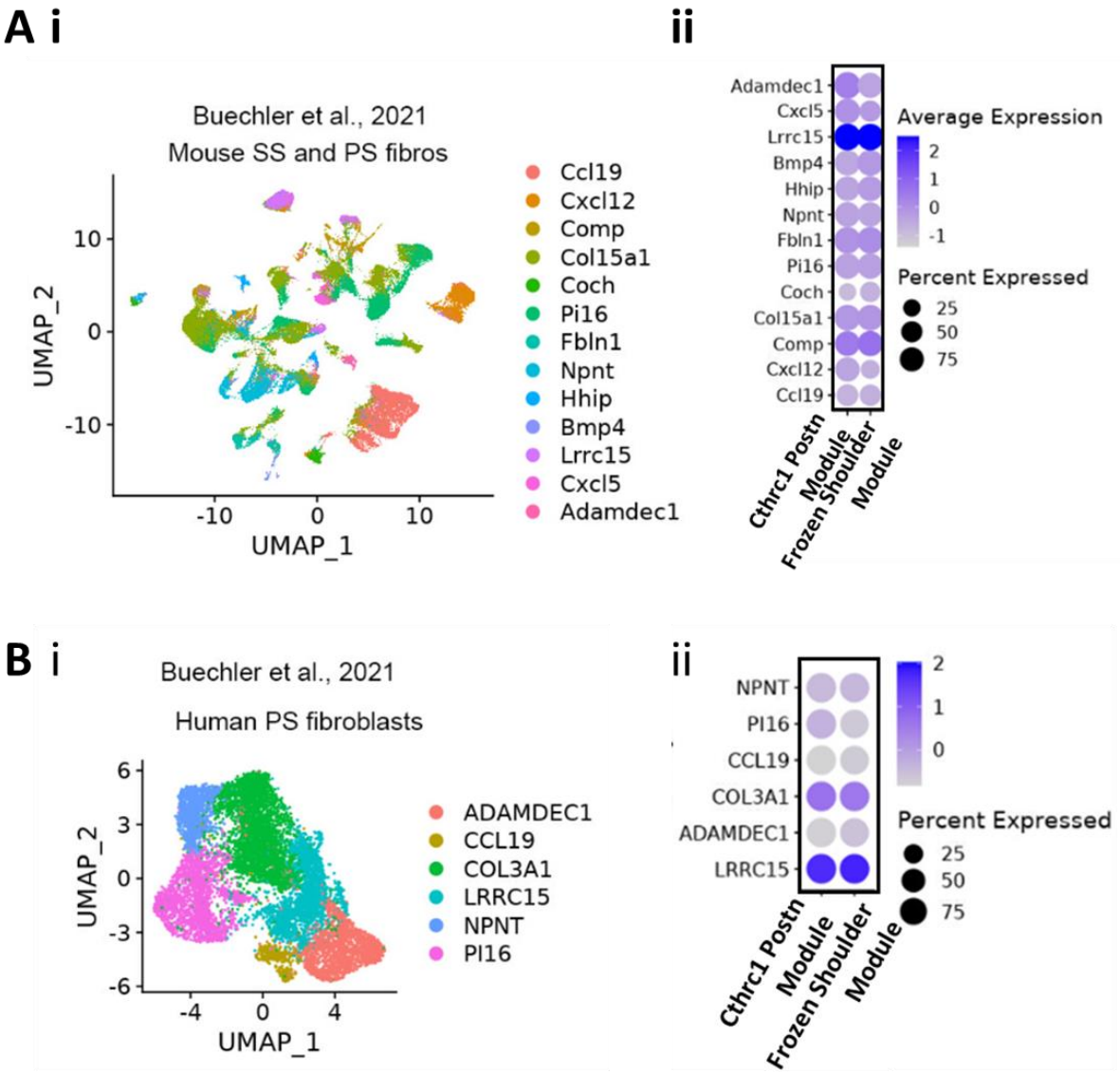

Figure 5.4 Mapping of Cthrc1 Postn and Frozen Shoulder gene modules onto a publicly available scRNA-seq dataset from Buechler et al. (2021). (A) Data from mouse perturbed and steady state fibroblasts, (i) UMAP of fibroblast clusters identified in the dataset. (ii) Enrichment of gene modules per fibroblast cluster. (B) Data from human perturbed state fibroblasts. (i) UMAP of identified fibroblast clusters. (ii) Enrichment of genes modules per fibroblast cluster.

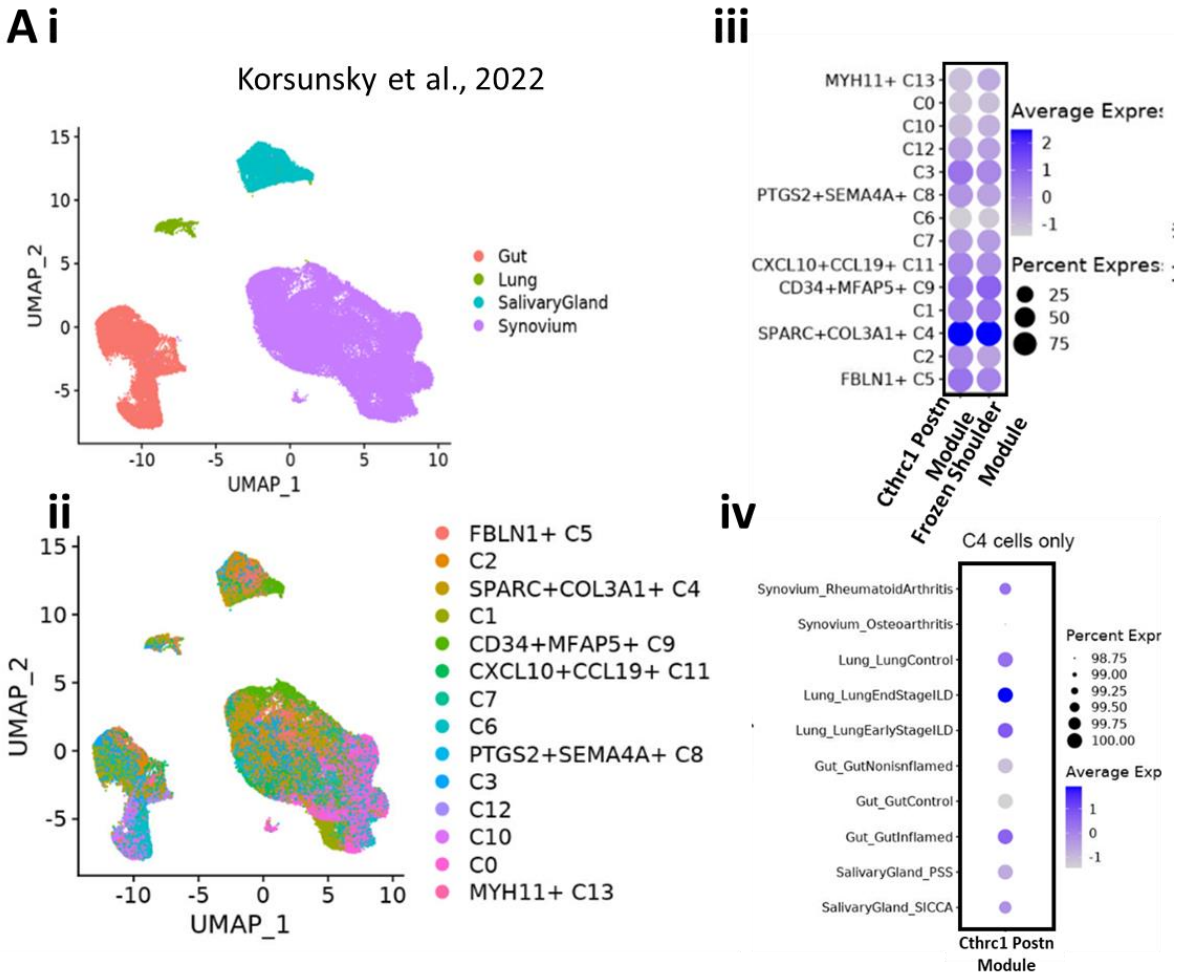

Figure 5.5 Mapping of Cthrc1 Postn and Frozen Shoulder gene modules onto a publicly available scRNA-seq dataset from Korsunsky et al. (2022). (A) Cross-tissue data from human fibroblasts, (i) UMAP of tissues present in the dataset. (ii) UMAP of fibroblast clusters identified in the dataset. (iii) Enrichment of gene modules per fibroblast cluster across tissues. (iv) Enrichment of Cthrc1 Postn gene module across tissues and disease conditions.

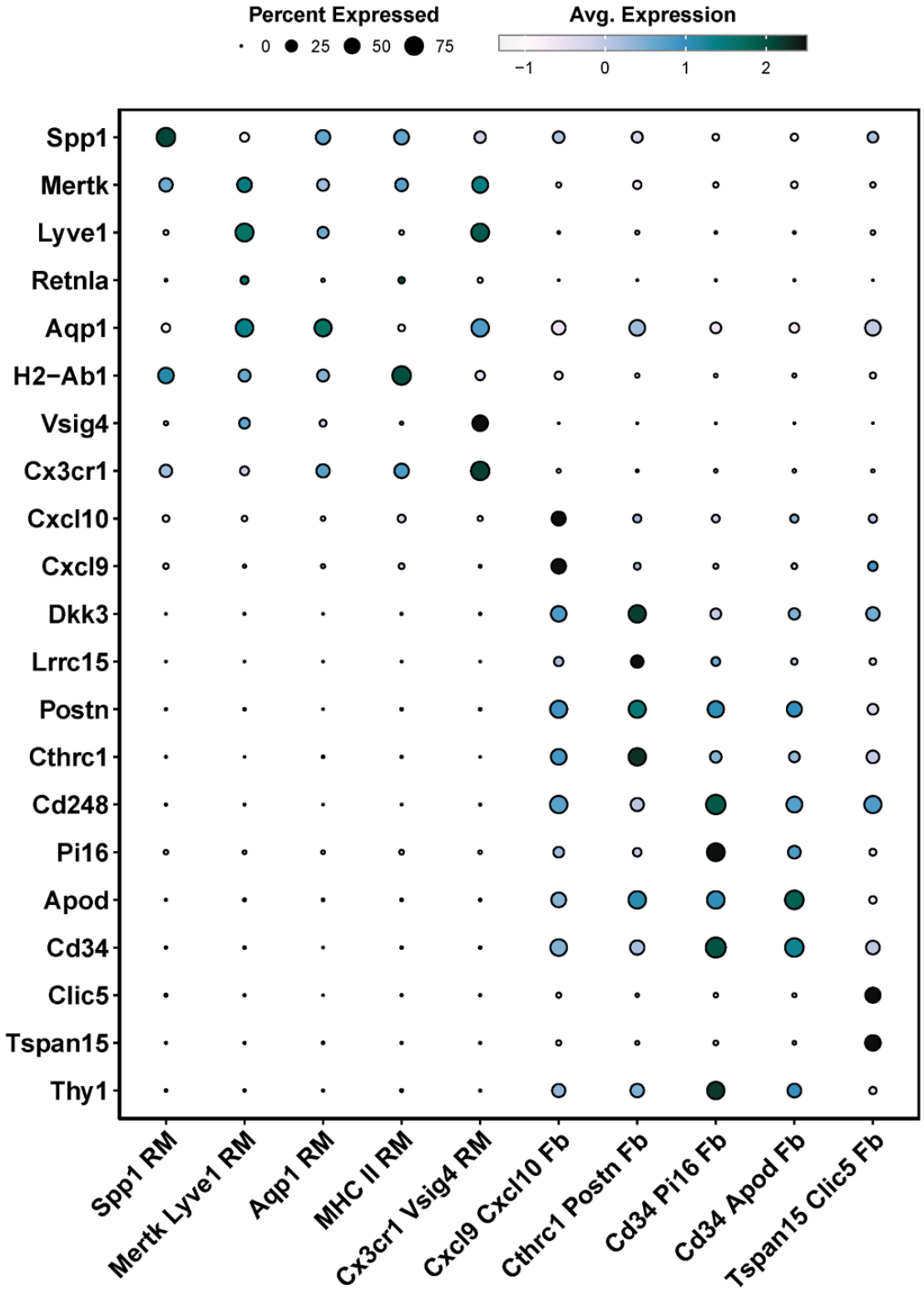

Figure 5.6 Marker genes of fibroblast and resident macrophage clusters in murine inflammatory arthritis. Dotplot showing expression of differentially expressed genes in each fibroblast and tissue resident macrophage cluster.

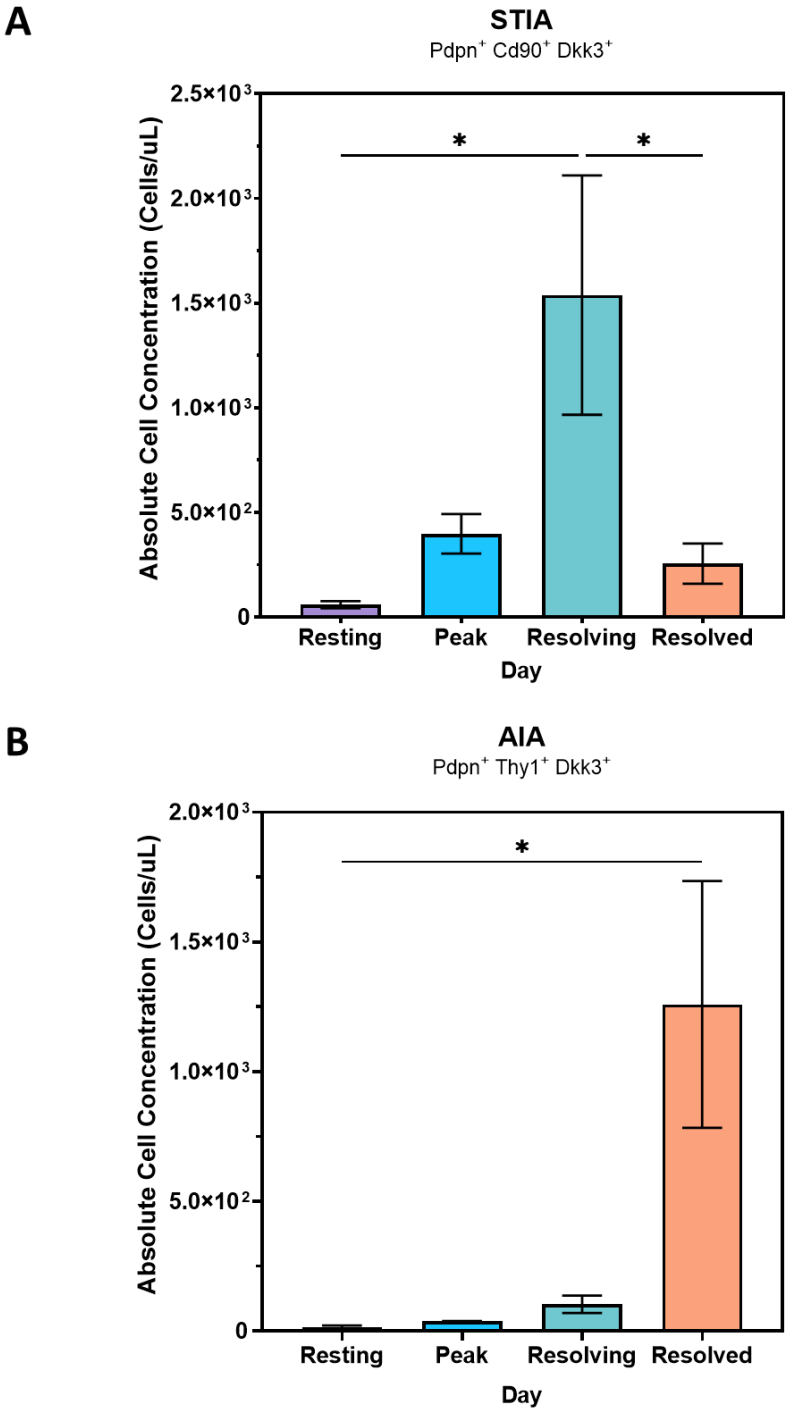

Figure 5.7 Concentration of Dkk3+ fibroblasts in a murine model of inflammatory arthritis. The absolute counts of Pdpn+ Thy1+ Dkk3+ fibroblasts are shown throughout the inflammatory arthritis time course. (A) Antigen-induced arthritis at Resting (Day 0), Peak (Day 2), Resolving (Day 7), and Resolved (Day 10) stages. (B) Serum transfer-induced arthritis at Resting (Day 0), Peak (Day 8), Resolving (Day 15), and Resolved (Day 22) stages. Significance was determined using Two-Way ANOVA followed by Tukey's Post-Hoc test. n=3 mice per timepoint. * $p<0.05$; ** $p<0.01$; *** $p<0.001$; **** $p<0.0001$.

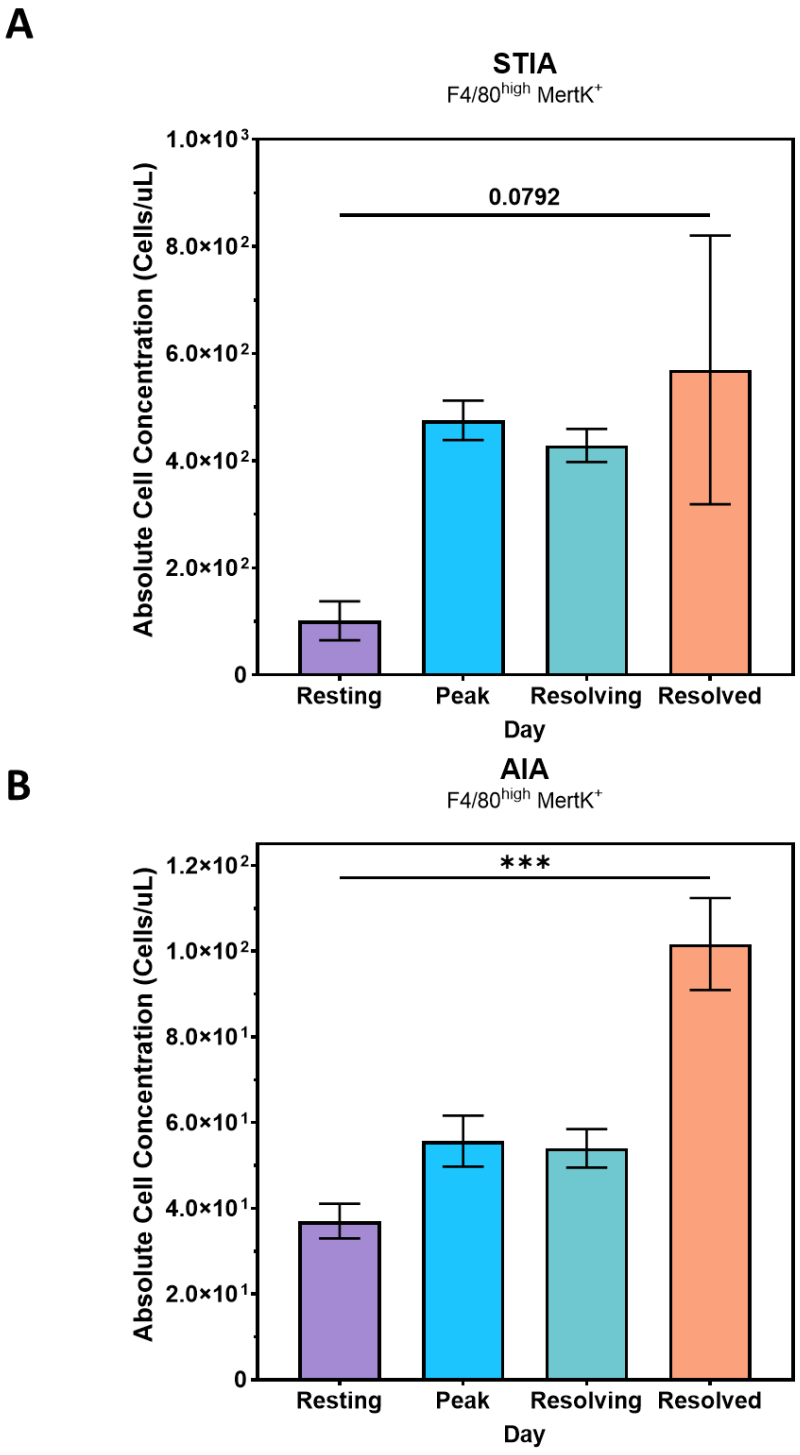

Figure 5.8 Concentration of Mertk+ fibroblasts in a murine model of inflammatory arthritis. The absolute counts of F4/80high Mertk+ macrophages are shown throughout the inflammatory arthritis time course. (A) Antigen-induced arthritis at Resting (Day 0), Peak (Day 2), Resolving (Day 7), and Resolved (Day 10) stages. (B) Serum transfer-induced arthritis at Resting (Day 0), Peak (Day 8), Resolving (Day 15), and Resolved (Day 22) stages. Significance was determined using Two-Way ANOVA followed by Tukey's Post-Hoc test. n = 3 mice per timepoint. * p<0.05; ** p<0.01; *** p<0.001; **** p<0.0001.

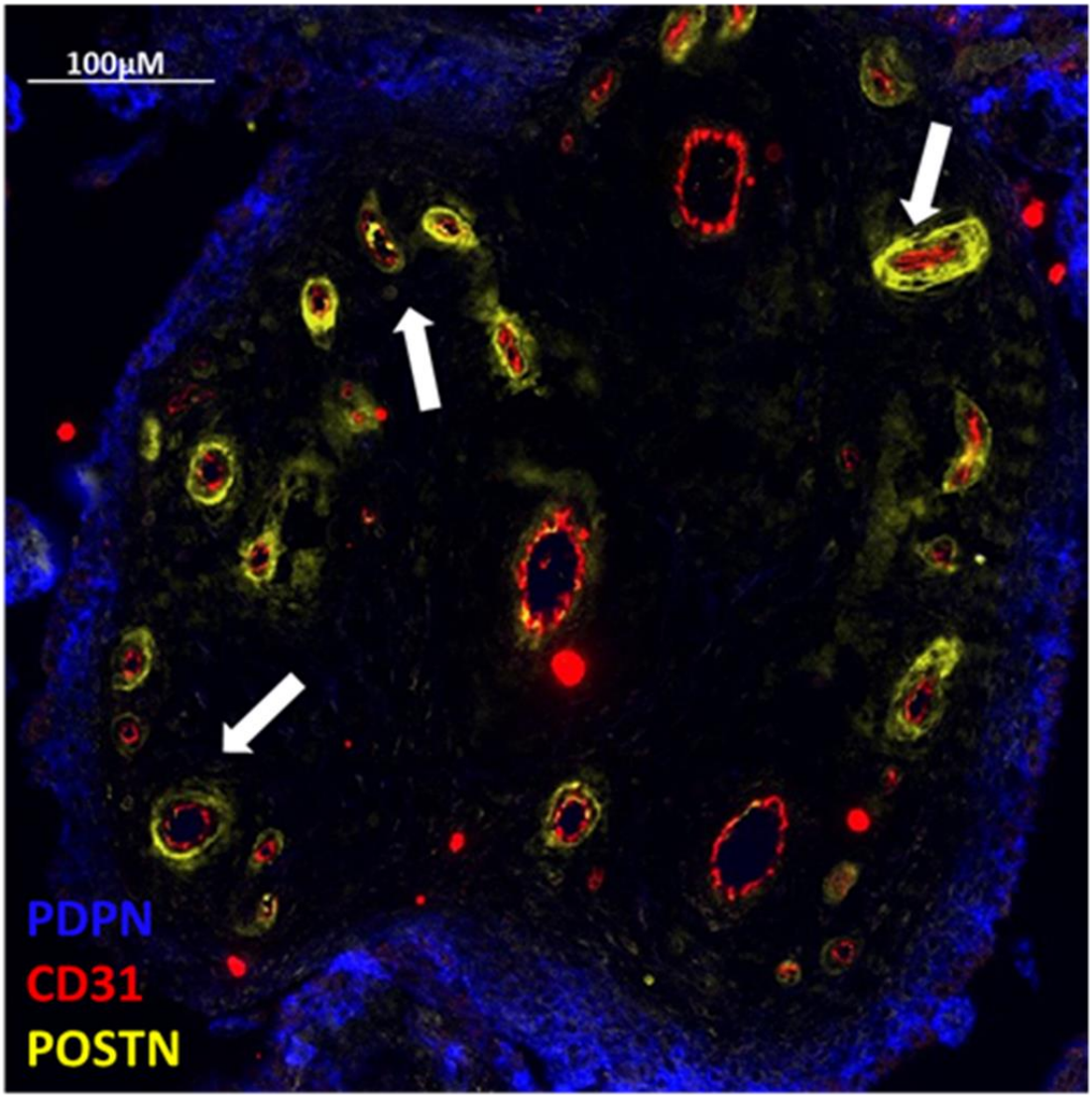

Figure 5.9 Immunofluorescent staining of human synovial tissue. Immunofluorescent imaging of human synovial RA biopsies, stained for PDPN (blue), CD31 (red) and POSTN (yellow). White arrows show localisation of POSTN+ fibroblasts.

5.4 TGF-β Signalling promotes expansion of pro-resolving fibroblasts

To investigate the key cellular and molecular signals driving the enrichment of Cthrc1 Postn fibroblasts during resolution, I performed cell communication analysis. This revealed bidirectional interactions between MerTK Lyve1 macrophages and Cthrc1 Postn fibroblasts, with a stronger signalling dynamic from the macrophages to the fibroblasts (Figure 5.10). Given this finding, I sought to determine whether MerTK Lyve1 macrophages provide the critical stimulus for the enrichment of Cthrc1 Postn fibroblasts during the resolution of inflammation.

I began by confirming that stimulation of primary murine bone marrow-derived macrophages (BMDMs) with dexamethasone enriched for MertK^{high} macrophages, consistent with previous studies[70] (Figure 5.11, A). When primary murine fibroblasts were co-cultured with dexamethasone-stimulated BMDMs, the frequency of DKK3+ Thy1+ fibroblasts increased compared to unstimulated controls (Figure 5.11, B). Interestingly, co-culture with LPS-stimulated BMDMs also elevated the frequency of these fibroblasts, suggesting that macrophage activation, regardless of stimulus type, promotes fibroblast enrichment.

I next investigated the molecular pathways involved in the expansion of the Cthrc1 Postn fibroblast phenotype. Gene Ontology analysis identified a significant enrichment of TGF-β signalling pathways during the resolution phase in both MerTK Lyve1 macrophages (Figure 5.12, A) and Cthrc1 Postn fibroblasts (Figure 5.12, B). Ligand-receptor analysis revealed that MerTK Lyve1 macrophages produced TGF-β1

(Tgfb1), which signalled to TGF-βR3 (Tgfbr3) on Cthrc1 Postn fibroblasts (Figure 5.12, C). In contrast, Cthrc1 Postn fibroblasts primarily signalled to macrophages through the production of collagens (Figure 5.12, D).

To test whether TGF-β could drive the Cthrc1 Postn phenotype, I stimulated primary murine fibroblasts with TGF-β and other cytokines and assessed expression of key marker genes via RT-PCR (Figure 5.13). TGF-β stimulation led to a significant upregulation of Cthrc1 (Figure 5.13, A) and Col1a1 (Figure 5.13, D), while Postn (Figure 5.13, B) and Thy1 (Figure 5.13, E) expression remained unchanged. Notably, TGF-β resulted in downregulation of Dkk3 (Figure 5.13, C). Stimulation with DLL4, a Notch ligand associated with pro-inflammatory Thy1+ fibroblasts, significantly reduced expression of Cthrc1, Postn, and Dkk3. However, when cells were co-stimulated with both TGF-β and DLL4, expression of Cthrc1 and Postn was partially restored, though Dkk3 expression did not.

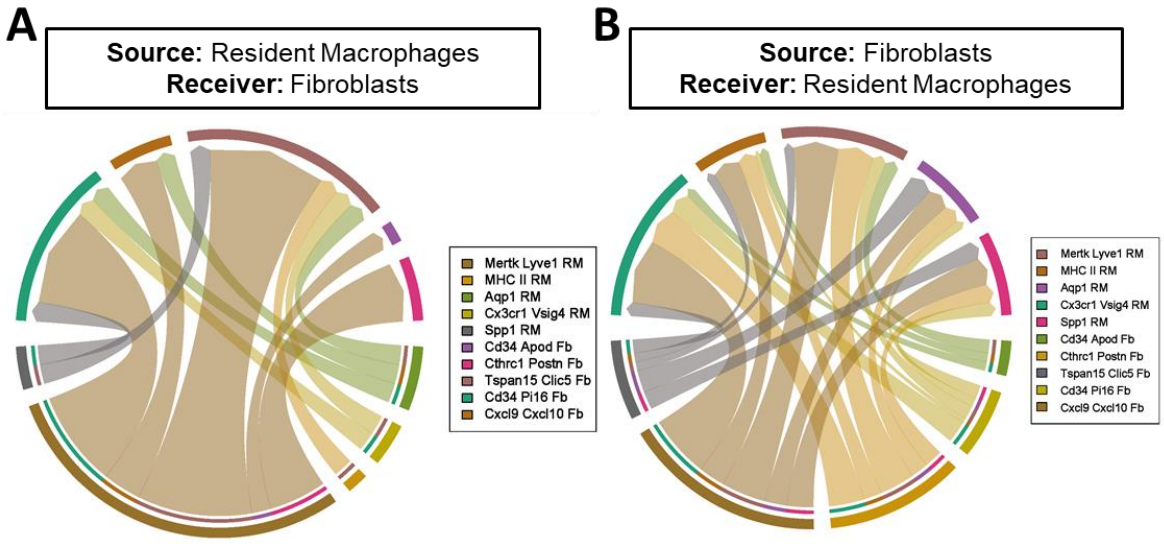

Figure 5.10 Cell Communication Strength Between Fibroblasts and Resident Macrophages. Chord diagrams illustrating the communication pathways (A) from resident macrophage clusters to fibroblast clusters and (B) from fibroblast clusters to resident macrophage clusters. Each arrow shows the direction of communication, originating from the source cluster and pointing to the receiving cluster. The width of each arrow reflects the volume of interactions between the clusters from Liana predicted communications.

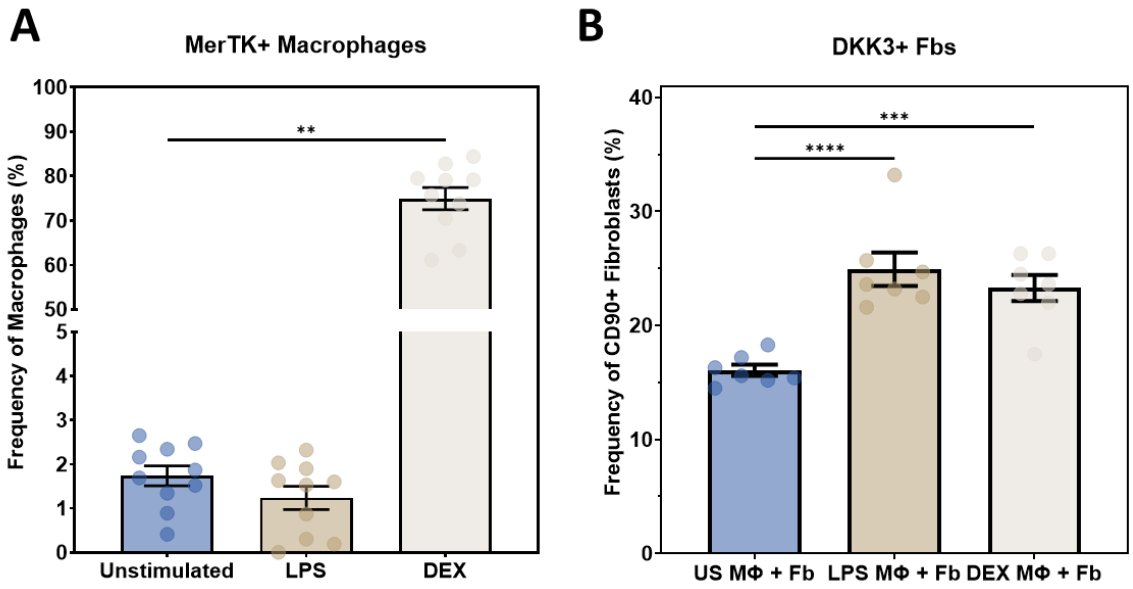

Figure 5.11 Impact of MerTK+ Macrophages on Fibroblast Phenotype. (A) Frequency of MerTK+ bone marrow-derived murine macrophages in conditions of unstimulated, LPS-stimulated, or Dexamethasone-stimulated states. n = 10. (B) Frequency of Dkk3+ fibroblasts following co-culture with unstimulated, LPS-stimulated, or Dexamethasone-stimulated bone marrow-derived macrophages (BMDMs). n = 7 per condition. Statistical analysis was performed using One-Way ANOVA followed by Tukey's Post Hoc test. * $p<0.05$; ** $p<0.01$; *** $p<0.001$; **** $p<0.0001$.

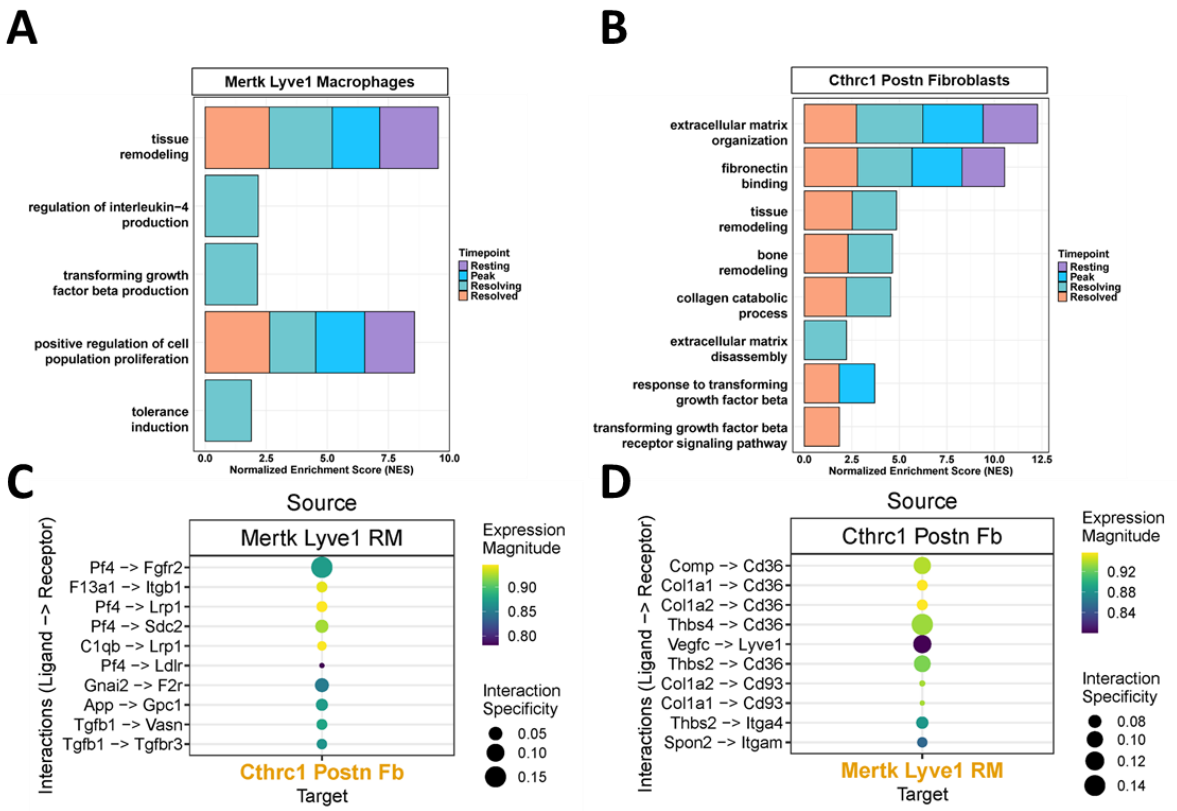

Figure 5.12 Enriched Gene Pathways in Murine Inflammatory Arthritis. Bar plots displaying enriched Gene Ontology (GO) terms at different time points for (A) MerTK+ Lyve1 macrophages and (B) Cthrc1+ Postn fibroblasts. Dot plots illustrate the top significant ligand-receptor pairings: (A) from MerTK+ Lyve1 macrophages to Cthrc1+ Postn fibroblasts and (B) from Cthrc1+ Postn fibroblasts to MerTK+ Lyve1 macrophages.

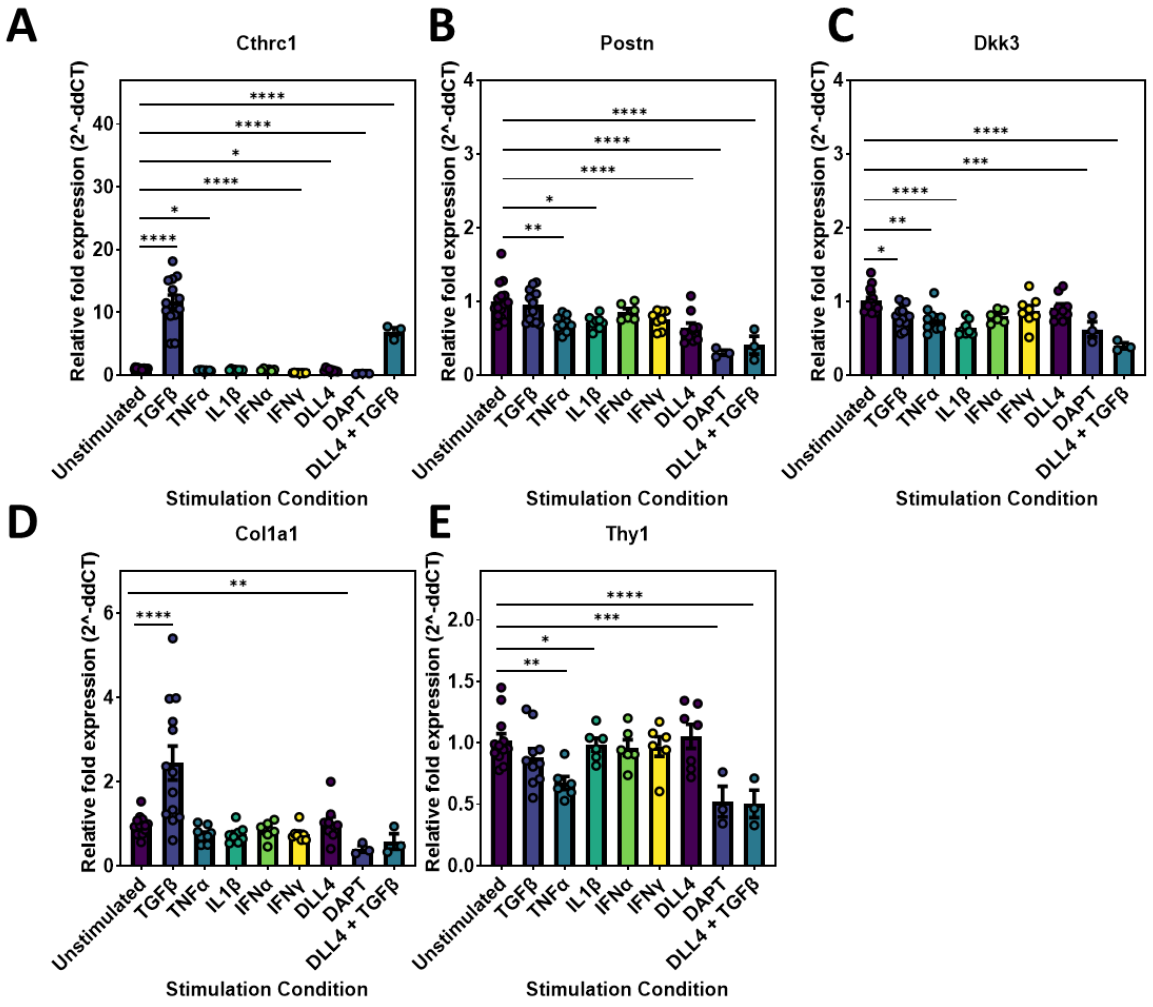

Figure 5.13 Expression of Fibroblast Marker Genes Following Stimulation. Expression levels of key genes associated with Cthrc1+ Postn fibroblasts under various stimulation conditions: (A) Cthrc1, n = 3-15 replicates per stimulation condition, (B) Postn, n = 3-15 replicates per stimulation condition, (C) Dkk3, n = 3-15 replicates per stimulation condition, (D) Col1a1, n = 3-15 replicates per stimulation condition, and (E) Thy1, n = 3-12 replicates per stimulation condition. Statistical analysis was conducted using One-Way ANOVA followed by Tukey's Post Hoc test.* p<0.05; ** p<0.01; *** p<0.001; **** p<0.0001.

5.5 Fibroblast expression of DKK3 correlates with resolution of inflammatory arthritis

I next sought to investigate the mechanisms by which Cthrc1 Postn fibroblasts contribute to the resolution of inflammatory arthritis. I hypothesised that genes upregulated during resolution could actively drive the resolution process. Many of the genes upregulated in all fibroblast populations during resolution were also identified as key markers of the Cthrc1 Postn fibroblast cluster, reinforcing the importance of this fibroblast subset in resolution (Figure 5.14, A). Specifically, within the Cthrc1 Postn fibroblasts, genes such as Lrrc15, Cthrc1, and Dkk3 were notably upregulated during resolution (Figure 5.14, B).

Among these, Dkk3 appeared as a key target for further study due to its highly specific upregulation during the resolution phase. Dkk3 expression in murine fibroblasts was largely confined to the Cthrc1 Postn population (Figure 5.15, A). Furthermore, Dkk3 expression significantly increased during all phases of inflammation compared to the resting state, with the highest levels seen at the resolution timepoint (Figure 5.15, B). Single-cell ATAC-seq analysis of STIA at various timepoints (resting, peak inflammation, and resolution) showed increased chromatin accessibility at the Dkk3 gene locus during the resolved phase, supporting the gene's active role during this stage (Figure 5.15, C). Additionally, synovial biopsies from patients with active rheumatoid arthritis (RA) or in remission demonstrated that DKK3 expression was strongly enriched in sublining fibroblasts from patients in remission (Figure 5.15, D).

To further explore DKK3 expression in RA, I performed RNA-Scope on synovial tissue from patients with active disease, detecting DKK3 alongside the macrophage marker CD68 and the endothelial marker VE-cadherin. DKK3 was seen in both the sublining (Figure 5.16, A, i) and lining regions (Figure 5.16, A, ii) of the synovium. Interestingly, DKK3 expression was found near VE-cadherin in the perivascular sublining areas (Figure 5.16, A, iii) and to CD68 in the synovial lining (Figure 5.16, A, iv), suggesting that DKK3+ fibroblasts may serve distinct functions—interacting with macrophages in the lining and vascular endothelial cells in the sublining.

Unlike other Dickkopf proteins, DKK3's role in Wnt signalling appears to be highly context-dependent, varying across cell types, tissues, and disease states. While some studies suggest that DKK3 can modulate Wnt signalling both positively and negatively, the exact mechanism remains unclear[250].

To determine if Dkk3 was involved in Wnt signalling in this context, I analysed the expression of Wnt-related genes across our dataset (Figure 5.17). Similar to the whole cell atlas analysed in Chapter 4, I observed enrichment of canonical Wnt receptors and co-receptors, including Fzd1, Fzd2, and Lrp6, however, Dkk3 does not interact with any of these proteins. Similarly, we found enrichment of Wnt inhibitor genes Dkk2, Sfrp1, and Sfrp2 in fibroblasts, but again, no evidence of interaction between Dkk3 and these inhibitors. These findings suggest that Dkk3 likely functions independently of Wnt signalling in this context.

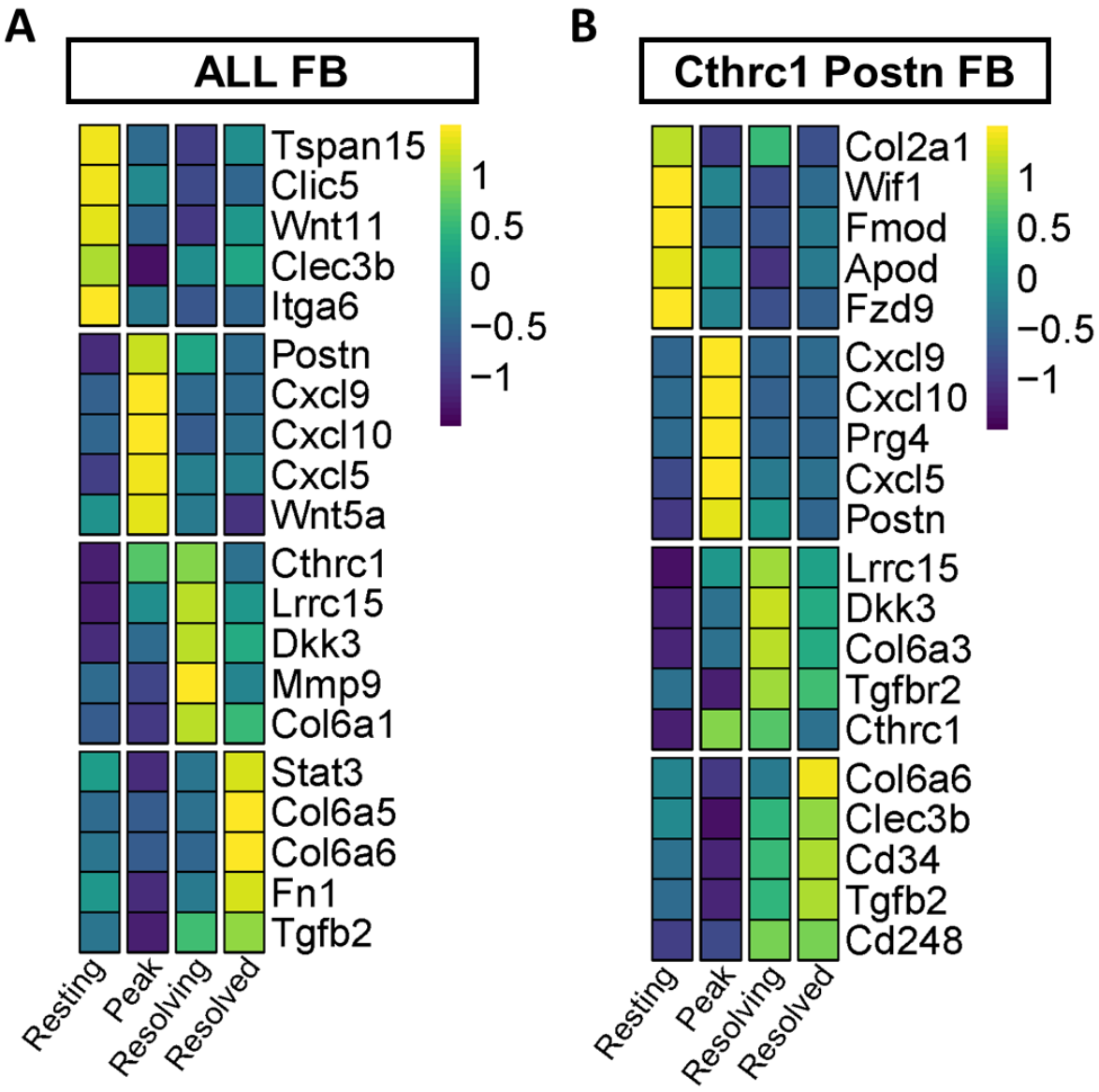

Figure 5.14 Fibroblast Transcriptional Changes Over the Time Course of Inflammatory Arthritis. Genes that are upregulated at each time point during inflammatory arthritis are shown for (A) all fibroblast clusters and (B) Cthrc1+ Postn fibroblasts.

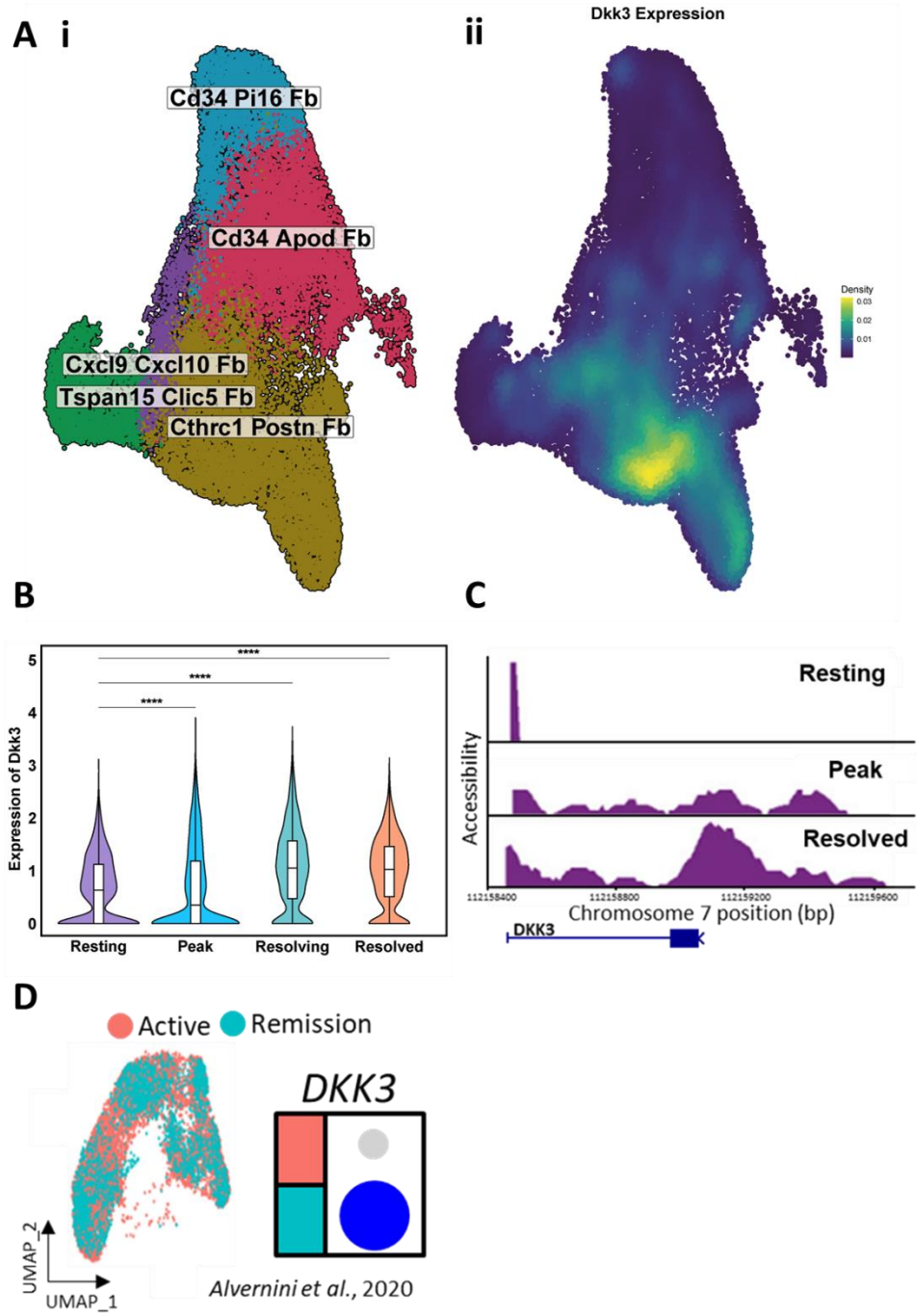

Figure 5.15 DKK3 as a Marker of Resolution in Fibroblasts. (A) UMAP representation of fibroblasts in inflammatory arthritis, displaying (i) cluster identities and (ii) expression density of Dkk3. (B) Violin plots illustrating Dkk3 expression in murine fibroblasts at each time point. n = 3 per timepoint. (C) Chromatin accessibility profile of the Dkk3 gene locus at Resting, Peak, and Resolved time points in serum transfer-induced arthritis (STIA). (D) (i) UMAP of human fibroblasts from Alvernini et al., 2020, comparing patients with active rheumatoid arthritis (RA) and those in remission. (ii) Dot plot depicting DKK3 expression in fibroblasts from patients with active RA versus remission. Statistical analyses were performed using One-Way ANOVA followed by Tukey's Post Hoc test. * $p<0.05$; ** $p<0.01$; *** $p<0.001$; **** $p<0.0001$.

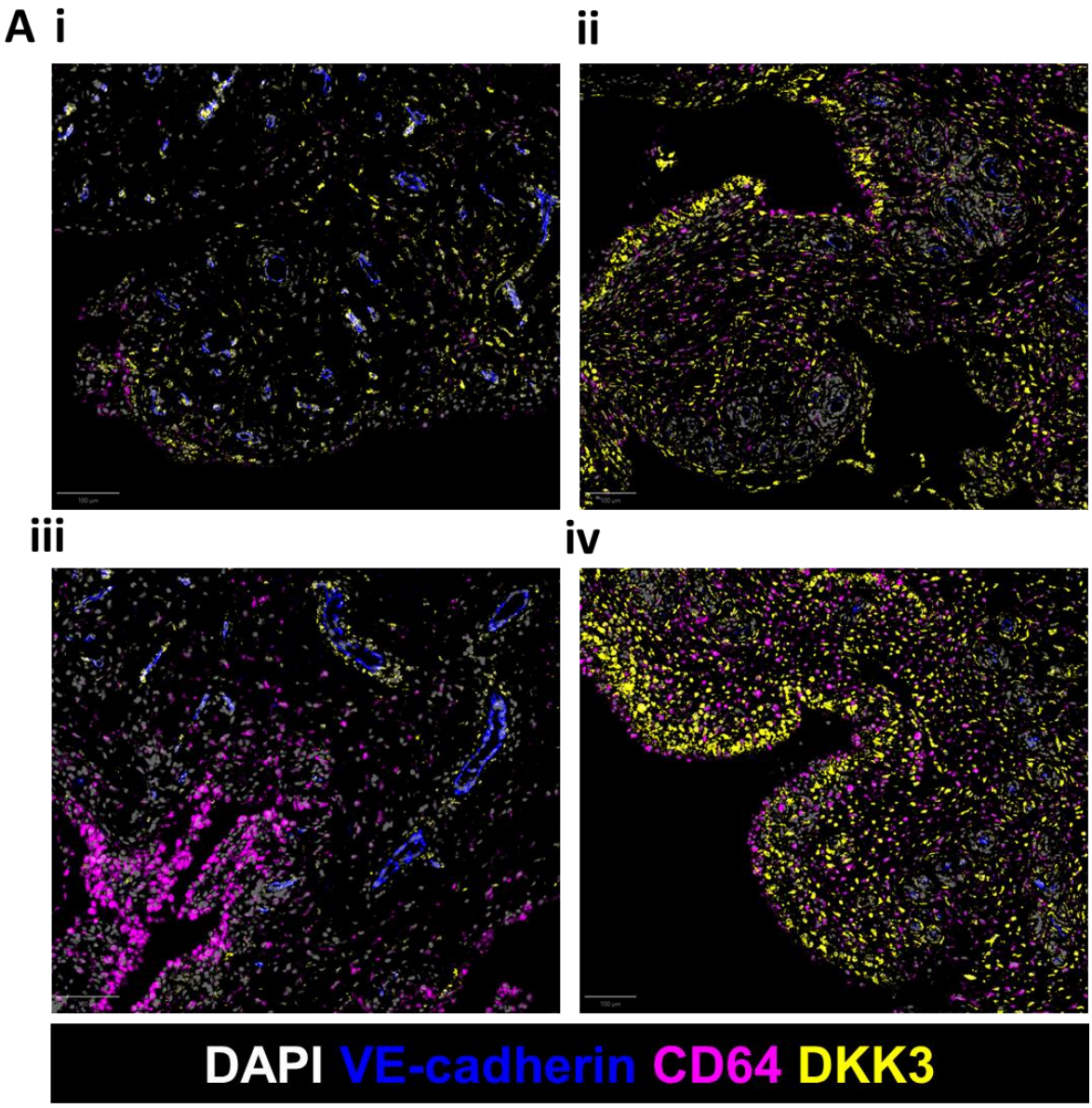

Figure 5.16 Localisation of DKK3 in RA Synovial Biopsies. RNA-Scope staining of four representative regions (i-iv) of synovial tissue from three patients with active rheumatoid arthritis (RA), demonstrating the expression of DAPI (grey), VE-cadherin (blue), CD68 (pink), and DKK3 (yellow).

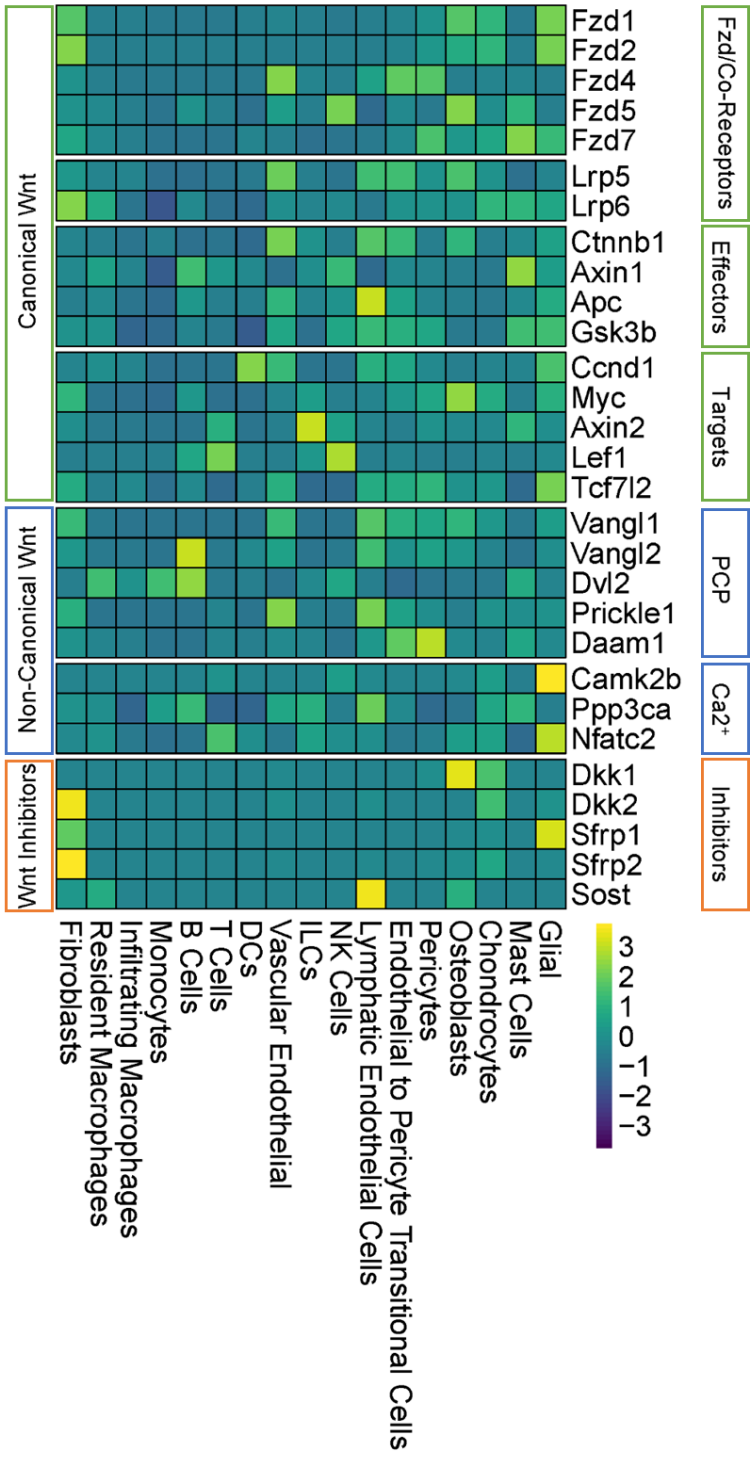

Figure 5.17 Enrichment of Wnt Signalling in Murine Inflammatory Arthritis. Heatmap illustrating the expression of key Wnt signalling genes across various cell types in murine inflammatory arthritis. Gene modules are categorised by the Canonical Wnt pathway, including Frizzled receptors, co-receptors, downstream effector genes, and target genes; Non-canonical Wnt pathways, comprising the planar cell polarity (PCP) pathway and the Ca^{2+} pathway; and Wnt inhibitor genes.

5.6 DKK3 directly promotes resolution of inflammatory arthritis

To investigate whether Dkk3 plays an active role in the resolution of inflammatory arthritis, I injected mice undergoing antigen-induced arthritis (AIA) with either PBS or recombinant DKK3 (rDKK3) protein into the knee joint at the peak of inflammation (Day 2). Dose optimisation details are available in Supplementary Figure 6.

For Final experiments, I determined a single dose of 500ng rDkk3 into the knee joint at day 2 of AIA to be ideal.

Injection of rDKK3 significantly reduced knee swelling at days 3, 4, and 5 of AIA (Figure 5.18, A,i), and when assessed over the entire model duration by calculating the area under the curve (Figure 5.18, A,ii). Additionally, I observed a marked, though non-significant, reduction in global arthritis severity scores at days 3 and 5 (Figure 5.18, B,i and B,ii).

To determine the impact of rDKK3 on the synovial environment, I harvested synovial tissue at Day 4 and conducted flow cytometry analysis. I observed minimal impact on total fibroblasts (Figure 5.19, A), lining fibroblasts (Pdpn+ Thy1-) (Figure 5.19, B), sublining fibroblasts (Pdpn+ Thy1+) (Figure 5.19, C), or pro-inflammatory fibroblasts (Pdpn+ Thy1+ Fap+) (Figure 5.19, D). A trend toward reduced numbers of total leukocytes (Figure 5.20, A), neutrophils (Figure 5.20, B), eosinophils (Figure 5.20, C), macrophages (Figure 5.20, D), B cells (Figure 5.20, E), and T cells (Figure 5.20, F) was observed in the rDKK3-injected group compared to PBS controls, but no effects

were noted on Ly6Chigh (Figure 5.21, C) or Ly6Clow monocytes (Figure 5.21, D). These findings suggest that Dkk3 may exert anti-inflammatory effects in AIA.

Upon examining macrophage populations, I found no effect of rDKK3 on Cx3cr1- macrophages (Figure 5.22, A), a slight increase in Cx3cr1+ barrier macrophages (Figure 5.22, B), a decrease in pro-inflammatory Cx3cr1- MHC-II+ macrophages (Figure 5.22, C), and a significant increase in Mertk+ Lyve1+ sublining macrophages (Figure 5.22, D).

I further analysed T cell populations and found that rDKK3 treatment significantly reduced the frequency of CD4+ T cells (Figure 5.23, A) while increasing the frequency of regulatory T cells (Figure 5.23, F), with no notable effect on other T cell subsets.

Histological analysis confirmed reduced inflammation, showing significant reductions in synovial hyperplasia (Figure 5.24, B,i) and synovial inflammation (Figure 5.24, B,iii) with no change in overall cellularity (Figure 5.24, B,ii). Combined synovitis severity was significantly lower with rDKK3 injection compared to PBS (Figure 5.24, B,iv).

To further assess Dkk3's role in resolving inflammation, I induced AIA in Dkk3-/- mice and compared them with wild-type controls. Although there was a trend toward increased knee swelling (Figure 5.25, A) and higher global arthritis severity (Figure 5.25, B) in Dkk3-/- mice, the differences were not statistically significant, possibly due to compensatory mechanisms.

Given the increase in Mertk+ Lyve1+ macrophages after rDKK3 treatment, I conducted an in vitro experiment to determine whether this effect was a direct result of Dkk3 stimulation. Co-culture of BMDMs with primary murine fibroblasts revealed that unstimulated macrophages co-cultured with fibroblasts resulted in a higher frequency of Mertk Lyve1 macrophages compared to dexamethasone-stimulated macrophages (Figure 5.26, A), and Dkk3-stimulated fibroblasts did not influence the frequency of these macrophages. Direct stimulation of BMDMs with rDKK3 at various doses revealed that 50 ng/mL rDKK3 significantly increased Mertk Lyve1 macrophages, although the effect was not as pronounced as dexamethasone.

To explore the impact of Dkk3 on T cells, I stimulated murine T cells with rDKK3 (Figure 5.27). A dose of 200 ng/mL rDKK3 significantly reduced the frequency of CD4+ (Figure 5.27, A) and CD8+ T cells (Figure 5.27, B) while three different doses of rDKK3 (100 ng/mL, 200 ng/mL, 400 ng/mL) significantly increased the frequency of regulatory T cells (Figure 5.27, C), suggesting that Dkk3 promotes resolution by driving regulatory T cell differentiation.

Single-cell RNA sequencing of synovial tissue from mice treated with PBS or rDKK3 at Day 4 of AIA revealed no significant changes in the proportions of regulatory T cells (Figure 5.28, B,i), Cthrc1 Postn fibroblasts (Figure 5.28, B,ii), or Mertk Lyve1 macrophages (Figure 5.28, B,iii), though there was a trend toward an increase in these populations in the Dkk3 condition.

Cell communication analysis confirmed that Cthrc1 Postn fibroblasts signal to regulatory T cells in both conditions, with stronger interactions observed in the rDKK3-treated group (Figure 5.29, A,i & B,i). In contrast, interactions from regulatory T cells to Cthrc1 Postn fibroblasts were absent in the control condition (Figure 5.29, A,ii) but present in the rDKK3 group (Figure 5.29, B,ii), highlighting the significance of these cell-cell interactions in Dkk3-mediated resolution.

Furthermore, Cthrc1 Postn fibroblasts from rDKK3-treated mice were enriched for pathways related to tissue remodelling, TGF-β signalling, anti-angiogenesis, and apoptosis (Figure 5.30). rDKK3-treated synovial cells showed downregulation of pro-inflammatory genes and upregulation of anti-inflammatory genes (Figure 5.31, A), as well as enrichment of genes associated with apoptosis (Figure 5.30, B), anti-angiogenesis (Figure 5.31, C), tissue remodelling (Figure 5.31, D), and regulatory T cells (Figure 5.31, E).

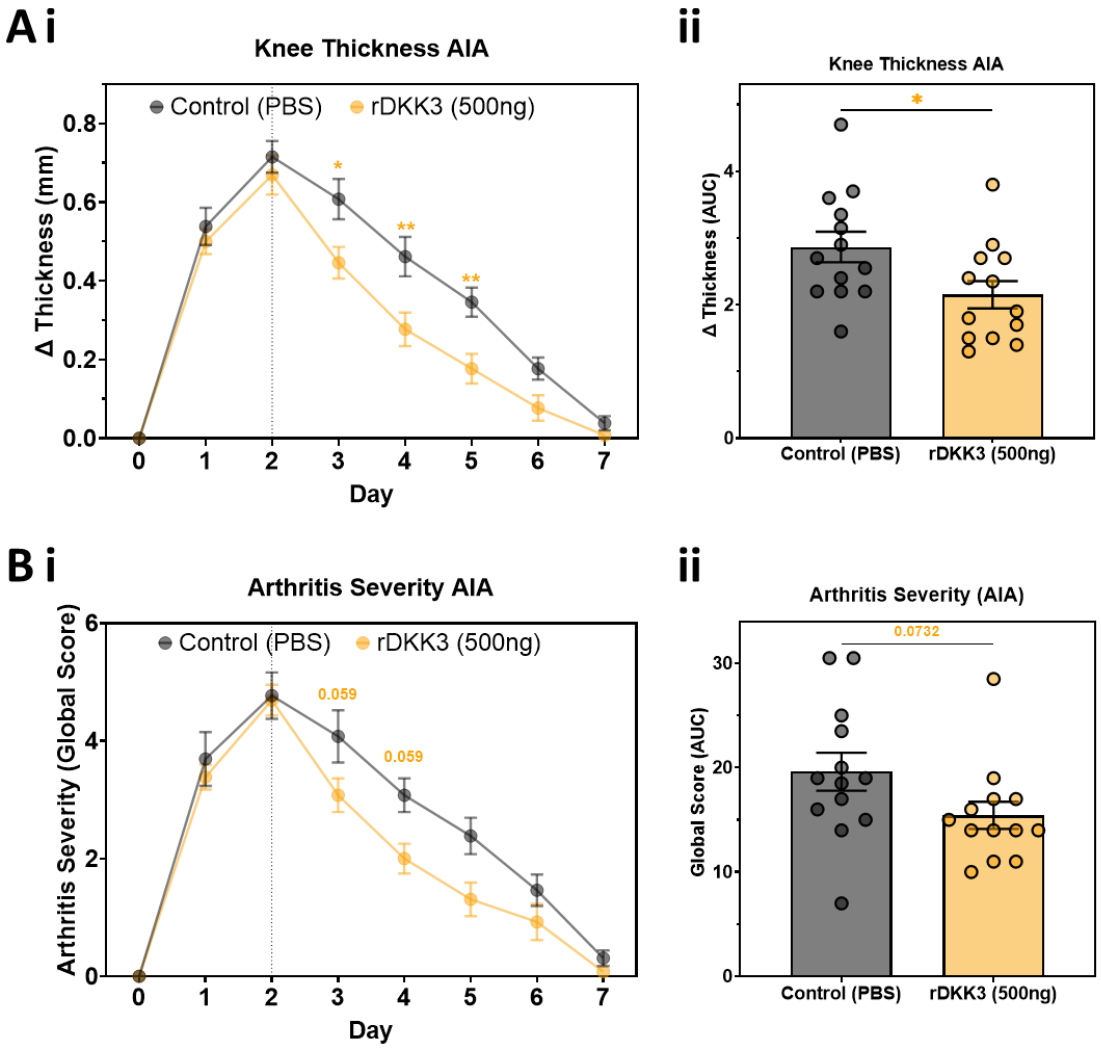

Figure 5.18 rDKK3 Ameliorates Antigen-Induced Arthritis in Mice. (A) Measurements of knee swelling in mice subjected to antigen-induced arthritis (AIA), treated on day 2 with either PBS control or 500 ng murine rDKK3 protein. (i) Change in knee swelling over time. (ii) Change in knee swelling quantified by the area under the curve. (B) Arthritis severity assessed using a global arthritis score sheet: (i) over time and (ii) calculated area under the curve. Statistical analyses were performed using Two-Way ANOVA followed by Tukey's Post Hoc test and unpaired t-tests. * p<0.05; ** p<0.01; *** p<0.001; **** p<0.0001. n = 13 per condition.

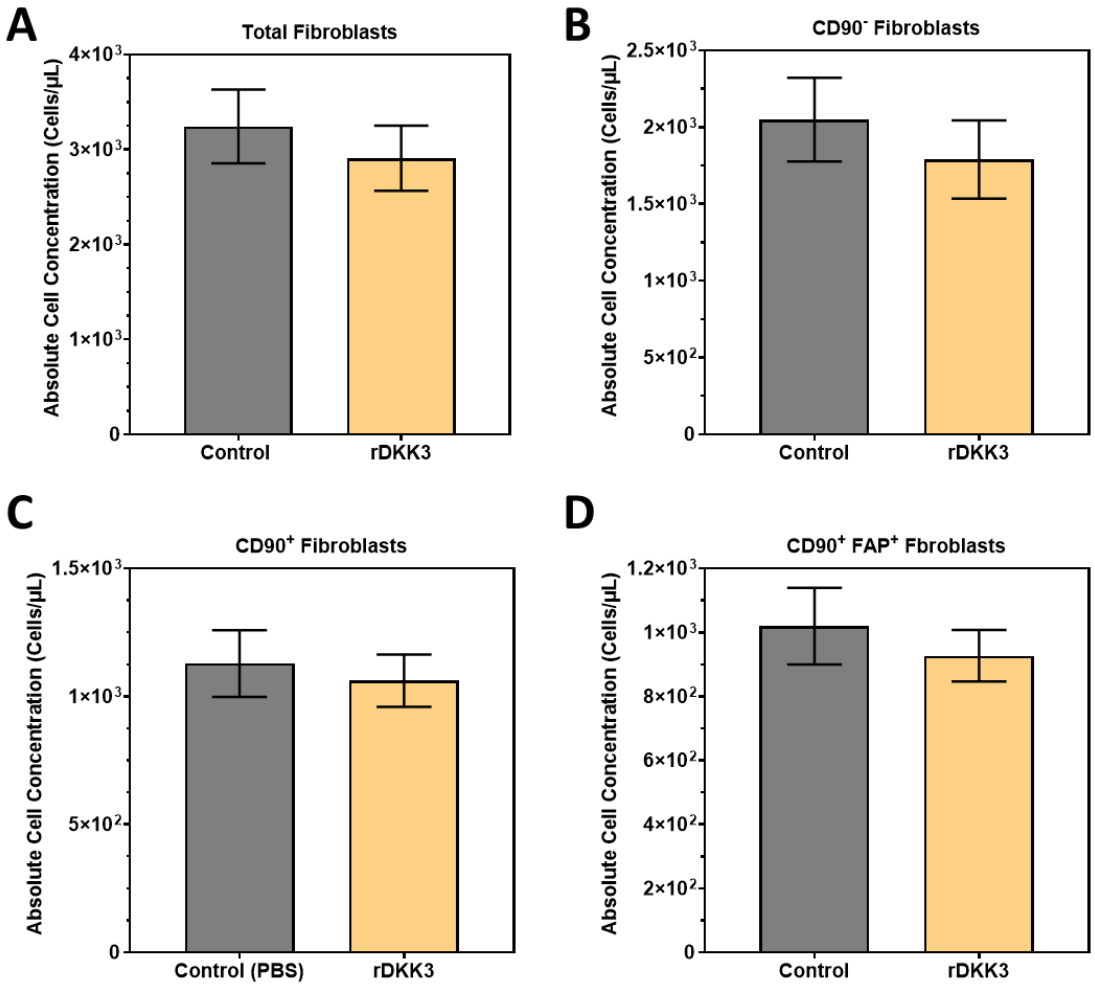

Figure 5.19 rDKK3 Does Not Influence Fibroblast Cellularity in AIA. Bar plots showing the absolute concentrations of (A) Total fibroblasts, (B) Thy1- fibroblasts, (C) Thy1+ fibroblasts, and (D) Thy1+ FAP+ fibroblasts on day 5 of AIA, following injection of PBS or rDKK3 on day 2. n = 3 per condition. Statistical analyses were performed using unpaired t-tests. * $p<0.05$; ** $p<0.01$; *** $p<0.001$; **** $p<0.0001$.

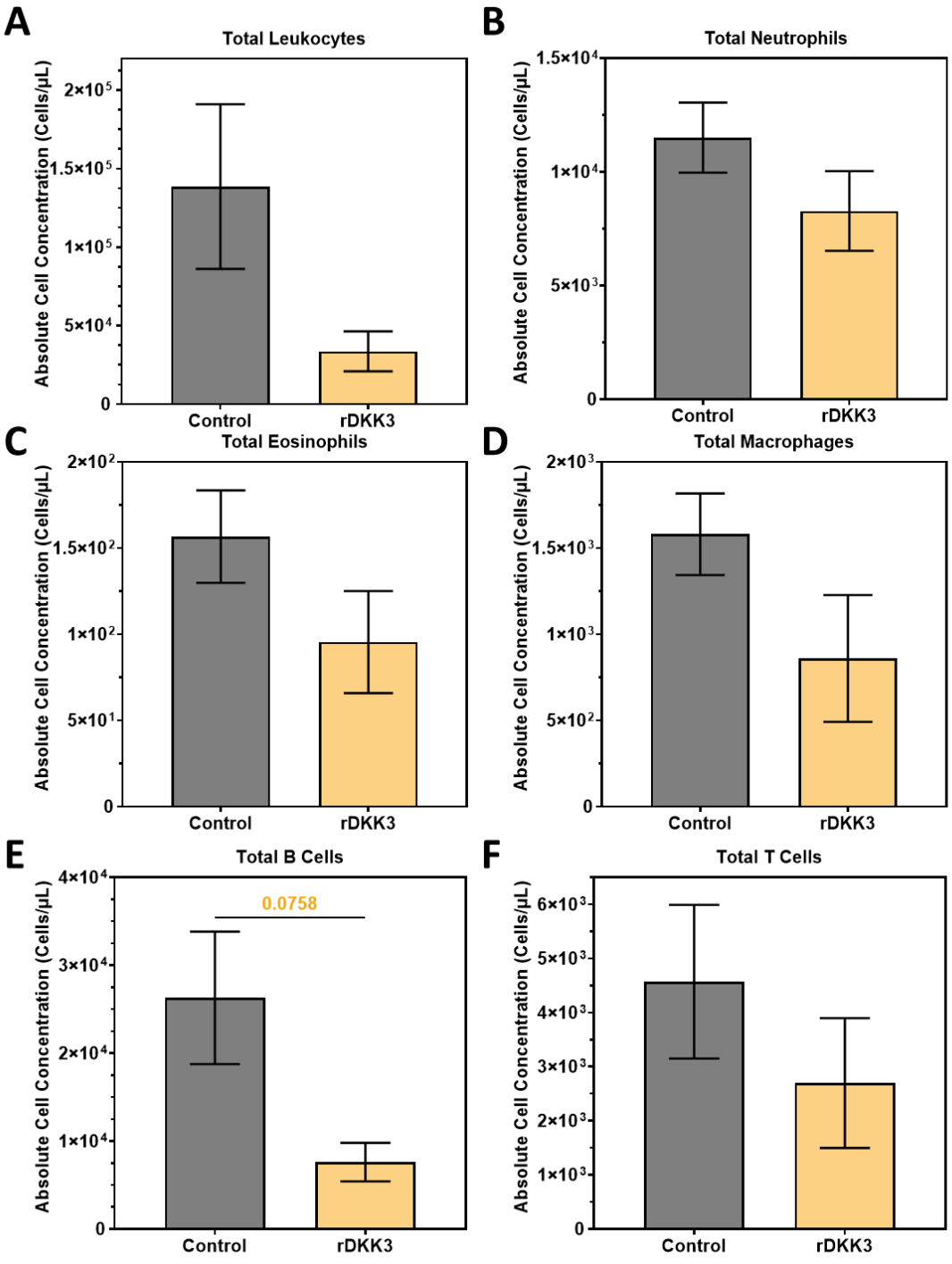

Figure 5.20 rDKK3 May Influence Leukocyte Cellularity in AIA. Bar plots showing absolute concentrations of (A) Total leukocytes (CD45+), (B) Neutrophils (CD11b+ CD11c- Ly6G+ Siglec-F-), (C) Eosinophils (CD11b+ CD11c- Ly6G- Siglec-F+), (D) Macrophages (CD11b+ CD11c- Ly6G- Siglec-F- F4/80+ CD64+), (E) B cells (CD45+ CD3- B220+), and (F) T cells (CD45+ CD3+ B220-) on day 5 of AIA, following injection of PBS or rDKK3 on day 2. n = 3 per condition. Statistical analyses were performed using unpaired t-tests. * $p<0.05$; ** $p<0.01$; *** $p<0.001$; **** $p<0.0001$.

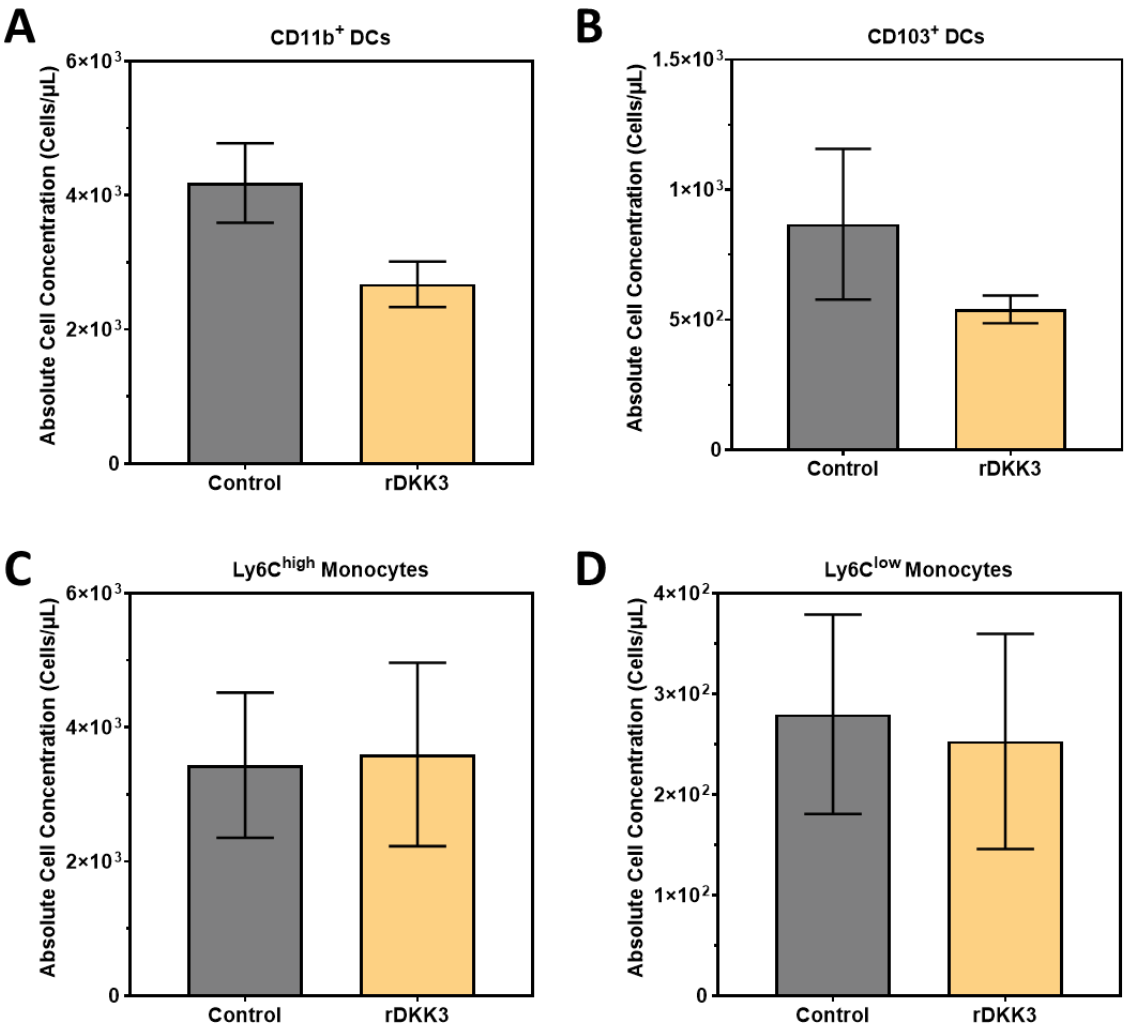

Figure 5.21 rDKK3 May Influence Myeloid Cellularity in AIA. Bar plots showing absolute concentrations of (A) CD11b+ DCs (CD11c+ CD11b+), (B) CD103+ DCs (CD11c+ CD11b-), (C) Ly6Chigh Monocytes (CD11c- CD11b+ Ly6G- Siglec-F- Ly6C++), (D) Ly6Clow Monocytes (CD11c- CD11b+ Ly6G- Siglec-F- Ly6C+), on day 5 of AIA, following injection of PBS or rDKK3 on day 2. n = 3 per condition. Statistical analyses were performed using unpaired t-tests. * p<0.05; ** p<0.01; *** p<0.001; **** p<0.0001.

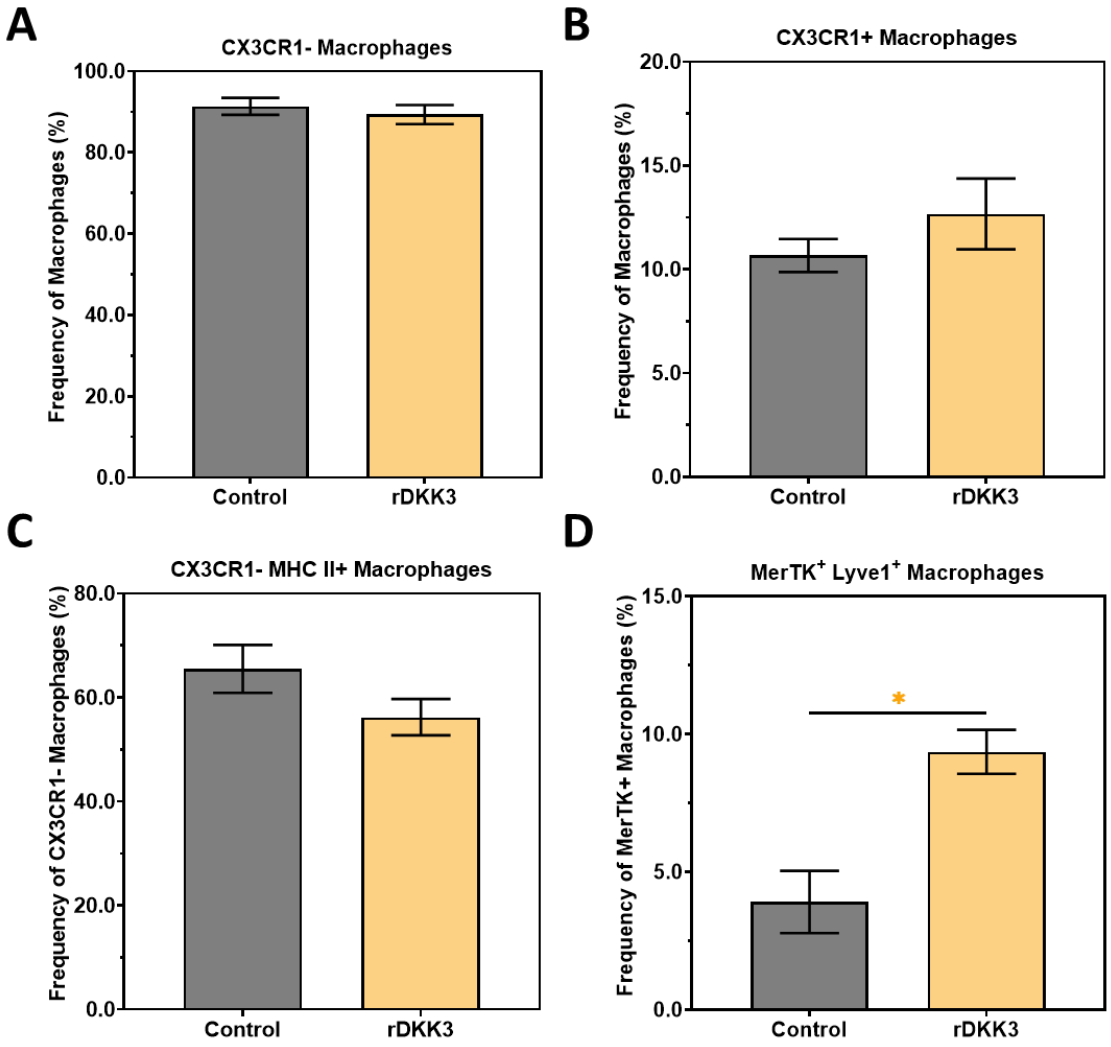

Figure 5.22 rDKK3 May Influence Macrophage Phenotypes in AIA. Bar plots showing proportional frequencies of (A) CX3CR1- Macrophages (F4/80+ CD64+ CX3CR1-), (B) CX3CR1+ Macrophages (F4/80+ CD64+ CX3CR1+), (C) CX3CR1- MHC II+ Macrophages (F4/80+ CD64+ CX3CR1- MerTK- MHC-II+), (D) MerTK+ Lyve1+ Macrophages (F4/80+ CD64+ CX3CR1- MerTK+ Lyve1+), on day 5 of AIA, following injection of PBS or rDKK3 on day 2. n = 3 per condition. Statistical analyses were performed using unpaired t-tests. * $p<0.05$; ** $p<0.01$; *** $p<0.001$; **** $p<0.0001$.

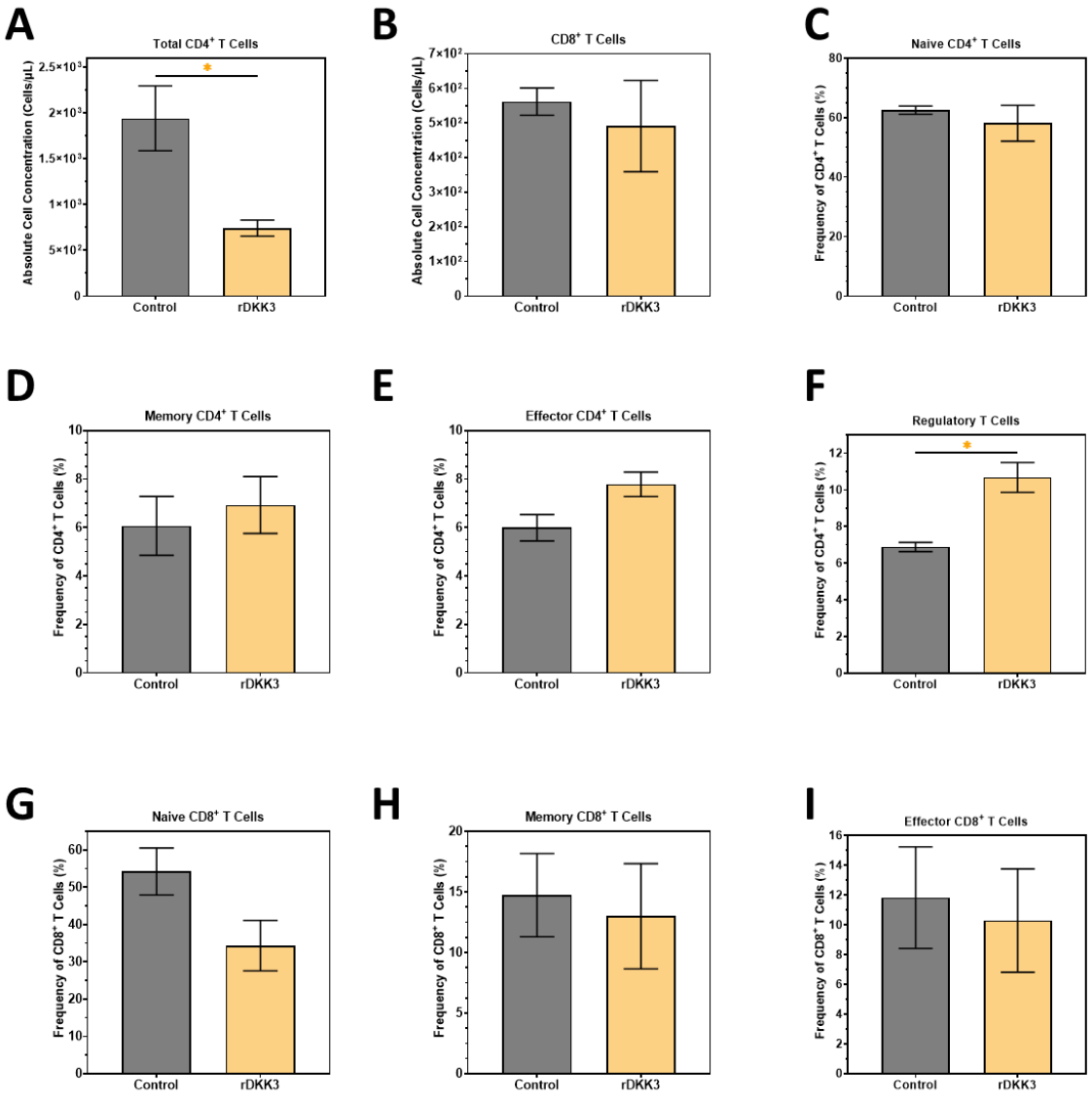

Figure 5.23 rDKK3 May Influence T Cell Phenotypes in AIA. Bar plots showing proportional frequencies of (A) CD4+ T Cells (CD3+ CD4+ CD8-), (B) CD8+ T Cells (CD3+ CD4- CD8+), (C) Naïve CD4+ T Cells (CD4+ CD62L+ CD44-), (D) Memory CD4+ T Cells (CD4+ CD62L+ CD44+), (E) Effector CD4+ T Cells (CD4+ CD62L- CD44+), (F) Regulatory T Cells (CD4+ FOXP3+ CD25+), (G) Naïve C84+ T Cells (CD8+ CD62L+ CD44-), (H) Memory CD8+ T Cells (CD8+ CD62L+ CD44+), (I) Effector CD8+ T Cells (CD8+ CD62L- CD44+), on day 5 of AIA, following injection of PBS or rDKK3 on day 2. n = 3 per condition. Statistical analyses were performed using unpaired t-tests. * p<0.05; ** p<0.01; *** p<0.001; **** p<0.0001.

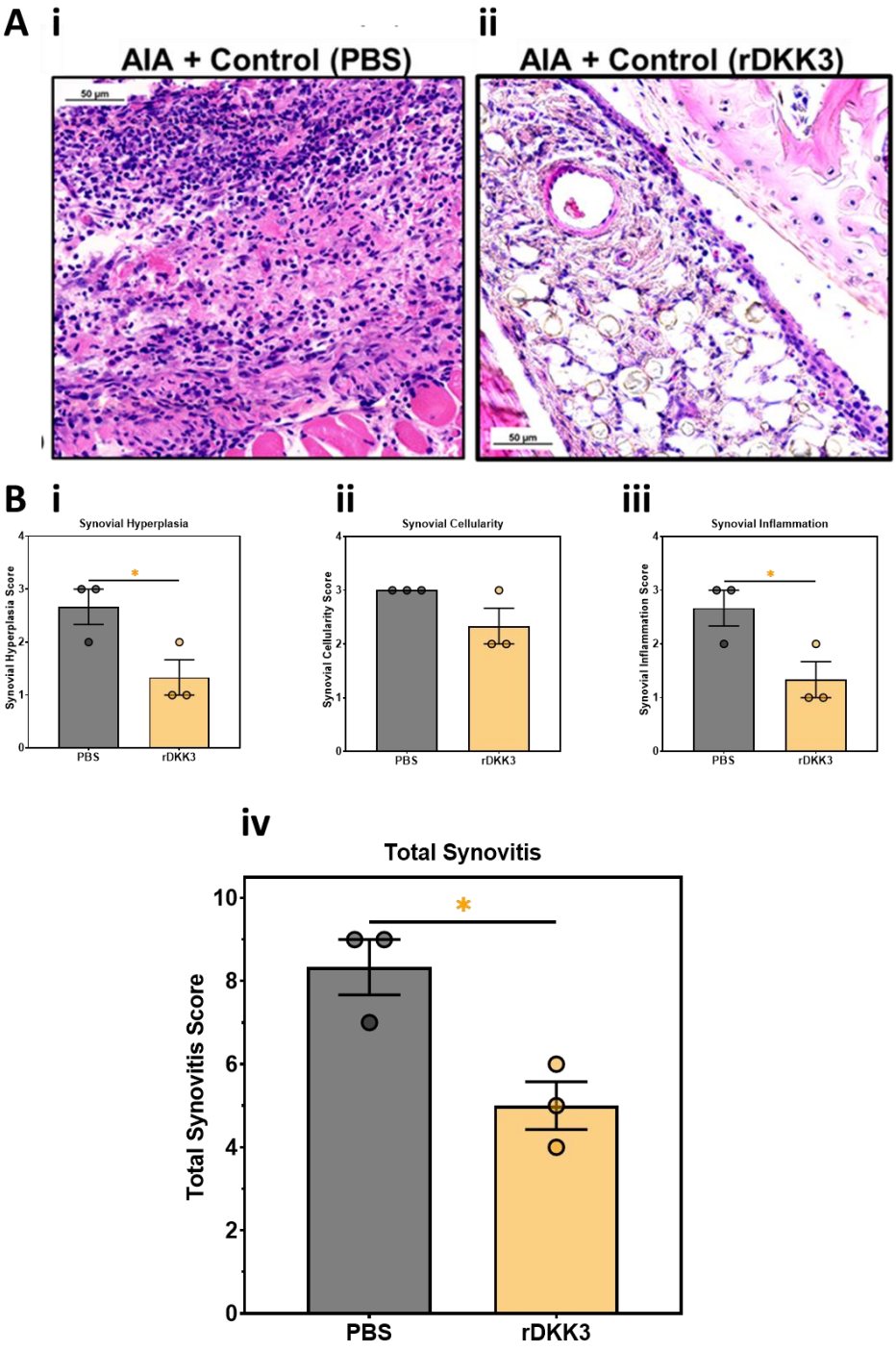

Figure 5.24 H&E Histology of rDKK3-Injected Knees in AIA. Knee joints from mice undergoing AIA were harvested on day 5, sectioned, and stained with H&E. (A) Representative images from mice injected with (i) PBS or (ii) rDKK3 on Day 2 of AIA. (B) H&E sections were scored for arthritis severity, assessing (i) synovial hyperplasia, (ii) synovial cellularity, (iii) synovial inflammation, and (iv) a combined score for total synovitis. n = 3 per condition. Statistical analyses were performed using unpaired t-tests. * $p<0.05$; ** $p<0.01$; *** $p<0.001$; **** $p<0.0001$.

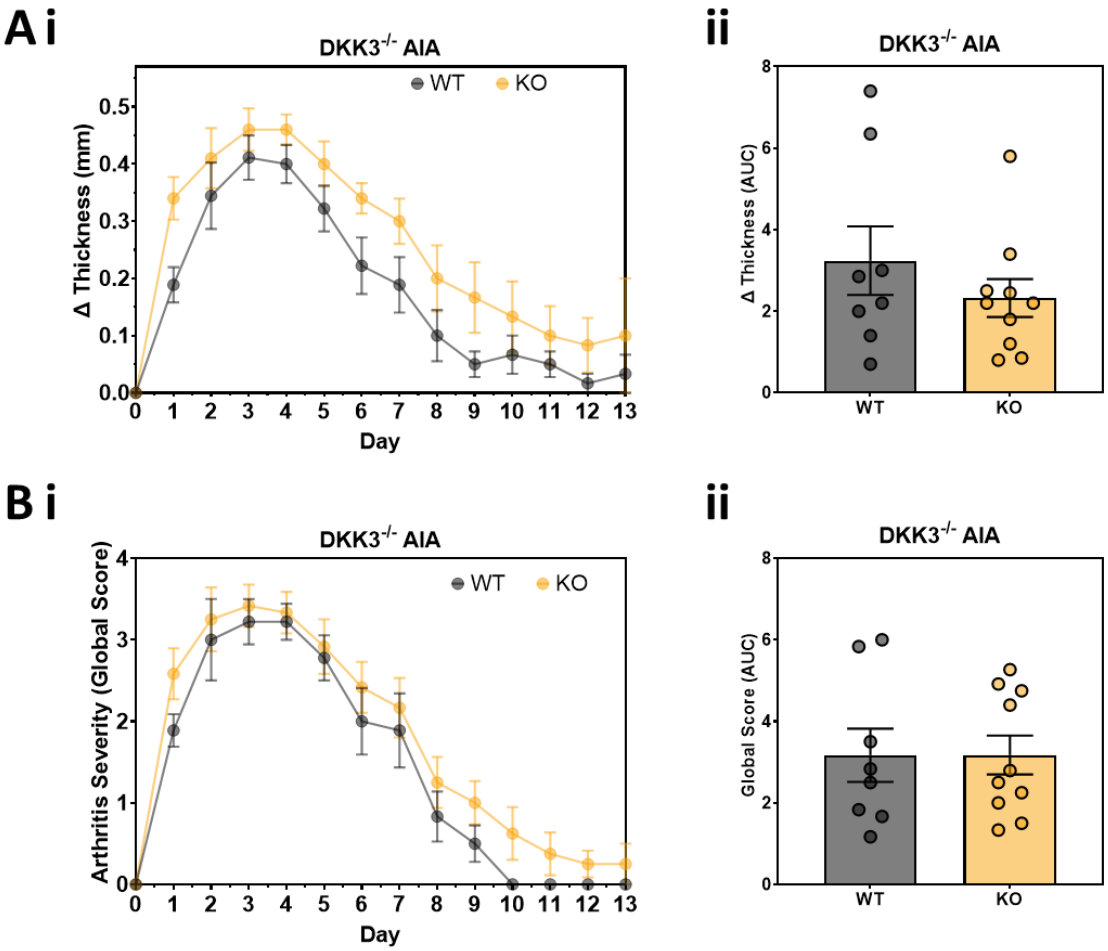

Figure 5.25 AIA in DKK3-/- Mice. (A) Measurements of knee swelling in mice subjected to antigen-induced arthritis (AIA), from either Wild-Type (WT) or DKK3-/- genotypes. (i) Change in knee swelling over time. (ii) Change in knee swelling quantified by the area under the curve. (B) Arthritis severity assessed using a global arthritis score sheet: (i) over time and (ii) calculated area under the curve. n = 8-10 per condition. Statistical analyses were performed using Two-Way ANOVA followed by Tukey's Post Hoc test and unpaired t-tests. * $p<0.05$; ** $p<0.01$; *** $p<0.001$; **** $p<0.0001$.

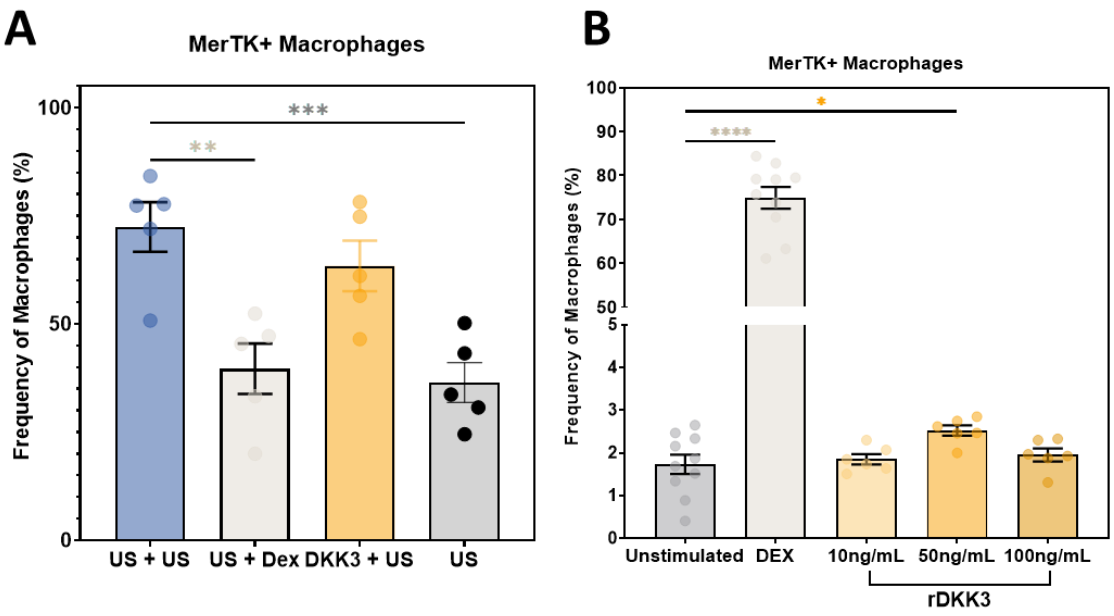

Figure 5.26 In-vitro Assays of rDKK3 Stimulation of Fibroblasts and Macrophages. Bar plots showing proportional frequencies of MerTK+ bone marrow-derived macrophages (BMDMs) (A) in co-culture with primary murine fibroblasts and (B) in monoculture with direct stimulation under various conditions. n = 4-10 per condition. Statistical analyses were performed using one-way ANOVA followed by Tukey's post hoc test. * $p<0.05$; ** $p<0.01$; *** $p<0.001$; **** $p<0.0001$.

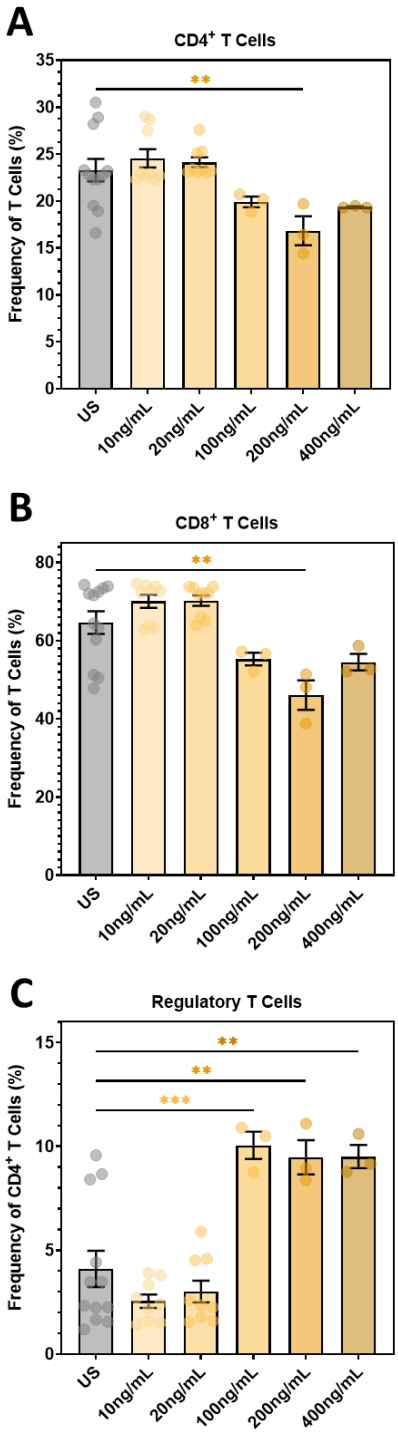

Figure 5.27 In-vitro Assays of rDKK3 Stimulation of murine isolated T Cells. Bar plots showing proportional frequencies of T Cell populations following various stimulations with rDKK3 protein (A) CD4+ T Cells (CD3+ CD4+ CD8-). (B) CD8+ T Cells (CD3+ CD4- CD8+). (C) Regulatory T Cells (CD3+ CD4+ CD8- FOXP3+ CD25+). n = 3-11 per condition. Statistical analyses were performed using one-way ANOVA followed by Tukey's post hoc test. * $p<0.05$; ** $p<0.01$; *** $p<0.001$; **** $p<0.0001$.

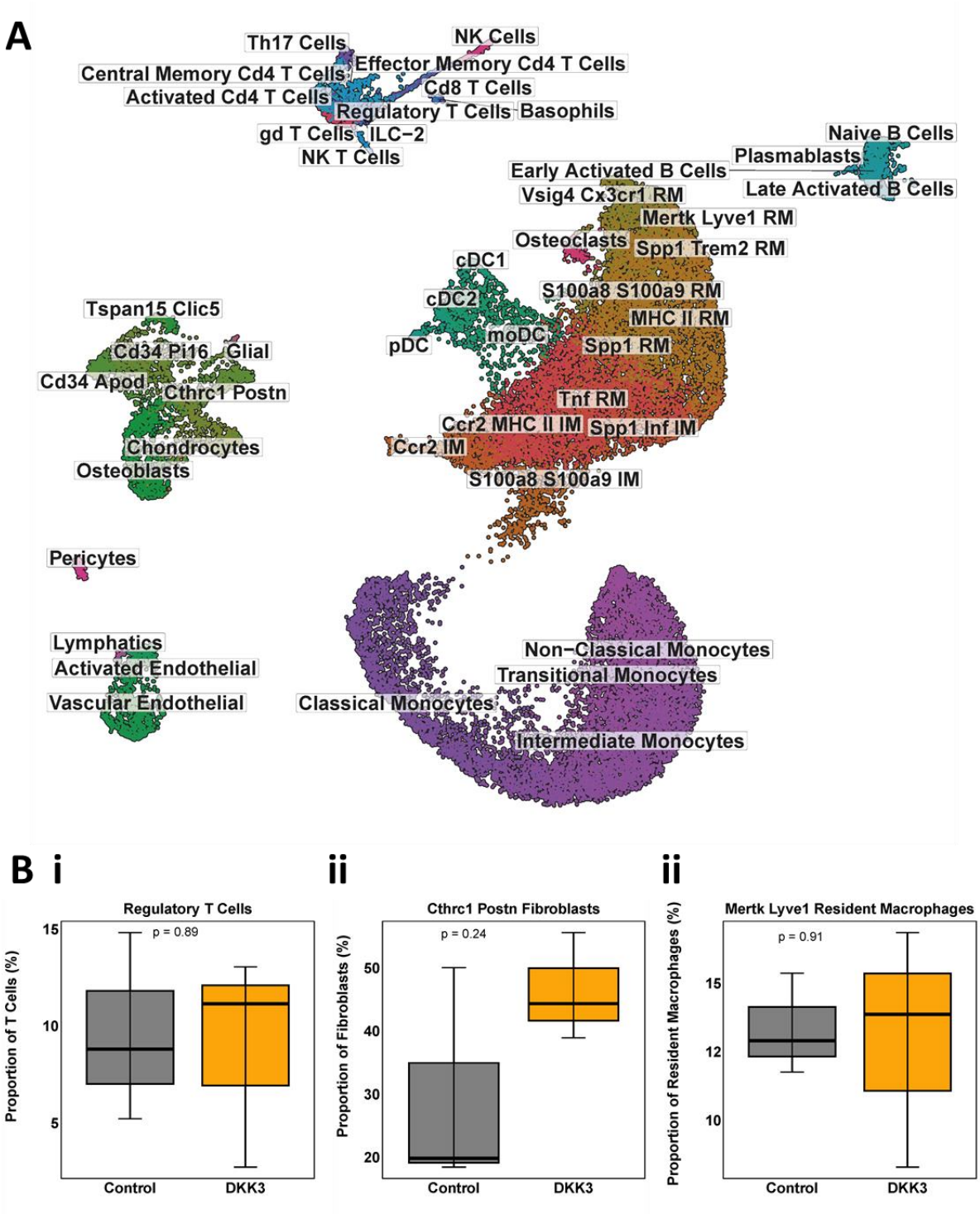

Figure 5.28 Single Cell RNA Sequencing of AIA mice treated with rDKK3 protein. (A) UMAP plot showing cell populations present in mice at Day 5 of AIA, in both Control (PBS) and rDKK3 injected conditions. (B) Box Plots showing proportional frequencies of (i) Regulatory T Cells (ii) Cthrc1 Postn Fibroblasts (iii) MerTK Lyve1 Resident Macrophages in either Control or rDKK3 treated mice. Statistical analyses were performed using unpaired t-tests. * $p<0.05$; ** $p<0.01$; *** $p<0.001$; **** $p<0.0001$. n = 3 per condition.

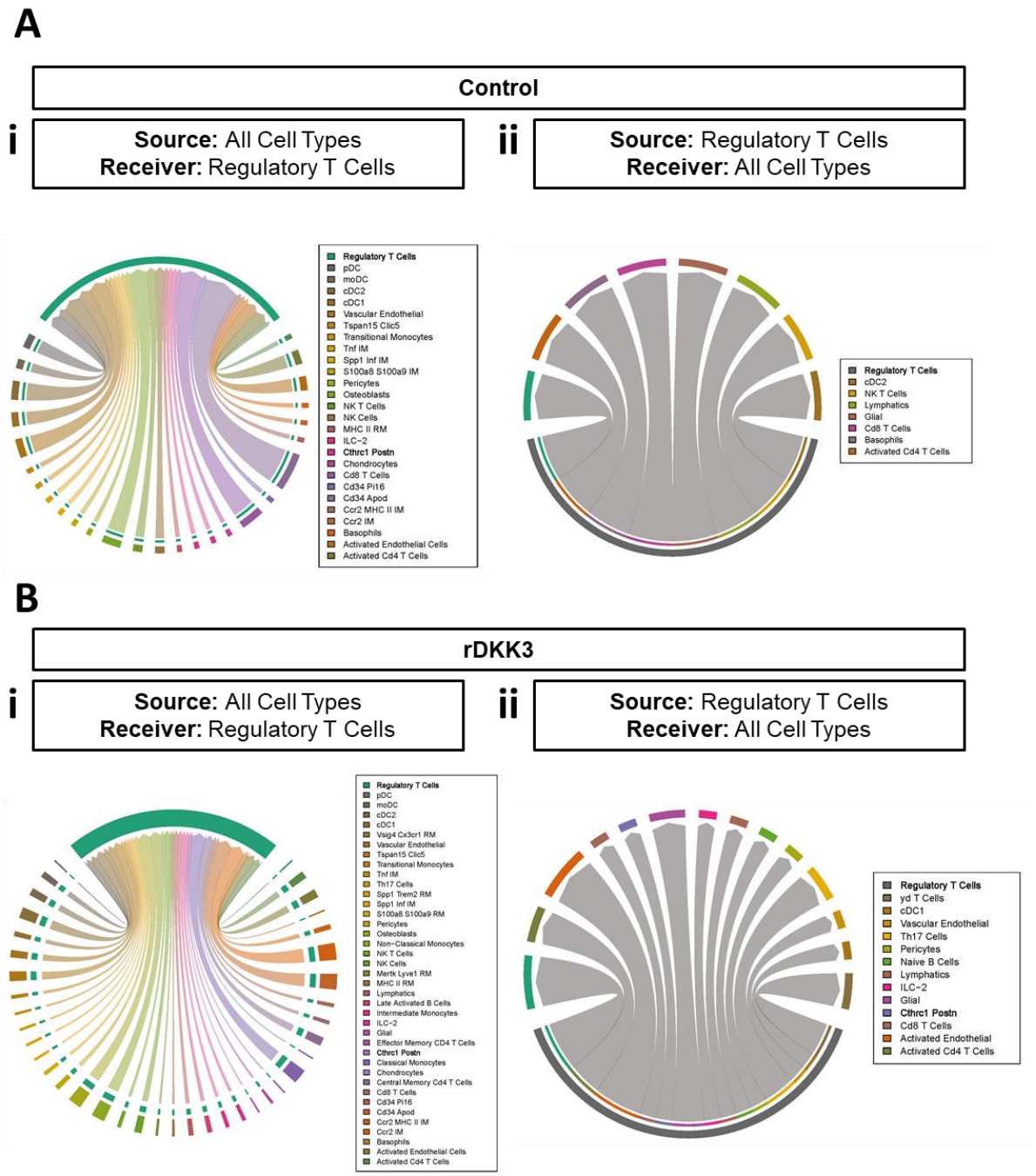

Figure 5.29 Cell Communication Strength Between Regulatory T Cells and All Synovial Cells. Chord diagrams illustrating the communication pathways (A) in the control condition from all cells to Regulatory T Cells (i) and from Regulatory T Cells to all cells (ii). (B) in the rDkk3 condition from all cells to Regulatory T Cells (i) and from Regulatory T Cells to all cells (ii). Each arrow shows the direction of communication, originating from the source cluster and pointing to the receiving cluster. The width of each arrow reflects the volume of interactions between the clusters.

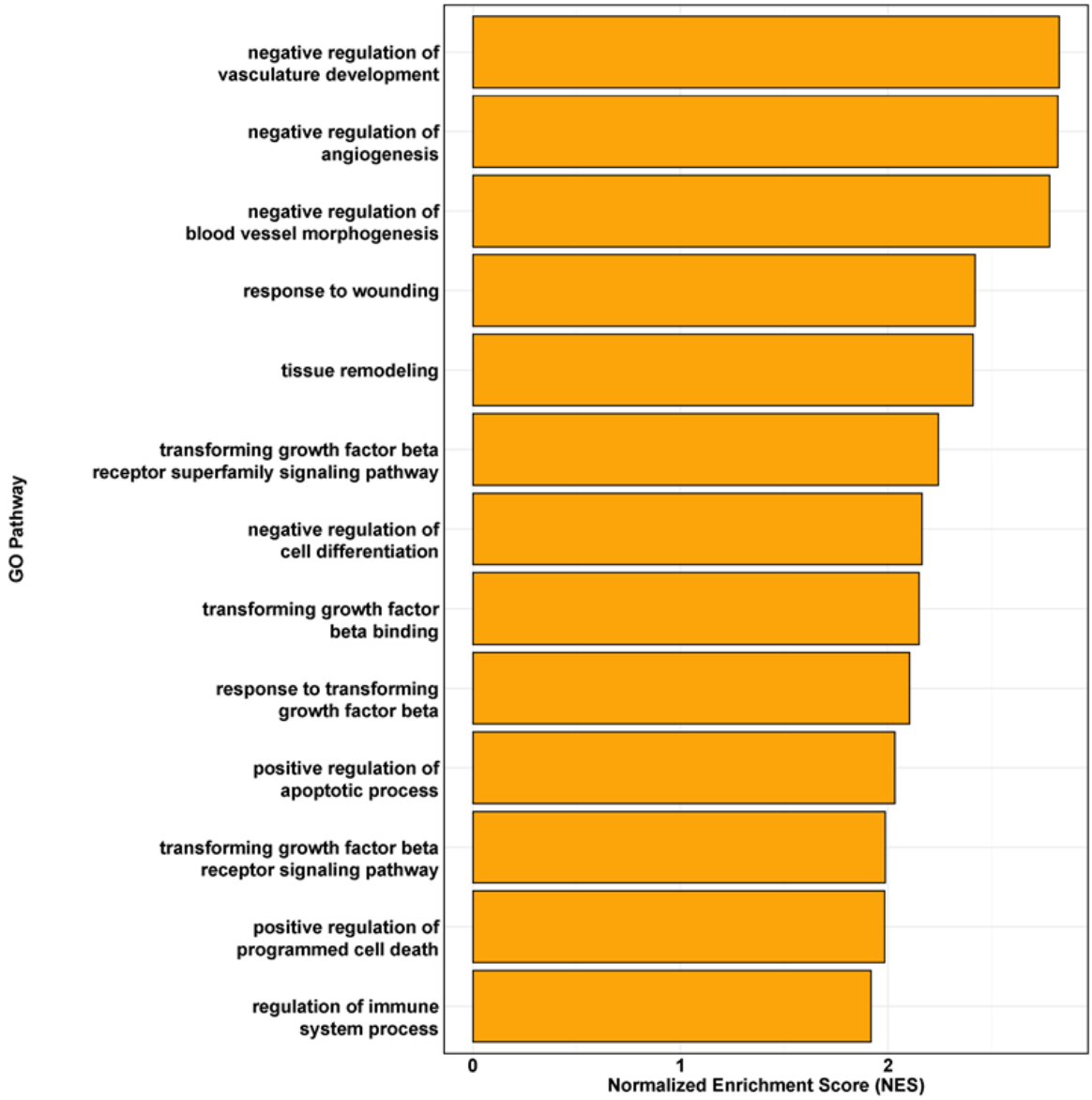

Figure 5.30 Enriched Gene Pathways with rDKK3 Injection. Bar Plot showing top significantly enriched Gene Ontology (GO) Pathways at Day 5 of AIA, in rDKK3 injected mice compared to PBS injected mice.

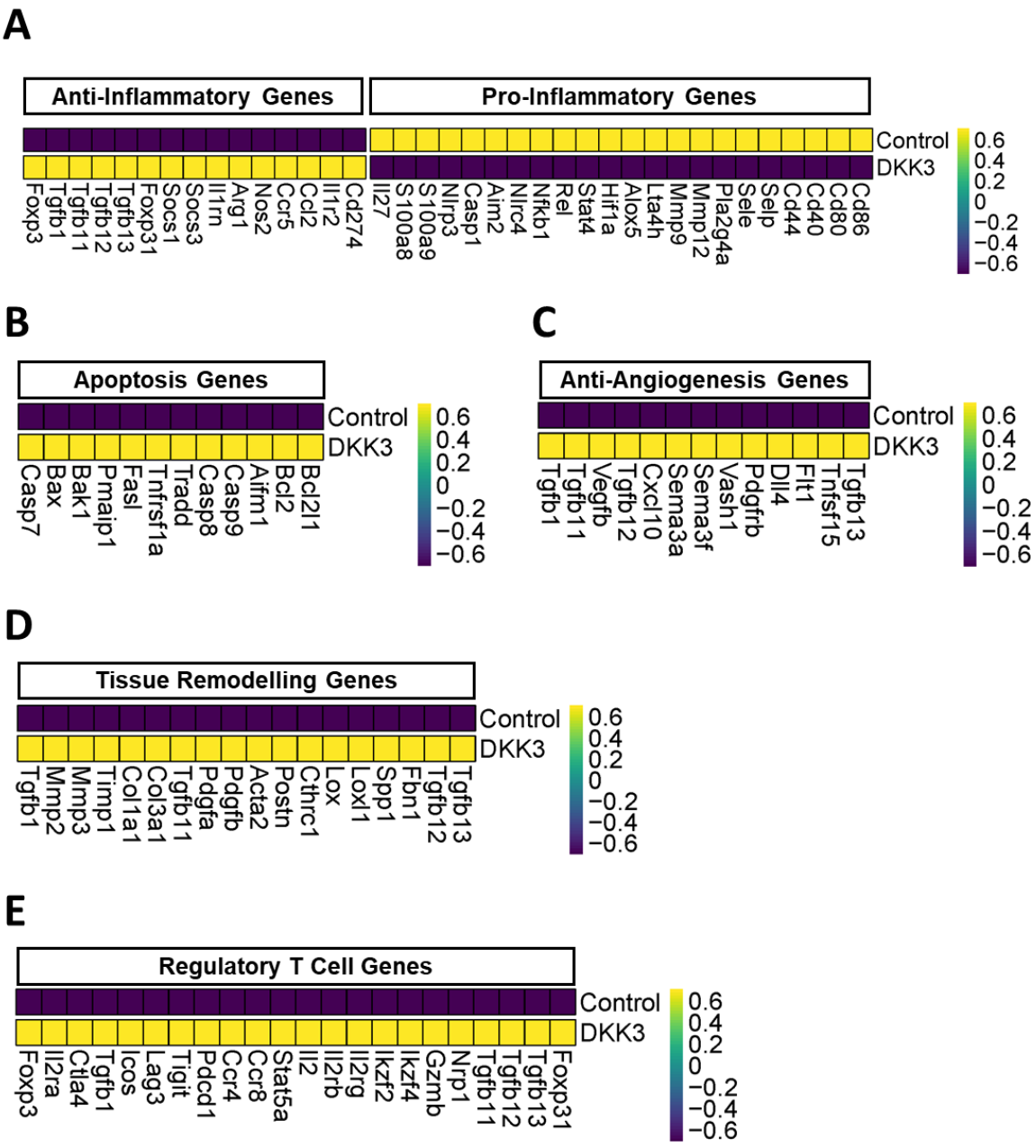

Figure 5.31 Expression of genes involved in key pathways identified with rDKK3 injection. Heatmaps showing scaled expression of genes across the whole dataset in either Control or DKK3 injected mice. (A) Genes implicated in inflammation, sorted as either pro- or anti-inflammatory. (B) Genes implicated in apoptosis. (C) Genes implicated in suppression of angiogenesis. (D) Genes implicated in tissue remodelling. (E) Genes implicated in differentiation, recruitment and activation of Regulatory T Cells.

5.7 Chapter discussion

5.7.1 Meeting the aims

I successfully characterised the roles of fibroblast and macrophages during the resolution phase of inflammatory arthritis. I identified key populations driving resolution, and the molecular cues between Cthrc1 Postn fibroblasts and Mertk Lyve1 macrophages. I revealed DKK3 as a novel marker of resolution in inflammatory arthritis, and displayed that administration of rDkk3 reduced disease severity in mice by promoting apoptotic clearance of leukocytes and polarising regulatory T cells.

5.7.2 Overall findings

This chapter clarifies the critical roles of Cthrc1+ Postn+ fibroblasts and MerTK+ Lyve1+ macrophages in the resolution of inflammatory arthritis.

The persistence of Cthrc1+ Postn+ fibroblasts and MerTK+ Lyve1+ macrophages in the resolution phase of inflammation supports their proposed roles in tissue homeostasis and repair [70,181]. Cross-disease relevance of these subsets emphasises the potential for therapeutic strategies aimed at modulating these cell populations.

Exploration of the signalling dynamics between macrophages and fibroblasts reveals that TGF-β plays a pivotal role in promoting the Cthrc1+ Postn+ fibroblast phenotype. MerTK Lyve1 macrophages promoted the enrichment of Cthrc1 Postn fibroblasts during inflammation resolution. These macrophages signal predominantly to fibroblasts through TGF-β1, driving the expansion of this fibroblast subset. The identification of this signalling pathway enhances our understanding of the cellular

interactions that drive resolution. TGF-β is widely accepted to play an anti-inflammatory role in the synovium, promoting tissue repair and inhibiting inflammation[259,260]. However previous attempts at direct targeting of TGF-β were unsuccessful, perhaps due to its widespread systemic role in biology[261]. This could suggest that TGF-β is just one important factor in a complex cellular and molecular network that results in resolution of inflammation. This is validated by in vitro stimulation experiments, where I found that TGF-β stimulation did not expand the full repertoire of key marker genes of the Cthrc1 Postn fibroblast population, suggesting other factors may be needed for full enrichment of the phenotype. Interestingly, Notch signalling via DLL4 antagonises this effect, with co-stimulation partially restoring Cthrc1 and Postn expression, suggesting a complex regulatory interplay between TGF-β and Notch pathways in fibroblast phenotype regulation. Notch-3 was previously identified as a driver of the pathological Thy1+ fibroblast phenotype[58], so it could be that a balance between these signalling pathways is required to restore tissue homeostasis.

Dkk3 emerged as a particularly interesting factor in this work, given its specific upregulation during the resolution phase and its enriched expression in fibroblasts from patients in remission. While Dkk3 has been implicated in Wnt signalling modulation, although not particularly well clarified, our data suggest that its role in the context of inflammatory arthritis may be independent of canonical Wnt pathways.

The administration of recombinant DKK3 demonstrated significant anti-inflammatory effects, evidenced by reduced joint swelling and inflammation in AIA models. Moreover, my findings indicate that Dkk3 influences T cell dynamics, promoting regulatory T cell differentiation. Although the mechanisms of DKK3 in inflammation

have not been widely studied, work has previously shown that DKK3 can promote T Cell tolerance and polarisation of regulatory T Cells[258], and regulate the immune response, with particular effects on $CD8^+$ T Cells and pro-inflammatory macrophages[262]. One study found that DKK3 was crucial to promote regulatory T Cells and suppress CD8+ T Cells in dormant tumours, allowing them to evade adaptive immunity, confirming the role of DKK3 in immune regulation[262]. The observed interactions between Cthrc1+ Postn+ fibroblasts and regulatory T cells in the presence of Dkk3 suggest that enhancing these communication pathways may be a promising therapeutic strategy.

In addition, the data implicated roles for promotion of apoptosis and inhibition of angiogenesis and vasculogenesis following DKK3 treatment, which have been validated in other studies[255,257].

Whilst not yet studied in the field of rheumatology, DKK3 has emerged as a key therapeutic target in cancer for quite some time. DKK3 was shown to be associated with positive disease outcomes in several types of cancer[263–266]. There are currently two ongoing clinical trials assessing the use of DKK3 in the treatment of cancer[267,268].

By fostering a microenvironment permissive to tissue repair and immune regulation, interventions targeting these cell types, and DKK3 directly could potentially mitigate the damaging effects of chronic inflammation.

5.7.3 Conclusion

In conclusion, these findings contribute to a deeper understanding of the cellular and molecular mechanisms underlying the resolution of inflammatory arthritis. By

highlighting the roles of Cthrc1+ Postn+ fibroblasts, MerTK+ Lyve1+ macrophages, and Dkk3, I propose a model in which these factors collaboratively orchestrate the repair process to restore tissue homeostasis (Figure 5.32).

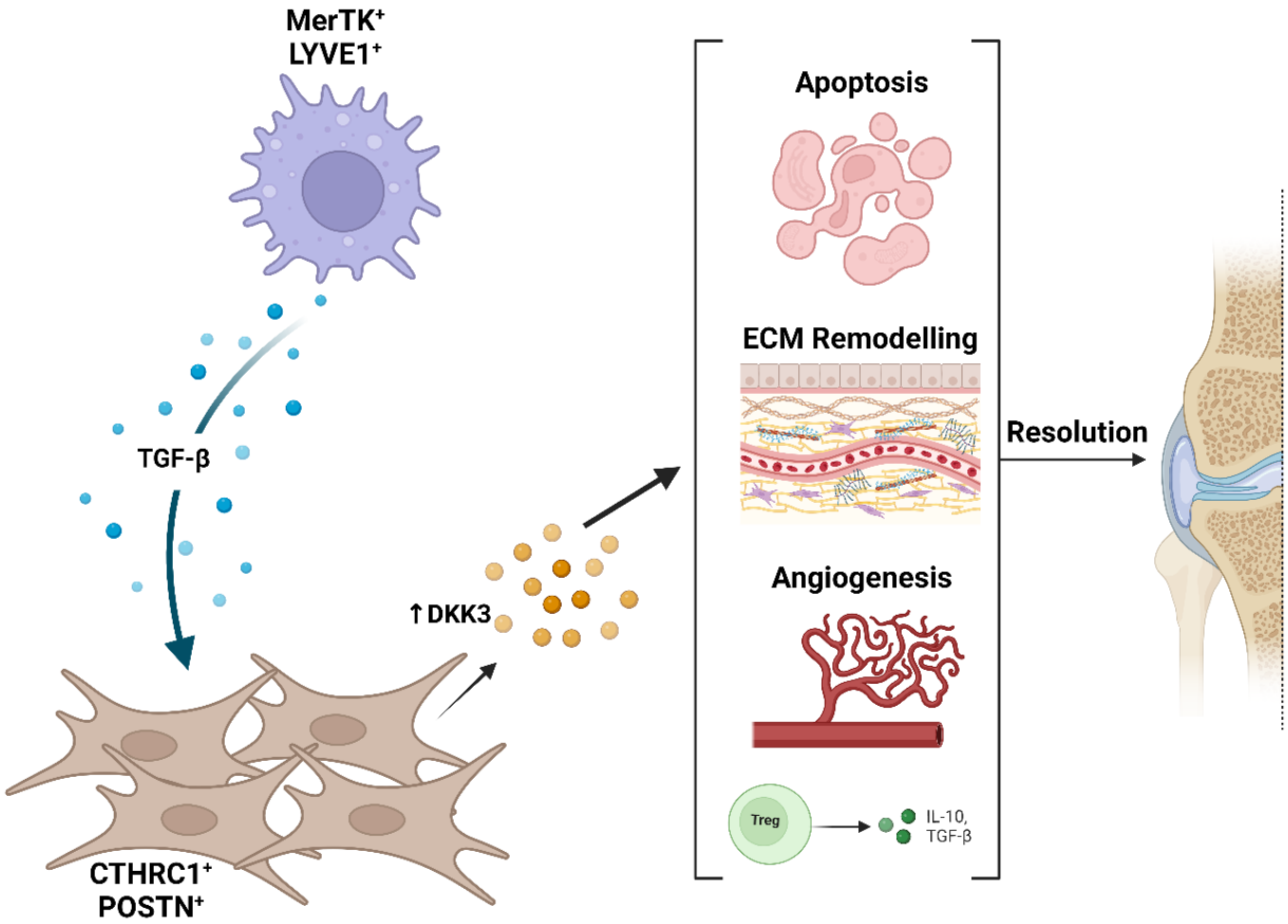

Figure 5.32 Schematic of fibroblast-macrophage cross talk in resolution of inflammatory arthritis. MerTK+ LYVE1+ macrophages are enriched in resolution and produce TGF-β. This stimulates expansion of CTHRC1+ POSTN+ fibroblasts, which in turn upregulate expression of DKK3. DKK3 promotes apoptosis of infiltrating leukocytes, tissue remodelling, inhibition of angiogenesis and polarisation of regulatory T Cells. These mechanisms contribute to the resolution of inflammation.

6 DISCUSSION

6.1 Meeting the thesis aims

The original aims of this thesis are presented in section 1.8. Below I will address how I did or did not meet each.

1. **Define the fibroblast subsets present in the synovium throughout the course of inflammatory arthritis from initiation to resolution of joint inflammation.**

Through generation of a comprehensive cellular atlas of murine inflammatory arthritis over several time points during disease, I have significantly characterised the fibroblast subsets present over the course of inflammation. I have determined the importance of each fibroblast subtype at each stage of inflammation, and also the dynamic changes that occur in each subset throughout the course of inflammation and resolution. Whilst I initially set out to characterise and validate all of the fibroblast subsets identified, this became unfeasible with time and resource constraints. I chose to focus on subsets and mechanisms I identified as particularly interesting.

2. **Determine the mechanisms underpinning the specialisation of fibroblasts during specific stages of inflammatory arthritis.**

I used several techniques to investigate the mechanisms involved in driving inflammation and damage in inflammatory arthritis. I was able to identify model-specific, and timepoint-specific mechanisms, allowing for highly tailored future experimental design. I identified a key regulator (WNT5A) of inflammation in pathogenic synovial fibroblasts, how it contributes to joint inflammation, and how it can be targeted to improve disease outcomes. Additionally, I identified key cell types and mechanisms during the resolution phase of inflammation, and began to unravel

the mechanisms involved in promoting joint resolution. In particular, I wanted to determine the exact molecular stimulus that expanded the pro-resolving phenotype in the joint. However, despite several attempts I was unable to determine this in full, leaving a clear gap for future exploration.

3. **Investigate the specific role of synovial fibroblasts in the resolution of joint inflammation.**

I undertook an in-depth assessment of the role of synovial fibroblasts in resolution. I identified a fibroblast subset that is expanded in resolution, and resembles other pro-resolving fibroblasts reported in the literature. I analysed the mechanisms underpinning the expansion of the subset, and its cross talk with tissue resident macrophages. I also identified TGF-β signalling as a driver of the pro-resolving fibroblast phenotype. I was able to isolate DKK3 as both a marker of resolution in Cthrc1 Postn fibroblasts, and a modulator of joint resolution. I displayed that DKK3 can promote resolution by clearance of the leukocyte infiltrate, and differentiation of regulatory T cells. As previously discussed, I wanted to be able to stimulate the full Cthrc1 Postn fibroblast phenotype, as well as figure out the stimulus that upregulates expression of DKK3 during resolution, but was unable to do so. I attempted isolate DKK3+ fibroblast from the joint during inflammatory arthritis, to use in in vitro experiments and adoptive transfer murine models, but was unable to isolate enough cells. Additionally, I tried to overexpress DKK3 in fibroblasts, using a commercially available overexpression plasmid, but this was also unsuccessful (supplementary figure).

6.2 Overview of findings

This thesis presents a comprehensive investigation into the mechanisms governing the temporal dynamics of inflammatory arthritis. Emphasising the roles of specific cell populations, signalling pathways, and molecular mechanisms.

My findings highlight the role of Wnt signalling in pathogenic synovial fibroblasts during inflammatory arthritis. Whilst Wnt signalling has been previously implicated in inflammatory disease and RA[215–225,225–228] the relevance and importance of its role has not been characterised, nor have the cellular cues involved in driving inflammation.

I have shown that fibroblasts upregulate Wnt signalling during inflammation, especially expression of Wnt5a, which has been increasingly linked to inflammation[225]. The role of WNT5A is better characterised in cancer, where cancer associated fibroblasts have been shown to produce WNT5A, which promotes a pro-inflammatory tumour microenvironment, leading to tumour progression and metastasis[234]. I displayed that Wnt5a upregulates pro-inflammatory cytokines such as IL-6 in vivo, which supports previous published work where in vitro stimulation of cells with WNT5A led to upregulation of TNF-α, IL-6 and IL-β[269]. Additionally, I observed an increase in leukocyte populations in the joint with Wnt5a administration, as well as upregulated Csf1. This highlights a key role of Wnt5a in recruiting pro-inflammatory macrophages to the joint.

Cthrc1+ Postn+ fibroblasts and MerTK+ Lyve1+ macrophages contribute to inflammation resolution, highlighting their potential as therapeutic targets.

MerTK+ Lyve1+ macrophages were identified as key players in the resolution of inflammatory arthritis[70]. These macrophages exhibited a pro-repair phenotype,

facilitating tissue regeneration. My findings corroborate previous studies emphasising macrophage polarisation's importance in inflammation and tissue repair[270,271], suggesting strategies to enhance this macrophage subset could prove beneficial in inflammatory arthritis.

The upregulation of Dkk3 during the resolution phase, particularly its expression in fibroblasts from patients in remission, underscores its relevance in mediating anti-inflammatory responses. The administration of recombinant DKK3 in murine models significantly reduced joint swelling and arthritis severity, indicating its potential as a therapeutic agent. This finding extends previous knowledge regarding Dkk3's role in modulating immune responses[255,257,258,262,272], suggesting its effects may occur independently of canonical Wnt signalling pathways.

Our research revealed significant interactions between Cthrc1+ Postn+ fibroblasts and regulatory T cells in the presence of Dkk3, suggesting a complex network of signalling pathways that enhance tissue repair and promote an anti-inflammatory environment. The enhanced communication pathways observed in Dkk3-treated groups indicate that these interactions are critical for effective resolution of inflammation and tissue homeostasis.

The results demonstrated that Dkk3 promotes regulatory T cell differentiation while reducing the frequency of CD4+ and CD8+ T cells. This shift in T cell dynamics reinforces the notion that Dkk3 plays a pivotal role in shaping immune responses during the resolution phase of inflammatory arthritis. The modulation of T cell

populations aligns with findings from other studies, highlighting the significance of regulatory T cells in controlling inflammation[258,272].

Histological evaluations confirmed reduced inflammation and synovial hyperplasia following rDKK3 treatment, while flow cytometry analyses revealed trends towards decreased leukocyte populations, including neutrophils and B cells, in the rDKK3-treated group. These results provide additional evidence for the anti-inflammatory effects of Dkk3 and the potential for manipulating these cell populations to enhance resolution.

Within the Cthrc1 Postn fibroblast subset, I observed gene changes over the course of inflammation. Postn was more associated with inflammation, while Dkk3 and Lrrc15 were more associated with resolution. Similar genetic changes were observed in pro-resolving fibroblasts in frozen shoulder disease[181]. This could indicate a transitional change within this population from inflammation to resolution.

The findings presented in this thesis build on existing literature regarding the mechanisms of inflammation resolution and tissue repair. The identification of Cthrc1+ Postn+ fibroblasts and MerTK+ Lyve1+ macrophages as central players align with studies demonstrating the significance of these populations in other inflammatory contexts. Additionally, the novel insights into Dkk3's independent role from canonical Wnt pathways contribute to a deeper understanding of its multifaceted functions in inflammatory diseases.

Moreover, the observed trends in immune cell dynamics support the growing body of evidence that emphasises the interplay between different cell types in orchestrating

the resolution of inflammation. By highlighting these interactions, this research reinforces the notion that targeted therapeutic strategies could enhance the resolution process and improve outcomes in chronic inflammatory diseases.

6.3 Limitations

One of the main limitations of this study is the use of murine models of arthritis, which, while valuable, may not fully recapitulate the complex interactions in human RA. Although AIA is a well-established model, it does not encompass the full range of chronicity seen in human RA, and results obtained from murine models may not directly translate to clinical settings.

One potential drawback of this experimental design is the enzymatic digest used to extract synovial cells from the joint. It's crucial to gently remove cells from the synovium without damaging the bones to avoid contamination from bone marrow. The enzyme cocktail was optimised for extracting fibroblasts, often the hardest cells to isolate, leading to the use of higher enzyme concentrations and longer digest times. This approach may affect the quality and quantity of other cell types in the synovium, potentially skewing results. In fact, data from our lab suggests that this digest particularly impacts T Cells, which could explain the small population of T Cells sequenced in this dataset. For further functional experiments, I optimised a second digest method specifically for T Cells.

Sorting synovial cells based on CD45 expression aimed to eliminate data skewing from larger cell populations and enhance atlas resolution. However, certain previously identified cell types, like CD4 T Cell subsets, were not detected in this study, possibly due to resolution issues in sequencing the entire leukocyte and stromal populations. Highly specific sorting strategies are typically used to identify

these cell types at the single-cell RNA seq level and could be considered for future analyses.

To tightly control the experiments, specific time points were set for each model. However, variation in inflammation among mice can lead to dataset inconsistencies. A more effective approach would be to adjust tissue collection points based on each mouse's disease trajectory, but this presents logistical challenges since cell sorting must occur on the same day as tissue collection and requires advance booking. Alternatively, daily tissue collection could allow for defining inflammatory time points during data analysis, but this would incur significantly higher sequencing costs.

Identifying cell types within the scRNA-seq datasets proved extremely challenging and time consuming. As previously discussed in Chapter 3, many of the accepted markers for monocyte/macrophage populations did not align and were often contradictory. It’s clear that there is a need for a streamlined and standardised approach when labelling these populations in particular. In addition, there are no unique markers available to identify fibroblasts. Whilst PDPN, FAP and PDGFRα are commonly used, they are not uniquely expressed in fibroblasts. There is a particular cross over between other stromal populations such as osteoblasts and chondrocytes. Analysis of gene expression in the scRNA-seq datasets was more straightforward, but the possibility of contamination within cell isolation and flow cytometry experiments cannot be excluded.

Additionally, administering substances directly into the joint did allow for observation of local effects, however it does not give clear insight into the complex cellular communication networks that occur when these modulators (such as rWnt5a and

rDkk3) are produced directly in fibroblasts. To resolve this, I tried to isolate DKK3+ fibroblasts using cell sorting but was not able to obtain enough cells from the joint.I also tried to over-express Dkk3 in murine fibroblasts using a commercially available plasmid, but this was also unsuccessful. Thus, the mechanisms drawn from these experiments can only be correlated with gene expression data from the cellular atlas.

Some experiments, particularly those involving the injection of rWnt5a, LGK974, and rDKK3, have low sample sizes. This is primarily due to time constraints and challenges in optimising histology methods for murine paraffin-embedded synovial tissue. While all displayed data has a minimum of n=3, lower replicate values may affect the reliability of statistical analyses, and it is recommended that more replicates be included prior to publication.

There is a possibility that recombinant proteins may contain trace amounts of LPS (due to the manufacturing process), which could potentially trigger an inflammatory response upon utilisation. All recombinant proteins used were endotoxin-free, ≥90% pure, and do not indicate any LPS contamination in their accompanying data sheets.

6.4 Future work

Several things remain unanswered or unclear regarding the exact molecular mechanisms of fibroblasts during inflammation and resolution of inflammatory arthritis. Here I will put forward future experiments that could further this work:

- It’s clear that the joint microenvironment is a highly dynamic structure, undergoing significant changes during the course of inflammatory disease. Whilst work was done to characterise these changes, additional timepoints could be added to the cellular atlas, to further explore the transition of cells.

- Local injection of Wnt5a displayed biological effects, but can not be exclusively linked to fibroblasts. In order to show that the pro-inflammatory effects of Wnt5a are mediated by fibroblasts, Wnt5a could be specifically overexpressed in fibroblasts or knocked out in mouse models, using conditional knockout methods. Alternatively, Wnt5a+ fibroblasts could be isolated and adoptively transferred into the joints of mice to determine the direct effect of these fibroblasts on joint inflammation.
- With that in mind, the same could be done for DKK3. Both of the above experiments were attempted but unsuccessful. When I first tried those experiments, antibodies for key markers of the Cthrc1 Postn population were not available. However, our group has recently obtained antibodies for Cthrc1 and Lrrc15, so isolation and adoptive transfer experiments can be re-attempted with these markers.
- Similar to the use of LGK974, a direct inhibitor of DKK3 could be administered into the joint to determine the effects of DKK3 blockade in inflammatory arthritis. Our group has recently obtained a DKK3 blocking antibody and will attempt this.
- TGF-β upregulated some marker genes of the Cthrc1 Postn fibroblast population, but not all. It would be useful to perform bulk RNA sequencing on TGF-β stimulated fibroblasts and compare the phenotype to that observed in our other datasets.
- Additionally, MerTK^{+} macrophages stimulated the Cthrc1 Postn phenotype, bulk RNA sequencing could be performed on fibroblasts following co-culture with MerTK^{+} macrophages to determine if this stimulus recapitulates the Cthrc1 Postn phenotype observed in vivo.

6.5 Conclusion

In conclusion, this thesis advances our understanding of the cellular and molecular mechanisms underlying the resolution of inflammatory arthritis. By highlighting the critical roles of Cthrc1+ Postn+ fibroblasts, MerTK+ Lyve1+ macrophages, and Dkk3, along with the relevance of Wnt signalling, I propose a model wherein these factors collaboratively orchestrate the repair processes essential for restoring tissue homeostasis. Continued exploration of these interactions will be crucial for developing effective therapeutic strategies aimed at enhancing resolution and preventing chronic inflammatory conditions.

7 REFERENCES

1. Marsh, L. J., Kemble, S., Reis Nisa, P., Singh, R. & Croft, A. P. Fibroblast pathology in inflammatory joint disease. *Immunol. Rev.* **302**, 163–183 (2021).

2. Smolen, J. S., Aletaha, D. & McInnes, I. B. Rheumatoid arthritis. *Lancet* **388**, 2023–2038 (2016).

3. Smolen, J. S. & Aletaha, D. Rheumatoid arthritis therapy reappraisal: Strategies, opportunities and challenges. *Nat. Rev. Rheumatol.* **11**, 276–289 (2015).

4. Catrina, A. I., Svensson, C. I., Malmström, V., Schett, G. & Klareskog, L. Mechanisms leading from systemic autoimmunity to joint-specific disease in rheumatoid arthritis. *Nature Reviews Rheumatology* vol. 13 79–86 (2017).

5. Winthrop, K. L. *et al.* Unmet need in rheumatology: Reports from the Targeted Therapies meeting 2019. *Ann. Rheum. Dis.* **79**, 88–93 (2020).

6. Schett, G., Tanaka, Y. & Isaacs, J. D. Why remission is not enough: underlying disease mechanisms in RA that prevent cure. *Nature Reviews Rheumatology* vol. 17 135–144 (2021).

7. Patel, R., Filer, A., Barone, F. & Buckley, C. D. Stroma: Fertile soil for inflammation. *Best Pract. Res. Clin. Rheumatol.* **28**, 565–576 (2014).

8. Filer, A. The fibroblast as a therapeutic target in rheumatoid arthritis. *Current Opinion in Pharmacology* vol. 13 413–419 (2013).

9. Kurowska-Stolarska, M. & Alivernini, S. Synovial tissue macrophages: Friend or foe? *RMD Open* **3**, (2017).

10. Yang, X., Chang, Y. & Wei, W. Emerging role of targeting macrophages in rheumatoid arthritis: Focus on polarization, metabolism and apoptosis. *Cell Proliferation* vol. 53 (2020).

11. Smith, M. D. *The Normal Synovium*. *The Open Rheumatology Journal* vol. 5 (2011).

12. Rhee, D. K. *et al.* The secreted glycoprotein lubricin protects cartilage surfaces and inhibits synovial cell overgrowth. *J. Clin. Invest.* **115**, 622–631 (2005).

13. D. Smith, M. The Normal Synovium. *Open Rheumatol. J.* **5**, 100–106 (2012).

14. Kiener, H. P. *et al.* Synovial fibroblasts self-direct multicellular lining architecture and synthetic function in three-dimensional organ culture. *Arthritis Rheum.* **62**, 742–752 (2010).

15. McInnes, I. B. & Schett, G. The Pathogenesis of Rheumatoid Arthritis. *N. Engl. J. Med.* **365**, 2205–2219 (2011).

16. Firestein, G. S. Evolving concepts of rheumatoid arthritis. *Nature* vol. 423 356–361 (2003).

17. Derer, A. *et al.* Rsk2 controls synovial fibroblast hyperplasia and the course of arthritis. *Ann. Rheum. Dis.* **75**, 413–421 (2016).

18. O'sullivan, F. X., Fassbender, H. -G, Gay, S. & Koopman, W. J. Etiopathogenesis of the rheumatoid arthritis–like disease in MRL/1 mice. I. The histomorphologic basis of joint destruction. *Arthritis Rheum.* **28**, 529–536 (1985).

19. Nygaard, G. & Firestein, G. S. Restoring synovial homeostasis in rheumatoid arthritis by targeting fibroblast-like synoviocytes. *Nat. Rev. Rheumatol.* **16**,

316–333 (2020).

20. Buckley, C. D., Ospelt, C., Gay, S. & Midwood, K. S. Location, location, location: how the tissue microenvironment affects inflammation in RA. *Nat. Rev. Rheumatol.* **17**, 195–212 (2021).

21. Koliaraki, V., Prados, A., Armaka, M. & Kollias, G. The mesenchymal context in inflammation, immunity and cancer. *Nature Immunology* vol. 21 974–982 (2020).

22. LeBleu, V. S. & Neilson, E. G. Origin and functional heterogeneity of fibroblasts. *FASEB J.* **34**, 3519–3536 (2020).

23. Kalluri, R. & Zeisberg, M. Fibroblasts in cancer. *Nat. Rev. Cancer* **6**, 392–401 (2006).

24. Filer, A., Pitzalis, C. & Buckley, C. D. Targeting the stromal microenvironment in chronic inflammation. *Curr. Opin. Pharmacol.* **6**, 393–400 (2006).

25. Lynch, M. D. & Watt, F. M. Fibroblast heterogeneity: implications for human disease. *J. Clin. Invest.* **128**, 26–35 (2018).

26. Buechler, M. B. & Turley, S. J. A short field guide to fibroblast function in immunity. *Semin. Immunol.* **35**, 48–58 (2018).

27. Lemos, D. R. & Duffield, J. S. Tissue-resident mesenchymal stromal cells: Implications for tissue-specific antifibrotic therapies. *Sci. Transl. Med.* **10**, (2018).

28. Roelofs, A. J. *et al.* Joint morphogenetic cells in the adult mammalian synovium. *Nat. Commun.* **8**, (2017).

29. Driskell, R. R. *et al.* Distinct fibroblast lineages determine dermal architecture in skin development and repair. *Nature* **504**, 277–281 (2013).

30. Rinn, J. L., Bondre, C., Gladstone, H. B., Brown, P. O. & Chang, H. Y. Anatomic demarcation by positional variation in fibroblast gene expression programs. *PLoS Genet.* **2**, 1084–1096 (2006).

31. Ospelt, C. & Frank-Bertoncelj, M. Why location matters — site-specific factors in rheumatic diseases. *Nat. Rev. Rheumatol. 2017 137* **13**, 433–442 (2017).

32. Mizoguchi, F. *et al.* Functionally distinct disease-associated fibroblast subsets in rheumatoid arthritis. *Nat. Commun.* **9**, (2018).

33. Buechler, M. B. *et al.* Cross-tissue single-cell transcriptomics reveals organizing principles of fibroblasts in health and disease. *bioRxiv* 1–58 (2021) doi:10.1101/2021.01.15.426912.

34. Korsunsky, I. *et al.* Cross-tissue, single-cell stromal atlas identifies shared pathological fibroblast phenotypes in four chronic inflammatory diseases. *Med* **3**, 481-518.e14 (2022).

35. Huber, L. C. *et al.* Synovial fibroblasts: Key players in rheumatoid arthritis. *Rheumatology* vol. 45 669–675 (2006).

36. Lee, D. M. *et al.* Cadherin-11 in synovial lining formation and pathology in arthritis. *Science (80-.).* **315**, 1006–1010 (2007).

37. Culemann, S. *et al.* Locally renewing resident synovial macrophages provide a protective barrier for the joint. *Nature* **572**, 670–675 (2019).

38. Buechler, M. B. *et al.* A Stromal Niche Defined by Expression of the Transcription Factor WT1 Mediates Programming and Homeostasis of Cavity-

Resident Macrophages. *Immunity* **51**, 119-130.e5 (2019).

39. Filer, A. *et al.* Identification of a transitional fibroblast function in very early rheumatoid arthritis. *Ann. Rheum. Dis.* **76**, 2105–2112 (2017).

40. Mcgettrick, H. M., Ward, L. S. C., Rainger, G. E. & Nash, G. B. Mesenchymal stromal cells as active regulators of lymphocyte recruitment to blood vascular endothelial cells. *Methods Mol. Biol.* **1591**, 121–142 (2017).

41. Zhang, F. *et al.* Defining inflammatory cell states in rheumatoid arthritis joint synovial tissues by integrating single-cell transcriptomics and mass cytometry. *Nat. Immunol.* **20**, 928–942 (2019).

42. Croft, A. P. *et al.* Distinct fibroblast subsets drive inflammation and damage in arthritis. *Nature* **570**, 246–251 (2019).

43. About Human Cell Atlas. 1–1 www.humancellatlas.org (2021).

44. Baldwin, M. J., Cribbs, A. P., Guilak, F. & Snelling, S. J. B. Mapping the musculoskeletal system one cell at a time. *Nat. Rev. Rheumatol.* **17**, 247–248 (2021).

45. Bartok, B. & Firestein, G. S. Fibroblast-like synoviocytes: Key effector cells in rheumatoid arthritis. *Immunological Reviews* vol. 233 233–255 (2010).

46. Croft, A. P. *et al.* Rheumatoid synovial fibroblasts differentiate into distinct subsets in the presence of cytokines and cartilage. *Arthritis Res. Ther.* **18**, (2016).

47. Bottini, N. & Firestein, G. S. Duality of fibroblast-like synoviocytes in RA: Passive responders and imprinted aggressors. *Nat. Rev. Rheumatol.* **9**, 24–33 (2013).

48. Chang, S. K. *et al.* Cadherin-11 regulates fibroblast inflammation. *Proc. Natl. Acad. Sci. U. S. A.* **108**, 8402–8407 (2011).

49. Kiener, H. P., Lee, D. M., Agarwal, S. K. & Brenner, M. B. Cadherin-11 induces rheumatoid arthritis fibroblast-like synoviocytes to form lining layers in vitro. *Am. J. Pathol.* **168**, 1486–1499 (2006).

50. Kiener, H. P. *et al.* Cadherin 11 promotes invasive behavior of fibroblast-like synoviocytes. *Arthritis Rheum.* **60**, 1305–1310 (2009).

51. Valencia, X. *et al.* Cadherin-11 provides specific cellular adhesion between fibroblast-like synoviocytes. *J. Exp. Med.* **200**, 1673–1679 (2004).

52. Lafyatis, R. *et al.* Anchorage-independent growth of synoviocytes from arthritic and normal joints. Stimulation by exogenous platelet-derived growth factor and inhibition by transforming growth factor-beta and retinoids. *J. Clin. Invest.* **83**, 1267–1276 (1989).

53. Korb, A., Pavenstädt, H. & Pap, T. Cell death in rheumatoid arthritis. *Apoptosis* **14**, 447–454 (2009).

54. Kato, M., Ospelt, C., Gay, R. E., Gay, S. & Klein, K. Dual role of autophagy in stress-induced cell death in rheumatoid arthritis synovial fibroblasts. *Arthritis Rheumatol.* **66**, 40–48 (2014).

55. Shin, Y. J. *et al.* Autophagy induction and CHOP under-expression promotes survival of fibroblasts from rheumatoid arthritis patients under endoplasmic reticulum stress. *Arthritis Res. Ther.* **12**, (2010).

56. Firestein, G. S. & McInnes, I. B. Immunopathogenesis of Rheumatoid Arthritis. *Immunity* **46**, 183–196 (2017).

57. Burman, A. *et al.* A Chemokine-Dependent Stromal Induction Mechanism for Aberrant Lymphocyte Accumulation and Compromised Lymphatic Return in Rheumatoid Arthritis. *J. Immunol.* **174**, 1693–1700 (2005).

58. Wei, K. *et al.* Notch signalling drives synovial fibroblast identity and arthritis pathology. *Nature* **582**, 259–264 (2020).

59. Dennis, G. *et al.* Synovial phenotypes in rheumatoid arthritis correlate with response to biologic therapeutics. *Arthritis Res. Ther.* **16**, (2014).

60. Pitzalis, C., Kelly, S. & Humby, F. New learnings on the pathophysiology of RA from synovial biopsies. *Current Opinion in Rheumatology* vol. 25 334–344 (2013).

61. Lewis, M. J. *et al.* Molecular Portraits of Early Rheumatoid Arthritis Identify Clinical and Treatment Response Phenotypes. *Cell Rep.* **28**, 2455-2470.e5 (2019).

62. Humby, F. *et al.* Synovial cellular and molecular signatures stratify clinical response to csDMARD therapy and predict radiographic progression in early rheumatoid arthritis patients. *Ann. Rheum. Dis.* **78**, 761–772 (2019).

63. Lliso-Ribera, G. *et al.* Synovial tissue signatures enhance clinical classification and prognostic/treatment response algorithms in early inflammatory arthritis and predict requirement for subsequent biological therapy: Results from the pathobiology of early arthritis cohort (PEA. *Ann. Rheum. Dis.* **78**, 1642–1652 (2019).

64. Mendez-Huergo, S. P. *et al.* Clinical relevance of galectin-1 and galectin-3 in rheumatoid arthritis patients: Differential regulation and correlation with

disease activity. *Front. Immunol.* **10**, (2019).

65. Ohshima, S. *et al.* Galectin 3 and Its Binding Protein in Rheumatoid Arthritis. *Arthritis Rheum.* **48**, 2788–2795 (2003).

66. Neidhart, M. *et al.* Galectin-3 is induced in rheumatoid arthritis synovial fibroblasts after adhesion to cartilage oligomeric matrix protein. *Ann. Rheum. Dis.* **64**, 419–424 (2005).

67. Filer, A. *et al.* Galectin 3 induces a distinctive pattern of cytokine and chemokine production in rheumatoid synovial fibroblasts via selective signaling pathways. *Arthritis Rheum.* **60**, 1604–1614 (2009).

68. Müller-Ladner, U. *et al.* Synovial fibroblasts of patients with rheumatoid arthritis attach to and invade normal human cartilage when engrafted into SCID mice. *Am. J. Pathol.* **149**, 1607–1615 (1996).

69. Rengel, Y., Ospelt, C. & Gay, S. Proteinases in the joint: Clinical relevance of proteinases in joint destruction. *Arthritis Res. Ther.* **9**, (2007).

70. Alivernini, S. *et al.* Distinct synovial tissue macrophage subsets regulate inflammation and remission in rheumatoid arthritis. *Nat. Med.* **26**, 1295–1306 (2020).

71. McInnes, I. B., Buckley, C. D. & Isaacs, J. D. Cytokines in rheumatoid arthritis-shaping the immunological landscape. *Nat. Rev. Rheumatol.* **12**, 63–68 (2016).

72. Geiler, T., Kriegsmann, Jöu., Keyszer, G. M., Gay, R. E. & Gay, S. A new model for rheumatoid arthritis generated by engraftment of rheumatoid synovial tissue and normal human cartilage into scid mice. *Arthritis Rheum.* **37**,

1664–1671 (1994).

73. Kurowska-Stolarska, M. *et al.* Inhibitor of DNA binding/differentiation 2 induced by hypoxia promotes synovial fibroblast-dependent osteoclastogenesis. *Arthritis Rheum.* **60**, 3663–3675 (2009).

74. Jüngel, A. *et al.* Effect of the oral application of a highly selective MMP-13 inhibitor in three different animal models of rheumatoid arthritis. *Ann. Rheum. Dis.* **69**, 898–902 (2010).

75. Takayanagi, H. *et al.* Involvement of receptor activator of nuclear factor κB ligand/osteoclast differentiation factor in osteoclastogenesis from synoviocytes in rheumatoid arthritis. *Arthritis Rheum.* **43**, 259–269 (2000).

76. Seemayer, C. A. *et al.* P53 in Rheumatoid Arthritis Synovial Fibroblasts At Sites of Invasion. *Ann. Rheum. Dis.* **62**, 1139–1144 (2003).

77. Pap, T. *et al.* Differential expression pattern of membrane-type matrix metalloproteinases in rheumatoid arthritis. *Arthritis Rheum.* **43**, 1226–1232 (2000).

78. Neumann, E. *et al.* Migratory potential of rheumatoid arthritis synovial fibroblasts: Additional perspectives. *Cell Cycle* **9**, 2286–2291 (2010).

79. Lefèvre, S. *et al.* Synovial fibroblasts spread rheumatoid arthritis to unaffected joints. *Nat. Med.* **15**, 1414–1420 (2009).

80. Rinn, J. L. *et al.* A dermal HOX transcriptional program regulates site-specific epidermal fate. *Genes Dev.* **22**, 303–307 (2008).

81. Filer, A. *et al.* Stromal transcriptional profiles reveal hierarchies of anatomical site, serum response and disease and identify disease specific pathways.

PLoS One **10**, (2015).

82. Fassbender, H. G. Histomorphological Basis of Articular Cartilage Destruction in Rheumatoid Arthritis. *Top. Catal.* **3**, 141–155 (1983).

83. Palmer, D. G., Selvendran, Y., Allen, C., Revell, P. a & Hogg, N. Features of synovial membrane identified with monoclonal antibodies. *Clin. Exp. Immunol.* **59**, 529–38 (1985).

84. Stephenson, W. *et al.* Single-cell RNA-seq of rheumatoid arthritis synovial tissue using low-cost microfluidic instrumentation. *Nat. Commun.* **9**, (2018).

85. Malhotra, D. *et al.* Transcriptional profiling of stroma from inflamed and resting lymph nodes defines immunological hallmarks. *Nat. Immunol.* **13**, 499–510 (2012).

86. Ekwall, A. K. H. *et al.* The tumour-associated glycoprotein podoplanin is expressed in fibroblast-like synoviocytes of the hyperplastic synovial lining layer in rheumatoid arthritis. *Arthritis Res. Ther.* **13**, (2011).

87. Bauer, S. *et al.* Fibroblast activation protein is expressed by rheumatoid myofibroblast-like synoviocytes. *Arthritis Res. Ther.* **8**, (2006).

88. Miyake, K. *et al.* Inflammatory cytokine-induced expression of vasohibin-1 by rheumatoid synovial fibroblasts. *Acta Med. Okayama* **63**, 349–358 (2009).

89. Middleton, J. *et al.* A comparative study of endothelial cell markers expressed in chronically inflamed human tissues: MECA-79, Duffy antigen receptor for chemokines, von Willebrand factor, CD31, CD34, CD105 and CD146. *J. Pathol.* **206**, 260–268 (2005).

90. Snelling, S. J. B. *et al.* Dickkopf-3 is upregulated in osteoarthritis and has a

chondroprotective role. *Osteoarthr. Cartil.* **24**, 883–891 (2016).

91. Li, Y. *et al.* DKK3 regulates cell proliferation, apoptosis and collagen synthesis in keloid fibroblasts via TGF-β1/Smad signaling pathway. *Biomed. Pharmacother.* **91**, 174–180 (2017).

92. Sakaguchi, M. *et al.* Overexpression of REIC/Dkk-3 in normal fibroblasts suppresses tumor growth via induction of interleukin-7. *J. Biol. Chem.* **284**, 14236–14244 (2009).

93. Nakamura, M. *et al.* Osteoprotegerin Regulates Bone Formation through a Coupling Mechanism with Bone Resorption. *Endocrinology* **144**, 5441–5449 (2003).

94. Sun, S., Liu, W. & Li, Y. CADM1 enhances intestinal barrier function in a rat model of mild inflammatory bowel disease by inhibiting the STAT3 signaling pathway. *J. Bioenerg. Biomembr.* **52**, 343–354 (2020).

95. Pilecki, B. *et al.* Characterization of microfibrillar-associated protein 4 (MFAP4) as a tropoelastin- and fibrillin-binding protein involved in elastic fiber formation. *J. Biol. Chem.* **291**, 1103–1114 (2016).

96. Ramirez-Montagut, T. *et al.* FAPα, a surface peptidase expressed during wound healing, is a tumor suppressor. *Oncogene* **23**, 5435–5446 (2004).

97. McGettrick, H. M. *et al.* Fibroblasts from different sites may promote or inhibit recruitment of flowing lymphocytes by endothelial cells. *Eur. J. Immunol.* **39**, 113–125 (2009).

98. Buckley, C. D. Why does chronic inflammation persist: An unexpected role for fibroblasts. *Immunology Letters* vol. 138 12–14 (2011).

99. Jones, S., Horwood, N., Cope, A. & Dazzi, F. The Antiproliferative Effect of Mesenchymal Stem Cells Is a Fundamental Property Shared by All Stromal Cells. *J. Immunol.* **179**, 2824–2831 (2007).

100. Haniffa, M. A. *et al.* Adult Human Fibroblasts Are Potent Immunoregulatory Cells and Functionally Equivalent to Mesenchymal Stem Cells. *J. Immunol.* **179**, 1595–1604 (2007).

101. McGettrick, H. M., Butler, L. M., Buckley, C. D., Ed Rainger, G. & Nash, G. B. Tissue stroma as a regulator of leukocyte recruitment in inflammation. *J. Leukoc. Biol.* **91**, 385–400 (2012).

102. Xiao, L. Z., Topley, N., Ito, T. & Phillips, A. Interleukin-6 regulation of transforming growth factor (TGF)-β receptor compartmentalization and turnover enhances TGF-β1 signaling. *J. Biol. Chem.* **280**, 12239–12245 (2005).

103. Dominitzki, S. *et al.* Cutting Edge: Trans- Signaling via the Soluble IL-6R Abrogates the Induction of FoxP3 in Naive CD4+CD25− T Cells . *J. Immunol.* **179**, 2041–2045 (2007).

104. Nguyen, H. N. *et al.* Autocrine Loop Involving IL-6 Family Member LIF, LIF Receptor, and STAT4 Drives Sustained Fibroblast Production of Inflammatory Mediators. *Immunity* **46**, 220–232 (2017).

105. Wong, P. K. K. *et al.* SOCS-3 negatively regulates innate and adaptive immune mechanisms in acute IL-1-dependent inflammatory arthritis. *J. Clin. Invest.* **116**, 1571–1581 (2006).

106. Ospelt, C. *et al.* Overexpression of toll-like receptors 3 and 4 in synovial tissue

from patients with early rheumatoid arthritis: Toll-like receptor expression in early and longstanding arthritis. *Arthritis Rheum.* **58**, 3684–3692 (2008).

107. Carrión, M. *et al.* RNA sensors in human osteoarthritis and rheumatoid arthritis synovial fibroblasts: Immune regulation by vasoactive intestinal peptide. *Arthritis Rheum.* **63**, 1626–1636 (2011).

108. Ichise, Y. *et al.* Soluble CD14 Induces Pro-inflammatory Cytokines in Rheumatoid Arthritis Fibroblast-Like Synovial Cells via Toll-Like Receptor 4. *Cells* **9**, (2020).

109. Yu, H., Lin, L., Zhang, Z., Zhang, H. & Hu, H. Targeting NF-κB pathway for the therapy of diseases: mechanism and clinical study. *Signal Transduct. Target. Ther.* **5**, 5 (2020).

110. Hu, X. *et al.* RGS1 silencing inhibits the inflammatory response and angiogenesis in rheumatoid arthritis rats through the inactivation of Toll-like receptor signaling pathway. *J. Cell. Physiol.* **234**, 20432–20442 (2019).

111. Kato, H., Endres, J. & Fox, D. A. The roles of IFN-γ versus IL-17 in pathogenic effects of human Th17 cells on synovial fibroblasts. *Mod. Rheumatol.* **23**, 1140–1150 (2013).

112. Tran, C. N. *et al.* Presentation of arthritogenic peptide to antigen-specific T cells by fibroblast-like synoviocytes. *Arthritis Rheum.* **56**, 1497–1506 (2007).

113. Carmona-Rivera, C. *et al.* Synovial fibroblast-neutrophil interactions promote pathogenic adaptive immunity in rheumatoid arthritis. *Sci. Immunol.* **2**, (2017).

114. Ueno, A. *et al.* The production of CXCR3-agonistic chemokines by synovial fibroblasts from patients with rheumatoid arthritis. *Rheumatol. Int.* **25**, 361–367

(2005).

115. Tanaka, Y. *et al.* Safety, pharmacokinetics, and efficacy of E6011, an antifractalkine monoclonal antibody, in a first-in-patient phase 1/2 study on rheumatoid arthritis. *Mod. Rheumatol.* **28**, 58–65 (2018).

116. Davies, L. C., Jenkins, S. J., Allen, J. E. & Taylor, P. R. Tissue-resident macrophages. *Nat. Immunol.* **14**, 986–995 (2013).

117. Kuo, D. *et al.* HBEGF+ macrophages in rheumatoid arthritis induce fibroblast invasiveness. *Sci. Transl. Med.* **11**, (2019).

118. Neumann, E. *et al.* Cell culture and passaging alters gene expression pattern and proliferation rate in rheumatoid arthritis synovial fibroblasts. *Arthritis Res. Ther.* **12**, (2010).

119. Zimmermann, T. *et al.* Isolation and characterization of rheumatoid arthritis synovial fibroblasts from primary culture - Primary culture cells markedly differ from fourth-passage cells. *Arthritis Res.* **3**, 72–76 (2001).

120. Firestein, G. S. Invasive fibroblast-like synoviocytes in rheumatoid arthritis: Passive responders or transformed aggressors? *Arthritis Rheum.* **39**, 1781–1790 (1996).

121. Ham, S. *et al.* Epigenetic analysis in rheumatoid arthritis synoviocytes. *Exp. Mol. Med.* **51**, (2019).

122. Nemtsova, M. V. *et al.* Epigenetic changes in the pathogenesis of rheumatoid arthritis. *Front. Genet.* **10**, (2019).

123. Karami, J. *et al.* Epigenetics in rheumatoid arthritis; fibroblast-like synoviocytes as an emerging paradigm in the pathogenesis of the disease. *Immunol. Cell*

Biol. **98**, 171–186 (2020).

124. Gibney, E. R. & Nolan, C. M. Epigenetics and gene expression. *Heredity (Edinb).* **105**, 4–13 (2010).

125. Hayer, S. *et al.* 'SMASH' recommendations for standardised microscopic arthritis scoring of histological sections from inflammatory arthritis animal models. *Ann. Rheum. Dis.* **80**, 714–726 (2021).

126. Grün, D. & Van Oudenaarden, A. Design and Analysis of Single-Cell Sequencing Experiments. *Cell* **163**, 799–810 (2015).

127. Papalexi, E. & Satija, R. Single-cell RNA sequencing to explore immune cell heterogeneity. *Nat. Rev. Immunol.* **18**, 35–45 (2018).

128. Trentham, D. E., Townes, A. S. & Kang, A. H. Autoimmunity to type II collagen: An experimental model of arthritis*. *J. Exp. Med.* **146**, 857–868 (1977).

129. Courtenay, J. S., Dallman, M. J., Dayan, A. D., Martin, A. & Mosedale, B. Immunisation against heterologous type II collagen induces arthritis in mice [13]. *Nature* **283**, 666–668 (1980).

130. Holmdahl, R., Jansson, L., Larsson, E., Rubin, K. & Klareskog, L. Homologous type II collagen induces chronic and progressive arthritis in mice. *Arthritis Rheum.* **29**, 106–113 (1986).

131. Inglis, J. J., Šimelyte, E., McCann, F. E., Criado, G. & Williams, R. O. Protocol for the induction of arthritis in C57BL/6 mice. *Nat. Protoc.* **3**, 612–618 (2008).

132. Miyoshi, M. & Liu, S. Collagen-induced arthritis models. *Methods Mol. Biol.* **1868**, 3–7 (2018).

133. Campbell, I. K., Hamilton, J. A. & Wicks, L. P. Collagen-induced arthritis in C57BL/6 (H-2b) mice: New insights into an important disease model of rheumatoid arthritis. *Eur. J. Immunol.* **30**, 1568–1575 (2000).

134. Hashida, R. *et al.* New studies of pathogenesis of rheumatoid arthritis with collagen-induced and collagen antibody-induced arthritis models: New insight involving bacteria flora. *Autoimmune Dis.* **2021**, (2021).

135. Brand, D. D., Kang, A. H. & Rosloniec, E. F. Immunopathogenesis of collagen arthritis. in *Springer Seminars in Immunopathology* (ed. Semin, S.) vol. 25 3–18 (2003).

136. Inglis, J. J. *et al.* Collagen-induced arthritis in C57BL/6 mice is associated with a robust and sustained T-cell response to type II collagen. *Arthritis Res. Ther.* **9**, (2007).

137. Holmdahl, R. *et al.* Incidence of arthritis and autoreactivity of anti-collagen antibodies after immunization of DBA/1 mice with heterologous and autologous collagen II. *Clin. Exp. Immunol.* **62**, 639–46 (1985).

138. Holmdahl R, Jansson L, Larsson A, J. R. Arthritis in DBA/1 Mice Induced with Passively Transferred Type II Collagen Immune Serum. *Scand. J. Immunol.* **31**, 147–157 (1990).

139. Seki, N. *et al.* Type II collagen-induced murine arthritis. I. Induction and perpetuation of arthritis require synergy between humoral and cell-mediated immunity. *J. Immunol.* **140**, 1477–1484 (1988).

140. Goodfellow, R. M., Williams, A. S., Levin, J. L., Williams, B. D. & Morgan, B. P. Soluble complement receptor one (sCR1) inhibits the development and

progression of rat collagen-induced arthritis. *Clin. Exp. Immunol.* **119**, 210–216 (2000).

141. Wang, Y., Rollins, S. A., Madri, J. A. & Matis, L. A. Anti-C5 monoclonal antibody therapy prevents collagen-induced arthritis and ameliorates established disease. *Proc. Natl. Acad. Sci. U. S. A.* **92**, 8955–8959 (1995).

142. Mauri, C., Williams, R. O., Walmsley, M. & Feldmann, M. Relationship between Th1/Th2 cytokine patterns and the arthritogenic response in collagen-induced arthritis. *Eur. J. Immunol.* **26**, 1511–1518 (1996).

143. Klareskog, L. & McDevitt, H. Rheumatoid arthritis and its animal models: The role of TNF-α and the possible absence of specific immune reactions. *Curr. Opin. Immunol.* **11**, 657–662 (1999).

144. Hom, J. T., Bendele, A. M. & Carlson, D. G. In vivo administration with IL-1 accelerates the development of collagen-induced arthritis in mice. *J. Immunol.* **141**, 834–841 (1988).

145. Müssener, Å., Litton, M. J., Lindroos, E. & Klareskog, L. Cytokine production in synovial tissue of mice with collagen-induced arthritis (CIA). *Clin. Exp. Immunol.* **107**, 485–493 (1997).

146. Stasiuk, L. M., Abehsira-Amar, O. & Fournier, C. Collagen-induced arthritis in DBA/1 mice: cytokine gene activation following immunization with type II collagen. *Cell. Immunol.* **173**, 269–275 (1996).

147. Doncarli, A., Stasiuk, L. M., Fournier, C. & Abehsira-Amar, O. Conversion in vivo from an early dominant Th0/Th1 response to a Th2 phenotype during the development of collagen-induced arthritis. *Eur. J. Immunol.* **27**, 1451–1458

(1997).

148. Machold, K. P. *et al.* Very recent onset rheumatoid arthritis: Clinical and serological patient characteristics associated with radiographic progression over the first years of disease. *Rheumatology* **46**, 342–349 (2007).

149. Shiozawa, S. & Ziff, M. Immunoelectron microscopic demonstration of fibronectin in rheumatoid pannus and at the cartilage-pannus junction. *Ann. Rheum. Dis.* **42**, 254–263 (1983).

150. Ishikawa, H. *et al.* An immunohistochemical and immunoelectron microscopic study of adhesion molecules in synovial pannus formation in rheumatoid arthritis. *Rheumatol. Int.* **16**, 53–60 (1996).

151. Kobayashi, I. & Ziff, M. Electron microscopic studies of the cartilage-pannus junction in rheumatoid arthritis. *Arthritis Rheum.* **18**, 475–483 (1975).

152. Shiozawa, S., Shiozawa, K. & Fujita, T. Morphologic observations in the early phase of the cartilage-pannus junction. *Arthritis Rheum.* **26**, 472–478 (1983).

153. Sudoł-Szopińska, I. *et al.* The pathogenesis of rheumatoid arthritis in radiological studies. Part I: Formation of inflammatory infiltrates within the synovial membrane. *J. Ultrason.* **12**, 202–213 (2012).

154. Kulka, J. P. The pathogenesis of rheumatoid arthritis. *J. Chronic Dis.* **10**, 388–402 (1959).

155. Rooney, M. *et al.* Analysis of the histologic variation of synovitis in rheumatoid arthritis. *Arthritis Rheum.* **31**, 956–963 (1988).

156. Ødegård, S. *et al.* Association of early radiographic damage with impaired physical function in rheumatoid arthritis: A ten-year, longitudinal observational

study in 238 patients. *Arthritis Rheum.* **54**, 68–75 (2006).

157. Cooke, T. D. & Jasin, H. E. The pathogenesis of chronic inflammation in experimental antigen-induced arthritis. I. The role of antigen on the local immune response. *Arthritis Rheum.* **15**, 327–337 (1972).

158. van den Berg, W. B., Joosten, L. A. B. & van Lent, P. L. E. M. Murine antigen-induced arthritis. *Methods Mol. Med.* **136**, 243–253 (2007).

159. Brackertz, D., Mitchell, G. F. & Mackay, I. R. Antigen-induced arthritis in mice. *Arthritis Rheum.* **20**, 841–850 (1977).

160. Simon, J. *et al.* Systemic macrophage activation in locally-induced experimental arthritis. *J. Autoimmun.* **17**, 127–136 (2001).

161. Frey, O. *et al.* The role of regulatory T cells in antigen-induced arthritis: aggravation of arthritis after depletion and amelioration after transfer of CD4+CD25+ T cells. *Arthritis Res. Ther.* **7**, 1–11 (2005).

162. Brackertz, D., Mitchell, G. F. & Mackay, I. R. Antigen-induced arthritis in mice. *Arthritis Rheum.* **20**, 841–850 (1977).

163. Pinto, L. G. *et al.* IL-17 mediates articular hypernociception in antigen-induced arthritis in mice. *Pain* **148**, 247–256 (2010).

164. Ji, H. *et al.* Critical roles for interleukin 1 and tumor necrosis factor α in antibody-induced arthritis. *J. Exp. Med.* **196**, 77–85 (2002).

165. van de Loo AA, Arntz OJ, van den B. W. Flare-up of experimental arthritis in mice with murine recombinant IL-1. *Clin. Exp. Immunol.* **87**, 196 (1992).

166. Van De Loo, A. A. J. *et al.* Role of interleukin 1 in antigen-induced

exacerbations of murine arthritis. *Am. J. Pathol.* **146**, 239–249 (1995).

167. Pohlers, D. *et al.* Expression of cytokine mRNA and protein in joints and lymphoid organs during the course of rat antigen-induced arthritis. *Arthritis Res. Ther.* **7**, 7 (2005).

168. Kouskoff, V. *et al.* Organ-specific disease provoked by systemic autoimmunity. *Cell* **87**, 811–822 (1996).

169. Matsumoto, I. & Staub, A. Arthritis provoked by linked T and B cell recognition of a glycolytic enzyme. *Science (80-.).* **286**, 1732–1735 (1999).

170. Ji, H. *et al.* Arthritis critically dependent on innate immune system players. *Immunity* **16**, 157–168 (2002).

171. Wipke, B. T. & Allen, P. M. Essential Role of Neutrophils in the Initiation and Progression of a Murine Model of Rheumatoid Arthritis. *J. Immunol.* **167**, 1601–1608 (2001).

172. Lee, D. M. *et al.* Mast cells: A cellular link between autoantibodies and inflammatory arthritis. *Science (80-.).* **297**, 1689–1692 (2002).

173. Wang, Y. *et al.* A Role for Complement in Antibody-Mediated Inflammation: C5-Deficient DBA/1 Mice Are Resistant to Collagen-Induced Arthritis. *J. Immunol.* **164**, 4340–4347 (2000).

174. Germann, T. *et al.* Administration of interleukin 12 in combination with type II collagen induces severe arthritis in DBA/1 mice. *Proc. Natl. Acad. Sci. U. S. A.* **92**, 4823–4827 (1995).

175. Zhang, F. *et al.* Deconstruction of rheumatoid arthritis synovium defines inflammatory subtypes. *Nature* **623**, 616–624 (2023).

176. Du, L. *et al.* Single cell and lineage tracing studies reveal the impact of CD34+ cells on myocardial fibrosis during heart failure. *Stem Cell Res. Ther.* **14**, (2023).

177. Hanley, C. J. *et al.* Single-cell analysis reveals prognostic fibroblast subpopulations linked to molecular and immunological subtypes of lung cancer. *Nat. Commun.* **14**, 1–18 (2023).

178. Richmond, J. M. *et al.* CXCL9 Links Skin Inflammation and Fibrosis through CXCR3-Dependent Upregulation of Col1a1 in Fibroblasts. *J. Invest. Dermatol.* **143**, 1138-1146.e12 (2023).

179. Pein, M. *et al.* Metastasis-initiating cells induce and exploit a fibroblast niche to fuel malignant colonization of the lungs. *Nat. Commun.* **11**, (2020).

180. Klingberg, F., Hinz, B. & White, E. S. The myofibroblast matrix: Implications for tissue repair andfibrosis. *J. Pathol.* **229**, 298–309 (2013).

181. Ng, M. T. H. *et al.* A single cell atlas of frozen shoulder capsule identifies features associated with inflammatory fibrosis resolution. *Nat. Commun.* **15**, 1394 (2024).

182. Austyn, J. M. & Gordon, S. F4/80, a monoclonal antibody directed specifically against the mouse macrophage. *Eur. J. Immunol.* **11**, 805–815 (1981).

183. McKnight, A. J. *et al.* Molecular cloning of F4/80, a murine macrophage-restricted cell surface glycoprotein with homology to the G-protein-linked transmembrane 7 hormone receptor family. *J. Biol. Chem.* **271**, 486–489 (1996).

184. Malorny, U., Michels, E. & Sorg, C. A monoclonal antibody against an antigen

present on mouse macrophages and absent from monocytes. *Cell Tissue Res.* **243**, 421–428 (1986).

185. Gouon-Evans, V., Lin, E. Y. & Pollard, J. W. Requirement of macrophages and eosinophils and their cytokines/chemokines for mammary gland development. *Breast Cancer Res.* **4**, 155–164 (2002).

186. McGarry, M. P. & Stewart, C. C. Murine eosinophil granulocyte bind the murine macrophage-monocyte specific monoclonal antibody F4/80. *J. Leukoc. Biol.* **50**, 471–478 (1991).

187. Waddell, L. A. *et al.* ADGRE1 (EMR1, F4/80) is a rapidly-evolving gene expressed in mammalian monocyte-macrophages. *Front. Immunol.* **9**, 414893 (2018).

188. Hume, D. A. *et al.* The mononuclear phagocyte system revisited. *J. Leukoc. Biol.* **72**, 621–627 (2002).

189. Caminschi, I. *et al.* Molecular Cloning of F4/80-Like-Receptor, a Seven-Span Membrane Protein Expressed Differentially by Dendritic Cell and Monocyte-Macrophage Subpopulations . *J. Immunol.* **167**, 3570–3576 (2001).

190. Misharin, A. V., Morales-Nebreda, L., Mutlu, G. M., Budinger, G. R. S. & Perlman, H. Flow cytometric analysis of macrophages and dendritic cell subsets in the mouse lung. *Am. J. Respir. Cell Mol. Biol.* **49**, 503–510 (2013).

191. Liyanage, S. E. *et al.* Flow cytometric analysis of inflammatory and resident myeloid populations in mouse ocular inflammatory models. *Exp. Eye Res.* **151**, 160–170 (2016).

192. Wang, Y. Y. *et al.* Macrophage-to-myofibroblast transition contributes to

interstitial fibrosis in chronic renal allograft injury. *J. Am. Soc. Nephrol.* **28**, 2053–2067 (2017).

193. dos Anjos Cassado, A. F4/80 as a major macrophage marker: The case of the peritoneum and spleen. *Results Probl. Cell Differ.* **62**, 161–179 (2017).

194. Lee, Y. S. *et al.* CX3CR1 differentiates F4/80low monocytes into pro-inflammatory F4/80high macrophages in the liver. *Sci. Rep.* **8**, 15076 (2018).

195. Shi, T., Denney, L., An, H., Ho, L. P. & Zheng, Y. Alveolar and lung interstitial macrophages: Definitions, functions, and roles in lung fibrosis. *J. Leukoc. Biol.* **110**, 107–114 (2021).

196. Félix, I. *et al.* Single-Cell Proteomics Reveals the Defined Heterogeneity of Resident Macrophages in White Adipose Tissue. *Front. Immunol.* **12**, 719979 (2021).

197. Kurowska-Stolarska, M. & Alivernini, S. Synovial tissue macrophages in joint homeostasis, rheumatoid arthritis and disease remission. *Nat. Rev. Rheumatol.* **18**, 384–397 (2022).

198. Montgomery, A. B. *et al.* Tissue-resident, extravascular Ly6c− monocytes are critical for inflammation in the synovium. *Cell Rep.* **42**, 112513 (2023).

199. Barone, F. *et al.* Stromal Fibroblasts in Tertiary Lymphoid Structures: A Novel Target in Chronic Inflammation. *Front. Immunol.* **7**, 477 (2016).

200. Nusse, R. & Clevers, H. Wnt/β-Catenin Signaling, Disease, and Emerging Therapeutic Modalities. *Cell* **169**, 985–999 (2017).

201. Sen, M. Wnt signalling in rheumatoid arthritis. *Rheumatology* **44**, 708–713 (2005).

202. Niehrs, C. The complex world of WNT receptor signalling. *Nat. Rev. Mol. Cell Biol. 2012 1312* **13**, 767–779 (2012).

203. van Amerongen, R. Alternative Wnt pathways and receptors. *Cold Spring Harb. Perspect. Biol.* **4**, (2012).

204. Huang, Y., Xue, Q., Chang, J., Wang, X. & Miao, C. Wnt5a: A promising therapeutic target for inflammation, especially rheumatoid arthritis. *Cytokine* **172**, 156381 (2023).

205. Rauner, M. *et al.* WNT5A is induced by inflammatory mediators in bone marrow stromal cells and regulates cytokine and chemokine production. *J. Bone Miner. Res.* **27**, 575–585 (2012).

206. Sen, M. *et al.* Expression and function of wingless and frizzled homologs in rheumatoid arthritis. *Proc. Natl. Acad. Sci. U. S. A.* **97**, 2791–2796 (2000).

207. Kobayashi, Y. *et al.* Wnt5a-induced cell migration is associated with the aggressiveness of estrogen receptor-positive breast cancer. *Oncotarget* **9**, 20979 (2018).

208. Vuga, L. J. *et al.* WNT5A Is a Regulator of Fibroblast Proliferation and Resistance to Apoptosis. *Am. J. Respir. Cell Mol. Biol.* **41**, 583 (2009).

209. Luo, J. *et al.* Wnt signaling and human diseases: what are the therapeutic implications? *Lab. Investig. 2007 872* **87**, 97–103 (2007).

210. Zheng, S., Liu, J., Wu, Y., Huang, T. L. & Wang, G. Small-molecule inhibitors of Wnt signaling pathway: towards novel anticancer therapeutics. *Future Med. Chem.* **7**, 2485 (2015).

211. Liu, J. *et al.* Targeting Wnt-driven cancer through the inhibition of Porcupine by

LGK974. *Proc. Natl. Acad. Sci. U. S. A.* **110**, 20224–20229 (2013).

212. Kim, H. K. *et al.* Blockers of Wnt3a, Wnt10a, or β-Catenin Prevent Chemotherapy-Induced Neuropathic Pain In Vivo. *Neurotherapeutics* **18**, 601–614 (2021).

213. Jang, J. *et al.* LGK974 suppresses lipopolysaccharide-induced endotoxemia in mice by modulating the crosstalk between the Wnt/β-catenin and NF-κB pathways. *Exp. Mol. Med. 2021 533* **53**, 407–421 (2021).

214. Rodon, J. *et al.* Phase 1 study of single-agent WNT974, a first-in-class Porcupine inhibitor, in patients with advanced solid tumours. *Br. J. Cancer* **125**, 28–37 (2021).

215. Gordon, M. D. & Nusse, R. Wnt signaling: multiple pathways, multiple receptors, and multiple transcription factors. *J. Biol. Chem.* **281**, 22429–22433 (2006).

216. Jridi, I., Canté-Barrett, K., Pike-Overzet, K. & Staal, F. J. T. Inflammation and Wnt Signaling: Target for Immunomodulatory Therapy? *Front. Cell Dev. Biol.* **8**, 615131 (2020).

217. Villaseñor, T. *et al.* Activation of the Wnt Pathway by Mycobacterium tuberculosis: A Wnt–Wnt Situation. *Front. Immunol.* **8**, 50 (2017).

218. Clevers, H. Wnt/beta-catenin signaling in development and disease. *Cell* **127**, 469–480 (2006).

219. Gill, A. K., McCormick, P. J., Sochart, D. & Nalesso, G. Wnt signalling in the articular cartilage: A matter of balance. *Int. J. Exp. Pathol.* **104**, 56 (2023).

220. Baarsma, H. A. *et al.* Activation of WNT / β-Catenin Signaling in Pulmonary

Fibroblasts by TGF-β1 Is Increased in Chronic Obstructive Pulmonary Disease. *PLoS One* **6**, (2011).

221. Ma, B. & Hottiger, M. O. Crosstalk between Wnt/β-Catenin and NF-κB Signaling Pathway during Inflammation. *Front. Immunol.* **7**, 1 (2016).

222. Pap, T., Müller-Ladner, U., Gay, R. E. & Gay, S. Fibroblast biology: Role of synovial fibroblasts in the pathogenesis of rheumatoid arthritis. *Arthritis Res.* **2**, 361 (2000).

223. Yap, H. Y. *et al.* Pathogenic Role of Immune Cells in Rheumatoid Arthritis: Implications in Clinical Treatment and Biomarker Development. *Cells* **7**, (2018).

224. Cici, D., Corrado, A., Rotondo, C. & Cantatore, F. P. Wnt Signaling and Biological Therapy in Rheumatoid Arthritis and Spondyloarthritis. *Int. J. Mol. Sci.* **20**, (2019).

225. Sen, M. Wnt signalling in rheumatoid arthritis. *Rheumatology (Oxford).* **44**, 708–713 (2005).

226. vanLoosdregt, J. *et al.* Canonical Wnt Signaling Negatively Modulates Regulatory T Cell Function. *Immunity* **39**, 298–310 (2013).

227. Diarra, D. *et al.* Dickkopf-1 is a master regulator of joint remodeling. *Nat. Med.* **13**, 156–163 (2007).

228. Miao, C. G. *et al.* Wnt signaling pathway in rheumatoid arthritis, with special emphasis on the different roles in synovial inflammation and bone remodeling. *Cell. Signal.* **25**, 2069–2078 (2013).

229. MacLauchlan, S. *et al.* Genetic deficiency of Wnt5a diminishes disease

severity in a murine model of rheumatoid arthritis. *Arthritis Res. Ther.* **19**, 1–11 (2017).

230. Zhao, Y. *et al.* Wnt5a Promotes Inflammatory Responses via Nuclear Factor κB (NF-κB) and Mitogen-activated Protein Kinase (MAPK) Pathways in Human Dental Pulp Cells. *J. Biol. Chem.* **289**, 21028 (2014).

231. Rodriguez-Trillo, A. *et al.* Non-Canonical WNT5A Signaling Through RYK Contributes to Aggressive Phenotype of the Rheumatoid Fibroblast-Like Synoviocytes. *Front. Immunol.* **11**, 1 (2020).

232. Blom, A. B. *et al.* Synovial lining macrophages mediate osteophyte formation during experimental osteoarthritis. *Osteoarthr. Cartil.* **12**, 627–635 (2004).

233. Carmona-Fontaine, C. *et al.* Contact inhibition of locomotion in vivo controls neural crest directional migration. *Nature* **456**, 957–961 (2008).

234. Asem, M. S., Buechler, S., Wates, R. B., Miller, D. L. & Stack, M. S. Wnt5a Signaling in Cancer. *Cancers (Basel).* **8**, (2016).

235. Shao, Y. *et al.* Biological functions of macrophage-derived Wnt5a, and its roles in human diseases. *Oncotarget* **7**, 67674 (2016).

236. Suryawanshi, A., Tadagavadi, R. K., Swafford, D. & Manicassamy, S. Modulation of Inflammatory Responses by Wnt/β-Catenin Signaling in Dendritic Cells: A Novel Immunotherapy Target for Autoimmunity and Cancer. *Front. Immunol.* **7**, 460 (2016).

237. Klavdianou, K., Liossis, S. N. & Daoussis, D. Dkk1: A key molecule in joint remodelling and fibrosis. *Mediterr. J. Rheumatol.* **28**, 174 (2017).

238. Tian, F., Mauro, T. M. & Li, Z. The pathological role of Wnt5a in psoriasis and

psoriatic arthritis. *J. Cell. Mol. Med.* **23**, 5876 (2019).

239. Fitzgerald-Bocarsly, P. & Feng, D. The role of type I interferon production by dendritic cells in host defense. *Biochimie* **89**, 843 (2007).

240. Swafford, D. & Manicassamy, S. Wnt Signaling in Dendritic Cells: Its Role in Regulation of Immunity and Tolerance. *Discov. Med.* **19**, 303 (2015).

241. Ma, M. H. Y. *et al.* Remission in early rheumatoid arthritis: predicting treatment response. *J. Rheumatol.* **39**, 470–475 (2012).

242. Shammas, R. M., Ranganath, V. K. & Paulus, H. E. Remission in Rheumatoid Arthritis. *Curr. Rheumatol. Rep.* **12**, 355 (2010).

243. Martinec, R., Pinjatela, R. & Balen, D. QUALITY OF LIFE IN PATIENTS WITH RHEUMATOID ARTHRITIS – A PRELIMINARY STUDY. *Acta Clin. Croat.* **58**, 157 (2019).

244. Kondo, N., Kuroda, T. & Kobayashi, D. Cytokine Networks in the Pathogenesis of Rheumatoid Arthritis. *Int. J. Mol. Sci.* **22**, 10922 (2021).

245. Rosenblum, M. D., Way, S. S. & Abbas, A. K. Regulatory T cell memory. *Nat. Rev. Immunol.* **16**, 90–101 (2016).

246. Sakaguchi, S., Wing, K., Onishi, Y., Prieto-Martin, P. & Yamaguchi, T. Regulatory T cells: how do they suppress immune responses? *Int. Immunol.* **21**, 1105–1111 (2009).

247. Shuai, Z. *et al.* Reestablish immune tolerance in rheumatoid arthritis. *Front. Immunol.* **13**, 1012868 (2022).

248. Niehrs, C. Function and biological roles of the Dickkopf family of Wnt

modulators. *Oncogene* **25**, 7469–7481 (2006).

249. Giralt, I. *et al.* Dickkopf Proteins and Their Role in Cancer: A Family of Wnt Antagonists with a Dual Role. *Pharmaceuticals (Basel).* **14**, (2021).

250. Kikuchi, A., Matsumoto, S. & Sada, R. Dickkopf signaling, beyond Wnt-mediated biology. *Semin. Cell Dev. Biol.* **125**, 55–65 (2022).

251. Mao, B. & Niehrs, C. Kremen2 modulates Dickkopf2 activity during Wnt/LRP6 signaling. *Gene* **302**, 179–183 (2003).

252. Shailesh, H., Siveen, K. S. & Sif, S. Protein arginine methyltransferase 5 (PRMT5) activates WNT/β-catenin signalling in breast cancer cells via epigenetic silencing of DKK1 and DKK3. *J. Cell. Mol. Med.* **25**, 1583–1600 (2021).

253. Nakamura, R. E. I. & Hackam, A. S. Analysis of Dickkopf3 interactions with Wnt signaling receptors. *Growth Factors* **28**, 232–242 (2010).

254. Zhao, S., Hao, C. L., Zhao, E. H., Jiang, H. M. & Zheng, H. C. The Suppressing Effects of Dkk3 Expression on Aggressiveness and Tumorigenesis of Colorectal Cancer. *Front. Oncol.* **10**, (2020).

255. Snelling, S. J. B. *et al.* Dickkopf-3 is upregulated in osteoarthritis and has a chondroprotective role. *Osteoarthr. Cartil.* **24**, 883–891 (2016).

256. Chen, T. *et al.* DKK3 (Dikkopf-3) Transdifferentiates Fibroblasts Into Functional Endothelial Cells-Brief Report. *Arterioscler. Thromb. Vasc. Biol.* **39**, 765–773 (2019).

257. Li, Y. *et al.* DKK3 regulates cell proliferation, apoptosis and collagen synthesis in keloid fibroblasts via TGF-β1/Smad signaling pathway. *Biomed.*

Pharmacother. **91**, 174–180 (2017).

258. Meister, M. *et al.* Dickkopf-3, a Tissue-Derived Modulator of Local T-Cell Responses. *Front. Immunol.* **6**, (2015).

259. Brescia, A. C., Simonds, M. M., McCahan, S. M., Fawcett, P. T. & Rose, C. D. The Role of Transforming Growth Factor β Signaling in Fibroblast-like Synoviocytes From Patients With Oligoarticular Juvenile Idiopathic Arthritis: Dysregulation of Transforming Growth Factor β Signaling, Including Overexpression of Bone Morphogenetic Protein 4, May Lead to a Chondrocyte Phenotype and May Contribute to Bony Hypertrophy. *Arthritis Rheumatol. (Hoboken, N.J.)* **66**, 1352 (2014).

260. Gonzalo-Gil, E. & Galindo-Izquierdo, M. Role of Transforming Growth Factor-Beta (TGF) Beta in the Physiopathology of Rheumatoid Arthritis. *Reumatol. Clínica (English Ed.* **10**, 174–179 (2014).

261. Gonzalo-Gil, E. *et al.* Transforming growth factor (TGF)-β signalling is increased in rheumatoid synovium but TGF-β blockade does not modify experimental arthritis. *Clin. Exp. Immunol.* **174**, 245 (2013).

262. Lu, K. H. *et al.* Dickkopf-3 contributes to the regulation of anti-tumor immune responses by mesenchymal stem cells. *Front. Immunol.* **6**, 173871 (2015).

263. LEE, E. J., NGUYEN, Q. T. T. & LEE, M. Dickkopf-3 in Human Malignant Tumours: A Clinical Viewpoint. *Anticancer Res.* **40**, 5969–5979 (2020).

264. Gondkar, K. *et al.* Dickkopf homolog 3 (Dkk3) acts as a potential tumor suppressor in gallbladder cancer. *Front. Oncol.* **9**, 1121 (2019).

265. Al Shareef, Z., Ershaid, M. N. A., Mudhafar, R., Soliman, S. S. M. & Kypta, R.

M. Dickkopf-3: An Update on a Potential Regulator of the Tumor Microenvironment. *Cancers (Basel).* **14**, (2022).

266. Mourtada, J., Thibaudeau, C., Wasylyk, B. & Jung, A. C. The Multifaceted Role of Human Dickkopf-3 (DKK-3) in Development, Immune Modulation and Cancer. *Cells 2024, Vol. 13, Page 75* **13**, 75 (2023).

267. A Phase 1/2a Study of In-Situ REIC/DKK-3 Therapy in Patients with Localized Prostate Cancer | Dana-Farber Cancer Institute. https://www.dana-farber.org/clinical-trials/16-601.

268. Katase, N., Nishimatsu, S. ichiro, Yamauchi, A., Okano, S. & Fujita, S. Establishment of anti-DKK3 peptide for the cancer control in head and neck squamous cell carcinoma (HNSCC). *Cancer Cell Int.* **22**, 1–16 (2022).

269. Rauner, M. *et al.* WNT5A is induced by inflammatory mediators in bone marrow stromal cells and regulates cytokine and chemokine production. *J. Bone Miner. Res.* **27**, 575–585 (2012).

270. Watanabe, S., Alexander, M., Misharin, A. V. & Budinger, G. R. S. The role of macrophages in the resolution of inflammation. *J. Clin. Invest.* **129**, 2619 (2019).

271. Wynn, T. A. & Vannella, K. M. Macrophages in Tissue Repair, Regeneration, and Fibrosis. *Immunity* **44**, 450–462 (2016).

272. Trotter, T. N. *et al.* Dormant tumors circumvent tumor-specific adaptive immunity by establishing a Treg-dominated niche via DKK3. *JCI Insight* **8**, (2023).

8 SUPPLEMENTARY INFORMATION

Table 8.1 Global Arthritis Score Sheet for STIA & CIA

Score sheet for K/BxN serum-induced arthritis:												
Experiment:												
Animal ID :	**Date**											
	Day	**0**	**1**	**2**	**3**	**4**	**5**	**6**	**7**	**8**	**9**	**10**
Behaviour (assessed in home cage prior to handling)		**Score**	**Score**	**Score**	**Score**	**Score**	**Score**	**Score**	**Score**	**Score**	**Score**	**Score**
Normal interactions with cage mates	0											
Reduced interest in roaming behaviour	2											
Isolated from cagemates (provide additional house)	5											
Coat condition (prior to scruffing)												
Normal	0											
Lack of grooming	1											
Staring coat	2											
Body weight (compared to an age-matched control)												
Weight												
Normal (within 10% of age matched control)	0											
>10 % weight loss (ensure food on cage floor)	2											
>15% (provide soft, palatable food)	5											
Mobility (assessed in a separate cage)												
Normal	0											
Abnormal gait	1											
Paddling (give analgesia)	2											
Reluctance to stand up on hind legs (give analgesia)	3											
Absence of load bearing (give analgesia)	5											
Mouse Grimace Scale												
Orbital Tightening (+1)												
Nose Bulge (+1)												
Cheek Swelling (+1)												
Ear Position (+1)												
Whisker Change (+1)												
Hunched Posture (+3)												
Involuntary Shaking / Shivering (+5)												
Altered Breathing (+5)												
Total Score Out of 18												
Arthritic paw score (see table below)												
Front Left		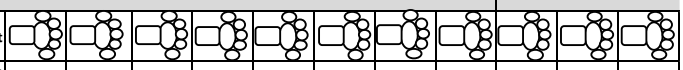										
Score out of 3												
Front Right		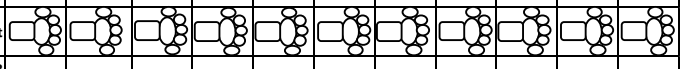										
Score out of 3												
Rear Left		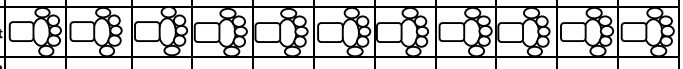										
Score out of 3												
Rear Right		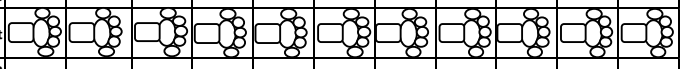										
Score out of 3												
Normal	0											
Total 1 - 3	1											
Total 4 – 7	2											
Total 8– 10	3											
Total 11 - 12 (give analgesia)	4											
Caliper measurement												
Front Left												
Front Right												
Rear Left												
Rear Right												
Left Ankle												
Right Ankle												
Abnormal response to caliper measurement	2											
>4.5mm on any individual foot pad/ankle	HEP											
Total score												
Sum all parameters	**/41**											

Arthritic paw score	
No swelling	**0**
Swelling affecting a single digit or joint	**1**
Localised swelling affecting multiple joints	**2**
Generalised swelling affecting multiple joints	**3**

Outcome	
1–7	Disease evident, monitor carefully
7– 12	Implement pain management
13-21	Seek advice from NACWO or vet
>21	Humane endpoint
HEP	Humane endpoint

Table 8.2 Global Arthritis Score Sheet for AIA

Score sheet for Mono-arthritis								
Experiment:								
Animal ID :	**Date**							
	Day							
Behaviour (assessed in home cage prior to handling)		**Score**	**Score**	**Score**	**Score**	**Score**	**Score**	**Score**
Normal interactions with cage mates	0							
Reduced interest in roaming behaviour	2							
Isolated from cagemates (provide additional house)	5							
Coat condition (prior to scruffing)								
Normal	0							
Lack of grooming	1							
Stary coat	2							
Redness/roughness/loss of fur at injection site	1							
Dry scab	2							
Wet ulceration (If maintained >2 days = HEP)	5							
Body weight (compared to an age-matched control)								
Weight								
Normal (within 10% of age matched control)	0							
>10 % weight loss (provide soft, palatable food)	2							
>20%	HEP							
Mobility (assessed in a separate cage)								
Normal	0							
Abnormal gait (e.g shuffles)	1							
Hobbling (e.g reluctance to put full weight on one leg during normal walking)	2							
Paddling with effected leg	3							
Absence of load bearing on effected leg (e.g. when standing on hind paws)	5							
Sledging (using tail to move) or absence of load bearing on both legs	HEP							
Mouse Grimace Scale								
Orbital Tightening (+1)								
Nose Bulge (+1)								
Cheek Swelling (+1)								
Ear Position (+1)								
Whisker Change (+1)								
Hunched Posture (+3)								
Involuntary Shaking / Shivering (+5)								
Altered Breathing (+5)								
Total Score Out of 18								
Caliper measurement								
Rear Left								
Rear Right								
10 - 20% increase from baseline	1							
20-30% increase from baseline	2							
30-40% increase from baseline	3							
40-50% increase from baseline	4							
> 50% increase (If maintained >2 days = HEP)	5							
Abnormal response to caliper measurement	2							
Knee joint ≥100% increase from baseline	HEP							
Total score								
Sum all parameters	**/44**							

Outcome	Normal, no action required
1–13	Disease evident, monitor carefully
13-25	Seek advice from NACWO or vet
>25	Humane endpoint
HEP	Humane endpoint

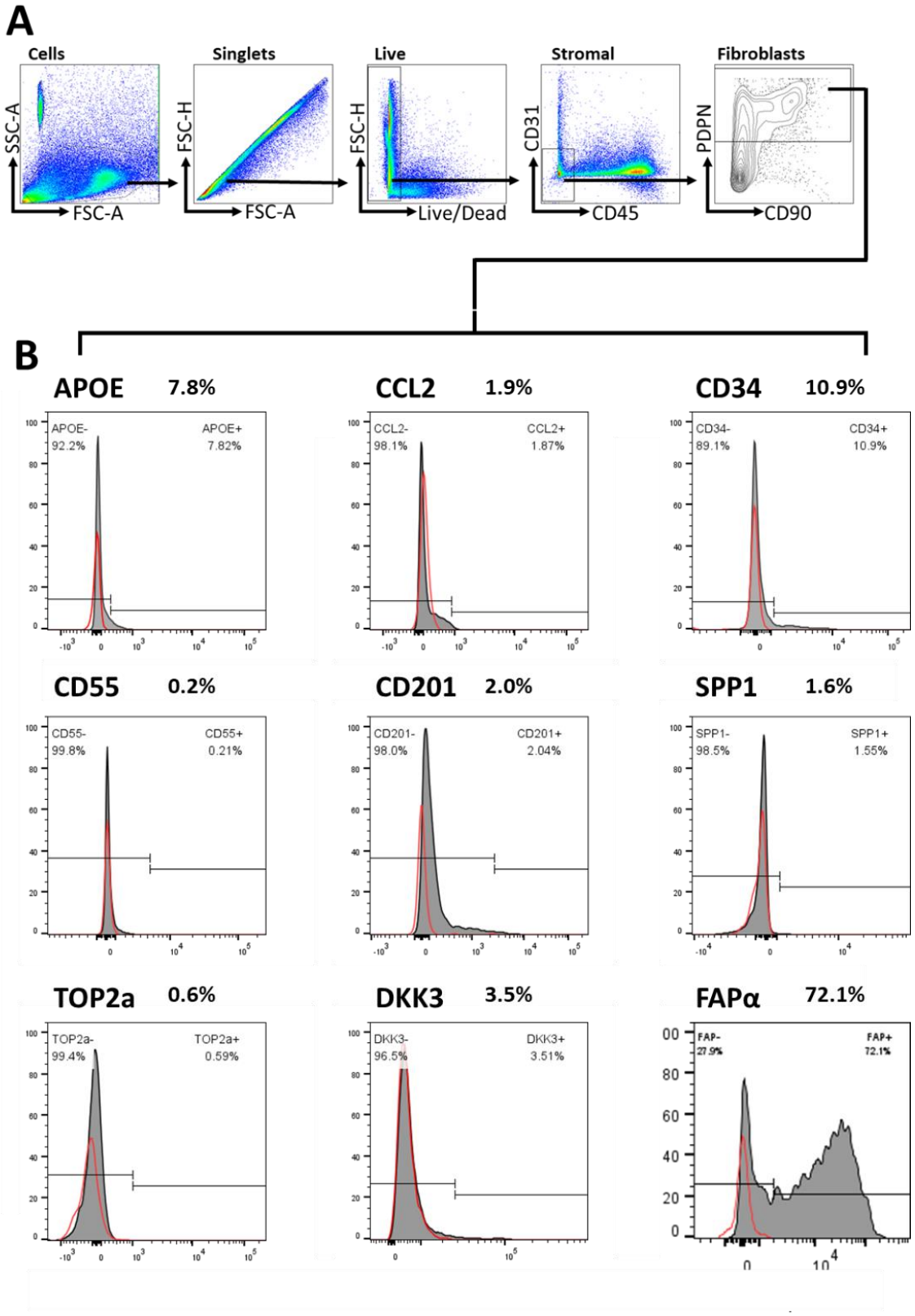

Figure 8.1 Optimisation of mouse fibroblast markers. Mouse synovial fibroblasts were isolated and stained as indicated. A) Gating strategy used to define all synovial fibroblasts. B) Individual markers compared against FMO controls. Percentages shown indicate proportion of fibroblasts positive for each marker.

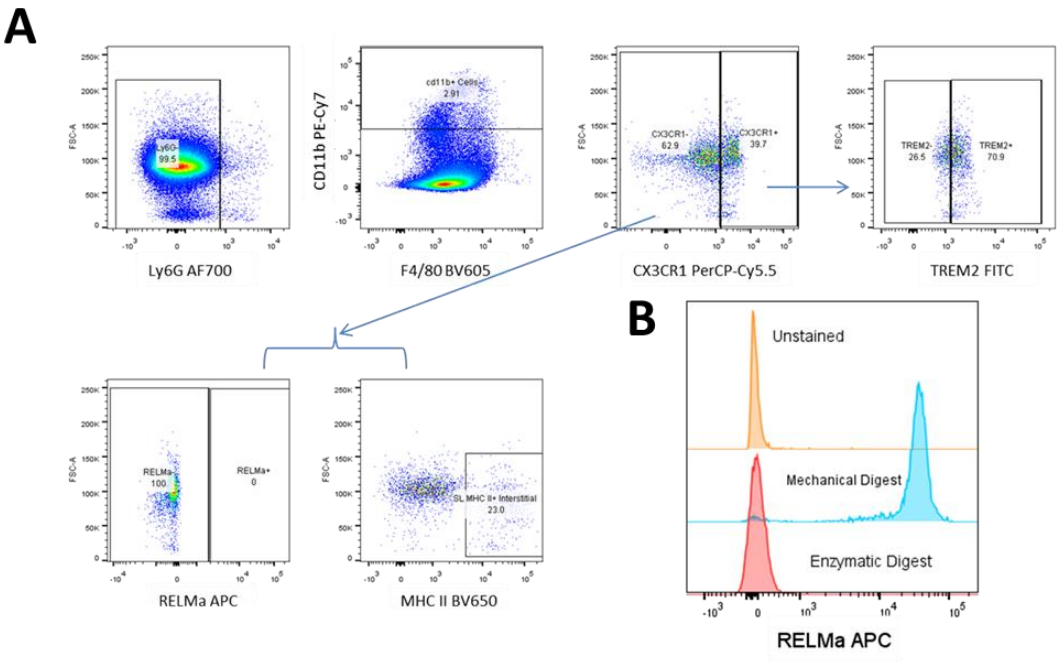

Figure 8.2 Optimisation of Relmα staining with flow cytometry. Mouse synovial cells were isolated by either enzymatic digest or mechanically by crushing tissue through a cell strainer. Sublining macrophages were identified from Cx3cr1 expression, and expression of Relmα was evaluated (A). Relmα appears to be cleaved by the enzymatic digest process (B).

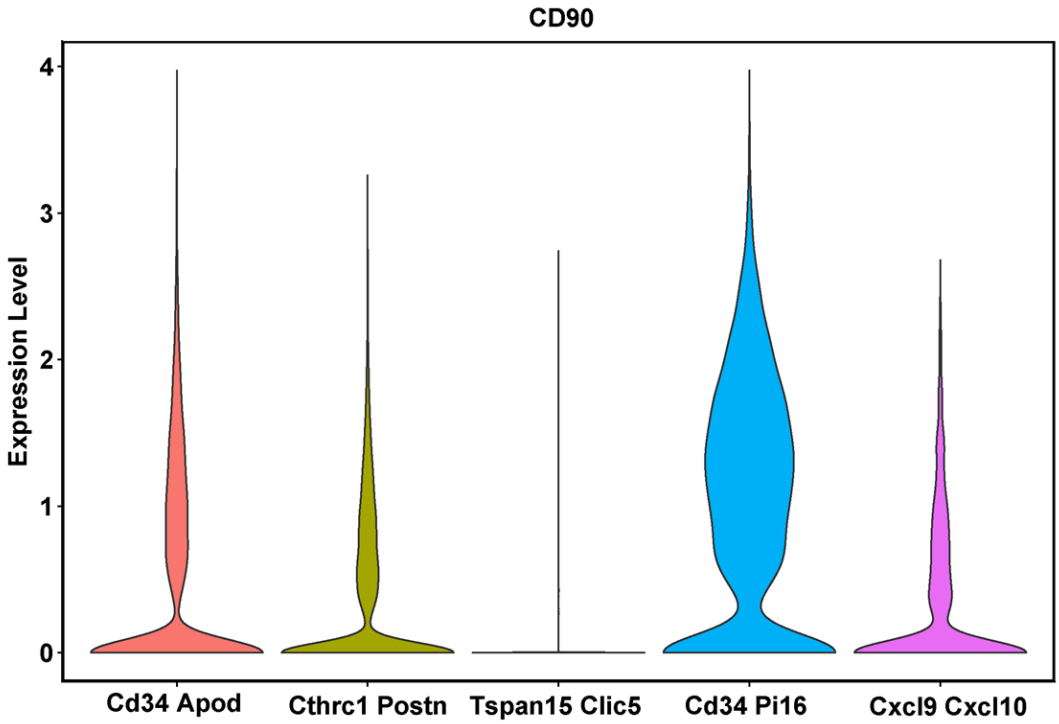

Figure 8.3 Characterising lining vs sub-lining fibroblasts in single cell RNA sequencing. Fibroblasts were identified using established markers, and subsets were labelled by top differentially regulated gene markers. Expression of Thy1 (CD90) was evaluated to determined if each subset was a lining or sublining fibroblast.

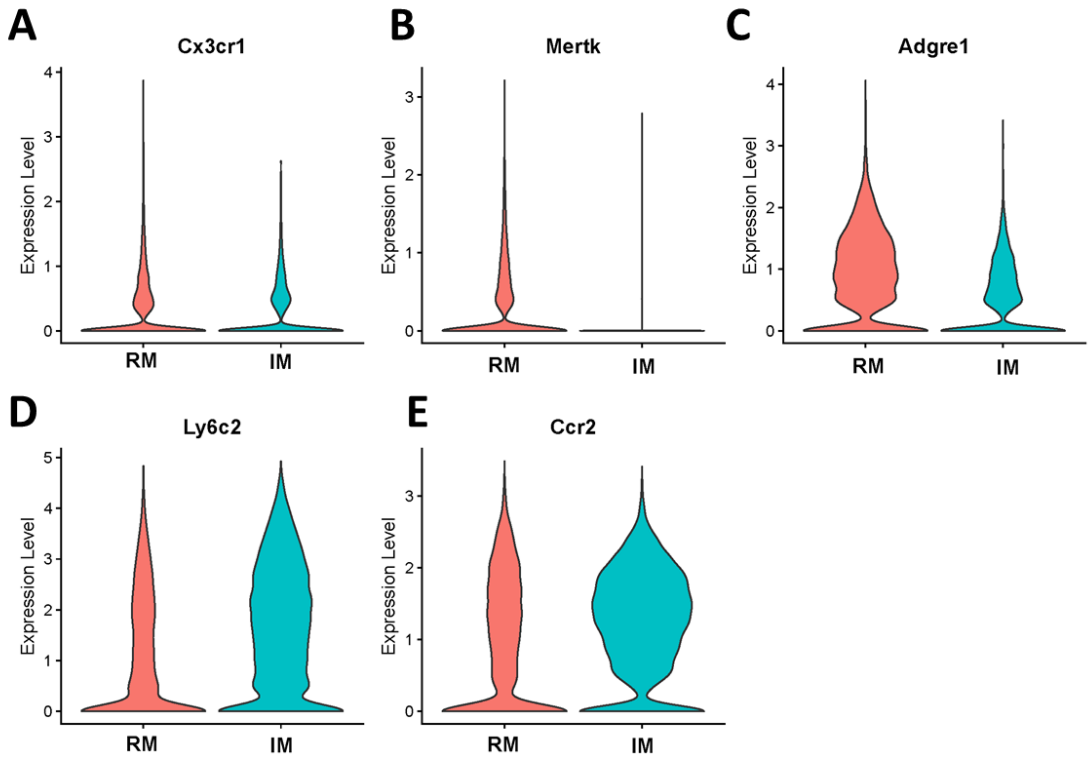

Figure 8.4 Characterising infiltrating vs resident macrophages in single cell RNA sequencing. Macrophages were identified using established markers. Sub-clusters were identified as being resident or infiltrating based on expression of: Cx3cr1 (A), Mertk (B), Adgre1 (C), Ly6c2 (D) and Ccr2 (E).

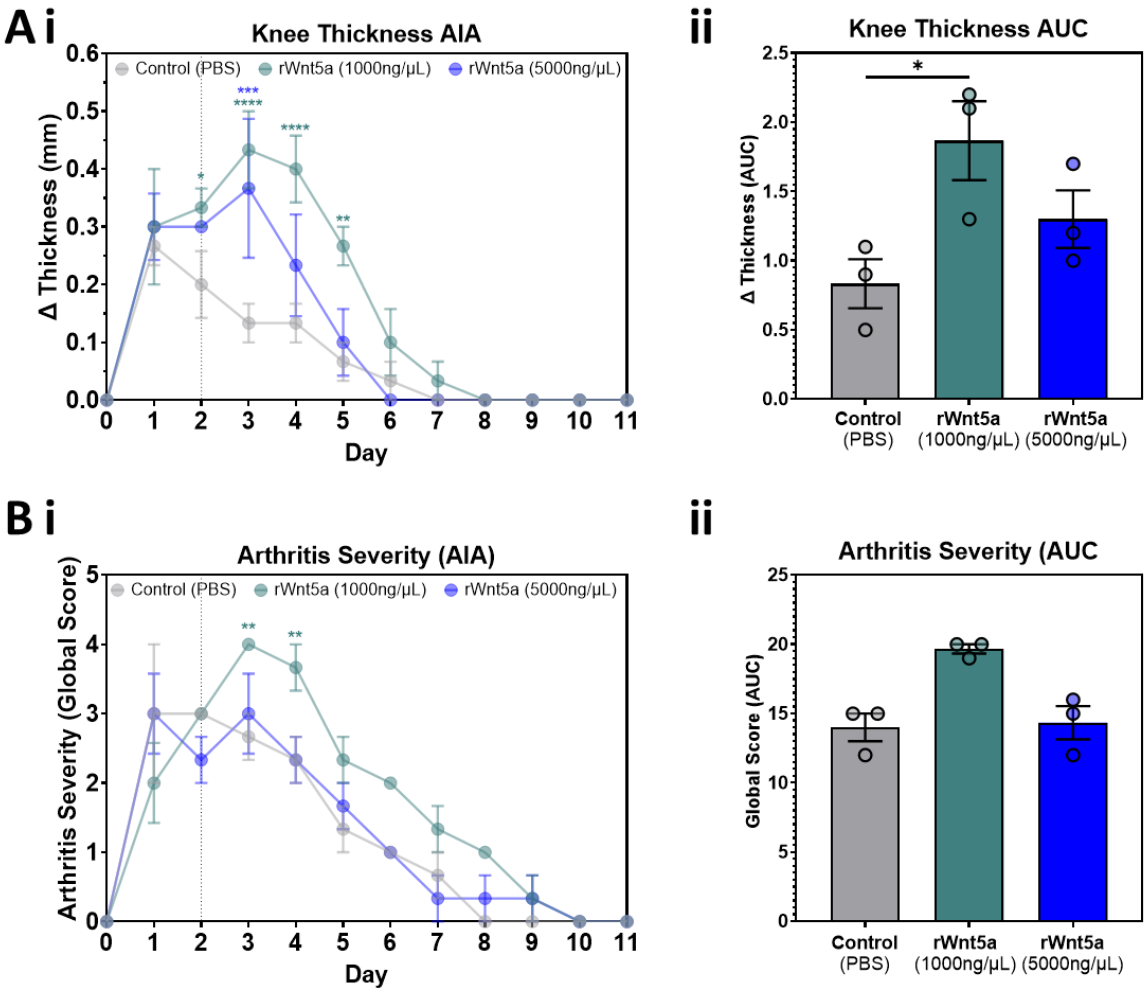

Figure 8.5 Dose optimisation of rWnt5a. AIA was initiated in mice at day 0. At Day 2, rWnt5a or a PBS control was injected directly into the knee joint at either 1000 ng/uL or 5000 ng/uL. Joint thickness (A,i) and arthritis severity (B,i) were scored daily. Overall change in joint thickness (A,ii) and arthritis severity (B,ii) were determined by calculating the area under the curve. Statistical analyses were performed using Two-Way ANOVA followed by Tukey's Post Hoc test and unpaired t-tests. * p<0.05; ** p<0.01; *** p<0.001; **** p<0.0001. n = 3 per condition.

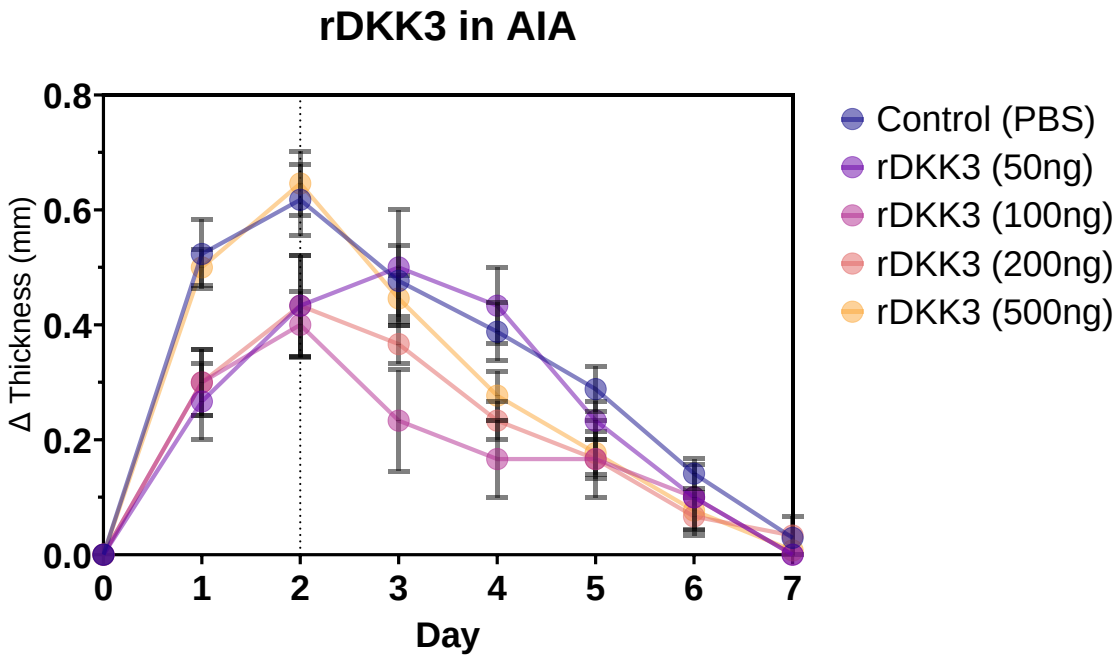

Figure 8.6 Dose optimisation of rDkk3. AIA was initiated in mice at day 0. At Day 2, rDkk3 or a PBS control was injected directly into the knee joint at 50ng, 100ng, 200ng or 500ng. Joint thickness was scored daily. Statistical analyses were performed using Two-Way ANOVA followed by Tukey's Post Hoc test and unpaired t-tests. * $p<0.05$; ** $p<0.01$; *** $p<0.001$; **** $p<0.0001$. n = 3 per condition.

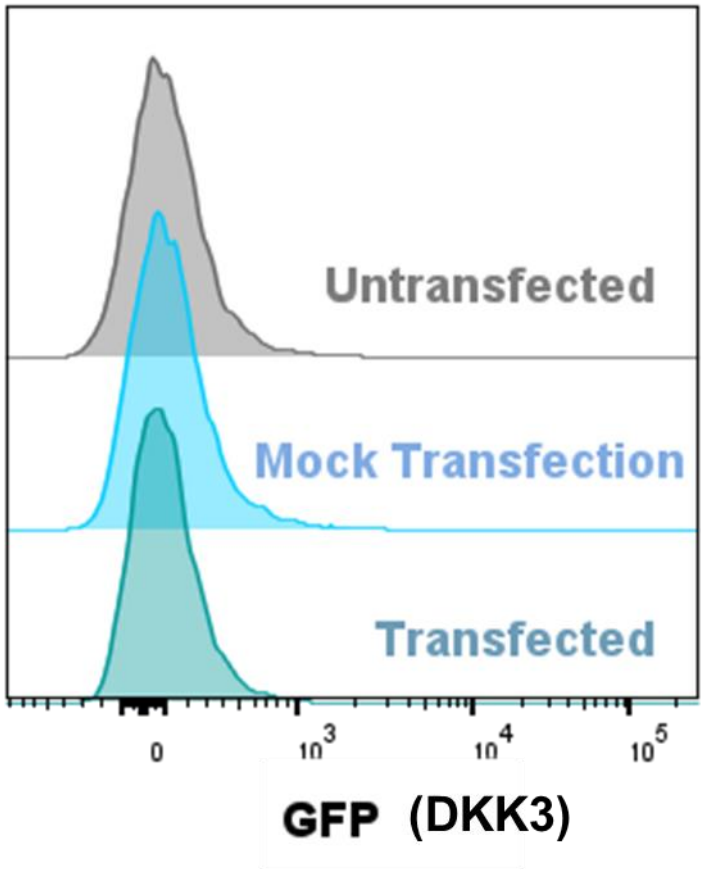

Figure 8.7 Overexpression of Dkk3 in mouse synovial fibroblasts. Murine synovial fibroblasts were isolated and cultured, then transfected with a plasmid for Dkk3 over expression, or a mock control, both of which contain a GFP tag. Following transfection, cells were prepared for flow cytometry and expression of GFP was analysed. This was work conducted with the help of Dr Paulynn Chin.